Pulse Position Modulation Coding Schemes for Optical Inter-satellite Links in Free Space

Fadi Jawdat Ghosna

A thesis submitted to the University of Huddersfield
in partial fulfilment of the requirements for
the degree of Doctor of Philosophy

The University of Huddersfield

July 2010

ABSTRACT

The rapid and significant development of communications links between satellites has made it possible to use various applications such as relay voice, video, multimedia, etc. As a result, a great deal of research has been done in this field during the last few years to reduce power consumption and increase transmission reliability.

This thesis is concerned with an analysis of intersatellite links in free space, with optical links using laser sources being considered in particular. It includes a literature survey and a thorough theoretical investigation into designing the model of the link in free space. This thesis describes the novel technique of designing the optical receiver that consists of PIN photodiode as a photodetector, Semiconductor optical amplifier (SOA) and a 3rd order Butterworth filter with central decision detection. In addition, it discusses the use of several different coding schemes for use in such links: multiple pulse position modulation (MPPM); digital pulse position modulation (DPPM); Dicode pulse position modulation (Dicode PPM).

This novel technique of an optical receiver is investigated and new work is presented in order to examine the noise performance of this optical receiver and hence determine its sensitivity and the number of photons received for a specified error rate. Further new work is carried out to compare these coding schemes in terms of error weightings and coding efficiency through showing how the PCM error rate is affected by false alarm and erasure errors for MPPM, DPPM and Dicode PPM coding 3, 4, 5 and 6 bits of PCM. An original maximum likelihood sequence detector (MLSD) is presented in this thesis in order to perform these comparisons. In addition, computer simulations models (using MCAD) are performed to compare these three coding schemes operating with 3, 4, 5 and 6 bits of PCM in terms of sensitivity and bandwidth efficiency. These comparisons show that MPPM coding 3, 4, 5 and 6 bits of PCM is the appropriate coding scheme to be used in optical inter-satellite links in free space and PCM data rates of 1 Gbit/s.

Acknowledgment

The work presented in this document has been carried out in the Department of Engineering and Technology at the University of Huddersfield, in collaboration with Ministry of Higher Education in Syria. The author wishes to acknowledge the Ministry of Higher Education in Syria for their financial support throughout the duration of the project.

The author wishes to express his sincere appreciation and is particularly indebted to his supervisor Dr. Martin J N Sibley for his guidance, encouragement, acting as a mentor throughout the project and for sharing his academic and practical expertise.

Special thanks for support, encouragement, patience and understanding go to my parents, brother (Basel), sisters and my best friend (Loiy).

Table of content

List of Figures

List of Tables

Glossary of Symbols

Symbol	Definition
P_t	Power transmitted
A_b	Beam area at the detector
A_1	Detector lens area
β	Beam divergence assumed small
D_1	Lens diameter
d	Distance between the transmitter and the receiver
A_r	Receiver antenna effective areas
A_t	Transmit antenna effective areas
g_r	Receive antenna gain
g_t	Transmit antenna gain
$\left(\frac{\lambda}{4\pi d}\right)^2$	Free space loss
A_R	Receiver aerial area
G_T	Transmitter antenna gain
L	Loss factor
$\frac{S}{N}$	Signal-to-noise ratio
N	Number of PCM bits
I_s	Photo-generated current
I_d	Dark current
I_{diode}	Reverse bias current

E_1	Valence band (VB) electron energy
E_2	Conduction band (CB) electron energy
$E_2 - E_1$	Change in energy
E_g	Band-gap energy
h	Planck's constant (6.624×10^{-34} Js)
c	Velocity of light in a vacuum ($3\times10^{8}\, ms^{-1}$)
λ_0	Cutoff wavelength
L_n	Diffusion length for electrons
L_p	Diffusion length for holes
τ_n	Carrier lifetime for electrons
τ_p	Carrier lifetime for holes
I_p	Primary photocurrent
q	Electron charge
hv	Photon energy
R_f	Reflectivity at the entrance face of the photodiode
ω	Width of the depletion region
P_0	Incident optical power level
$\alpha_s(\lambda)$	Absorption coefficient
η	Photodiode quantum efficiency
R_o	Photodiode responsivity
I_M	Average value of the total multiplied output current
M	Multiplication for all carriers created in the photodiode
$F(M)$	Photodiode noise figure
i_Q	Photodiode quantum or shot noise
i_{DB}	Photodiode dark current noise
i_{DS}	Photodiode surface leakage current noise
I_L	Photodiode surface leakage current
i_N	Photodiode total noise current

K_B	Boltzmann's constant ($K_B = 1.38 \times 10^{-23} JK^{-1}$)
T	Absolute temperature
i_T	Thermal (Johnson) noise current of load resistor
G	Amplifier gain
$P_{s,in}$	Amplifier the input power
$P_{s,out}$	Amplifier output power
Γ	Optical confinement factor in the cavity
g_m	Material gain coefficient
$\overline{\alpha}$	Effective absorption coefficient of the material in the optical path
L	Amplifier length
$g(z)$	Overall gain per unit length
ε_r	Relative permittivity of the active region
τ_{sp}	Carrier lifetime for spontaneous emission
$g(f)$	Lorenztian curve
n_1	Electron density in the conduction band CB
n_2	Electron density in the valence band VB
v_g	Group velocity of the light in the semiconductor material
J_{th}	Threshold current density
ϕ	Optical flux density
τ_r	Radiative recombination time
τ_{ph}	Stimulated photon lifetime in the active region
n_{th}	Threshold electron density
σ	Linewidth of the laser output
β	Propagating constant
$I(z)$	Optical field intensity
R_{sp}	Rate of spontaneous emission into the lasing mode
τ_{sp}	Spontaneous recombination lifetime
η_i	Internal quantum efficiency
η_{ext}	External differential quantum efficiency
λ_B	Bragg wavelength

n_e	Effective refractive index of the mode
Λ	Period of the corrugations
V_B	Bias voltage
NF	Amplifier noise figure
$A(\omega)$	Amplifier transfer function
C_d	Detector capacitance
S_I	Shunt noise generator
S_E	Series noise generator
T_b	PCM bit time
B	PCM bit rate
I_2, I_3	Bandwidth integrals in A.c. equivalent circuit of an optical receiver
R_{in} and C_{in}	Parallel combination modeling the input impedance of the preamplifier
C_T	Total input capacitance which equals ($C_d + C_{in}$)
N_A	Input noise of the Semiconductor optical amplifier (SOA)
P	Mean optical power required in the receiver
Q	Signal-to-noise ratio parameter
P_o	Received power
NP	Number of received photons
T_s	Slot time
P_s	Probability of a wrong-slot error
$\left\langle n_o^{\,2} \right\rangle$	Noise on the detected signal
$slope(t_d)$	Slope of the received pulse at the threshold crossing instant
t_d	Threshold crossing instant
P_f	Probability of a false alarm error
$v_o(t_d)$	The signal voltage in the slot considered
v_d	Decision or threshold level voltage

T_s / τ_R	Number of uncorrelated samples per time slot
τ_R	Autocorrelation time
P_e	Probability of an erasure error
ω_{Pn}	Preamplifier bandwidth
ω_{Bn}	Bandwidth of the Butterworth filter
V_d	Threshold crossing voltage
V_{pk}	Peak voltage of the pulse
f_n	Channel bandwidth for free space
t_{pk}	Peak time
t_{d_i}	Decision time

1. INTRODUCTION

The connectivity, coverage, flexibility, reliability and efficiency of future satellite networks can be improved by utilising optical intersatellite links (OISL). Some applications might include geosynchronous to geosynchronous communications, geosynchronous to earth communications and geosynchronous to low-orbit communications. In addition, the potential of high data rate transmission is offered by using an OISL, and relatively small transmitter and receiver antennae are used compared to microwave transmission as a result of the high directivity associated with the optical beam.

Further advantages of an optical transponder are that it provides greater protection against interference and security as a result of the narrow transmit beams. There is greater opportunity to collocate a large number of these with reduction in power consumption and weight compared to a microwave system.

A number of basic system characteristics should be possessed by an optical intersatellite link, low mass (< 50 Kg), low power (< 50 W), low volume and very accurate pointing. The overall mass of the system should permit it to be utilised as a secondary payload. The use of laser diodes for coherent optical communication is a considerable choice due to the additional requirements of long lifetime, reliability and cost effectiveness. Therefore, high sensitivity receivers are required because, in this application, laser diodes provide a power limited transmitter source and the link budget should be met.

The main aim of the research is to investigate the design of an optical inter-satellite link in free space and PCM data rates of 1 Gbit/s, and to select the appropriate coding scheme to be used in such links. Therefore, this thesis is concerned with an analysis of intersatellite links in free space, with optical links using laser sources being considered in particular. An initial assumption will be considered that the input speed is of the order of 128 Mbit/s and the output speed is of the order of 1 Gbit/s. The novel technique of designing an optical receiver will be investigated and new work will be presented in order to examine the noise performance of this optical receiver and hence determine its sensitivity and the number of photons received for a specified error rate. Furthermore, the use of several different coding schemes in such links will be discussed, and hence a comprehensive comparison between these coding schemes will be performed and the appropriate coding scheme to be used in such links will be addressed.

Chapter 2 will present a literature survey of some significant topics which will form the core concepts of the investigation in designing of the model of the link. It will be divided into five sections: a review of the work of other researchers in the field of comparison between optical and microwave systems is given in the first section; the second section provides an idea of some technological studies in the domain of optical intersatellite links for the assessment of modulators for high-data- rate laser links in space, such as Semiconductor laser Intersatellite Link Experiment (SILEX) and Optical Inter-Orbit Communications Engineering Test Satellite (OICETS); a detailed literature reviews of a photodetector, which is the first and most important element of the receiver, and the types of photodiode will be comprehensively discussed throughout the third section; a basic discussion of optical amplifiers in general and Semiconductor Optical Amplifier (SOA) in particular, and also Mach Zehnder interferometer device as an external modulator of the continuous wave (CW) laser source will be studied within the fourth section in term of types and applications; a detailed and fundamental discussion of several different coding schemes for use in optical intersatellite links in space such as: Multiple Pulse Position Modulation (MPPM), Digital Pulse Position Modulation (DPPM), and Dicode Pulse Position Modulation (Dicode PPM), will be presented within the fifth section.

Chapter 3 will give a detailed information and in-depth analysis for two types of sources which are in use at present: Semiconductor Laser Diodes (SLDs) and Light Emitting Diodes (LEDs). This, in turn, will help select the appropriate emission wavelength and the suitable semiconductor material of the laser source to be used in free space links and speed of 1 Gbit/s. This information will represent the main goal of designing the transmitter in such links.

Chapter 4 will be concerned with the use of optically preamplified receiver for such links. It contains a comparative review with an in-depth analysis between PIN photodiode and Avalanche Photodiode (APD) which will be comprehensively presented and conducted in order to select the appropriate detector for the receiver through checking the possibility of using avalanche photodiodes (APDs) or PIN photodiodes with semiconductor optical amplifier (SOA), and to support selecting the appropriate semiconductor material that could be used in fabricating the suitable photodetector to be used in free space links and speed of 1 Gbit/s. Additionally, a computer simulation model (using MCAD) will be performed to examine the noise performance of an optical receiver and hence determine its sensitivity and the number of photons received for a specified error rate. This information will form the main goal of designing the receiver in such links.

In chapter 5, work will be presented to compare MPPM, DPPM and Dicode PPM coding schemes in terms of error weightings and coding efficiency through showing how the PCM error rate is affected by false alarm and erasure errors for MPPM, DPPM and Dicode PPM coding 3, 4, 5 and 6 bits of PCM. An original maximum likelihood sequence detector (MLSD) will be analyzed in this chapter. In addition, computer simulations models (using MCAD) will be performed to compare these three coding schemes in terms of sensitivity and bandwidth efficiency. This chapter will be concluded with a discussion of these comparisons in order to select the optimum PPM coding scheme to be used in optical intersatellite links in free space. This information forms the main target of this research.

Following a comparison of the computer-predicted results obtained for the receiver design and comparisons of coding schemes, a discussion of the results and an outline of possible future work will be given in chapters 6 and 7.

2. Literature Review

2.1 Comparison between Optical and Microwave Systems:

McCullagh and Wisely [1] performed a direct comparison of both optical free space and microwave point to point links through expressing the optical path loss equation in the traditional microwave form. They concluded that microwave radio systems can operate with much lower received power levels than optical systems due to their ability to use superheterodyne receiver techniques in which the received signal and a local oscillator are mixed to produce a much lower intermediate frequency (IF). Furthermore, the microwave systems accomplish much lower outage figures for terrestrial links, less than 0.01 % due to their capability to penetrate thick fogs that would cut off optical links. However, they also concluded that the path loss with an optical link is much lower because the shorter wavelength leads to a much larger antenna gain. In addition, optical systems have the potential of operation at Gbit/s data rates due to the almost limitless spectrum available and the high speed modulation ability of laser sources. A comparison was made between a typical optical link and the microwave equivalent. A 1.55μm, 4km, terrestrial link might have a receiving lens area of 0.03m² (i.e. 10cm diameter) and the beam diameter might be 2m at 4km. A total propagation loss of 20dB was presented by noting that the beam diameter is 20 times the lens diameter and by direct substitution in the following equation which gives the power falling on the detector from a traditional optics point of view:

$$P_r = \frac{P_t A_1}{A_b} = \frac{P_t D_1^{\,2}}{4\beta^2 d^2} \qquad (1)$$

where P_t is the power transmitted, A_b is the beam area at the detector, A_1 is the detector lens area, β is the beam divergence assumed small, D_1 is the lens diameter and d is the distance between the transmitter and the detector.

The transmit antenna gain and the receive antenna gain are expressed as follows, respectively:

$$g_t = \frac{4\pi A_t}{\lambda^2} \qquad g_r = \frac{4\pi A_r}{\lambda^2} \tag{2}$$

where A_r and A_t are the receiver and transmit antenna effective areas respectively. The effective area of a well designed antenna is typically in the range 0.55 to 0.65 of the physical aperture. Therefore, the path loss equation is expressed as follows:

$$PathLoss = g_t g_r \left(\frac{\lambda}{4\pi d}\right)^2 \tag{3}$$

where $\left(\frac{\lambda}{4\pi d}\right)^2$ is free space loss, and *d* is the distance between the receiver and transmitter which are assumed to be isotropic (omnidirectional) elements.

Table 1 demonstrates the comparison for point to point, terrestrial microwave and optical free space links in terms of path loss:

	Free Space Loss(dB)	Tx Antenna Gain(dB)	Rx Antenna Gain(dB)	Total path Loss (dB)
Microwave	136	20	20	94
Optical	210	78	112	20

Table 1. Path Loss comparison for point to point, terrestrial microwave and optical free space links [1].

Table 1 shows that optical links have a much greater free space loss than the microwave ones. However, this loss is compensated for by correspondingly greater transmitter and receiver gains. Therefore, the total path loss of optical links is much lower than microwave ones.

Turbulence destroys the spatial and temporal coherence of the beam and so coherent detection can not be used in an optical terrestrial link. Thus, it's important to use a direct detection receiver and, moreover, one with a large collecting area and correspondingly large capacitance, again due to turbulence-induced spot broadening. The need for this direct detection in the optical link results in the receiver for the optical point to point system having a poor sensitivity compared with the microwave system. In addition, such receivers will always be subjected to high levels of preamplifier noise and a typical example, suitable for use on a 4km link operating at 155Mbit/s, will have a sensitivity around -32dBm at 10^{-9} bit error rate [1]. A transmit power of +23dBm (200mW) is required for the 20dB path loss because allowance must be made for scintillation fading of 10 dB and, for an outage of 5 %, another 25dB is required to allow for fog, rain etc [1].

Coherent detection can be utilized in optical links where atmospheric turbulence is not an issue. However, since the optical receiver is ultimately limited by signal quantum noise, whereas the microwave receiver is limited by the background thermal noise, the receiver sensitivity in optical links is still much poorer than in the microwave case. The following table shows the comparison of thermal and quantum noise for microwave and optical free space links at 300K, 100MHz noise bandwidth and the signal to noise ratio used to determine the optical receiver's noise figure is 8dB:

	Frequency	Thermal Noise	Quantum Noise	Sensitivity	Rx Noise Fig
Microwave	29 GHz	-94 dBm	-117 dBm	-70 dBm	10 dB
Optical	194 THz	-214 dBm	-79 dBm	-32 dBm	39 dB

Table 2. Comparison of thermal and quantum noise for microwave and optical free space links at 300 K and 100 MHz noise bandwidth [1].

McCullagh and Wisely [1] found that the optical receiver has a much poorer noise figure than in the microwave case. Thus the terrestrial microwave receiver can operate close to its thermal noise limit whereas the free space optical receiver has to operate at power levels which are much higher than its quantum noise limit. In addition , they justify the reason behind giving great attention to the optical wireless systems for use in satellite to satellite links through computing the range of an optical system transmitting 200mW of 1.55μm radiation at 155Mbit/s across space (ie in a vacuum). The transmitter antenna gain is in this case:

$$g_t = \frac{4(\pi\omega)^2}{\lambda^2} \tag{4}$$

Therefore, transmitter antenna gain equals +113dB for a 10cm diameter transmitting telescope, modest by space standards. The receiver antenna gain is 112dB from the table 1. Additionally, a typically receiver sensitivity of -53dBm was already presented for a suitable receiver which used coherent detection without turbulence-induced phase destruction. Consequently, the total power margin, which is the difference between the transmit power and receiver sensitivity, is 76dBm. This system has resulted in the value of the free space loss that is expressed by the term $(\lambda/4\pi d)^2$ of -301dB producing a maximum range of 138,000km. In view of these figures, optical wireless systems for use in satellite to satellite links have been receiving a great deal of attention.

Ekberg [2] considered that the transmission parameter, which is dependent on the signal-to-noise ratio and amplifier bandwidth, is an appropriate basis for comparison of the microwave link and the optical link. This transmission parameter is given by:

$$R_0 = \frac{S}{N} B \tag{5}$$

For the microwave link, this parameter is expressed as follows:

$$R_0 = P_T G_T \frac{1}{4\pi R^2} A_R L \frac{B}{KTB} \tag{6}$$

where A_R is the receiver aerial area, G_T is transmitter antenna gain and L is loss factor (<1). For the optimum optical link, this parameter becomes:

$$R_0 = P_T \frac{1}{\pi R^2 \beta^2} A_R L \frac{B}{2h\nu B} \tag{7}$$

where 2β is optical beam width.

The lines shown in the following figure were derived by Ekberg [2] for various frequencies, a fixed transmission range for which these above parameters are calculated, and with up-to-date transmitter powers and optimum design taken into account at that time:

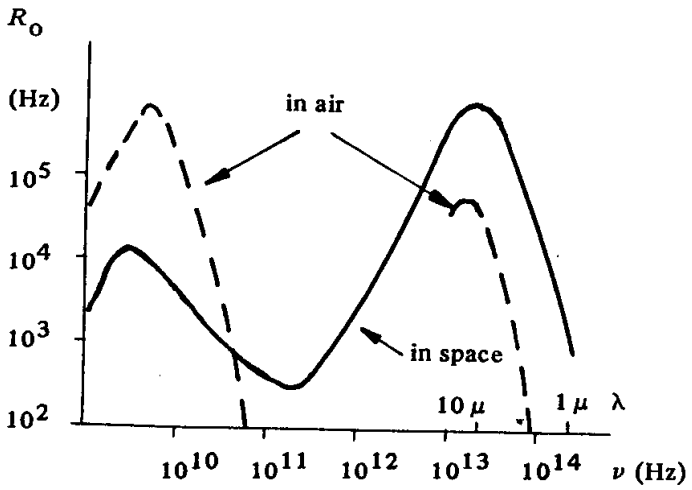

Figure 1. Transmission parameter as a function of frequency, reproduced from Ekberg [2]

Ekberg [2] deduced that as a result, the IR link is much more dependent on weather conditions than the microwave one; the microwave link emerges to be about ten times as efficient as the IR link in the atmosphere. The IR link can only compete with its microwave counterpart in applications where the transmission range is small .In such cases, full utilization can be achieved from the compactness and the simplicity of the IR link parts. In addition, he defined the optimum optical transmission system "*is obviously a system in which a transmitted coherent beam is received coherently by means of a powerful coherent local light source (oscillator), or non-coherently by means of an appropriate avalanche photodiode. Coherent reception is used when the efficient coherent area of the received beam is sufficiently large, and non-coherent reception when the spatial coherence of the received beam is too much disturbed*". Moreover, he demonstrated that the optical link is superior to the microwave one in space because large microwave antennas can't be used in space, and

additionally there is no atmosphere to attenuate the optical beam and ruin the spatial coherence in it.

Toyoshima et al [3] predicted that optical communication systems can make a revolution in space system architectures. This is because optical communication systems have many advantages compared with RF systems: wider bandwidth; larger capacity; lower power consumption; more compact equipment; greater security against eavesdropping; and immunity from interference. However, they concluded, in a straight comparison, that RF systems offer greater maximum data rates than optical communications ones for space applications over long distances. In addition, they stated that only a few in-orbit demonstrations have been done. However, the advantages of in-orbit optical communications could be verified by experiments which should be continued and full-scale demonstrations would follow. Thus, it is essential that the suitable characteristics of such communication systems be examined and the best suited systems for various configurations of space networks be recognized.

Two optical systems and one RF system were examined by Toyoshima et al [3]. The first optical system operated at a wavelength of 0.8μm using intensity modulation (IM) and direct detection (DD) with an avalanche photodiode based on Semiconductor Intersatellite Laser Experiment (SILEX) technology - the first in-orbit inter-satellite laser communication link launched in November 2001. The second optical system used 1.5μm wavelength optical preamplifiers with on-off keying. Erbium doped fibre amplifiers (EDFAs) were applied as a booster amplifier in the transmitter and as a low-noise preamplifier in the receiver. Transmitter and receiver antenna diameters of 10cm and 1m, respectively, were assumed for both systems. The RF system parameters were derived from GEO-TAIL, the spacecraft launched in 1992 to investigate the geomagnetic tail up to 1,000,000km from the earth. It operates in the X-band frequency of 8.47GHz, with transmitting and receiving antenna diameters of 18cm and 64m, respectively. Toyoshima et al [3] highlighted that the electrical power of the signal in optical systems is proportional to the square of the received optical power and that is considered as one of fundamental characteristics of optical systems, whereas the electrical power of the signal in RF systems is proportional to the received RF power. Furthermore, the

signal-to-noise ratio of optical systems decreases more rapidly over increasing distance than with RF systems as a result of the received optical power being inversely proportional to the square of the link distance. The following figure shows the maximum accomplishable data rates for the optical and RF communication systems at a bit error ratio of 10^{-6} versus distance (R):

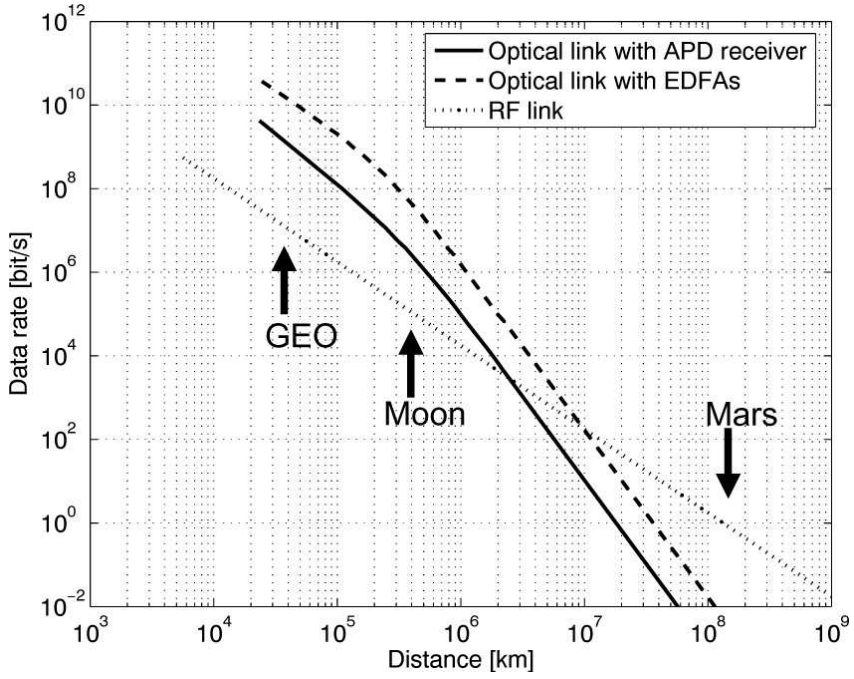

Figure 2. Maximum data rates for optical and RF communication systems versus link distance. GEO stands for geostationary earth orbit, and arrows show distances to GEO, Moon and Mars [3].

As can be seen, the data rates for the RF systems are lower than for the intensity modulation and direct detection (IM-DD) and the EDFA systems at distance less than 10^6 km. The data rate of the RF signal is always proportional to R^{-2}, in contrast to the dependence found in the optical systems, and the crossover in communication performance takes place at around 10^7 km. therefore, the RF system is preferable for the Mars-to-Earth communication link distance of around 10^8 km.

Toyoshima et al [3] deduced that optical systems are more appropriate for communicating over a relatively shorter distances in space than RF systems. In contrast, RF systems provide greater maximum data rates than optical communications systems for space applications over longer distances. Therefore, RF systems are preferable for communicating over long distances in space. However, novel technologies, such as particular modulation and coding techniques and antenna configurations, and further progress in quantum physics could open other possibilities for long-distance optical communications.

In this literature survey, McCullagh and Wisely [1], Ekberg [2] and Toyoshima et al [3] explored the competing technologies of optical and microwave systems. Generally speaking, these studies demonstrate that microwave radio systems can receive much lower power levels and operate in the atmosphere more efficiently than optical systems because they are capable of using superheterodyne receiver techniques [1]. Yet, in space, optical systems can operate with much lower path loss as the shorter wavelength leads to a much larger antenna gain [1], they are regarded as superior to microwave ones because large microwave antennas can not be used there, and there is no atmosphere to attenuate the optical beam and disrupt the spatial coherence in it [2]. Optical systems have many advantages compared with RF systems; wider bandwidth; larger capacity; lower power consumption; more compact equipment; greater security against eavesdropping; and immunity from interference [3]. In addition, they have the potential to operate at Gbit/s data rates due to the almost limitless spectrum available and the high speed modulation ability of laser sources [1]. Consequently, according to these considerations, optical links in space are receiving a great deal of attention and this work will focus on using optical intersatellite links.

2.2 Transmitter (Semiconductor Laser Diodes):

The first technological study in the domain of intersatellite optical links for the assessment of modulators for high-data- rate laser links in space was by the European Space Agency (ESA) in summer 1977. This was the beginning of a long and continued ESA involvement in space optical communications. Twenty years later, a huge number of study contracts and preparatory hardware development followed, conducted under various ESA R&D and support technology programmes. The Semiconductor laser Intersatellite Link Experiment (SILEX) laser terminals having been flight tested for integration with their host spacecraft was considered as a fundamental cornerstone as an optical link in space. Simultaneously, the European Space Agency (ESA) was preparing itself for a new challenge, which was the potential enormous use of optical cross links in satellite constellations for mobile communications and global multimedia services [4].

In summer 1977, European Space Agency (ESA) considered the use of optics for intersatellite communications when virtually there was no available component technology to support space system development. The available laser sources were rather bulky and primarily laboratory devices. ESA used the CO_2 gas laser for its first work. This laser was the most efficient and reliable laser available at that time and Europe had a considerable background in CO_2 laser technology for industrial applications. However, as a result of its weight, lifetime and operational problems, the 10μm CO_2 laser was not the winning technology for use in space [4]. Semiconductor diode lasers operating at room temperature became available by the end of 1970's, and provided a very promising transmitter source for optical intersatellite links. Therefore, ESA started the first studies to explore the potential of using this new device for intersatellite links in 1980 and simultaneously the French national space agency, CNES, started to look into a laser-diode-based optical data-relay system called Pastel. This line of development was followed and resulted in the Semiconductor laser Intersatellite Link Experiment (SILEX) pre-operational, in-orbit optical link experiment in 1985 [4].

SILEX is a free-space optical communication system that used semiconductor diode lasers and consisted of two optical communication payloads to be embarked on the ESA Advanced Relay and Technology Mission Satellite (ARTEMIS) spacecraft and on the French Earth-observation spacecraft SPOT-4. SILEX had two terminals, one on board the French Low Earth Orbit (LEO) observation satellite SPOT4 and one on ESA's Geostationary Orbit (GEO) telecommunication satellite ARTEMIS and data transmission at 50Mbit/s from LEO to GEO using GaAlAs laser-diodes and direct detection was achieved. Apart from launching ARTEMIS, Japan is participating in the SILEX programme with its own laser terminal, Laser Utilizing Communications Equipment (LUCE), to be carried onboard the Japanese Optical Inter-orbit Communications Engineering Test Satellite (OICETS). This programme launched in summer 2000 [4].

SILEX was barely considered as an attractive alternative to an RF terminal of comparable transmission capability because it’s mass of 157kg and electrical power consumption of 150W. SILEX had provided inflight testing of a pre-operational optical link in space and had stimulated the development of many new space-qualified optical, electronic and mechanical equipment items and technologies which can be considered as a basis for future optical terminals. Therefore, SILEX was a vital developmental step for Europe. In addition, its large telescope diameter (25 cm aperture) put very severe demands on the pointing, acquisition and tracking (PAT) subsystem and related components. As a result of these considerations and since an attractive Inter-Orbit Link (IOL) user terminal needs to keep mass, interface requirements to the host spacecraft and cost to a minimum, ESA embarked on a programme in January 1992 for the development and manufacturing of an elegant breadboard of a Small Optical User Terminal (SOUT). The SOUT activities were successfully completed in December 1994 demonstrating a data rate of 2 Mbit/s based on GaAlAs laser-diode technology, with a SILEX-compatible wavelength and polarization plan and with a mass of about 25 kg [4]. After the successful completion of the SOUT programme, the SOUT terminal concept was adapted by the United Kingdom for low-data-rate cross links between two communication satellites in geostationary orbit. However, the name SOUT was changed to SOTT, the first 'T' standing for 'Telecommunication' instead of 'User'. Maser-Oscillator-Power-

Amplifier (MOPA) laser diodes were used to boost the communication capacity. Matra Marconi Space (UK) has been working on the SOTT programme but directed towards new market needs requiring a 1 Gbps data rate and GEO-GEO link distances up to 83 000 km, such as in the Hughes Spaceway system [4].

As a result of the physical limits to the achievable laser power and detector sensitivity in the SILEX programme, ESA continued to examine other advanced system concepts and technologies in its search for smaller and more efficient laser terminals. Lutz [4] found that direct-detection, semiconductor laser-diode technology, as applied in SILEX, is suitable for moderate-data-rate systems which could be 1 Gbps data rate and GEO-GEO link distances up to 83 000 km as new market needs required. In addition, optical direct detection receivers using state-of-the-art Avalanche Photodiodes (APD) need about 50 photons/bit to achieve a Bit Error Rate (BER) better than 10^{-6}. Since 1989, ESA has stated strong emphasis on the development of Nd-YAG laser-based coherent laser communication systems and related hardware technologies because coherent systems based on Nd-YAG laser radiation are highly promising for high-data-rate systems and there is no fundamental limit to the achievable laser power and detector sensitivity can almost reach the theoretical quantum limit [4]. In addition, the investigation of advanced concepts such as optical amplifiers in fibre-optic and/or semiconductor technology was stimulated by the coherent Nd-YAG laser communication effort that also stimulated the possibility of synthesizing the input/output aperture of the terminal with the help of an array of smaller sub-apertures, coherently coupled together. However, ESA could not perform a full hardware implementation of such terminals because of funding difficulties, but Germany went on with this programme under the German national Solid State Laser Communications in Space (SOLACOS) programme [4].

Lutz [4] considered that, up to the early 1990's, the data-relay scenario dominated ESA's optical communication activities, but some potential future users of a data-relay service vanished and the interest in a near-term development of second-generation user terminals dropped considerably. In addition, a new class of potential users of optical intersatellite links

emerged with the intended deployment of extensive satellite networks for mobile communications and interactive multimedia services. However, based on the pervious perspective, ESA initiated internal studies in 1991 to examine probable design solutions for the compact laser terminals potentially required by such commercial satellite constellations. The Monolithic Mini Optical Terminal (MOMOT) was one of the initial results. In April 1996, a contract with an industrial team led by Oerlikon-Contraves Space (CH) was placed by ESA for the design, realization and testing of a demonstrator of a compact and lightweight optical terminal for short-range optical intersatellite links (SROIL). Lutz [4] deduced that "To be responsive to the projected market opportunities, the SROIL terminal was required to be capable of servicing the following mission classes: cross links between low-Earth-orbiting satellites in global satellite networks for mobile communication (IRIDIUM) and fixed-station data highways (Teledesic); cross links between co-located telecommunication satellites in geostationary orbit; cross links between extensively spaced geostationary satellites as proposed in ESA's On- Board Processing System or in the Spaceway system from Hughes". The model of the SROIL terminal was demonstrated by summer 1998 [4].

Lutz [4] concluded that Europe is in a leading position in the domain of space laser communications through twenty years of technology activities, sponsored by ESA and other European space agencies. Semiconductor laser Intersatellite Link Experiment (SILEX) was the most observable result of this effort as it was the world's first launch-ready civilian laser communication system. He believed that driven by this vast technological basis at hand, European industry is well ready to face the challenge of meeting the current requirements for optical intersatellite links in the emerging multimedia, Global Information Infrastructure (GII) satcom market. In addition, he considered that the question that remains is basically one of how space industry is able to adapt its practices and put the required resources into place, and found that old methods of space hardware design and qualification should be replaced by production-oriented, commercial manufacturing practices, with designed-in rather than tested-in quality and reliability.

The pre-launch optical adaptability of Optical Inter-Orbit Communications Engineering Test Satellite (OICETS) with the Advanced Relay and Technology Mission (ARTEMIS) was

confirmed by a successful optical communication experiment which was conducted by The National Space Development Agency of Japan (NASDA) for data transmission/ acquisition from September 9 to 14, 2003. This confirmation was successfully done by conducting two-way optical communications between ARTEMIS of the European Space Agency (ESA) in geostationary orbit and an optical communication equipment engineering model of OICETS, which was the same as the flight model and installed at ESA's Optical Ground Station (OGS) located in Tenerife Island of the Spanish territory's Canarias Islands in the Atlantic Ocean. The adaptability of optical equipment of two satellites was verified by the successful result of this experiment and considered as one of the significant pre-launch verification items for OICETS. In March 2003, ARTEMIS had the successful intersatellite communication experiment using microwave with NASDA’s Advanced Earth Observing Satellite II (ADEOS-II), "Midori II" [5].

Japan Aerospace Exploration Agency (JAXA) [5] identified the OICETS as a satellite to pursue orbital verification of element technologies such as acquisition, tracking and pointing technologies between ARTEMIS in geostationary orbit (GEO) and OICETS in low earth orbit (LEO) under international cooperation. They considered this optical inter-orbit communication technology is essential for future space activities in terms of large-volume communication and miniaturized on-board equipment.

The first bidirectional optical inter-orbit communication experiment in the world was successfully carried out by the JAXA and the ESA on December 9, 2005 [5]. This experiment used a laser beam, through the mechanism of Laser Utilizing Communications Equipment (LUCE), between the Optical Inter-orbit Communications Engineering Test Satellite "Kirari" (OICETS) in LEO and the Advanced Relay and Technology Mission (ARTEMIS) of the ESA in GEO.

Many advantages have been achieved by the success of this experiment through enabling different technologies such as collecting data for improving transmission speed, and for making onboard communication equipment smaller and lighter, which are fundamental for a future data relay satellite; acquisition and tracking technology for essentially on-orbit laser

beam; and obtaining technology for future international mutual operations through international cooperation with ESA. In addition, this experiment enabled optical inter-orbit communications system to be a highly advanced technology and as a method for satellites that are moving several kilometres per second in particular orbits to transmit and receive laser beams. The distance between them can be as far as 40,000 kilometres. This communication method has many advantages such as: more stable communication since laser beam, unlike radio waves, does not result in interference; onboard equipment can be smaller and lighter; higher transmission speed; and large volume data can be smoothly exchanged. Therefore, JAXA expected that Kirari's optical inter-orbit communication technology is going to be a fundamental technology for supporting various future space activities including global data acquisition by an earth observation satellite as a communication method between a low earth orbit satellite and a data relay satellite in geostationary orbit [5].

The first successful optical communication experiment in the world that connected a low earth orbit satellite and a ground station was successfully performed by the National Institute of Information and Communication Technology (NICT) and the JAXA on March 31, 2006. This experiment used laser beams between the Optical Inter-orbit Communications Engineering Test Satellite "Kirari (OICETS)" of JAXA orbiting at an altitude of about 600 km and the optical ground station of NICT in Koganei, Tokyo [5]. Moreover, a highly sophisticated technology is required by optical communications between a low earth orbit satellite like "Kirari" and a ground station. The satellite must keep sending laser beams precisely to the ground station while moving at a very high speed although the optical reception level fluctuates remarkably as a result of atmospheric attenuation and flicker. This successful experiment demonstrates the quality of Japanese technology in the area of optical inter-orbit communication equipment and accurate satellite acquisition and tracking [5].

Another successful bi-directional optical communication experiment that connected a low earth orbit satellite and a ground station was carried out for 3 minutes by the German Aerospace Center (DLR) and the JAXA on June 7, 2006. This experiment also used laser beams between the Optical Inter-orbit Communications Engineering Test Satellite "Kirari (OICETS)" of JAXA orbiting at an altitude of about 600 km and the optical ground station of

"OGS-OP" of DLR [5]. The possibility of establishing a flexible optical communication network with a satellite and a mobile optical ground station was demonstrated by this successful experiment because the DLR optical ground station is unique as it is a mobile station, and this is what distinguishes this experiment from the last one with the optical ground station of the NICT.

The "Kirari" found that to verify the performance of the optical inter-orbit communication equipment in a space environment as well as to evaluate the influence of the atmosphere and acquire statistical data, they had to continue optical inter-orbit experiments with the ARTEMIS of the European Space Agency (ESA) in addition to communication experiments with optical ground stations including NICT and German Space Agency (DLR) stations [5].

To summarize, the first significant optical intersatellite link (2000) was Semiconductor Laser Intersatellite Link Experiment by the European Space Agency using semiconductor laser diode technology [4]. The most recent project (2005) is Optical Inter-orbit Communications Engineering Test Satellite “Kirari” by Japan Aerospace Exploration Agency using Laser Utilizing Communications Equipment [5]. This enabled optical inter-orbit communications system using a semiconductor laser between satellites that are tens of thousands of kilometers apart. There were various advantages: more stable communications with less interference; lighter; more compact communications equipment; and higher data transmission rates. These tests led to new technologies that will support the development and utilization of space, including global data reception from Earth Observation satellites and continuous communication links with a manned space station. These studies show that, in general, for many applications, laser diodes have many advantages: small size; high electrical to optical efficiencies; tightly focused beam. In addition, it is possible to adapt the technology used in fibre optic links to free-space communications and so multi-Gbit/s transmission is possible using readily available integrated driver chips.

Detailed information and in-depth analysis of laser diodes will be extensively presented and conducted in the 3rd chapter of this research to select the appropriate emission wavelength

and the suitable semiconductor material of the laser source to be used in free space links and speed of 1 Gbit/s. This information will form the main goal of designing the transmitter in such links.

2.3 Receiver (Photodetector/ PIN + APD Photodiode):

An optical receiver consists of a photodetector, an amplifier, and signal-processing circuitry. The first task of an optical receiver is the conversion of the received optical energy into an electric signal, and then amplification of this signal to a large enough level so that it can be processed by the electronics following the receiver amplifier. Therefore, the main characteristics and operation of photodetector as a first element of the receiver will be discussed within this section, while the major characteristics and operation of the amplifier as a second element of the receiver will be discussed in the next section.

As mentioned, a photodetector is the first and most important element of the receiver which must be at the receiving end of an optical intersatellite link. It must sense the optical power falling upon it and convert the variation of this optical power into a varying electric current. Since the light at the end of any optical link is usually of very low intensity and generally weakened and distorted when it emerges from the end of the link, this photodetector must meet very high performance requirements. Among these requirements are a high sensitivity to the emission wavelength range of the optical source being used; a high conversion efficiency at the operating wavelength; a minimum addition of noise to the system; it must be possible to operate continuously over a wide range of temperatures for many years; and a fast response time or sufficient bandwidth to handle the desired data rate to ensure that signal distortion does not occur. Several different types of photodetectors are in existence. Among these are photomultipliers, pyroelectric detectors, and semiconductor-based photoconductors, phototransistors, and photodiodes. However, many of these detectors do not meet one or more of the foregoing requirements. At present, these requirements are met by reverse biased p-n photodiodes which are the PIN photodetector and the Avalanche Photodiode (APD).

Detailed literature reviews of these photodiodes [6, 15] will be briefly discussed throughout this section. The most important parameters that determine the characteristic and the performance of these photodiodes will be defined in order to support the selection of the

appropriate semiconductor material that could be used in fabricating a suitable photodetector in optical intersatellite link. Additionally, detailed information and in-depth analysis of photodetectors (PIN, APD) will be presented and conducted in the 4th chapter of this research to select the appropriate detector for the receiver through checking the possibility of using avalanche photodiodes (APDs) or PIN photodiodes with semiconductor optical amplifier (SOA) to be used in free space links and speed of 1 Gbit/s. This information will form the main goal of designing the receiver in such links.

As the result of the absorption of a photon of light by the semiconductor material, an electron can be excited from the valence band (VB) to the conduction band (CB) in reverse biased p-n photodiodes. This raises the material conductivity, so-called *photoconductivity,* because electron-hole pairs are generated and this leads to an increase in the diode current which can be given by:

$$I_{diode} = (I_d + I_s)(\exp[Vq/\eta kT] - 1) \qquad (8)$$

Where I_d is the dark current that is the current that arises from the flowing of the current through the bias circuit when there is no incident light on the photodiode, and I_s is the photo-generated current due to the incident optical signal.

Figure 3 shows that there are three operating regions: forward bias (region 1), reverse bias (region 2) and avalanche breakdown (region 3), through the following plot of the last equation for varying amounts of incident optical power [6]:

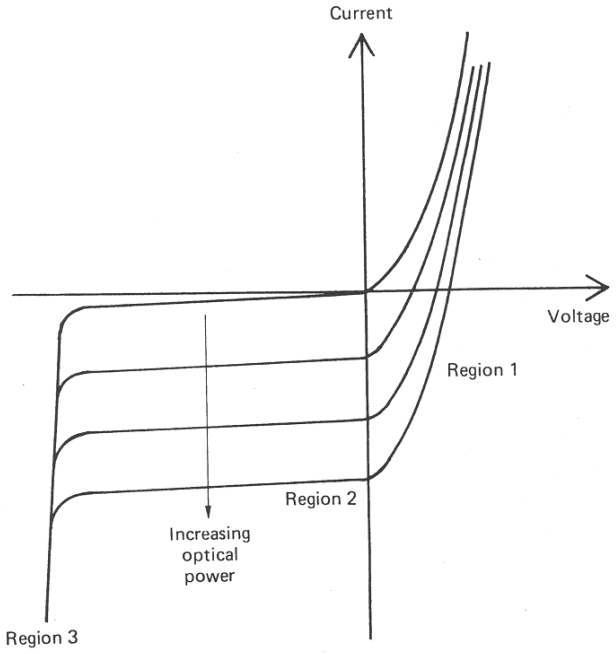

Figure 3. V-I characteristic of a photodiode, with varying amounts of incident optical power [6]

Forward bias, region (1) so-called *photovoltaic mode*, is infrequently used in optical links because the frequency response of the diode is poor. In this mode, a change in incident power is resulted by a change in terminal voltage.

Reverse bias, region (2) so-called *photoconductive mode*, is mostly used for detectors in optical links. In this mode, a proportional change in diode current is produced by a change in optical power. The exponential term in the last equation can be neglected and the reverse bias current is expressed as:

$$I_{diode} = I_d + I_s \tag{9}$$

Avalanche breakdown, region (3) so-called *avalanche photodiodes*, *APDs*, has the V-I characteristic which is very steep. Therefore, in order to prevent spontaneous breakdown, the

bias voltage has to be tightly controlled. In this region, avalanche breakdown is caused by a photo-generated electron-hole pair and results in a large diode current for a single incident photon.

The wavelength of the incident photon accepted by the photodiode is given by:

$$\lambda_0 = \frac{hc}{E_2 - E_1} \tag{10}$$

where E_1 is valence band (VB) electron energy in J, h is Planck's constant (6.624×10^{-34} Js), c is velocity of light in a vacuum ($3\times10^{8} ms^{-1}$), E_2 is the conduction band (CB) electron energy in J, and $E_2 - E_1$ is the change in energy in J. The cutoff wavelength beyond which the material becomes transparent is set by the band-gap energy of the material which is the lowest possible energy change.

The absorption coefficient, α, is a very significant parameter when considering the design of photodiodes because it is a measure of how good the material is at absorbing light of a specific wavelength and it depends strongly on the wavelength. Photon absorption can take place in either the p-type region, the depletion region, or the n-type region which can be neglected as the result of the low light intensity in this region. This results from the planar structure of most photodiodes that means the incident light must pass through the p-type region before reaching the depletion region.

As the result of the low penetration depth (1/ α) that is given by the low wavelength of the incident light, electron-hole generation can occur in the p-type region. If this carrier generation does not take place within a diffusion length of the depletion layer boundary, the diode current does not change because these carriers recombine. While if photon absorption takes place within a diffusion length of the depletion layer boundary, the diode current increases as the result of the diffusion of the electrons into the depletion region where a high electric field exists. Thus useful absorption in the p-type takes place within a diffusion length in the depletion layer.

When the photon absorption is in the depletion region, the photo-generated electron-hole pairs are separated by the electric field with electrons to the n-type, and holes to the p-type. These carriers raise the majority carrier density in these regions and so the diode current rises.

This is more efficient than absorption in the p-type, and so an efficient photodiode should have a thin p-type layer, less than a diffusion length, and a thick depletion region. Thus a PIN photodiode is preferred.

An equivalent circuit for a PIN photodiode is shown in the following diagram:

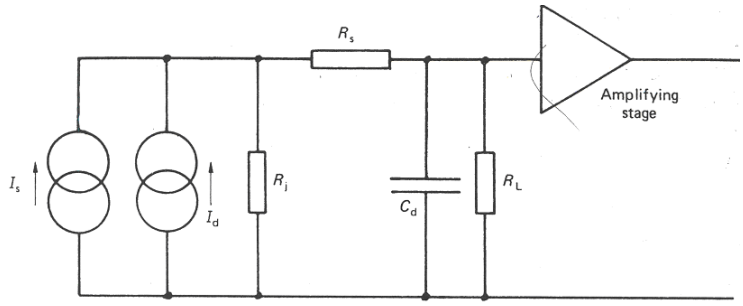

Figure 4. A circuit model for a typical photodiode [6]

Where I_s is the photoconductive current which has been represented as a current source, I_d is the constant current source represents the dark current that is the leakage current and any photoconductive current due to background radiation, R_s is series resistance of the bulk semiconductor and the contact resistance, R_i is the shunt resistance that models the slope of the reverse bias characteristic, C_d is the total diode capacitance representing the depletion and diffusion capacitances, R_L is the load resistor that shunts this capacitance and it is this time constant that usually limits the speed of response. R_i and R_s can generally be neglected, so that bandwidth of the detector is expressed as:

$$f = \frac{1}{2\pi R_L C_d} \tag{11}$$

The PIN photodetector consists of p and n regions separated by a very lightly n-doped intrinsic (i) region and sufficiently large reverse-bias voltage is applied across this device. The following schematic represents the circuit of PIN photodiode with an applied reverse bias [7]:

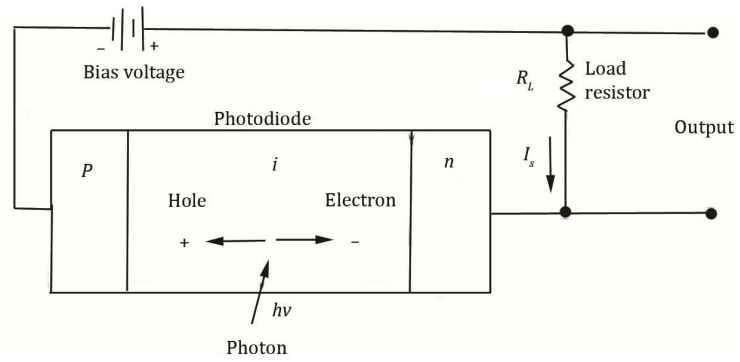

Figure 5. Schematic representation of a PIN photodiode circuit with an applied reverse bias [7]

Keiser [7] clarified that free electron-hole pairs, which are known as photocarriers, are mainly generated in the depleted intrinsic region by exciting electrons from the valence band to the conduction band when an incident photon can give up its energy which is greater than or equal to the band-gap energy of the semiconductor material. As a result of the high electric field in this depletion region where the incident light is absorbed, these carriers will be separated and collected across the reverse-biased junction and this gives rise to a current, known as the photocurrent, which flows in an external circuit. However, some electron-hole pairs will combine during their flow through the material .So, they will move a distance, which is known as diffusion length, L_n for electrons or L_p for holes and will take time to combine, which is known as carrier lifetime, τ_n for electrons and τ_p for holes to combine.

Keiser [7] found that the cutoff wavelength λ_c is identified by the band-gap energy E_g of the material and given by:

$$\lambda_c(\mu m) = \frac{h_c}{E_g} = \frac{1.24}{E_g(eV)} \quad (12)$$

He clarified that when the wavelengths is longer than λ_c , an electron does not excite from the valence band to the conduction band because the photon energy is not sufficient. Whereas, there will be very large values of the absorption coefficient $\alpha_s(\lambda)$ at the shorter wavelengths where the photons are absorbed very close to the photodetector surface and the recombination time of the generated electron-hole pairs is very short .

The primary photocurrent I_p is expressed as:

$$I_p = \frac{q}{hv} P_0 (1 - e^{-\alpha_s w})(1 - R_f) \quad (13)$$

where q is the electron charge, hv is the photon energy, R_f is a reflectivity at the entrance face of the photodiode, ω is the width of the depletion region, P_0 is the incident optical power level, $\alpha_s(\lambda)$ is the absorption coefficient.

Keiser [7] considered that the two most important characteristics of a photodetector are its quantum efficiency η which is the number of the electron-hole carrier pairs generated per incident photon of energy hv and is given by:

$$\eta = \frac{I_p / q}{P_0 / hv} \quad (14)$$

and its response speed. However, Keiser [7] clarified that a comparison must be made between these two parameters because high quantum efficiency requires that the depletion layer has to be thick to allow a large part of the incident light to be absorbed. But, the time taken for a photogenerated carrier to drift across the reverse-biased junction will be longer and this time determines the response speed of the photodiode.

Keiser [7] found that the responsivity determines the performance of a photodiode and is a function of the wavelength and of the photodiode material (since different materials have different band-gap energies); hence the responsivity drops quickly beyond the cutoff wavelength, and is given by:

$$R_0 = \frac{I_p}{P_0} = \frac{\eta q}{hv} \tag{15}$$

For Si: 0.65 A/W at 900 nm

For Ge: 0.45 A/W at 1.3 μm

For InGaAs: 0.9 A/W at 1.3 μm and 1.0 A/W at 1.55 μm.

The quantum efficiency is not a constant at all wavelengths, since it varies according to the photon energy. Consequently, the responsivity is a function of the wavelength and of the photodiode material (since different materials have different band-gap energies). For a given material, as the wavelength of the incident photon becomes longer, the photon energy becomes less than that required to excite an electron from the valence band to the conduction band. The responsivity thus falls off rapidly beyond the cutoff wavelength. The following plot compares the responsivity and quantum efficiency as a function of wavelength for pin photodiodes constructed of different materials [7]:

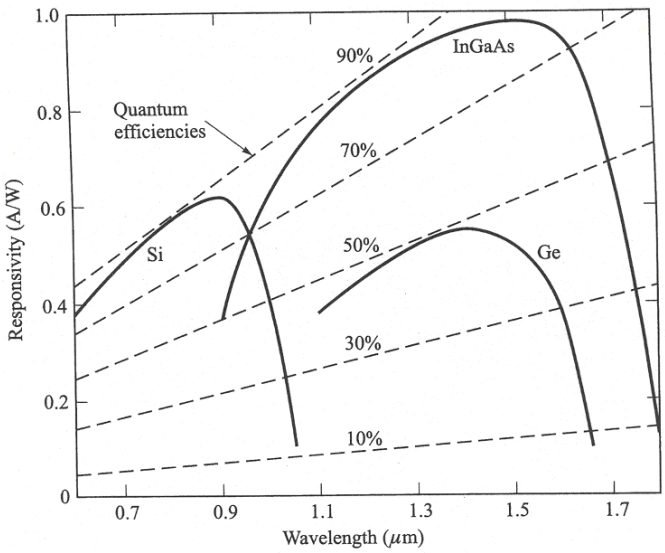

Figure 6. Comparison of the responsivity and quantum efficiency as a function of wavelength for PIN photodiodes constructed of different materials [7].

As regards avalanche photodiodes, Keiser [7] demonstrated that the receiver sensitivity rises as the result of the multiplication of the primary photocurrent before meeting the thermal noise associated with the receiver circuit. He identified the carrier multiplication mechanism by impact ionization where this carrier multiplication occurs when the photogenerated carriers pass through a very high electric field region so that photogenerated electron or hole can earn enough energy to ionize bound electrons in the valence band upon collide with them, and this high electric field also accelerates the newly created carriers .This phenomenon is the avalanche effect.

Keiser [7] also demonstrated the commonly used structure for performing carrier multiplication that is the reach-through avalanche photodiode (RAPD) which consists of p+ π p n+ where p+ and n+ are high-doped p and n type respectively and the π layer is intrinsic material but inadvertently has some p doping as the result of imperfect purification. In practical usage, light passes through the p+ region and the π material absorbs it .Thus the electron-hole pairs will be generated as the result of the given photon energy and will be separated by the electric field in the π depletion region. Consequently, carrier multiplication occurs in the high electric field presented in the p n+ junction when the photogenerated carriers pass through the π region in this junction.

The ratio $K = \beta/\alpha$ can be used to measure the photodetector performance, where α is electron ionization rates and is β hole ionization rates and the ionization rate is the average number of electron-hole pairs generated by a carrier per unit distance travelled. The multiplication M for all carriers created in the photodiode is expressed as:

$$M = \frac{I_M}{I_p} \tag{16}$$

where I_M is the average value of the total multiplied output current and I_p is the primary unmultiplied photocurrent. As not every carrier pair created in the diode undergoes the same multiplication, the avalanche mechanism has a statistical nature and M is measured as an average quantity.

In order for M to be large, there must be a large number of impact ionization collisions in the avalanche region. The probability that a carrier will generate an electron-hole pair in a unit distance is known as the ionisation coefficient. M is highly dependent on these coefficients which, in turn, depends upon the E-field and the device structure. A large M requires a low value of k. in silicon, k ranges from 0.1 to 0.01, and this leads to value of M ranging from 100 to 1000. However, in germanium and III-V materials, k ranges from 0.3 to 1 and, in practice, it is difficult to fabricate and control devices with gains above 15.

Similar to the PIN photodiode, the responsivity also determines the performance of an APD, and is given by:

$$R_{APD} = \frac{\eta q}{hv} M = R_0 M \tag{17}$$

where R_0 is the unity gain responsivity.

Since the optical signal is generally very weak, the signal-to-noise ratio S/N for the photodetector and the following amplification should be high to detect the weakest possible optical signals. This ratio is expressed as [7]:

$$\frac{S}{N} = \frac{\text{Signal power from photocurrent}}{\text{Photodetector noise power + amplifier noise power}} \tag{18}$$

The statistical nature of photon-to-electron conversion process in the photodiode causes the photodetector noise and thermal and shot noise causes the amplifier noises. It is noticeable that the quantum efficiency of the photodetector and the photodetector and amplifier noises determine the signal-to-noise ratio. Thus, when the quantum efficiency of the photodetector is high and the noises of photodetector and amplifier are low; this ratio will be high .However, due to the photodiode quantum efficiency for most applications is normally close to its maximum possible value, the noise currents determine the detected minimum optical signal and consequently the sensitivity of a photodetector which is describable in terms of the minimum detectable optical power.

Keiser [7] divided the main noises of the photodetector that have no internal gain into quantum or shot noise, bulk dark current noise, and leakage current noise. The statistical nature of photon-to-electron conversion processes, which is the production and collection of photoelectrons, follows a Poisson process, resulting in the quantum or shot noise:

$$\left\langle i_Q{}^2 \right\rangle = \sigma_Q{}^2 = 2qI_p BM^2 F(M) \qquad (19)$$

where *B* is bandwidth, I_p is the average value of photocurrent, and $F(M)$ is a noise figure associated with the random nature of the avalanche process.

The photodiode dark current, which is composed of bulk and surface current (leakage current), arises from the flowing of the current through the bias circuit when there is no incident light on the photodiode. The thermally created electrons or/and holes in the p n junction causes the bulk dark current. These thermally created carriers will be multiplied by the avalanche mechanism after they are also accelerated by the high electric field existed at the p n junction. The mean-square value of this current is expressed as:

$$\left\langle i_{DB}{}^2 \right\rangle = \sigma_{DB}{}^2 = 2qI_D BM^2 F(M) \qquad (20)$$

where I_D is the primary unmultiplied detector bulk dark current. The following figure shows a comparison of typical dark currents for Si, Ge, GaAs, and InGaAs photodiodes as a function of normalized bias voltage [7]:

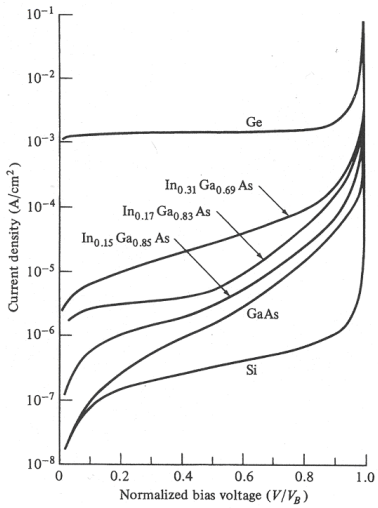

Figure 7. A comparison of typical dark currents for Si, Ge, GaAs, and InGaAs photodiodes as a function of normalized bias voltage [7]

The surface leakage current depends on surface area, bias voltage, and surface defects. It can be decreased by using the guard ring structure and its mean-square value is given by:

$$\left\langle i_{DS}{}^2 \right\rangle = \sigma_{DS}{}^2 = 2qI_L B \tag{21}$$

where I_L is the surface leakage current, and it is noticeable that the avalanche multiplication gain does not affect this current because it has bulk effect.

The total mean-square photodetector noise current is expressed as:

$$\left\langle i_N{}^2 \right\rangle = \sigma_N{}^2 = \left\langle i_Q{}^2 \right\rangle + \left\langle i_{DB}{}^2 \right\rangle + \left\langle i_{DS}{}^2 \right\rangle = \sigma_Q{}^2 + \sigma_{DB}{}^2 + \sigma_{DS}{}^2 = 2q(I_p + I_D)M^2F(M)B + 2qI_LB \tag{22}$$

It is assumed that the photodetector load resistor is much smaller than the amplifier input impedance. Therefore its thermal noise is much greater than that of the amplifier input. The mean-square thermal (Johnson) noise current of load resistor is given by:

$$\left\langle i_T{}^2 \right\rangle = \sigma_T{}^2 = \frac{4K_BT}{R_L} B \tag{23}$$

where K_B is Boltzmann's constant, and T is the absolute temperature. Using a large load resistor decreases this noise, but this load resistor should be consistent with the receiver bandwidth requirements.

Consequently, the signal-to-noise ratio at the input of the amplifier is expressed as:

$$\frac{S}{N} = \frac{\left\langle i_P{}^2 \right\rangle M^2}{2q(I_P + I_D)M^2F(M)B + 2qI_LB + 4K_BTB/R_L} \tag{24}$$

With avalanche photodiodes, the photodetector noise normally dominates and the thermal noise is of lesser importance. Whereas, the thermal noise of the detector load resistor and the active elements of the amplifier circuitry will be dominated when the PIN photodiodes are used [7].

It can be seen that the signal power is multiplied by M^2 and the quantum noise plus bulk dark current is multiplied by $M^2 F(M)$. The surface leakage current is not altered by the avalanche gain mechanism. Since the noise figure $F(M)$ increases with M ; there always exists an optimum value of M that maximizes the signal-to-noise ratio.

The excess noise factor can be approximated by:

$$F = M^x \tag{25}$$

X takes value of 0.3 for Si, 0.7 for InGaAs, and 1.0 for Ge avalanche photodiodes.

To keep the excess noise factor at a minimum, it is desirable to have small values of effective ionization rate ratio k_{eff} . The effective ionization rate ratio k_{eff} varies between 0.015 and 0.035 for silicon, between 0.6 and 1.0 for germanium. Figure 8 shows the superiority of silicon over other material for making avalanche photodiodes [7]:

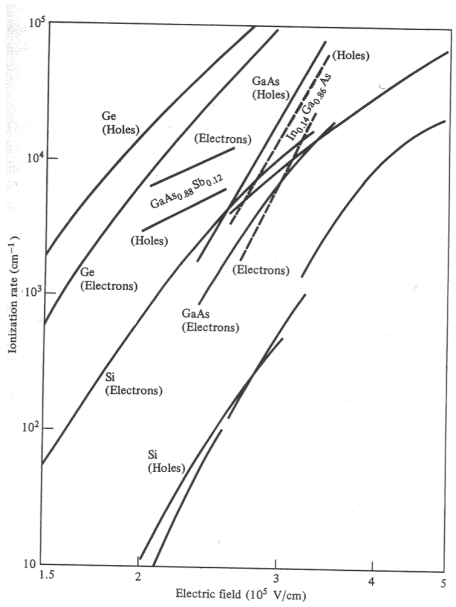

Figure 8. Carrier ionization rates obtained experimentally for silicon, germanium, gallium arsenide, gallium arsenide antimonide, and indium gallium arsenide [7].

The gain mechanism of an avalanche photodiode is very temperature-sensitive because of the temperature dependence of the electron and hole ionization rates. This temperature dependence is particularly critical at high bias voltages, where small changes in temperature can cause large variations in gain. For example, if the operating temperature decreases and the applied bias voltage is kept constant, the ionization rates for electrons and holes will increase and so will the avalanche gain. Figure 9 shows how the gain mechanism of a silicon avalanche photodiode depends on temperature [7]:

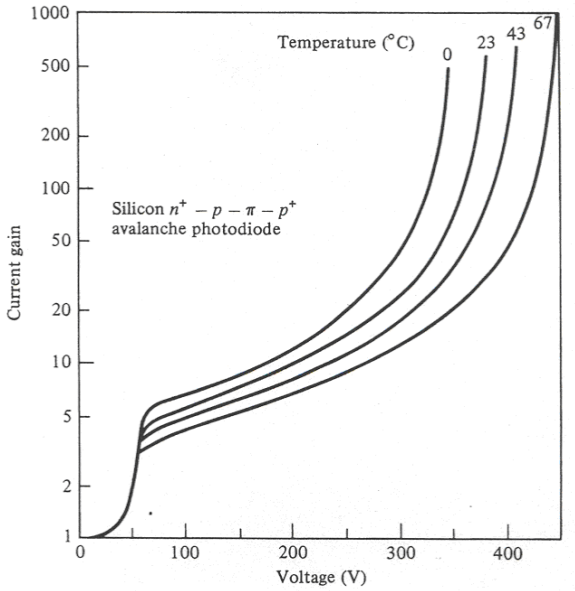

Figure 9. Example of how the gain mechanism of a silicon avalanche photodiode depends on temperature. The measurements for this device were performed at 825 nm [7].

To maintain a constant gain as the temperature changes, the electric field in the multiplying region of the p n junction must also be changed. This requires that the receiver incorporate a compensation circuit which adjusts the applied bias voltage on the photodetector when the temperature changes.

Yariv [8] concluded that avalanche photodiodes are analogous to normal photodiodes in their construction excluding a particular care has to made to achieve very uniform junctions for avalanche photodiodes as a result of the steep dependence of M on the applied field in the avalanche region. Corresponding to normal photodiode, the frequency response, which is the ability of the diode to respond to variations in the incident intensity such as those caused by

high-frequency modulation, of the avalanche photodiode is limited by the three following main mechanisms: the effect of the finite transit time of the carriers drifting across the depletion layer; the effect of the finite diffusion time of carriers created in the p and n regions which can be reduced by an appropriate choice of the length of the depletion layer; and the shunting effect of the signal current by the junction capacitance.

Brain & Smith [9] considered that using avalanche gain to raise the signal power relative to the noise of the preamplifier is the potential advantage of using an APD in an optical receiver. But, the generation of excess noise is presented in the avalanche process where how much this excess noise is created determines the possibility of an APD to compensate the noise of the preamplifier.

Brain & Smith [9] summarised the requirements for an APD receiver which are : a minimum level of shot noise due to the multiplied bulk leakage current which has to be produced at the highest operating temperature for the receiver before the reduction of any other noise source becomes worthwhile; either decreasing the effective ratio of ionisation rates or decreasing the preamplifier noise could produce further improvement in performance , but either would require further reduction in the bulk leakage current to be worthwhile.

McIntyre [12] found that the semiconductor p-n junctions have been used as high-gain photodiodes when they have more or less uniform avalanche multiplication characteristics over significant parts of their areas. These high-gain photodiodes present significant advantages over normal photodiodes in wide-band applications where these photodiodes will produce an improved signal-to-noise ratio, which is defined by thermal or amplifier noise and not by the shot noise in the diode current, provided that the noise created in the multiplication process does not become extreme, and present gain through the mechanism of impact ionization.

McIntyre [13] concluded that there are a number of significant applications in which avalanche photodiodes can be excellent light detectors at very low light levels. These applications, in which it is necessary to use quite different detection techniques, can be classified into two classes:

Photon-Counting Applications: in this class, photons with detection probabilities comparable to the best available photomultipliers (especially in the near infrared) and with excessively low dark-current rates can be detected while the detection of every photon incident on the detector, as it is desirable, is not possible. The detection mode of photon counting is considered as the most desirable for some low light level applications such that if the flux from the source is very weak, or, in the case of a pulsed laser signal, if the intensity is sufficiently low that it is unlikely for there to be more than a few photons per pulse. Under these conditions, it is not feasible to discriminate against background (by discriminating against single-photon-induced events) as a result of the desired signal would also be discriminated against. In these applications, it can be operated below the breakdown voltage provided the dark current is sufficiently low where it is practical to operate well above the breakdown voltage in a “Geiger-tube” mode. Once the avalanche is started, the current will raise until limited by the diode resistance or the external circuit provided a quenching circuit is presented which decreases the voltage temporarily below the breakdown voltage, the diode can be made ready to receive another photon.

Laser Pulse Detection Applications: in this class, discriminating against single-photon-induced events (background) is desirable and simultaneously detecting a package of photons within time duration of a laser pulse with a high detection probability. It can be noted that the avalanche photodiode compares favorably, under the suitable conditions, with the best available photomultipliers. Since laser pulses consist of more than a few photons, its detection is quite different. The desirable goal now is the detection of all pulses, with as high a probability as possible, which arise from more than one photoelectron, while simultaneously discriminating against single-photoelectron-induced pluses, which are as a result of either dark current (thermally excited electrons) or background radiation (assumed low enough so

that the arrival of more than one photon with the resolving time of the detection system is unlikely).

As a conclusion, a photodetector at the receiver is needed to convert the modulated light signal back into an electrical one. There are two types of detector in use at present: avalanche photodiodes (APDs) or PIN photodiodes [6, 7]. The optimum choice depends on the wavelength of operation which, in turn, depends on how the laser source is to be modulated. In optical fibre communications it is common practice to modulate a continuous wave (CW) laser with an external Mach- Zehnder interferometer. As these devices operate at a wavelength of 1.55 μm, this must be the wavelength of operation for the link.

2.4 Semiconductor Optical Amplifier (SOA):

When setting up an optical link in traditional method, a power budget is formulated and repeaters are added in case the available power margin is exceeded by the path loss. An optical signal can be amplified with a conventional repeater by performing photon-to-electron conversion, electrical amplification, retiming, pulse shaping, and then electron-to-photon conversion. Despite the fact that this operates well for moderate-speed single-wavelength operation, a few obstructions might affect the adoption of this process in terms of complexity and high installation-cost for high-speed multi-wavelength systems. Therefore, huge effort has been carried out to develop all-optical amplifiers. These devices are used to compensate for the signal-splitting losses in multi-access networks and to amplify the optical signal in long-distance point-to-point optical fibre links. Moreover, optical amplifiers involve various features which have resulted in diversification of applications with different design challenges for each application. The general applications of optical amplifiers are: In-line optical amplifiers; preamplifier; power amplifier. Basic information of optical amplifiers in general and Semiconductor Optical Amplifier (SOA) in particular will be discussed within this section in term of types and applications. However, more detail of SOAs and the most important parameters that determine the performance of these SOAs will be extensively presented and conducted in chapter 4.

Keiser [7] classified the two fundamental types of optical amplifier as semiconductor optical amplifiers (SOAs) and active-fibre or doped-fibre amplifiers (DFAs). The power level of incident light is increased in all optical amplifiers through a stimulated emission process which, in turn, can be produced by generating a population inversion. The same mechanism which is used in laser diodes to produce the population inversion needed for stimulated emission is used in optical amplifiers. Despite the fact that optical amplifiers have a similar structure to that of a laser, they do not have the optical feedback mechanism that is necessary for lasing to occur. Thus an optical amplifier can boost incoming signal levels, but it can not produce a coherent optical output by itself [7].

Keiser [7] compared the two types of optical amplifiers, semiconductor optical amplifiers (SOAs) and the active-fibre or doped-fibre amplifiers (DFAs). He found that semiconductor optical amplifiers consume less power, have fewer components, and are more compact than active-fibre or doped-fibre amplifiers (DFAs). He justified the attractiveness of SOAs through their possibility of working in both the 1300-nm and the 1550-nm low-attenuation windows and can be easily integrated on the same substrate as other optical devices and circuits such as couplers, optical isolators, and receiver circuits. In addition, the SOAs have a more rapid gain response, which is on the order of 1ps to 0.1ns. This leads to both limitations and advantages. The limitation is that the rapid carrier response results in the gain at a particular wavelength to fluctuate with the signal rate for bit rates up to several Gb/s. Consequently, the overall gain is affected and thus the signal gain at other wavelengths also fluctuates which, in turn, produces crosstalk effects when a broad spectrum of wavelengths has to be amplified. The advantage of SOAs is that they can be used when both switching and signal processing are called for in optical networks [7]. In contrast to SOAs, DFAs are immune from interference effects, such as crosstalk and intermodulation distortion, between different optical channels within a broad spectrum of wavelengths that are injected simultaneously into the amplifier. This is because DFAs are highly transparent to signal format and bit rate, as they display slow gain dynamics, with carrier lifetime on the order of 0.1-10 ms. consequently, the gain responses of DFAs are fundamentally constant for signal modulations greater than a few kilohertz [7].

Keiser [7] classified the two main types of SOAs as the resonant, Fabry-Perot amplifier (FPA) and the nonresonant, travelling-wave amplifier (TWA). In an FPA, a Fabry-Perot cavity is formed by the two cleaved facets of a semiconductor crystal which perform as partially reflective end mirrors and have a natural reflectivity of approximately 32 percent. When an optical signal enters the FPA, it reflects back and forth between the mirrors until it is amplified and emitted at a higher intensity. Despite the fact that FPAs are easy to fabricate, very careful stabilization of temperature and injection current are required due to the optical signal gain being very sensitive to variations in amplifier temperature and input optical frequency [7]. However, in a TWA, the input light gets amplified only once during a single pass through the

TWA because its structure is the same as that of an FPA except that the end facets are either antireflection-coated or cleaved at an angle, so that internal reflection does not occur.

Keiser [7] compared TWAs and FPAs and found that TWAs have a large optical bandwidth, high saturation power, and low polarization sensitivity. Therefore, TWAs have been used more extensively than FPAs. In addition, he concluded that TWAs have become the SOA of choice for networking applications and are particularly used as amplifiers in the 1300-nm window and as wavelength converters in the 1550-nm region. The 3-dB bandwidth of TWAs is about three orders of magnitude greater than that of FPAs. The pumping method used to generate the population inversion is an external current injection.

Keiser [7] considered that the signal gain or amplifier gain G is one of the most important parameters of an optical amplifier and is defined as:

$$G = \frac{P_{s,out}}{P_{s,in}} \tag{26}$$

where $P_{s,in}$ and $P_{s,out}$ are the input and output powers, respectively, of the optical signal being amplified.

The single-pass gain in the active medium of the SOA is:

$$G = \exp[\Gamma(g_m - \bar{\alpha})L] \equiv \exp[g(z)L] \tag{27}$$

Where Γ is the optical confinement factor in the cavity, g_m is the material gain coefficient, $\bar{\alpha}$ is the effective absorption coefficient of the material in the optical path, L is the amplifier length, and $g(z)$ is the overall gain per unit length. This equation shows that the gain rises with device length. However, the carrier density in the gain region of the amplifier depends on

the optical input intensity. This means the internal gain is limited by gain saturation. Excited carriers (electron-hole pairs) are depleted from the active region because the input signal level is raised. Because there are not enough excited carriers to keep stimulated emission, further increases in the input signal level no longer yield an appreciable change in the output level when there is a sufficiently large optical input power. Thus, it can be noted that the carrier density at any point z in the amplifying cavity depends on the signal level Ps(z) at that point. . In particular, near the input where z is small, incremental portions of the device may not have reached saturation simultaneously as the sections further down the device, where incremental portions may be saturated due to higher values of Ps(z) [7].

Semiconductor optical amplifiers (SOAs) can be indentified as essentially laser diodes without end mirrors, which have fibre attached to both ends. They amplify any optical signal that comes from either fibre and transmit an amplified version of the signal out of the second fibre. SOAs are typically constructed in a small package, and they work for 1310 nm and 1550 nm systems. In addition, they transmit bidirectionally, making the reduced size of the device an advantage over regenerators using EDFAs. However, the drawbacks to SOAs include polarization dependence, a higher noise figure, and high-coupling ratio/loss that is the ratio/loss of optical power from one output port to the total output power and is expressed as a percent. As mentioned before, optical amplifiers, in general, and SOAs, in particular, have a great deal of attention in modern optical networks because they have the features that led to many diverse applications, each having different design challenges.

The most important and widespread of these applications in modern optical networks are:

Power Boosters: Many tunable laser designs output low optical power levels and must be immediately followed by an optical amplifier. (A power booster can use either a SOA or EDFA).

In-Line Amplifier: Allows signals to be amplified within the signal path.

Wavelength Conversion: Involves changing the wavelength of an optical signal.

Receiver Preamplifier: SOAs can be placed in front of detectors to enhance sensitivity.

As a conclusion, there is currently much interest in all optical amplification for applications in a signal regeneration and receiver preamplification. For the majority of modern optical networks, the Semiconductor Optical Amplifier (SOA) is a highly versatile component that can be deployed for a wide range of amplification and routing functions within the telecommunications industry. The minimal space requirements, integration capability, and strong potential for cost reduction through scaled manufacturing processes will ensure that the SOA plays an increasingly important role in future advanced optical networks. SOAs are a cost-effective solution to implementing optical amplification in advanced optical networking subsystems for core, metro, and ultimately access applications.

2.5 Mach-Zehnder Interferometer (MZI):

Optical transmission systems are generally based on one of two methods of modulation of a signal laser, either direct or external modulation. In the first of these, the bias current to the laser is modulated, turning the laser on and off. The disadvantage of this when applied to high capacity systems is that the semiconductor material dynamic behaviour introduces frequency distortion into the laser output, known as chirp. External modulation of the continuous wave (CW) source produces a modulated output signal with significantly reduced chirp, and sources of this type are preferred for use in high capacity systems. High speed electro-optic modulators such as Mach Zehnder interferometer devices are typically used.

Modulation is the process of imposing information on a light stream and it can be achieved either by directly varying the laser drive current with the information stream and thus a varying optical output power is produced, or by using an external modulator and thus a steady optical power level emitted by the laser is modified. For high-speed systems (> 2.5 Gb/s), external modulation is needed to minimize undesirable nonlinear effects such a chirping. A variety of external modulators are commercially available, either as a separate device or as an integral part of the laser transmitter package. The spontaneous and stimulated carrier lifetimes and the photon lifetime determine the fundamental limitation on the direct modulation rate of laser diodes.

External modulators can be classified as waveguide devices for use in optical fibre links, and bulk modulators for use in high power free-space links. At present, practically all waveguide modulators are made using lithium niobate. The refractive index varies according to the strength of an externally applied electric field, the so-called electro-optic effect, is one characteristic of a lithium niobate, *LiNbO3*, on which a single-mode waveguide coupler fabricated. This effect can be exploited to create phase and intensity modulators. The following figure shows the Mach-Zehnder interferometer [6]:

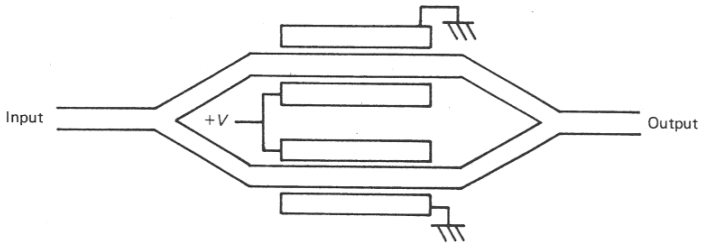

Figure 10. A Mach-Zehnder interferometer [6]

In this device, the input power is split equally between the two arms of the device by a Y-junction waveguide. The relative phases of the fields are altered by phase modulators, which are placed in the two arms, before recombination in another Y junction. The fields will add and light will appear at the output when the phase difference between the two paths is 2Nπ radians, where N is an integer. However, the waves will cancel each other out and the output will be zero when the phase difference is (2N+1) π radians [6]. The output power is simply given by:

$$P_{out} = P_{in} \cos^2(\frac{\Delta\phi}{2}) \qquad (28)$$

where $\Delta\phi$ is the phase difference between the two branches. The following figure shows the measured transmission/drive voltage characteristic of a typical Mach-Zehnder modulator [6]:

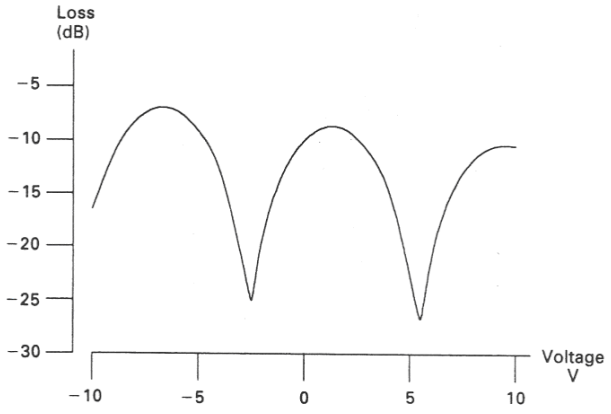

Figure 11. Measured transfer function of a Mach-Zehnder interferometer [6]

Mach-Zehnder modulators are of great use when a laser has to be modulated at high speed with the laser being operated continuously. Such a technique is extensively used at present. In addition, since the optical power density in a single-mode waveguide modulator would be

excessively high, and could result in damage to the device, bulk modulators must be used to modulate the light output of a high power laser - the power density will be lower and thus modulator damage is less likely to occur when a wide output beam is existed. Bulk modulators can be classified into two groups: those that use the electro-optic effect, and those that use the acousto-optic effect [6].

As a conclusion, the two methods of modulation of a signal laser in optical transmission systems can be classified as direct modulation and external modulation. External modulation of the continuous wave (CW) source, such as solid-state and gas lasers, is preferred for high capacity systems due to its modulated output signal with considerably reduces chirp. The high speed electrode-optic modulator such as Mach Zehnder interferometer device is considered as the most suitable external modulator to be used in optical intersatellite links.

2.6 Pulse Position Modulation Coding Schemes:

Various pulse position modulation (PPM) schemes have been proposed in the past for use in optical communications links. Despite the fact that these coding schemes operate with higher data rates than their pulse code modulation (PCM) counterparts, they do offer a better sensitivity. They can be used as a means of utilizing the bandwidth available in optical fibre links. A review of these pulse positions modulation coding schemes has been carried out. Detailed and fundamental information of several different coding schemes for use in optical intersatellite links in space such as: Multiple Pulse Position Modulation (MPPM); Digital Pulse Position Modulation (DPPM); Dicode Pulse Position Modulation (Dicode PPM), will be discussed within this section .Further in-depth analysis will be extensively presented and conducted in the 5th chapter of this research to make a thorough comparison between these coding schemes for optimum use in such links. This information will form the main target of this research.

The coding scheme currently popular is Digital Pulse Position Modulation (digital PPM). Digital PPM is an early form of signal modulation in which n bits of PCM are encoded by transmitting a single pulse in one of 2^n possible time slots. This is repeated every T seconds, such that the transmitted bit rate is *n*/T bits per second. In addition, a guard interval, which is composed of a certain number of empty time slots, is sometimes located at the end of the frame to minimize the impacts of inter-symbol interference (ISI) and inter-frame interference (IFI) resulted from pulse dispersion in optical fibre. This scheme gives an increase of between 5-11dB in receiver sensitivity in comparison with standard PCM. However, the bandwidth expansion results in an increased line rate such that the final data rate can be 10.7 times that of the original PCM if six bits are encoded into 64 data slots with no guard bits. This bandwidth expansion leads to significant demands on the processing electronics and thus the technique has limited appeal [16]. Many alternative coding schemes have been suggested that operate with a smaller bandwidth expansion such as differential PPM [17, 18], overlapping PPM [19], dicode PPM [20-22] and multiple PPM [23-27]. The most bandwidth-effective of these are dicode PPM and multiple PPM as they appear to offer the lowest bandwidth expansion [16].

Multiple PPM can provide the sensitivity of digital PPM without the large bandwidth expansion. For instance, the (12/2) multiple PPM scheme, where 6 bits of PCM can be converted into two data pulses used in 12 slot-frame, has a line rate that is twice that of the PCM. The (15/4) multiple PPM scheme can convert 10 bits of PCM into 4 data pulses used in 15 slot-frame and achieve line rate of 1.5 times the PCM rate [16]. Both schemes give sensitivities comparable to that of digital PPM.

Atkin and Fung [24] concluded that the predicted performance of a multiple PPM system with Reed Solomon (RS) coding using avalanche photodiodes (APD) was 0.1 nats/photon for an error rate of 1 in 10^9 bits, while an equivalent RS coded, digital PPM system required 0.03 nats/photon. Sugiyama and Nosu [23] analyzed the error performance of multiple PPM with maximum likelihood sequence detection (MLSD) scheme and found that multiple PPM is more efficient than digital PPM in terms of power and bandwidth utilization. The best predicted sensitivity was 0.58 bits/photon compared to 0.5 bits/photon for digital PPM (both operating with an error rate of 1 in 10^9). A power and bandwidth requirement comparison was made by Park and Barry [25] between digital PPM, overlapping PPM and multiple PPM. It was confirmed that multiple PPM is the most power and bandwidth-efficient of the three. Park and Barry [26] compared digital PPM, overlapping PPM and multiple PPM in terms of sensitivity and bandwidth efficiency and showed that an 8-level digital PPM system requires 4.4 dB less power than a (4/2) multiple PPM system when the channel bandwidth is high and MLSD is used in both cases. The increase is 2 dB for low channel bandwidth. In their paper [27], they concluded that multiple PPM provided a sensitivity advantage of less than 1 dB when compared with 8-level PPM.

Multiple PPM uses two or more pulses in a frame with the pulse positions being determined by the original PCM word, whereas dicode PPM only transmits a pulse when there is a transition between levels. Therefore, the timing diagram in the following figure shows examples of the MPPM, DPPM and Dicode PPM signals.

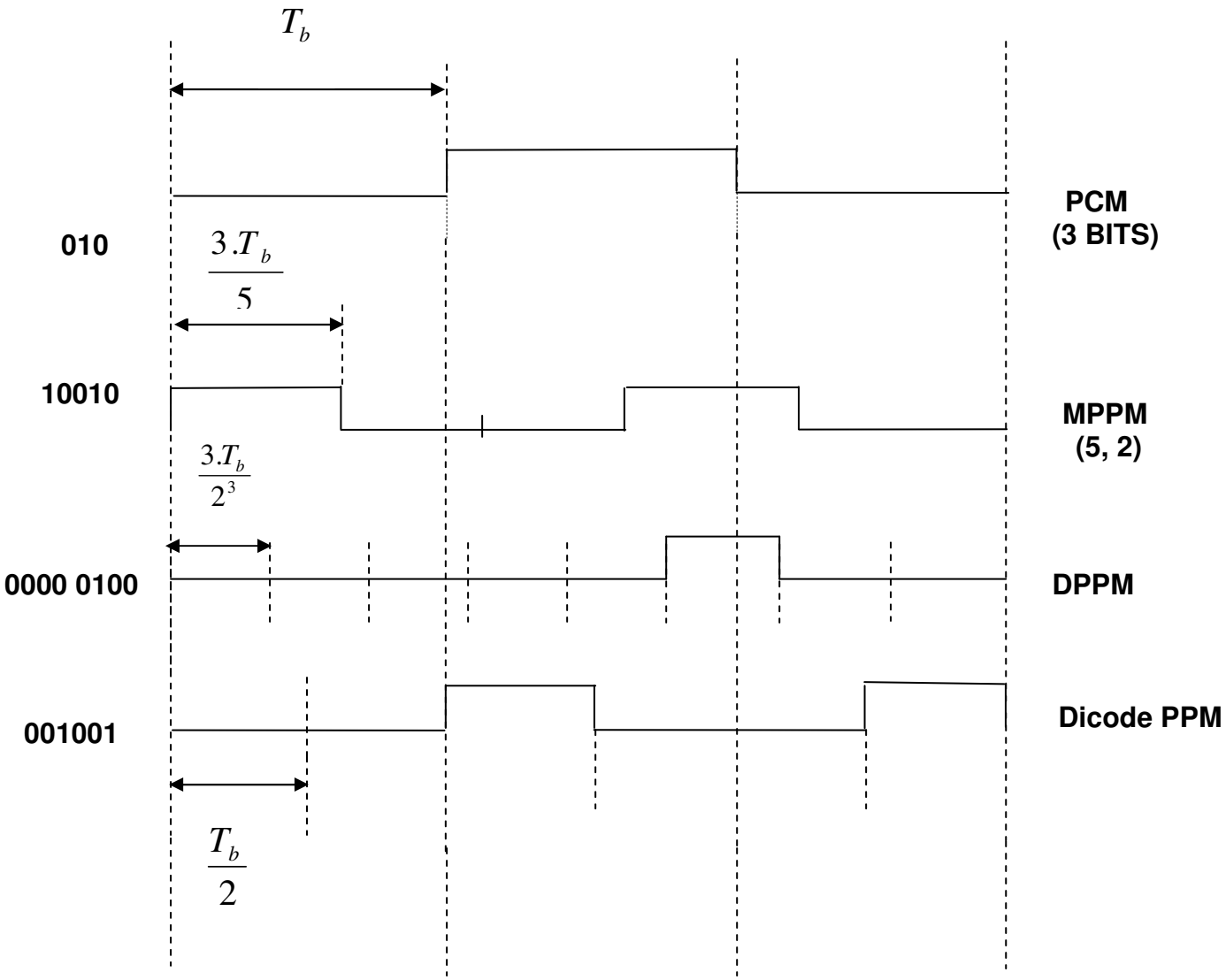

Figure 12. Examples of timing diagram for the MPPM, DPPM and Dicode PPM signals with the time slot width (T_s) for each scheme

The coding alphabet for digital PPM and multiple PPM for 3 and 4 bits of PCM is shown in tables 3, 4, respectively:

PCM (3 Bits)	DPPM	MPPM (5,2)
000	0000 0001	11000 (1,2)
001	0000 0010	10100 (1,3)
010	0000 0100	10010 (1,4)
011	0000 1000	10001 (1,5)
100	0001 0000	01100 (2,3)
101	0010 0000	01010 (2,4)
110	0100 0000	01001 (2,5)
111	1000 0000	00110 (3,4)

Table 3. Alphabet for coding 3 bits of PCM into digital PPM and multiple PPM

As regards the coding alphabet, digital PPM codes *n* bits of PCM into a single pulse which occupies one of 2^n time slots. So, table 3 shows digital PPM in which a single pulse occupies one of 8 time slots to code 3 bits of PCM. However, the multiple PPM scheme uses a number of pulses in a frame, with the pulse positions being determined by the original PCM word. Table 3 shows (5, 2) multiple PPM in which a 5-slot frame uses two data pulses to code 3 bits of PCM.

PCM (4 Bits)	DPPM	MPPM (7,2)
0000	0000 0000 0000 0001	1100000 (1,2)
0001	0000 0000 0000 0010	1010000 (1,3)
0010	0000 0000 0000 0100	1001000 (1,4)
0011	0000 0000 0000 1000	1000100 (1,5)
0100	0000 0000 0001 0000	1000010 (1,6)
0101	0000 0000 0010 0000	1000001 (1,7)
0110	0000 0000 0100 0000	0110000 (2,3)
0111	0000 0000 1000 0000	0101000 (2,4)
1000	0000 0001 0000 0000	0100100 (2,5)
1001	0000 0010 0000 0000	0100010 (2,6)
1010	0000 0100 0000 0000	0100001 (2,7)
1011	0000 1000 0000 0000	0011000 (3,4)
1100	0001 0000 0000 0000	0010100 (3,5)
1101	0010 0000 0000 0000	0010010 (3,6)
1110	0100 0000 0000 0000	0010001 (3,7)
1111	1000 0000 0000 0000	0001100 (4,5)

Table 4. Alphabet for coding 4 bits of PCM into digital PPM and multiple PPM

Table 4 shows digital PPM in which a single pulse occupies one of 16 time slots to code 4 bits of PCM and (7, 2) multiple PPM in which a 7-slot frame uses two data pulses to code 4 bits of PCM.

As regards the signaling format of dicode PPM, only data transitions are sent and no signal is transmitted when the data is constant. Data transitions from logic zero to logic one are coded as +V and transitions from logic one to logic zero are coded as –V. If there is no change in the PCM signal, a zero signal is transmitted. The positive pulse can be regarded as setting the data to logic one (pulse SET), whereas the negative pulse resets the data to logic zero (pulse

RESET) (as can be seen in figure 12). These SET and RESET signals are converted into two pulse positions in a data frame. Therefore, a pulse is generated in slot S by PCM transition from zero to one and a pulse is produced in slot R by one to zero PCM transition. In addition, there is no transmitted signal when the PCM data is constant [20].

As a conclusion, Digital PPM is the preferred coding scheme for use in optical inter-satellite links because it operates with very low average power and offers high sensitivity. However, it does suffer from a very large bandwidth expansion problem in that a scheme coding 5 bits of PCM will have a final line rate of 6.4 times the original PCM rate [16].This places a great strain on the processing electronics as the speed can be prohibitive. Many alternative coding schemes have been suggested that operate with a smaller bandwidth expansion such as differential PPM overlapping PPM, dicode PPM and multiple PPM. The most bandwidth-effective of these are dicode PPM and multiple PPM. Digital PPM and these two alternative coding schemes have been examined in this section. In addition, an in-depth analysis and comprehensive comparison between these three coding schemes in terms of sensitivity, bandwidth efficiency, error rate weightings and coding efficiency has been made and will be extensively discussed in the 5^{th} chapter of this research to select the optimum choice to be used in optical intersatellite links in free space. This information will form the main target of this research.

3. The model of the link (Transmitter (TX)/ the light source of the laser)

3.1 Introduction:

Space communication at optical frequencies has been seriously considered by various agencies such as ESA and NASA. Proposed mission scenarios are:

- Inter satellite links between two geosynchronous satellites.
- Inter orbit links between a low earth orbiting satellite and a geosynchronous data relay satellite.
- Optical communications to deep space probes.

As mentioned in the previous chapter, optical intersatellite links in space are receiving a great deal of attention and can make a revolution in space system architectures. This is resulted by the competing technologies of optical and microwave systems which have been examined by McCullagh [1], Ekberg [2], Toyoshima et al [3] and Allen et al [28]. These studies show that, in general, microwave radio systems can receive much lower power levels and operate in the atmosphere more efficiently than optical ones [1]. However, in space, optical systems can operate with much lower path loss and are considered superior to microwave ones [2]. In addition, they have the potential of operation at Gbit/s data rates.

Despite the fact that radio frequency (RF) links are considered as a reliable and well understood technology and have been used by the space industry for almost all space-based communications for decades, there are still various disadvantages of using RF in space: disrupting the communication link because the relatively broad beam widths raises susceptibility to jamming and interception; the bandwidth of the antenna limits the data throughput; antenna gain is small at RF wavelengths as a result of higher beam diffraction at longer wavelength leading to the need for higher transmitter power; one cannot design a DC to 10 GHz broadband RF antenna [29].

Wree et al [29] highlighted the various advantages of optical communications in space. The optical communication link produces much higher data rates where currently the light of a single laser in long-haul fibre optic transmission systems usually carries 2.5 Gb/s or 10 Gb/s and lately up to 40 Gb/s. The typical telecom satellite will have 15 RF transponders and achieve a total data rate of 150 Mb/s. A single RF transponder consumes anywhere from 30 Watts to 300 Watts, and to produce an equivalent data rate, a satellites would consume a power of up to 1 KW because it would need anywhere from 10 to 30 RF transponders.

There is insignificant chance of interference from another user in optical communication as it depends on lasers as the transmission source. The potential overlap area of multiple laser signals is radically decreased by the fact that lasers have very tight beam widths, and no side or back lobes. The interference can only occur if another laser is incident on the detector and this is extremely unlikely and can be designed around. In addition, optical communication is much more secure than RF communication because the tight beam width of lasers is virtually impossible for an outside observer to detect if a transmission is taking place while an RF transponder will spread its radiated energy over a much larger area. This is considered to be another advantage of the tight beam width of lasers [29]. Moreover, the eavesdropping on a transmission is almost impossible in optical systems and even detecting that a transmission is taking place is difficult because only scattered light can be seen off the optical path of the laser, and in space, there are few particles to produce such scatter. Therefore, optical links require less encryption to maintain the integrity and safety of the data stream. More complete use of the available bandwidth for actual data, in turn, is allowed, and the overall efficiency of the optical system is increased compared to an RF system [29]. However, a line of laser is a big challenge.

Phillips et al [30,31] highlighted that the bandwidth limitations of microwave satellite links traditionally resulted in greater restrictions on the bit rate in satellite communications, but for compatibility with the STM-1 signal in the new synchronous digital hierarchy (SDH) there is a requirement to operate at a bit rate of 155 Mbit/s and above. Therefore, laser satellite communications have been proposed for intersatellite links.

Cryan & Unwin [32] pointed out the advantages of optical technologies for space communications:

- The optical transmitter is a diode laser which is efficient, compact, reliable and inexpensive.
- The high frequency of the optical carrier leads to communications at data rates far in excess of those realisable using RF and microwave systems.
- The mass of the communication subsystems and hence the mass of the satellite host is reduced as a result of the use of transmission optics of modest dimensions which is resulted by the short emission wavelength.
- The antenna size and the power consumption of the communication subsystem are reduced in optical systems.

As well as considering the advantages of optical technologies for space communications, Cryan & Unwin [32] explained the tradeoffs between direct detection and coherent detection. This examination of the detection technique leads to the direct detection as the preferred technology for optical satellite communications as a result of the reduced complexity and greater potential sensitivity. In addition, the direct detection systems are being more actively pursued because they are insensitive to phase and frequency noise associated with lasers, whereas the coherent systems contain complicated optics and electronics in order to accomplish reasonable error rates as a result of excessive frequency and phase noise associated with semiconductor laser diodes. However, it should be noted that shot noise

limited coherent detection offers the best solution in the situation where background noise and noise associated with the receiver can not be ignored.

Therefore, according to these considerations, this research work is concerned with an analysis of intersatellite links in space, with optical links using laser diodes as sources being considered in particular because , generally, for many applications, they have many advantages: small size; high electrical to optical efficiencies; tightly focused beam. In addition, it is possible to adapt the technology used in fibre optic links to free-space communications and so multi-Gbit/s transmission is possible using readily available integrated driver chips. This chapter presents detailed information and in-depth analysis for two types of sources which are in use at present: semiconductor laser diodes (SLDs) and light emitting diodes (LEDs). Despite the fact that LED is used in fibre optic and can not be used with Mach-Zehnder interferometer device, which is used as an external modulator of the continuous wave (CW) laser source, but it is discussed into this chapter in order to clarify the operation process of the SLD. This, in turn, allows selecting the appropriate emission wavelength and the suitable semiconductor material of the laser source to be used in free space links and speed of 1 Gbit/s. This information represents the main goal of designing the transmitter in such links.

3.2 Comparative Review

3.2.1 Semiconductor Laser Diodes (SLDs) and Light-emitting Diodes (LEDs):

Cryan & Unwin [32] highlighted the laser diode as the attractive candidate for intersatellite optical communication transmitter as a result of its compactness, simplicity and high efficiency. The use of transmission optics of modest dimensions and reducing the mass of the communication subsystem are resulted by the short emission wavelength which is in the region of 0.85 μm as the majority of proposed communication systems are based upon GaAlAs laser diodes. Directly modulating the laser injection current performs the optical intensity modulation.

Ferrier et al [33] found that the technology of the semiconductor lasers is the enabling technology for coherent optical intersatellite links. They considered that very stringent requirements on the laser transmitter are required when using coherent detection system. These include mode stability, frequency response and a very narrow linewidth. In addition, they deduced that further stringent requirements should be met by the laser: it should be capable of high-speed modulation, where the lasers are modulated by direct modulation of the bias current; it should be capable of operating at high power; it should have low intensity noise to decrease the excess noise density produced at the receiver; it should be reliable, which is particularly significant for space applications. Furthermore, they highlighted that the buried heterostructure distributed feedback (BH) DFB InGaAsP laser is well suited to high-speed modulation and can be made very reliable. This is because this structure of the laser can, while maintaining a low leakage current, operate at current many times greater than the threshold current. In addition, the series resistance and the parasitic capacitance and inductance are kept at low levels as fabrication; mounting and packaging are permitted by this laser structure [33].

The principal light sources used for fibre optic communications applications are heterojunction-structured semiconductor laser diodes (also referred to as injection laser diodes or ILDs) and light-emitting diodes (LEDs). A heterojunction consists of two adjoining semiconductor materials with different band-gap energies. These devices are suitable for fibre transmission systems because they have adequate output power for a wide range of applications, their optical power output can be directly modulated by varying the input current to the device, they have a high efficiency, and their dimensional characteristics are compatible with those of the optical fibre. Comprehensive treatments of the major aspects of LEDs and laser diodes are presented in various books and journals [6-7, 34-39].

The light-emitting region of both LEDs and laser diodes consists of a pn junction constructed of direct-band-gap III-V semiconductor materials. When this junction is forward biased, electrons and holes are injected into the p and n regions, respectively. These injected minority carriers can recombine either radiatively, in which case a photon of energy hv is emitted, or nonradiatively, whereupon the recombination energy is dissipated in the form of heat. This p n junction is thus known as the active or recombination region.

A major difference between LEDs and laser diodes is that the optical output from an LED is non-coherent, whereas that from a laser diode is coherent. In a coherent source, the optical energy is produced in an optical resonant cavity. The optical energy released from this cavity has spatial and temporal coherence, which means it is highly monochromatic and the output beam is very directional. In a non-coherent LED source, no optical cavity exists for wavelength selectivity. The output radiation has a broad spectral width, since the emitted photon energies range over the energy distribution of the recombining electrons and hole, which usually lie between 1 and $2K_BT$. In addition, the non-coherent optical energy is emitted into a hemisphere according to a cosine power distribution and thus has a large beam divergence.

Sibley [6] highlighted the needed characteristics of the light source to be effective in an optical link: it must be possible to modulate the light output over a wide range of modulating frequencies and to operate the device continuously at a variety of temperatures for many years; the emitting area should be small in order to couple large amount of power into an optical fibre; the output spectrum should be narrow in order to decrease material dispersion in an optical fibre link; the wavelength of the output, for fibre links, should coincide with one of the transmission windows for the fibre type used.

Sibley [6] identified the differences between semiconductor laser diodes (SLDs) and light emitting diodes (LEDs) in several ways: SLDs emit light by stimulated emission, whereas LEDs emit light spontaneously; the application of a constant current is required by a laser diode to preserve stimulated emission; the output is more directional; and the response time is faster.

Stimulated emission takes place when a photon of light impinges on an already excited atom and, instead of being absorbed; the incident photon results in an electron to cross the band-gap, thus creating another photon. The stimulated photon has the same frequency and phase as the original and these two create more photons as they pass through the lattice that actually multiplies the original photon. Light amplification by the stimulated emission of radiation supported by the acronym laser. The light output is coherent and has a narrow linewidth because the created photons are all in phase. A quasi-stable state known as a population inversion is that the conduction band (CB) has to include a large number of electrons and the valence band (VB) a large number of holes before stimulated emission can take place, and arises from the injection of a large number of carriers into a heavily doped, ELED (the edge light emitting diode) active layer. If a population inversion exists then, some stimulated emission takes place by virtue of the light confinement from the heterojunction. It should be noted that some addition optical confinement has to be provided in order to guarantee that it is the principal light creating process.

This extra confinement arises in a laser diode from cleaving the end faces; therefore they form partial reflectors or facets. This resulting structure is called a Fabry-Perot etalon and is shown in the following figure [6]:

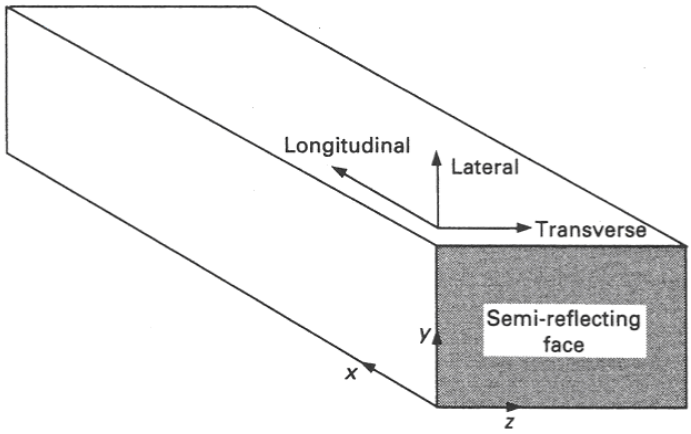

Figure 13. A basic Fabry-Perot cavity [6]

Stimulated emission and hence gain results from some of the spontaneously emitted light that is reflected back into the active region by these facets. Thus, provided the optical gain in the cavity exceeds the losses, stimulated emission will occur.

Sibley [6] examined the optical gain that is produced by stimulated emission and the spectral characteristics of SLDs for the simple stripe contact laser, which is analogous in construction to a stripe contact ELED. It should be noted that propagation can take place along all three axes; longitudinal, transverse and lateral propagation because light emission takes place in a rectangular cavity. He deduced that the optical gain for lasing is expressed as:

$$g = (n_2 - n_1)\frac{v_g^{\ 2}}{8\pi f^2 \tau_{sp}} g(f) \qquad (29)$$

Or

$$g = (n_2 - n_1)\frac{\lambda_0^{\ 2}}{8\pi \varepsilon_r \ \tau_{sp}} g(f) \qquad (30)$$

where ε_r is the relative permittivity of the active region, τ_{sp} is the carrier lifetime for spontaneous emission, $g(f)$ is the Lorenztian curve, n_1 is the electron density in the CB, n_2 is the electron density in the VB, v_g is the group velocity of the light in the semiconductor material, λ_0 is cut-off wavelength and f is the frequency of photons. For stimulated emission to take place, n_2 has to be greater than n_1. This is the quasi-stable state known as a population inversion that can be produced in SLDs by injecting a large number of electrons into the active region of a double heterojunction diode.

It should be noted that the SLD has to be biased at a certain current to preserve a population inversion. Below this threshold current, the SLD will emit light spontaneously as there will not be enough current to create a population inversion. The rate equations for a SLD have to be found in order to find the threshold current density (J_{th}).

The SLD rate equations are expressed as:

$$\frac{dn}{dt} = \frac{1}{q}\frac{J}{d} - \frac{n_2}{\tau_{sp}} - C(n_2 - n_1)\phi \qquad (31)$$

And

$$\frac{d\phi}{dt} = C(n_2 - n_1)\phi + \frac{Dn_2}{\tau_r} - \frac{\phi}{\tau_{ph}} \qquad (32)$$

where ϕ is the optical flux density (photons/m³), τ_r is radiative recombination time, d is the distance between the heterojunctions, *q* is the electronic charge, *J* is the diffusion current density, *C* is a constant of proportionality for stimulated emission, *D* is constant that helps to explain operation below threshold despite the fact that it is very low typically and τ_{ph} is the stimulated photon lifetime in the active region. For the first equation: the first term is the injected carrier density; the second term is the number of carriers lost due to recombination; and the third term is the total loss due to stimulated emission and absorption. As regards the second equation: the first term is the total increase in light due to stimulated emission and

absorption; the second term is the fraction of spontaneous emission coupled into a laser mode; and the third term is the loss due to photons being emitted by the cavity. For the steady-state rate equations, the last equations (31) and (32) then become:

$$0 = \frac{1}{q}\frac{J}{d} - \frac{n_2}{\tau_{sp}} - C(n_2 - n_1)\phi \qquad (33)$$

And

$$0 = C(n_2 - n_1)\phi + \frac{Dn_2}{\tau_r} - \frac{\phi}{\tau_{ph}} \qquad (34)$$

By combining these equations to give:

$$\frac{\phi}{\tau_{ph}} = \frac{Dn_2}{\tau_r} + \left[\frac{1}{q}\frac{J}{d} - \frac{n_2}{\tau_{sp}}\right] \qquad (35)$$

The first term in this equation is the spontaneous emission term, while the term in the brackets relates to stimulated emission. There are three regions of interest with a laser diode: operation below threshold, operation at threshold, and operation above threshold.

For operation below threshold, the stimulated emission term is zero and so:

$$\frac{1}{q}\frac{J}{d} = \frac{n_2}{\tau_{sp}} \qquad (36)$$

This implies

$$n_2 = \frac{\tau_{sp}}{q}\frac{J}{d} \qquad (37)$$

Thus, the equation (35) becomes:

$$\frac{\phi}{\tau_{ph}} = \frac{Dn_2}{\tau_r} \qquad (38)$$

$$\frac{\phi}{\tau_{ph}} = \frac{D}{\tau_r}\frac{\tau_{sp}}{q}\frac{J}{d} \qquad (39)$$

$$\frac{\phi}{\tau_{ph}} = \frac{D}{\tau_r}\frac{\tau_{sp}}{q}\frac{I}{Volume} \qquad (40)$$

The output optical power is then expressed as:

$$P = \frac{D}{\tau_r}\frac{\tau_{sp}}{q} I h_f \qquad (41)$$

This equation indicates that the power output of a SLD operating below threshold is directly proportional to the applied current, that is, it is operating as an LED. Taking into account, the factor h_f has been included as a photon density has been considered.

For operation at threshold, the light output will raise until there is sufficient spontaneously emitted light to result in stimulated emission as a result of increasing of the drive current. At this stage, the spontaneous emission can be neglected and the second equation from the steady-state rate equations, equation (34), becomes:

$$0 = C(n_{th} - n_1)\phi - \frac{\phi}{\tau_{ph}} \qquad (42)$$

And so

$$n_{th} = \frac{1}{C\tau_{ph}} + n_1 \qquad (43)$$

where n_{th} is the threshold electron density and *B* is the Einstein coefficient. The *C* is given by:

$$C = Bh_f g(f) \qquad (44)$$

And, from pervious equation of the optical gain, equation (29), the optical gain at threshold is:

$$g = (n_{th} - n_1)\frac{Bh_f}{v_g} g(f) \qquad (45)$$

And so

$$g = (n_{th} - n_1)\frac{C}{v_g} \qquad (46)$$

$$g = (\frac{1}{C\tau_{ph}} + n_1 - n_1)\frac{C}{v_g} \qquad (47)$$

$$g = \frac{1}{\tau_{ph} v_g} \qquad (48)$$

The optical gain at threshold is also given by:

$$g \geq \alpha + \frac{1}{2L} \times \ln(\frac{1}{R_1 R_2}) \qquad (49)$$

where α is the attenuation of the optical power per unit length (hence the factor 1/2), R_1 and R_2 are the reflectivity of the mirrors at x = 0 and x = L respectively, and *L* is the length of cavity.

Then the photon lifetime τ_{ph} is expressed as:

$$\frac{1}{\tau_{ph}} = v_g \left[\alpha + \frac{1}{2L} \times \ln(\frac{1}{R_1 R_2}) \right] \qquad (50)$$

The physical parameters of the SLD only determine the photon lifetime that also sets a limit on the maximum rate of modulation. Therefore, the threshold electron density becomes:

$$n_{th} = \frac{v_g}{B h_f g(f)} \left[\alpha + \frac{1}{2L} \times \ln(\frac{1}{R_1 R_2}) \right] + n_1 \qquad (51)$$

The bias current supplies these carriers, and so the threshold current density is:

$$J_{th} = \frac{q d n_{th}}{\tau_{sp}} \qquad (52)$$

By assuming $n_{th} >> n_1$, then:

$$J_{th} = \frac{qd}{g(f)} \frac{8\pi\varepsilon_r}{\lambda_0^{\,2}} \left[\alpha + \frac{1}{2L} \times \ln\left(\frac{1}{R_1 R_2} \right) \right] \qquad (53)$$

And so J_{th} at the nominal wavelength of emission is:

$$J_{th} = qd\frac{\pi\delta_f}{2}\frac{8\pi\varepsilon_r}{\lambda_0{}^2}\left[\alpha + \frac{1}{2L}\times\ln\left(\frac{1}{R_1R_2}\right)\right] \tag{54}$$

where δ_f is half-power spread propagating through the SLD. This δ_f can be found by one way that is to excite the SLD material with light of varying wavelength, and plot the variation of absorption with frequency. This equation shows that J_{th} is directly proportional to the width of the active region, and the linewidth of the ELED that makes up the SLD. Despite the fact that this equation is reasonably accurate at low temperature, it can be approximated under normal operating conditions by:

$$J_{th}(T) = 2.5J_{th}\exp(T/120) \tag{55}$$

For operation above threshold, the spontaneous emission is neglected, and so the resulted equation from combining the two rate equations, equation (35), becomes:

$$\frac{\phi}{\tau_{ph}} = \left[\frac{1}{q}\frac{J}{d} - \frac{n_2}{\tau_{sp}}\right] \tag{56}$$

In this case, the gain is effectively clamped at the value given by equation (49). And so any raise in carrier density will not raise the gain – it will, however, raise the light output. Under these conditions, it can be written:

$$\frac{\phi}{\tau_{ph}} = \left[\frac{1}{q}\frac{J}{d} - \frac{n_{th}}{\tau_{sp}}\right] \tag{57}$$

$$\frac{\phi}{\tau_{ph}} = \frac{1}{q}\left[\frac{J - J_{th}}{d}\right] \tag{58}$$

Sibley [6] considered that commonly with the planar optical waveguide, light waves of certain wavelengths only can propagate in the cavity. The condition for successful propagation is that the reflected and original waves have to be in phase.

Where N is an integer. The cut-off wavelength is expressed as:

$$\lambda_0 = \frac{2n_1}{N} L \qquad (59)$$

Therefore, the laser will only amplify wavelengths that satisfy λ_0. Each wavelength is known as a longitudinal mode, or simply a mode. The modes result in a line spectrum, and the mode spacing will be produced by solution of the last equation of λ_0.

The bias current determines highly the spectral emission of a laser. Below threshold, spontaneous emission predominates and so the linewidth is analogous to that of an LED. However, above threshold, the linewidth decreases because the cavity exponentially amplifies the first mode to reach threshold, at the expense of all other modes. To examine this, as mentioned above, the steady-state solution for the photon density is given by equation (34). By rearranging this equation to give the photon concentration:

$$\phi = \frac{Dn_2}{\tau_r}\left[\frac{1}{\tau_{ph}} - C(n_2 - n_1)\right]^{-1} \qquad (60)$$

The term outside the brackets is the amount of spontaneous emission coupled into a laser mode. Therefore, this equation can be interpreted as an amplification factor, G, which is acting on the spontaneous emission of an ELED, given by:

$$G = \left[\frac{1}{\tau_{ph}} - C(n_2 - n_1)\right]^{-1} \qquad (61)$$

Since the gain function has a Lorenztian distribution, it can be expressed as:

$$G(\omega) = \left[\frac{1}{\tau_{ph}} - \left\{C(n_2 - n_1) + b(\omega - \omega_0)^2\right\}\right]^{-1} \qquad (62)$$

When a SLD operates below threshold, the term in {} is small, and thus the cavity amplifies all the propagating modes to the same extent. The following figure shows the effect that the amplification increases when the diode current is increased, but the mode whose wavelength is closest to the nominal operating wavelength is amplified the most:

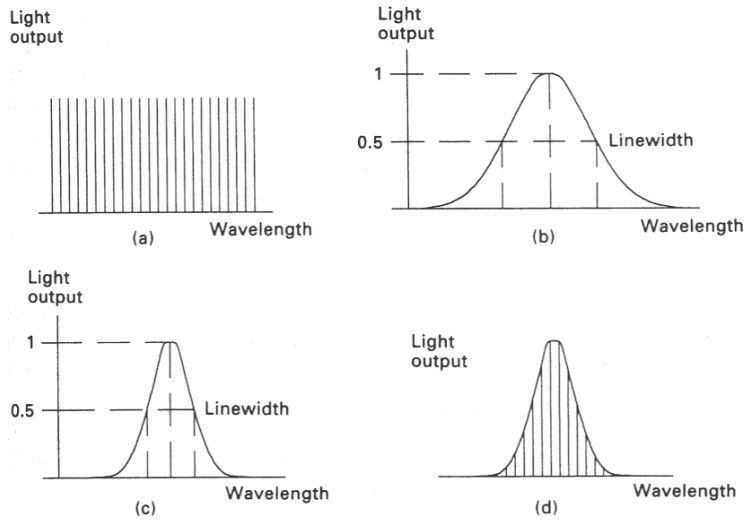

Figure 14. (a) Allowable modes in a SLD; (b) gain profile of a SLD operating below threshold; (c) gain profile of a SLD operating above threshold; and (d) resultant emission spectrum [6]

Therefore, when a SLD operates above threshold, the linewidth is considerably less than that of an ELED.

In practice, the output consists of a range of modes following a gain profile because modes close to the principle also pass through significant amplification. This profile can be approximated to the Gaussian distribution:

$$g(\omega) = g(\omega_0)\exp(\frac{-(\omega-\omega_0)^2}{2\sigma^2}) \qquad (63)$$

where σ is the linewidth of the laser output. The linewidth of typical stripe contact SLDs can vary from 2 to 5 nm.

The gain profile could shift slightly if the laser is operated at currents significantly higher than threshold. Therefore, one of the modes close to the nominal wavelength becomes control. This effect is known as mode-hopping and it is responsible for kinks in the power/current characteristic. This mode-hopping can modify the operating frequency if the laser is modulated by varying the drive current, and so dynamic mode-hopping is also known as

chirp. The stripe contact lasers are not commonly used in high-data-rate optical fibre links because mode-hopping can result in problems in these links. Any chirp on the optical pulse will alter the operating wavelength so resulting in pulse dispersion if the link is operating at a zero dispersion wavelength. Then, alternative laser structures have to be used.

As mentioned, there are also transverse and lateral as well as longitudinal modes. These tend to yield an output beam which is highly divergent, resulting in inefficient launching into an optical fibre. The ideal situation is one in which only the principle transverse and lateral modes are existed. This would produce a parallel beam of light of very small cross-sectional area. The condition for a single lateral mode is analogous to that for a planar dielectric waveguide, and so

$$d < \frac{\lambda_0}{2(n_1^{\,2} - n_2^{\,2})^{\frac{1}{2}}} \qquad (64)$$

where n_1 and n_2 are the refractive indices of the active region and the surrounding material respectively. In most laser diodes, the active region is typically less than 1 μm thick and the last equation is usually satisfied. The single transverse mode operation is more difficult to perform. This is because the width of the active region is set by the current density profile in the active layer, which can be difficult to dominate in the stripe contact lasers.

Sibley [6] concluded that the frequency response of the SLD has a peak at a frequency close to the natural frequency of the cavity, ω_0. This is known as a relaxation resonance, and it is caused by a resonance between the photon and electron populations in the laser. Under digital modulation, this gives rise to the ringing that the optical pulse suffers from it at an angular frequency given by $\omega_0^{\,2} = C^2 n_{th}\phi_s = \frac{\phi_s}{n_{th}\tau_{ph}^{\,2}}$. It should also be noted that the response falls off at a rate $\omega_0^{\,2} / \omega_m^{\,2}$ (where ω_m is an angular frequency at which the diode current is modulated) at frequencies above ω_0. Therefore, the bandwidth of the SLD is set by the frequency of the relaxation resonance. Since SLDs are normally used in long-haul, high-data-rate routes, which use SM fibres, it is generally desirable to minimise the linewidth and

operate with a single lateral mode. It is also significant to decrease the threshold current, as this will yield a more efficient device.

Sibley [6] found that the stripe contact design is the most common SLD structure for general use. The decreasing of the active region cross-sectional area is the most explicit way of decreasing the threshold current I_{th}. As this is set by the area of the stripe contact, the I_{th} could be decreased by decreasing of the cavity length. However, this causes increasing of the threshold current density, J_{th}, as a result of increasing of the gain required for threshold. The cavity length is usually limited to typically 150 μm because of heatsinking problems that result from a high current density. Therefore, the reduction of the contact width has to be made to decrease I_{th}. To a certain extent the width of the active region is set by the width of the contact. Since the injected current tends to diffuse outwards as it passes through the laser if the contact stripe width is less than about 6 μm, the threshold current I_{th} practically fails to fall in proportion to the contact stripe width. Ultimately, the threshold current of stripe contact lasers is usually no less than 120 mA because an existed active region that is independent of the contact width.

A different structure should be used to decrease the threshold current I_{th} further, and operate with a single lateral mode. The following figure shows that the diode current in a buried heterostructure, BH, laser is restricted to flow in a well-defined active region:

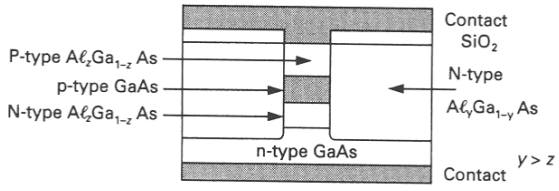

Figure 15. Cross-section through a buried-heterojunction, semiconductor laser diode [6]

In the heterojunctions, a carrier confinement is provided by either side of the active region, and thus the width of this region can be made very small, typically 2 μm or less. These heterojunctions will also yield a narrow optical waveguide, and so single lateral mode operation is often performable. The threshold current of these devices is typically 30 mA. The gain profile of the BH structure is considerably narrowed by using a small active region. This is considered as a further advantage of the BH structure. Therefore, the emission spectrum of some BH lasers can consist of a single line- a considerable advantage in long-haul routs operating at a zero dispersion wavelength. However, the wavelength of emission may alter during operation so resulting in dispersion because the gain profile is dependent on the junction temperature.

The distributed feedback, or DFB, laser that is distributing the feedback throughout the laser can produce a truly single-mode source. The following figure shows a cross-section through a distributed feedback semiconductor laser diode, where a grating replaces the Fabry-Perot cavity resonator:

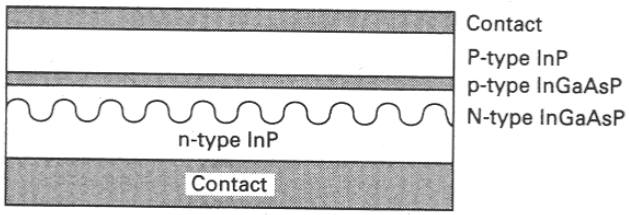

Figure 16. Cross-section through a distributed feedback semiconductor laser diode [6]

In these devices, each perturbation reflects some of the light and the phase of the twice reflected light has to match that of the incident light in order to propagate successfully. This produces the effect of grating that is to choose just one propagating mode. This condition is expressed as:

$$2n_2 \ddot{A} = m\lambda_0 \qquad (65)$$

where $\ddot{A}$ is the period of the grating, n_2 is the refractive index of the material above the grating, and m is an integer. The factor 2 appears in the lift-hand side of this equation

because the light has to be reflected twice in order to be in phase with the incident wave. The wave will not propagate and the scattered light from the grating will interfere destructively if this condition is not satisfied. On the other hand, this equation is a special case of Bragg's law. So, if m equals unity, the wave is said to be incident at the first Bragg condition. It is also possible for light to be reflected using the second Bragg condition that can be seen if $m = 2$, the grating period will increase, so making it easier to fabricate. It should be noted that a grating in the active region will result in surface dislocations, and this will increase the non-radiative recombination rate. Therefore, the grating is not part of the active layer. Instead, the grating usually exists in a waveguide layer where it interacts with the evanescent field.
The distributed Bragg reflector, DBR, laser is a modification of the DFB laser. In this device, short lengths of grating, which act as frequency selective reflectors, replace the Fabry-Perot resonator. In addition, despite of many modes propagate in the active region, a single wavelength only is reflected back and undergoes amplification.

The threshold current of both these devices is typically 20 mA, and their linewidth is quite narrow < 0.5 nm. Therefore, these devices are often used for high-data-rate/long-haul routes. As mentioned, these lasers depend on the grating period to choose a special wavelength. However, the wavelength will alter because changes in temperature will result in the grating to expanding or contracting. The laser temperature can be controlled by mounting the semiconductor on a peltier cooler. If a thermistor is placed close to the device, a simple control loop can be used to preserve the laser temperature.

Sibley [6] highlighted the packaging of SLDs in the laboratory and for commercial applications as the following:

For using in the laboratory*:* SLDs are usually mounted in brass studs. With this package, the body of the stud forms the anode of the SLD, and so the lead at the rear of the package has to be connected to a negative voltage, current source. A thread on the back of the stud enables the user to bolt the diode on to an efficient heatsink.

***For commercial applications**:* the SLD is commonly mounted on a Peltier cooler in a dual-in-line package. The power monitoring facility is provided by a photodiode that is placed on the non-emitting end of the laser. A fibre pig-tail, with a lens grown on the laser end of the fibre, provides the output. For launching into MM fibre, a hemispherical lens is often used, whereas for launching into SM fibres, a tapered lens is more common. The lenses can be made by dipping the fibre end into low-melting-point glass. With this technique, up to 66 per cent of the output power can be coupled into the fibre.

As a SLD ages, the threshold current requirement tends to increase because carrier lifetime reduces with age. Therefore, a feedback loop has to be used that monitors the laser output, and increases the drive current accordingly. However, the threshold point tends to become less well-defined as time passes, and so the control loop has to contain some means of raising an alarm if the threshold requirement becomes too great. Accelerated life testing suggests that this condition takes place after, typically, 20 to 25 years.

Sibley [6] concluded that semiconductor laser diodes are used in optical fibre links but are seldom used in free-space optical links as a result of their low output power. Instead, high-power solid-state or gas lasers are used. Such lasers are usually physically large, and modulation of the light output can prove difficult. In spite of this, such lasers are often used in the laboratory, and their application to free-space links is developing.

Sibley [6] highlighted that the recombination of the minority carriers in a p-n semiconductor diode, holes in the n-type and electrons in the p-type, can take place by electrons dropping down from the CB to the VB when a forward bias is applied to a semiconductor and thus the barrier voltage of a p-n semiconductor junction diode decreases. This recombination leads to the electrons losing a certain amount of energy equal to the band-gap energy difference. There are two different processes for this recombination: indirect transitions (also known as non-radiative recombinations) which generate lattice vibrations, or phonons; and direct transitions (or radiative recombinations) which generate photons of light.

The wavelength of the incident photon is given by:

$$\lambda_0 = \frac{hc}{E_2 - E_1} \tag{66}$$

Where E_1 is valence band (VB) electron energy, E_2 is the conduction band (CB) electron energy, and $E_2 - E_1$ is the change in energy. The lowest possible energy change is the band-gap energy of the material, and so this results in a cut-off wavelength beyond which the material becomes transparent. These cut-off wavelengths are identical to the emission wavelengths of sources made of the same material.

The following table lists the band-gap energy, and transition type, of a range of semiconductors. It can be seen from this table that the semiconductors have a direct band-gap, and so are most often used. However, all the common single element materials have an indirect band-gap and so are never used as light sources. This table is:

Characteristics of various semiconductor materials (D – direct, I – indirect band-gap)			
Semiconductor material	*Transition type*	*Band-gap Energy (eV)*	*Wavelength of emission (μm)*
InAs	D	0.36	3.44
PbS	I	0.41	3.02
Ge	I	0.67	1.85
GaSb	D	0.72	1.72
Si	I	1.12	1.11
InP	D	1.35	0.92
GaAs	D	1.42	0.87
CdTe	D	1.56	0.79
GaP	I	2.26	0.55
SiC	I	3.00	0.41

Table 5. Characteristics of various semiconductor materials (D-direct, I –indirect band-gap)

Silicon responds to light of wavelengths up to 1.1 μm, whereas germanium photodiodes operate up to 1.85 μm.

Keiser [7] considered that the lasing medium can be a gas, a liquid, an insulating crystal (solid state), or a semiconductor. Despite the fact that there are some differences between them, the basic principle of operation is the same for each type of laser and semiconductor laser diodes are similar to other lasers, such as the conventional solid-state and gas lasers, in that the emitted radiation has spatial and temporal coherence; that is, the output radiation is highly monochromatic and the light beam is very directional. However, semiconductor laser diodes are almost exclusively the laser sources used for optical fibre systems.

Keiser [7] demonstrated that Laser action is the consequence of three major processes: photon absorption, spontaneous emission, and stimulated emission. The following simple two-energy-level diagrams represent these three processes:

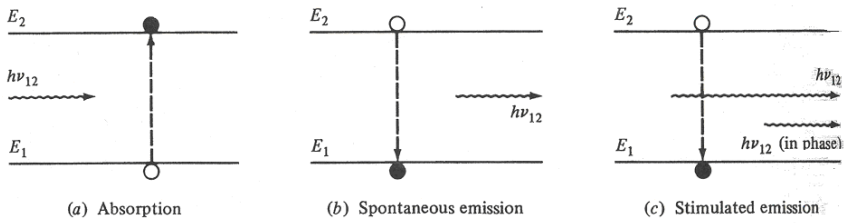

Figure 17. The three key transition processes involved in laser action [7]

The open circle represents the initial state of the electron and the filled circle represents the final state. Incident photons are shown on the left of each diagram and emitted photons are shown on the right.

where E_1 is the ground-state energy and E_2 is the excited-state energy. The absorption or emission of a photon of energy $h_{v12} = E_2 - E_1$ is involved by a transition between theses two states according to Planck's law. When a photon of energy h_{v12} collides on the system, that normally is in the group state, an electron in state E_1 can absorb the photon energy and be excited to state E_2, as shown in (a).

Since this is an unstable state, the electron will shortly return to the ground state, thereby emitting a photon of energy h_{v12} without any external stimulation. This is called spontaneous

emission, as shown in (b). However, these emissions come out as a narrowband Gaussian output because they are isotropic and of random phase.

The electron can also be induced to make a downward transition from the excited level to the ground-state level by an external stimulation. If photon of energy h_{v12} collides on the system while the electron is still in its excited state, the electron is directly stimulated to drop to the ground state and give off a photon of energy h_{v12}. This is called stimulated emission, as shown in (c). However, this emitted photon is in phase with the incident photon.

The stimulated emission is basically negligible when most of photons incident on the system will be absorbed because the density of excited electrons is very small in thermal equilibrium. Only if the population of the excited states is greater than that of the ground state, stimulated emission will go beyond absorption. This condition is known as population inversion that is performed by various pumping techniques as it is not an equilibrium condition. In a semiconductor laser, population inversion is achieved by injecting electrons into the material at the device contacts to fill the lower energy states of the conduction band.

Keiser [7] concluded that the semiconductor injection laser diode is preferred over the LED for optical fibre communication systems requiring bandwidth greater than approximately 200 MHz. However, the construction of laser diodes is more complicated, basically as a result of the additional requirement of current confinement in a small lasing cavity. The double-heterojunction LED configuration developed from the successful demonstration of both carrier and optical confinement in heterojunction injection laser diodes. The more quick development and utilization of LEDs as compared with laser diodes existed in the inherently simpler construction, the smaller temperature dependence of the emitted optical power, and the absence of decreasing in LEDs. In addition, he found that Laser diodes, which are typically have response times less than 1ns and have optical bandwidths of 2nm or less, are generally capable of coupling several tens of milliwatts of useful luminescent power into optical fibres with small cores and small mode-field diameters. Actually all laser diodes in use are multilayered heterojunction devices.

Optical transitions between distributions of energy states in the valence and conduction bands produce stimulated emission in semiconductor lasers. This varies from gas and solid-state lasers, in which radiative transitions take place between discrete isolated atomic or molecular levels.

The radiation in the laser diode is created within a Fabry-Perot resonator cavity that is much smaller, being approximately 250-500 μm long, 5-15 μm wide, and 0.1-0.2 μm thick. In the laser diode Fabry-Perot resonator, pair of flat, partially reflecting mirrors are directed toward each other to enclose the cavity. The aim of these mirrors is to give strong optical feedback in the longitudinal direction, thereby converting the device into an oscillator with gain mechanism that offsets for optical losses in the cavity. The laser cavity can have many resonant frequencies. The device will oscillate at those resonant frequencies for which the gain is sufficient to surmount the losses. The sides of the cavity are simply formed by roughening the edges of device to decrease unwanted emissions in these directions.

Keiser [7] found that a pattern of electric and magnetic fields lines called the modes of the cavity is produced by the optical radiation within the resonance cavity of a laser diode. These can adequately be separated into two independent groups of transverse electric (TE) and transverse magnetic (TM) modes. Each group of modes can be expressed in terms of the longitudinal, lateral, and transverse half-sinusoidal variations of electromagnetic fields along the major axes of the cavity.

The longitudinal modes: they are correlated to the length L of the cavity and define the main structure of the frequency spectrum of the emitted optical radiation. Many longitudinal modes can present because L is much larger than the lasing wavelength of approximately 1μm.

The lateral modes: they lie in the plane of the pn junction. The side wall preparation and the width of cavity determine these modes that define, in their turn, the shape of the lateral profile of the laser beam.

The transverse modes: these modes are of great importance, because they highly define such laser characteristics as the radiation pattern (the angular distribution of the optical output power) and the threshold current density. They are companioned with the electromagnetic field and beam profile in the direction perpendicular to the plane of the pn junction.

The lasing conditions and resonant frequencies can be defined by expressing the electromagnetic wave propagating in the longitudinal direction (along the axis normal to the mirrors) in terms of the electric field phasor

$$E(z,t) = I(z) \times e^{j(wt-\beta z)} \tag{67}$$

where $I(z)$ is the optical field intensity, ω is the optical radian frequency, and β is the propagating constant.

The requirement for lasing, that is the condition at which light amplification becomes possible in the laser diode, is that a population inversion be performed. The main relationship between the optical field intensity I, the absorption coefficient α, and the gain coefficient g in the Fabry-Perot cavity can clarify this condition. The stimulated emission rate into a given mode is proportional to the intensity of the radiation in that mode. The radiation intensity at a photon energy hv differs exponentially with the distance z that it passes through along the lasing cavity according to the relationship:

$$I(z) = I(0)\exp\left\{\left[\Gamma g(hv) - \bar{\alpha}(hv)\right]z\right\} \tag{68}$$

Where $\bar{\alpha}$ is the effective absorption coefficient of the material in the optical path and Γ is the optical-field confinement factor that is the fraction of optical power in the active layer. The feedback mechanism of the optical cavity produces the optical amplification of selected modes. In the repeated passes between the two partially reflecting parallel mirrors, a part of the radiation companied with those modes that have the highest optical gain coefficient is kept and further amplified during each trip through the cavity.

Keiser [7] considered that examining the laser diode rate equations that control the interaction of photons and electrons in the active region can define the relationship between optical output power and the diode drive current. As mentioned above, carrier injection, spontaneous recombination, and stimulated emission define the total carrier population. For a pn junction with carrier-confinement region of depth d, the rate equations are expressed as:

$$\frac{d\phi}{dt} = Cn\phi + R_{sp} - \frac{\phi}{\tau_{ph}} \tag{69}$$

This controls the number of photons ϕ. The first term is a source of photons arising from stimulated emission, the second term, describing the number of photons resulted by spontaneous emission, is relatively small compared with the first term, and the third term implies the decay in the number of photon resulted by loss mechanisms in the lasing cavity.

And:

$$\frac{dn}{dt} = \frac{J}{qd} - \frac{n}{\tau_{sp}} - Cn\phi \tag{70}$$

Which controls the number of electrons n. The first term represents the raise in the electron concentration in the conduction band as current flows into the device, and the second and third terms indicate the number of electrons lost from the conduction band as a result of spontaneous and stimulated transitions, respectively.

Where *C* is a coefficient describing the strength of the optical absorption and emission interactions, R_{sp} is the rate of spontaneous emission into the lasing mode, τ_{ph} is the photon lifetime, τ_{sp} is the spontaneous recombination lifetime, and J is the injection-current density.

The last two equations could be balanced by considering all the factors that affect the number of carriers in the laser cavity. Solving these two equations for a steady-state condition, which is characterized by the left-hand sides of these two equations being equal to zero, will produce an expression for the output power.

For the equation (69), assuming R_{sp} is negligible and noting that $\frac{d\phi}{dt}$ has to be positive when ϕ is small:

$$C_n - \frac{1}{\tau_{ph}} \geq 0 \qquad (71)$$

This indicates that n has to go beyond a threshold value n_{th} in order for ϕ to rise.

For the equation (70), this threshold value can be expressed in terms of the threshold current J_{th} needed to preserve an inversion level $n = n_{th}$ in the steady state when the number of photons $\phi = 0$:

$$\frac{n_{th}}{\tau_{sp}} = \frac{J_{th}}{qd} \qquad (72)$$

This expression determines the current required to support an excessive electron density in the laser when spontaneous emission is the only decay mechanism.

Keiser [7] identified the external differential quantum efficiency η_{ext} as the number of photons emitted per radiative electron-hole pair recombination above threshold. Under the assumption that above threshold the gain coefficient keeps fixed at g_{th}, η_{ext} is given by:

$$\eta_{ext} = \frac{\eta_i (g_{th} - \bar{\alpha})}{g_{th}} \qquad (73)$$

where η_i is the internal quantum efficiency. However, it is not well-defined quantity in laser diodes where most measurements result in $\eta_i \cong 0.6 - 0.7$ at room temperature.

Experimentally, η_{ext} is defined from the straight-line part of the curve for the emitted optical power P versus drives current I, which gives:

$$\eta_{ext} = \frac{q}{E_g}\frac{dP}{dI} = 0.8065\lambda(\mu m)\frac{dP(mW)}{dI(mA)} \qquad (74)$$

where E_g is the band-gap energy in electron volts, dP is the incremental change in the emitted optical power in milliwatts for an incremental change dI in the drive current (in milliamperes), and λ is the emission wavelength in micrometers. For standard semiconductor lasers, external differential quantum efficiencies of 15-20 percent per facet are typical. High-quality devices have differential quantum efficiencies of 30-40 percent.

Keiser [7] concluded that the current flow has to be limited laterally to a narrow stripe along the length of the laser that is a principle requirement for efficient operation of laser diodes, in addition to transverse optical and carrier confinement between heterojunction layers. Several methods of performing this have been suggested, but all strive for the same aims of limiting the number of lateral modes. Therefore, lasing is restricted to a single filament, stabilizing the lateral gain, and guaranteeing a relatively low threshold current.

Keiser [7] highlighted that a compromise has to be made between current density and output beam width when designing the width and the thickness of the optical cavity. Because when either the width or the thickness of the active region increases, a narrowing of the lateral or transverse beam width takes place, respectively, but at the expense of a raise in the threshold current density. Most waveguide devices have a lasing spot 3μm wide by 0.6μm high. This is significantly greater than the active-layer thickness, since about half the light runs in the confining layers.

The achievable threshold current density, modulation speed, and linewidth of the device are limited because the electronic and optical properties remain the same as in the bulk material despite that fact that the active layer in a standard double-heterostructure laser is thin enough (1-3 μm) to restrict electrons and the optical field. Quantum-well lasers surmount these limitations by having an active-layer thickness around 10 nm. This changes the electronic and optical properties dramatically, because the dimensionality of the free-electron motion is decreased from three to two dimensions. A quantization of the energy levels results from the confinement of the carrier motion normal to the active layer. The possible energy-level transitions which result in photon emission are designated by ΔEij . Both single quantum-well (SQW) and multiple quantum-well (MQW) lasers have been manufactured, where these structures include single and multiple active regions, respectively. Barrier layers are the layers separating the active regions. The MQW lasers have a better optical-mode restriction, which leads to a lower threshold current density. The wavelength of the output light can be changed by adapting the layer thickness *d*. The following figure shows energy-band diagram for a quantum layer in a multiple quantum-well (MQW) laser, the parameter ΔEij represents the allowed energy-level transitions [7]:

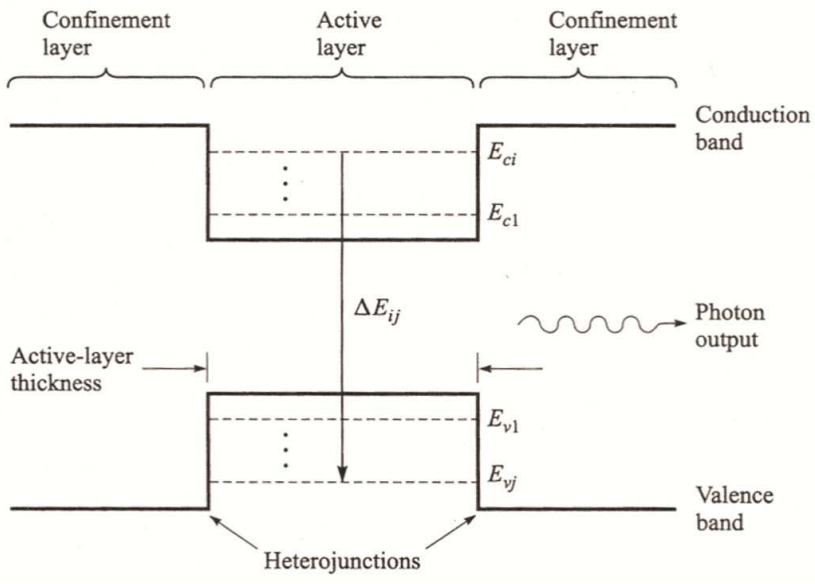

Figure 18. Energy-band diagram for a quantum layer in a multiple quantum-well (MQW) laser [7]

Keiser [7] demonstrated that single-mode lasers, which have to include only a single longitudinal mode and a single transverse mode, are needed for high-speed long-distance communications. Thus, the spectral width of the optical emission is very narrow. The decreasing of the length L of the lasing cavity to the point where the laser transition line width is lower than the frequency separation Δv of the adjacent modes is one method of confining a laser to have only one longitudinal mode. However, these lengths make the device hard to handle, and they are restricted to optical output powers of only a few milliwatts.

Vertical-cavity surface-emitting lasers are among alternative devices that were thus developed. The following figure shows a basic architecture of a vertical-cavity surface-emitting laser:

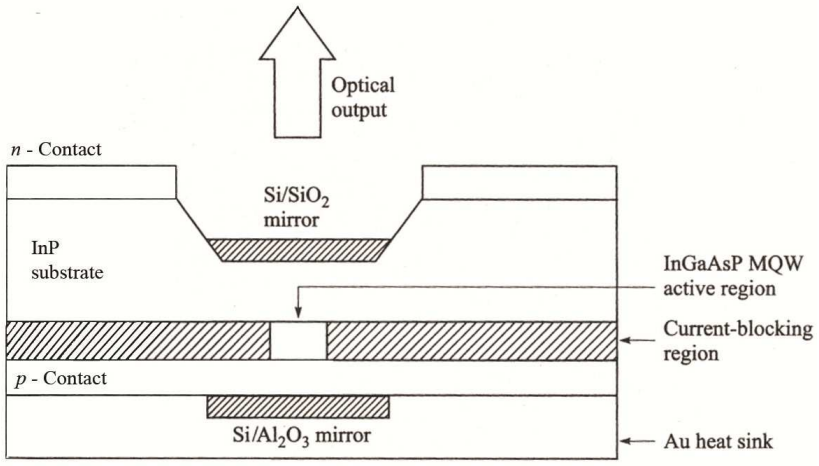

Figure 19. Basic architecture of a vertical-cavity surface-emitting laser [7]

The major aspect of a vertical-cavity surface-emitting laser (VCSEL or VCL), that makes the integration of multiple lasers easy onto a single chip in one- or two-dimensional arrays, which makes them attractive for wavelength-division-multiplexing applications, is that the light emission is perpendicular to the semiconductor surface. Very low threshold currents (< 100 μA) result from the very small active region volume of these devices. In addition, the modulation bandwidths are much greater for an equivalent output power compared to edge-emitting lasers because the higher photon densities decrease radiative lifetimes. A maximum reflectivity is needed for efficient operation, thus the mirror system used in VCSELs is of critical importance.

There are three types of laser configurations using a built-in frequency-selective reflector, which are: distributed-feedback (DFB) laser; distributed-Bragg-reflector (DBR) laser; and distributed-reflector (DR) laser. In each case, the frequency-selective reflector is a corrugated grating which is a passive waveguide layer adjacent to the active region. The optical wave propagates parallel to this grating. The distributed Bragg phase-grating reflector determines the operation of these types of lasers. A phase grating is mainly a region of periodically varying refractive index that results in two counterpropagating travelling waves to couple. The coupling is at a maximum for wavelengths close to the Bragg wavelength λ_B, which is related to the period Λ of the corrugations by:

$$\lambda_B = \frac{2n_e\Lambda}{K} \qquad (75)$$

Where n_e is the effective refractive index of the mode and K is the order of the grating. The strongest coupling is provided by first-order gratings ($K = 1$), but sometimes second-order gratings are used since their larger corrugation period facilitates manufacture. Lasers based on this architecture offer good single-mode longitudinal operation with low sensitivity to drive-current and temperature variations.

The distributed-feedback (DFB) laser: It can be shown by figure 20:

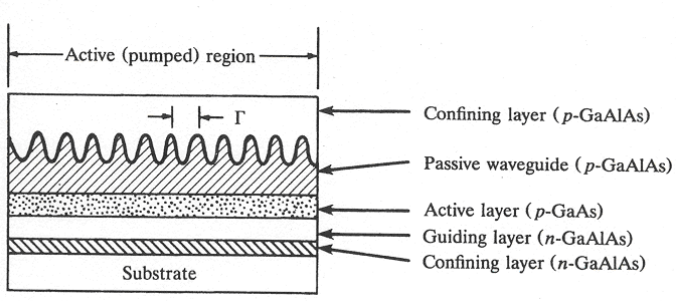

Figure 20. The distributed-feedback (DFB) laser [7]

In this configuration, the grating for wavelength selector is configured over the entire active region. The longitudinal modes in an ideal DFB laser are spaced identically around λ_B at wavelengths given by:

$$\lambda = \lambda_B \pm \frac{\lambda_B^{\ 2}}{2n_e L_e}(m + \frac{1}{2}) \qquad (76)$$

Where $m = 0,1,2,.....$ is the mode order and L_e is the effective grating length. The amplitudes of successively higher-order lasing modes are highly decreased from the zero-order amplitude. Theoretically, the two zero-order modes, in a DFB laser that has both ends antireflection-coated, on either side of the Bragg wavelength should experience the same lowest threshold gain and would lase simultaneously in an idealized identical structure. However, in practice, the degeneracy in the model gain is lifted and a single-mode operation is resulted by the randomness of the cleaving process. This facet asymmetry can be further raised by putting a high-reflection coating on one end and a low-reflection coating on the other.

The distributed-Bragg-reflector (DBR) laser: shown in the figure 21:

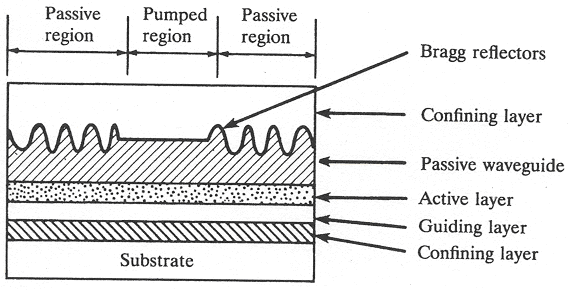

Figure 21. The distributed-Bragg-reflector (DBR) laser [7]

In this configuration, the cleaved end mirrors used in the Fabry-Perot optical resonator are replaced by the gratings that are located at the ends of the normal active layer of the laser.

The distributed-reflector (DR) laser: shown in the figure 22:

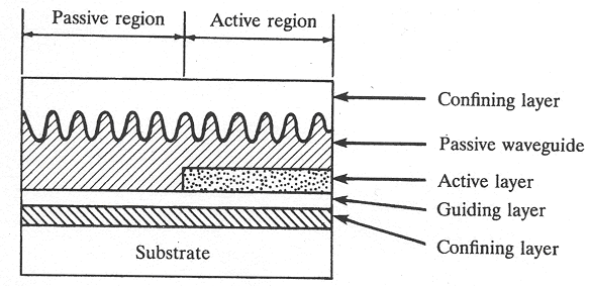

Figure 22. The distributed-reflector (DR) laser [7]

This configuration consists of active and passive distributed reflectors. The lasing features of conventional DFB and DBR lasers are improved by this structure that has a high efficiency and high output capability.

The second structure of vertical-cavity surface-emitting lasers is tunable laser sources that are significant instruments for tests that measure the wavelength-dependent response of an optical component or link. For example, Hewlett-Packard (Model 8168B) that creates a true single-mode laser line for every selected wavelength point. The source is an external-cavity semiconductor laser. A tunable filter for wavelength selection is a movable diffraction grating. According to the source and grating combination, a typical instrument is tunable over either the 1280-to-1330-nm band or the 1450-to-1565-nm band. The minimum output power of these instruments is -10 dBm and the absolute wavelength accuracy is typically ±0.1 nm.

Keiser [7] considered that the temperature dependence of the threshold current $I_{th}(T)$ is a significant factor in the application of laser diodes. Various complex temperature-dependent factors result in increasing this parameter with temperature in all types of semiconductor lasers. Despite of the fact that the formulation of a single equation that holds for all devices and temperature ranges is hindered by the complexity of these factors, the temperature variation of I_{th} can be approximated by the empirical expression:

$$I_{th}(T) = I_z e^{T/T_0} \tag{77}$$

where T_0 is a measure of the relative temperature insensitivity and I_z is a constant.

For a conventional stripe-geometry GaALAs laser diode, T_0 is typically $120-165C^o$ in the vicinity of room temperature. The following figure shows an example of a laser diode with $T_0 = 135C^o$ and $I_z = 52mA$:

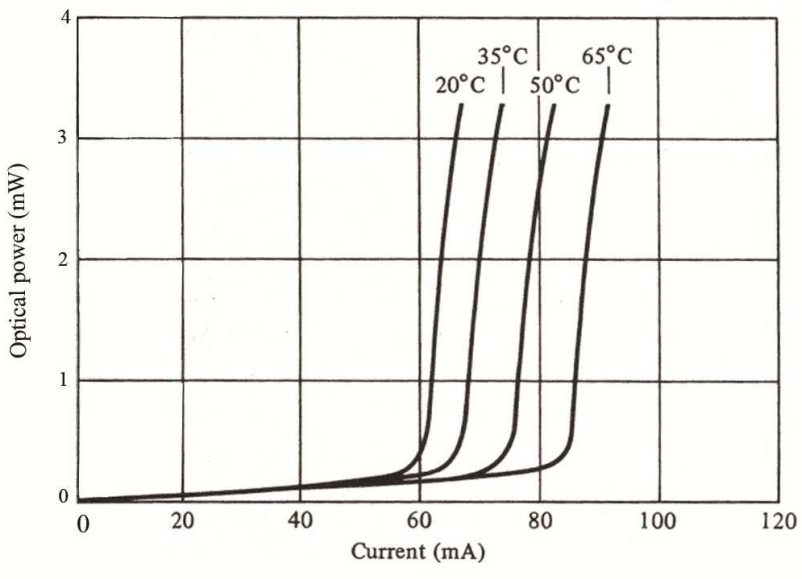

Figure 23. Temperature-dependent behavior of the optical output power as a function of the bias current for a particular laser diode [7].

For this laser diode, the threshold current increase by a factor of about 1.4 between 20 and 60 C^o. In addition, the lasing threshold can alter as the laser ages. Consequently, if a constant optical output power level is to be preserved as the temperature of the laser changes or as the laser ages, it is necessary to adapt the dc-bias current level. Possible ways for performing this automatically are optical feedback and feedforward schemes, temperature-matching transistors, and predistortion techniques.

The following figure shows the variation in I_{th} with temperature is 0.8 percent/C^o :

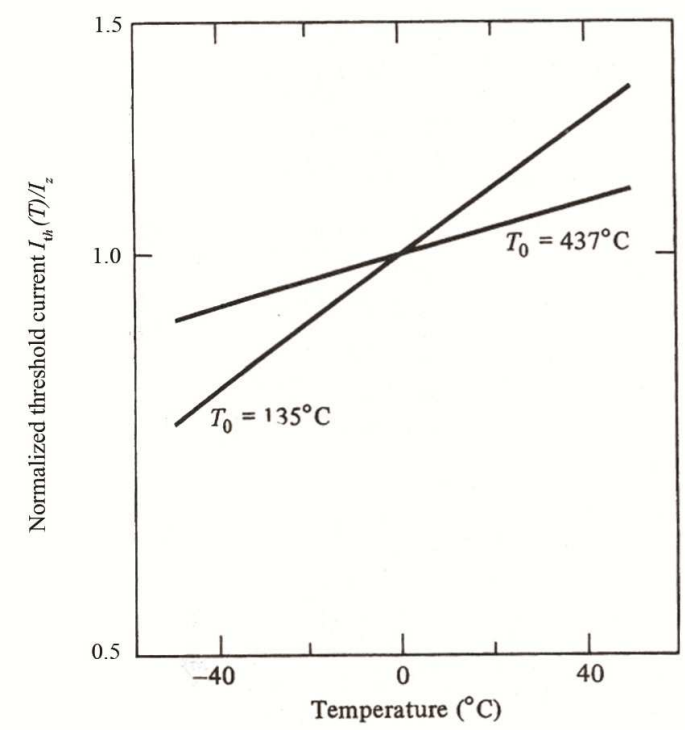

Figure 24. Variation with temperature of the threshold current I_{th} for two types of laser diodes, which are a conventional stripe-geometry GaALAs laser diode, $T_0 = 135C^o$, and GaALAs quantum-well heterostructure laser at, $T_0 = 437C^o$ [7].

This figure shows also the temperature dependence of I_{th} for GaALAs quantum-well heterostructure lasers. For these lasers, T_0 can be as high as 437 C^o. The threshold variation for this particular laser type is 0.23 percent/C^o. Experimental values of T_0 for 1300-nm InGaAsP lasers are typically 60-80 K (333-353 C^o).

3.2.2 The emission wavelength 1300 and 1550 nm:

Allen et al [28] chose the 1310-nm region for two reasons. First, the reflectance is about an order of magnitude greater at this wavelength than at 1550 nm. Second, driven by the cable TV market, fibre-optic technology supporting operation in the 1310-nm band has recently reached a maturity level such that these components are economical and reliable.

Wree et al [29] recently considered that the reasonable assumptions for component specifications used in 10.7 Gb/s optical transmitter-receiver for free-space system are: the wavelength of the laser is 1550 nm , and both satellites have 10 cm diameter apertures for the optical path length which is 46000 km.

Phillips et al [30, 31] demonstrated the possibility of employing an optically preamplified receiver for the purposes of intersatellite laser communication employing PPM. An optically preamplified on-off keyed (OOK) non-return to zero (NRZ) intersatellite system employing erbium-doped fibre amplifiers (EDFAs) was proposed by Phillips et al [30, 31]. They found that operation at a particular wavelength, which is normally between 1.53 and 1.55 μm, is required by the choice of an erbium-doped fibre amplifier (EDFA). Thus, feasibility of their system is dependent on the development of high power, and highly directional, laser sources for deployment at the transmitter. As a result of corresponding to a low loss wavelength region in silica optical fibre, sources at wavelength 1.55 μm are in common use in optical fibre communications.

Ferrier et al [33] concluded that Marconi Space Systems are considering the use of 1.55 μm distributed feedback lasers (DFB) and operation with a 100 Mbit/s data rate for a heterodyne detection space communications system. A breadboard was developed to simulate a Geo-Geo intersatellite link meeting post 2000 telecommunication traffic requirements. On the other hand, they mentioned that InGaAsP lasers operating at 1.55μm which utilize the distributed feedback (DFB) structure were existed in 1990.

Mikhrin et al [40] reported on GaAs-based broad area (100 µm) 1.3 µm quantum dot (QD) lasers with high CW output power (5 W) and efficiency (56%). The reliability of the devices has been demonstrated beyond 3000 h of CW operation at 0.9 W and 40 ℃ heat sink temperature with 2% degradation in performance. P-doped QD lasers with a temperature-insensitive threshold current and differential efficiency up to 80 ℃ have been realized.

Eric et al [41] simulated a transmission data link using a high speed digital signal to modulate a 1300 nm laser diode. A Nd:YAG laser was used to simulate ionizing effects induced by transient particle irradiation on the laser diode by creating carriers only in the laser cavity. With this method, calibration of ionizing effects, error amplitude and influence of operational parameters of the link (frequency, amplitude of modulation...) have been studied.

Rabinovich et al [42] considered that free-space optical links (lasercomm) are finding increasing use for commercial systems and are being considered for military systems. The narrow divergence and high bandwidth of optical beams enable point-to-point data links at rates exceeding 1 Gbit/s. However, these links require large telescopes, lasers, and highly accurate pointing systems to work. There are many situations in which one end of the link cannot accommodate the weight of a lasercomm terminal. These asymmetric links often have lower data requirements than a conventional lasercomm link because the smaller platform may have the capacity for only a moderate (1 to 100 Mbit/s) data rate sensor. An optical link may still be desirable in these cases because rf terminals for these data rates would be large, rf spectrum allocation may be limited, and because optical links are difficult to intercept.

Rabinovich et al [42] demonstrated a 1550-nm eye-safe, free-space optical communications link at rates up to 5 Mbits/s over a distance of 2 km in the Chesapeake Bay, using quantum-well-based modulating retroreflectors. Tests were conducted under various atmospheric conditions over a period of about a year. The experimental and theoretical link budgets were compared and statistical measurements of the effects of scintillation were collected.

3.3 Design of the Transmitter:

As can be seen, this research work is concerned with an analysis of intersatellite links in free space, with optical links using laser sources being considered in particular. Therefore, a detailed literature review for two types of sources which are in use at present: semiconductor laser diodes (SLDs) and light emitting diodes (LEDs), and comprehensive treatments of the major aspects of laser diodes have been presented. In addition, various techniques for modulating the output of a light source have been considered. With a semiconductor light source, such as the SLD or LED, the light output can be modulated by varying the drive current. However, some form of external modulator has to be used for solid-state and gas lasers because they are usually continuous wave (CW) devices. Therefore, a comprehensive literature review of Mach-Zehnder interferometer as an external modulator has been presented in the 2nd chapter to check the possibility of using it in such links. Since Mach-Zehnder interferometer is used as an external modulator at high speed, which is usually more than 1 Gb/s, it should be noted that some modifications have to be done with a Mach-Zehnder interferometer to be used as an external modulator in such links. These modifications have been mentioned into the previous chapter.

These treatments show that laser diodes have many advantages compared with LEDs for many applications: high electrical to optical efficiencies; small size; tightly focused beam; the optical output from a laser diode is coherent and thus the output beam is very directional, whereas that from an LED is non-coherent and hence the output radiation has a broad spectral width. In addition, it is possible to adapt the technology used in fibre optic links to free-space communications and so multi-Gbit/s transmission is possible using readily available integrated driver chips. In optical fibre communications, it is common practice to modulate a c.w. laser with an external Mach-Zehnder interferometer [6]. As these devices operate at a wavelength of 1.55 μm, this must be the wavelength of operation for the link.

On the other hand, investigations have been carried out to select the appropriate emission wavelength of the laser source and thus the comprehensive literature survey and in-depth analysis have been done. These studies considered that free-space optical links (lasercomm) are finding increasing use for commercial systems and are being considered for military systems. The narrow divergence and high bandwidth of optical beams enable point-to-point data links at rates exceeding 1 Gbit/s. However, these links require large telescopes, lasers, and highly accurate pointing systems to work.

These investigations reveal that using 1.55 μm as an emission wavelength is receiving a great deal of attention, and thus the suitable semiconductor material should be InGaAsP. This is because the wavelength 1.55 μm free-space optical communications link achieved significant results compared with 1.3 μm under various atmospheric conditions over a time period of about a year. Additionally, the wavelength of 850 nm that is working with vertical-cavity surface-emitting laser (VCSEL) and the semiconductor material is GaAsP has a too low power ≈ 5 mW. Further investigations have been presented in the 4th chapter to link between selecting the emission wavelength and the material of the light source with the cut-off wavelength and the material of the detector. However, it should be noted that although the emission wavelength of the light source does not commonly equal to the cut-off wavelength of the detector which is made of the same material of that light source is made because the emission wavelength can be changed by doping the semiconductor material with impurities and hence changing its band-gap. However, it is important to mention that the light source and detector in such links are made by the same semiconductor material that is InGaAsP and hence the cut-off wavelength equals the emission wavelength which is 1550 nm.

3.4 Conclusion:

This chapter highlighted the importance of using laser diodes as a light source in optical intersatellite links in space. The laser diode has many advantages over many applications. These advantages are: small size, high electrical to optical efficiencies, tightly focused beam, it is possible to adapt the technology used in fibre optic links to free-space communications and so multi-Gbit/s transmission is possible using readily available integrated driver chips. Therefore, comprehensive treatments of the major aspects of both two types of sources, which are in use at present: semiconductor laser diodes (SLDs) and light emitting diodes (LEDs), were presented in this chapter. This, in turn, support selecting the appropriate emission wavelength and the suitable semiconductor material of the laser source to be used in free space links and speed of 1 Gbit/s.

As a conclusion, initial assumption has been considered that the input speed of the link is of the order of 128 Mbit/s and the output speed is of the order of 1 Gbit/s. Therefore, work has been carried out to establish the model of the transmitter to be used in free space links and speed of 1 Gbit/s through selecting the appropriate emission wavelength of the laser source and suitable semiconductor material that is used in fabricating this source. These investigations reveal that the suitable emission wavelength is 1.55 μm and thus the suitable semiconductor material should be InGaAsP. This information represents the main goal of designing the transmitter in such links.

4. The model of the link (Receiver (RX))

4.1 Introduction:

In the field of high bit rate long distance optical transmissions, photoreceivers providing both high sensitivity and high bandwidth are of great interest. The use of optical preamplification can be attractive in this case, since it leads to separately optimise the noise performance of the receiver (mainly limited by the noise of the optical amplifier) and its speed (only given by the photodiode bandwidth). In other words, in order to obtain maximum sensitivity, an optically preamplified receiver must be optical amplifier noise limited rather than thermal noise limited.

As mentioned in chapter 2, an optical receiver consists of a photodetector, an amplifier, and signal-processing circuitry. Therefore, the basic structure of an optical receiver which consists of: a photodiode, a low-noise preamplifier, the front-end, feeds further amplification stages, the post-amplifier, before filtering. The following figure shows the basic structure of an optical receiver:

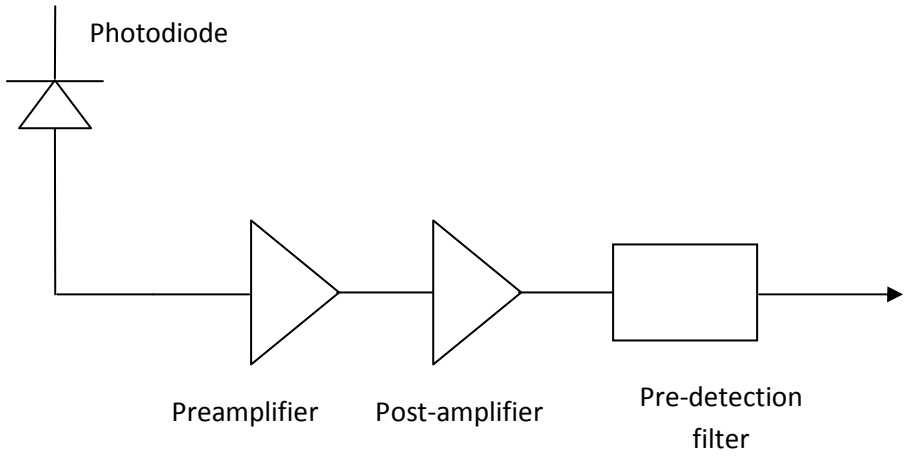

Figure 25 . The basic structure of an optical receiver

As can be seen, an optical receiver converts the received optical energy into an electric signal, and then amplifies it to a large enough level so that it can be processed by the electronics following the

receiver amplifier. Comprehensive treatments of the major aspects of an optical receiver are presented in various books [6-7, 43-57].

This basic structure can be considered as a fundamental base for design of the receiver in optical intersatellite links in free space. Therefore, this chapter is concerned with using an optically preamplified receiver for such links. It looks at a comparative review with an in-depth analysis between PIN photodiode and avalanche photodiode (APD) which is extensively presented and conducted in order to select the appropriate detector for the receiver through checking the possibility of using avalanche photodiodes (APDs) or PIN photodiodes with semiconductor optical amplifier (SOA), and to support selecting the appropriate semiconductor material that could be used in fabricating the suitable photodetector to be used in free space links and speed of 1 Gbit/s. in addition, a computer simulation model (using MCAD) has been carried out to examine the noise performance of an optical receiver and hence determine its sensitivity and the number of received photons in such links. This information will form the main goal of designing the receiver in such links.

4.2 Comparative Review:

4.2.1 Avalanche Photodiode (APD) and PIN Photodiode:

Cryan & Unwin [32] identified the photodetector as a device that performs the opto-electronic conversion operation in which the optical signal at the receiver is converted into an electrical signal for detection. They considered two types of detectors for direct detection optical satellite systems which are: Photomultiplier Tube and Avalanche Photodiode (APD). The photomultiplier has a very large internal gain (10^6), and so the additive Gaussian noise of the pre-amplifier is effectively eliminated and an extremely low dark current. High bias voltages and a relatively large electrical power requirement limit its appeal. The avalanche photodiode (APD), which is the solid state equivalent of a photomultiplier tube, is compact, requires low bias voltages and has lower power consumption. However, the additive receiver noise can no longer be ignored because APDs have lower gains. In addition, the gain induced excess noise is significant for an APD because the avalanche process is much noisier than the photomultiplier process. In spite of this, the APD is the detection device commonly used as the advantages overshadow the disadvantages.

Detailed literature reviews of APD and PIN photodiodes and the most important parameters that determine the characteristic and the performance of these photodiodes have been presented in chapter 2 in order to help selecting the appropriate detector that could be used with semiconductor optical amplifier for the receiver, and to support selecting the appropriate semiconductor material that could be used in fabricating the suitable photodetector in optical intersatellite link. Comprehensive treatments of the major aspects of both types of photodiodes are presented in various books and journals [6-15, 58-59].

Sibley [6] illustrated a comparison between PIN and APD photodiodes through calculating the sensitivity of analogue and digital receiver using an APD photodiode, and compared it with that of the same receiver using a PIN photodiode. The results show that a considerable increase in sensitivity

results by using an APD with a noisy digital receiver, compared with that by using a PIN detector. However, since the total receiver noise is dominated by the APD noise and hence any reduction in preamplifier noise will not generate a considerable change in sensitivity, the advantage is significantly reduced for the low-noise receiver. With a PIN detector, the total receiver noise is dominated by the preamplifier noise and hence a significant change in sensitivity results from a reduction in preamplifier noise. These results show that an APD detector is preferable to a PIN with noisy analogue receivers. However, the advantage of using an APD is significantly reduced for the low-noise analogue receiver and thus its use is a disadvantage. This is because a high level of multiplied shot noise comes from a standing photocurrent which is generated by the average received power. Therefore, it can be generally concluded that the sensitivity of a noisy preamplifier is increased by using an APD detector.

Keiser [7] summarized some general operating characteristics of Si, GE, and InGaAs photodiodes as comparisons between them in the following tables:

Parameter	Symbol	Unit	Si	Ge	InGaAs
Wavelength range	λ	nm	400-1100	800-1650	1100-1700
Responsivity	R_o	A/W	0.4-0.6	0.4-0.5	0.75-0.95
Dark Current	I_D	nA	1-10	50-500	0.5-2.0
Rise time	τ_r	ns	0.5-1	0.1-0.5	0.05-0.5
Bandwidth	B	GHz	0.3-0.7	0.5-3	1-2
Bias voltage	V_B	V	5	5-10	5

Table 6. Generic operating parameters of Si, Ge, and InGaAs PIN photodiodes

Parameter	Symbol	Unit	Si	Ge	InGaAs
Wavelength range	λ	nm	400-1100	800-1650	1100-1700
Avalanche gain	M	-	20-400	50-200	10-40
Dark Current	I_D	nA	0.1-1	50-500	10-50 $@M=10$
Rise time	τ_r	ns	0.1-2	0.5-0.8	0.1-0.5
Gain. Bandwidth	$M.B$	GHz	100-400	2-10	20-250
Bias voltage	V_B	V	150-400	20-40	20-30

Table 7. Generic operating parameters of Si, Ge, and InGaAs avalanche photodiodes

As can be seen, depending on the integrated photodiode the spectrum ranging from 400 – 1100 nm (Si diodes), 1100 – 1650 nm (InGaAs diodes), or 800 – 2100 nm (Ge diodes) can be detected very efficiently up to a bandwidth of 3.5 GHz. In addition, Keiser [7] concluded that relatively inexpensive solutions for short-distance links are provided by Si devices that operate around 850 nm. InGaAs-based devices are used for longer links as an operating in the 1300-nm and 1550-nm windows is usually required for these links.

Therefore, according to these considerations, these studies [6-7, 43-57] and further investigations reveal that using a PIN photodiode with semiconductor optical amplifier (SOA) is receiving a great deal of attention for using in optical intersatellite links in free space, because of an APD photodiode has multiplication that causes increase of excess noise, which are dark and signal noise, and poor bandwidth. In contrast, a PIN photodiode has a very good bandwidth and has a lower excess noise than APD photodiode because it does not have multiplication. In addition, using a PIN photodiode with semiconductor optical amplifier (SOA) has a very good bandwidth, multiplication and easy of use. However, using an APD photodiode with SOA is not sufficient as the noise with the signal will be highly amplified.

As regards to the appropriate semiconductor material that could be used in fabricating the PIN photodiode, previous studies [6-15, 58-59] and current investigations as a comprehensive comparison between Si, Ge and InGaAs have been carried out in order to select the appropriate semiconductor material that could be used in fabricating a photodiode and simultaneously should be suitable with the emission wavelength which is 1.55 µm. These comparisons are presented through the following points:

- The silicon can not be used in such links because it is transparent for the operation wavelength 1.55 µm.
- InGaAs has the highest responsivity at the wavelength of interest. As can be seen by the figure 6 in chapter 2/ section 2.3.
- In practice, it's difficult to fabricate and control devices with gains above 15. So, InGaAs, which has the lowest multiplication, is the best in terms of control and multiplication of excess noise.
- InGaAs has the lowest bias voltage. This is the main problem for Si that needs very high bias voltage.
- By using the separate-absorption-and-multiplication (SAM) to InGaAs APDs or PINs , InGaAs has high performance:

  To improve the performance of InGaAs APDs or PINs various complex device architectures have been devised. One widely used structure is the separate-absorption-and-multiplication (SAM) APD configuration.

The following figure shows cross-section of the multi-quantum well (MQW) SAM-APD [7]:

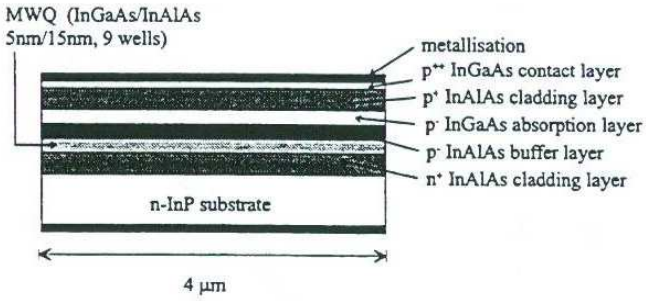

Figure 26. Cross-section of the multi-quantum well (MQW) SAM-APD [7]

This structure uses different materials in the absorption and multiplication regions, with each region being optimized for a particular function. Variations on the SAM structure include adding other layers to the device. These include:

1. Using a grading layer between the absorption and multiplication regions to increase the response time and bandwidth of the device.
2. Adding a charge layer that provides better control of the electric field profile.
3. Incorporating a resonant cavity that decouples the optical and electrical path lengths to achieve high quantum efficiencies and wide bandwidths simultaneously.

- InGaAs has the lowest rise time. So, it is faster than Si and Ge.
- Low band-gap means that photodiodes exhibit a high leakage current (>100 nA). InGaAs has the biggest band-gap (1.42 eV) and direct as well. So, it has the lowest leakage current and is used in long-haul routes.
- At long wavelengths, > 1 µm, detectors for 1.3 and 1.55µm wavelengths must be made out of low band-gap materials. Germanium has a band-gap of 0.67 eV, corresponding to a cut-off wavelength of 1.85 µm, and so would appear to be a suitable material. However, the low

band-gap means that Ge photodiodes exhibit a high leakage current (> 100 nA). As the dark current is an additional source of noise, and so Ge PIN photodiodes are rarely used in long-haul routes. The InGaAsP emits light in the band 1.0-1.7 μm. Thus detectors made of a similar material should respond to 1.3 or 1.55 μm light.

As mentioned in the 3rd chapter the cut-off wavelength preferably equals the emission wavelength which is 1550 nm, and hence the light source and detector in the link are made by the same semiconductor material that is InGaAsP. In addition, according to the above-mentioned considerations, InGaAsP is the best choice as a semiconductor material for using in fabricating a PIN photodiode in optical intersatellite links in free space. Before moving on to examine the noise performance and the sensitivity of the selected receiver, it is important to discuss in detail the SOA as a second element of the receiver and define the main parameters that determine its performance.

4.2.2 Semiconductor optical amplifier (SOA) as an optical amplifier:

There is currently much interest in all optical amplification for applications in a signal regeneration and receiver preamplification. Therefore, an optical amplifier is receiving a great deal of attention for using in an optical receiver as a preamplifier. There are two main types of optical amplifiers in use at present: semiconductor optical amplifiers (SOAs) and active-fibre or doped-fibre amplifiers (DFAs). Comprehensive treatments of the major aspects of both types of optical amplifier are presented in various books and journals [6-7, 60-69].

The most popular approach is based on erbium doped-fibre amplifiers (EDFAs) and leads to very good sensitivities around -40dBm input power at 10 Gbit/s for 10^{-9} bit error rate. This represents a very large improvement compared to the best photodiode-transistor sensitivity of -23.5 dBm, and also compared to the record APD sensitivity of -29.4 dBm reported recently at the same bit rate [45]. However, the EDFA configuration is rather bulky, complex (as it often includes two amplifying stages) and expensive. Owing to their compactness and their compatibility with further integration on semiconductor substrate, semiconductor optical amplifiers (SOA) have attracted attention for this application, where they stay perfectly linear.

The SOA is a highly versatile component that can be deployed for a wide range of amplification and routing. In addition, it has been considered as a better and widely used amplifier than DFA. This is because the SOA has many advantages compared with DFA: fewer components; less power consumption; more compact; more rapid gain response; higher performance and higher functionality; and the possibility of working in both 1300 nm and 1550 nm low-attenuation windows; can be easily integrated on the same substrate as other optical devices. Therefore, the SOA is receiving a great deal of attention to be used as an optical preamplifier in the receiver in the link, and thus the most significant parameters has been extensively presented within this section in order to determine the

performance of the SOA and hence supporting the examination of the noise performance for the receiver.

As mentioned in the 2nd chapter, the two major types of SOAs are the resonant, Fabry-Perot amplifier (FPA) and the nonresonant, travelling-wave amplifier (TWA).

FPA: they are easy to fabricate, the optical signal gain is very sensitive to variations in amplifier temperature and input optical frequency. Thus, they require very careful stabilization of temperature and injection current.

TWA: these devices have been used more widely than FPAs because they have a large optical bandwidth, high saturation power, and low polarization sensitivity. Since the 3-dB bandwidth of TWAs is about three orders of magnitude greater than that of FPAs, TWAs have become the SOA of choice for networking applications. Therefore, TWA is the appropriate choice of the SOA to be used in the link.

External current injection is the pumping method used to create the population inversion needed for having a gain mechanism in SOAs. This is similar to the operation of laser diodes. In addition, there are five main parameters which are used to characterize SOAs [64]:

1. Gain (G_s).
2. Gain Bandwidth.
3. Saturation Output Power (P_{sat}).
4. Noise Figure (NF).
5. Polarization Dependent Gain (PDG).

As a result of the physical limitations of the various processes occurring inside the SOA, an ideal SOA is impossible to implement. However, an ideal SAO can be achieved theoretically through the following conditions:

- A SOA must have the highest gain suitable to the application.
- A SOA must have a wide optical bandwidth so that can amplify a wide range of signal wavelengths.
- A SOA must have very high saturation output power to accomplish good linearity and to maximize its dynamic range with minimum distortion in order to avoid of the effects of gain saturation which causes undesirable distortion to the output.
- A SOA must have a very low noise figure (the physical limit is 3 dB) to minimize the amplified spontaneous emission (ASE) power at the output.
- A SOA must have very low polarization sensitivity to minimize the gain difference between the transverse-electric (TE) and transverse-magnetic (TM) polarization.

1. Gain (G_s):

One of the most important parameters of an optical amplifier is the signal gain or amplifier gain G, which is defined as:

$$G = \frac{P_{s,out}}{P_{s,in}} \tag{78}$$

Where $P_{s,out}$ and $P_{s,in}$ are the input and output powers, respectively, of the optical signal being amplified. The radiation intensity at photon energy h_v varies exponentially with the distance traversed in a lasing cavity.

As mentioned previously, an optical amplifier is essentially a laser without feedback. Therefore, SOAs amplify incident light through stimulated emission; the same mechanism used by semiconductor lasers. The optical gain has been considered as the most useful feature of SOA and it can be realized when the amplifier is pumped to accomplish population inversion. The optical gain depends on the local beam intensity at any point inside the amplifier, as well as its dependence on the frequency (or wavelength) of the incident signal. Therefore, the single pass optical gain (Gs) below saturation, where spectral effects and nonuniform distribution of the carrier density are not considered, is approximately determined by [64]:

$$G_s \propto e^{\Gamma(g_m-\alpha)L} = e^{\Gamma[g_0(N-N_0)-\alpha]L} = e^{\Gamma\left[g_0\left(\frac{\eta_i I\tau_s}{eLwd}-N_0\right)-\alpha\right]L} \quad (79)$$

Γ is the optical confinement factor, α is optical loss, g_m is the material gain, g_o is the gain coefficient, L is the cavity length, η_i is the current injection efficiency, W is the active width, d is the thickness of the active region in which the carriers are confined, e is the electronic charge, I is the operating current, N is the carrier density at the operating current I , N_o is the carrier density at transparency, τ_s is the spontaneous recombination lifetime of the carriers. In addition to, it can be indicated by this equation that a high gain may be accomplished with a high injection current, a large optical confinement, a long cavity, a multiple quantum well (MQW) structure, or a combination of them.

2. Gain Bandwidth:

The gain bandwidth is defined as the full width at the half-maximum (FWHM) height of the gain spectrum. Optical communication systems prefer the use of amplifiers with a relatively large bandwidth because the gain is almost constant over the entire bandwidth. A 3dB bandwidth can exceed 60 nm for quantum-well SOAs, where it is about 45 nm for bulk SOAs. The band filling effect increases the injection current which, in turn, will broaden the bandwidth that depends inversely on

the optical confinement and the cavity length. Moreover, wider bandwidth can be achieved by MQW SOAs compared with bulk SOAs.

3. Saturation Output Power:

The saturation output power is defined as the output power for which the amplifier gain is reduced by a factor of 2 (or by 3 dB) from its unsaturated value. It depends inversely on the optical confinement.

4. Noise Figure (F_n):

The amplifier noise figure (F_n) is defined as the ratio between the input signal-to-noise ratio of the amplifier $(SNR)_{in}$ and the output signal-to-noise ratio of the amplifier $(SNR)_{out}$. This parameter quantifies the degradation of the signal-to-noise ratio (SNR) of the amplified signal which is caused by spontaneous emissions that add to the signal during its amplification in all laser amplifiers.

The following sources essentially attribute the noise:

(1) Amplified signal shot noise.

(2) Spontaneous emission shot noise.

(3) Signal-spontaneous beat noise.

(4) Spontaneous-spontaneous beat noise.

(5) Signal excess noise.

The sources (1) and (2) are related to several detector parameters. The shot noise levels are usually 20 dB smaller than the beat noise. The spontaneous-spontaneous beat noise prevails in the low output power region, while the signal-spontaneous beat noise dominates in the high output power region. The SNR of the amplified signal is degraded by a factor of 2 (or 3 dB) for an ideal detector whose performance is limited by the shot noise only. As a result of the intrinsic internal loss of the SOA and the lower coupling efficiency on its input side, a SOA practically exhibits a higher noise

level. However, the SOA has the same theoretical lower noise figure limit of 3 dB as an EDFA. For most SOAs, F_n is typically in the range of 6-10 dB. In addition, an optical amplifier must have an F_n as low as possible to be used in optical communication systems. NF is also dependent on the operating wavelength, the operating current, and the input signal power [64].

5. Polarization Sensitivity:

The confinement factor and the effective mode index are different for each of the transverse-electric (TE) and transverse-magnetic (TM) polarizations. This leads to the amplifier gain differing for both of these polarizations and hence makes the gain sensitivity to input signal polarization of the SOA an undesirable characteristic. This feature makes the amplifier gain dependent on the polarization state of the input beam. The polarization sensitivity of SOAs can be reduced to less than 1 dB by using several possible approaches in geometric design of the active layers combined with a proper use of tensile strain (bulk or multi-quantum well).

4. 3 Design of the receiver:

As mentioned earlier in this chapter, the basic structure of an optical receiver consists of: a photodiode, a low-noise preamplifier, the post-amplifier, filtering. Moreover, PIN photodiode and SOA have been received a great deal of attention to be used as a suitable photodetector and amplifier, respectively, in the receiver for optical intersatellite links in free space.

In these processes, errors in the interpretation of the received signal can result from various noises and distortions which will unavoidably be introduced. The random noises associated with the photodetection process adversely affect the current generated by the photodetector that is generally very weak. When this electric signal output from the photodiode is amplified, further corruption of the signal will be caused by additional noises resulting from the amplifier electronics. Therefore, noise considerations are significant in the design of optical receivers, because the lowest limit for the signals that can be processed is generally set by the noise sources operating in the receiver.

A computer simulation model (using MCAD) has been performed in such links using three different coding schemes: multiple pulse position modulation (MPPM); digital pulse position modulation (DPPM); Dicode pulse position modulation (Dicode PPM). This simulation examines the noise performance of the selected optical receiver, and hence determines its sensitivity and the number of received photons for each coding scheme (the simulation is attached in the appendix E).

4. 3.1 Simulation Model:

These systems are operating in space at a wavelength of 1.55µm, 3 bits PCM and PCM data rates of 1 Gbit/s. A High speed InGaAs PIN photodiode C30637, @ 1550 nm (optoelectronics. PerkinElmer) and an SOA-High Power Operation (IEEE 802.3av) have been used as a photodetector and amplifier, respectively, (Datasheets are attached in appendixes A and B, respectively). The receiver has been considered as a linear channel and the a.c. equivalent circuit of an optical receiver shown in the following figure:

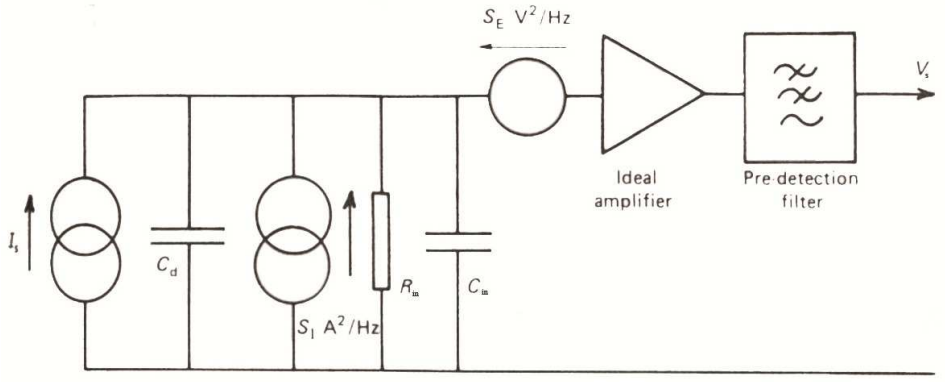

Figure 27. A.c. equivalent circuit of an optical receiver

The photodetector is modeled by an ideal current source, I_s, shunted by the detector capacitance, C_d.this feeds the parallel combination of R_{in} and C_{in}, modeling the input impedance of the preamplifier. A single voltage amplifier, with transfer function $A(\omega)$, models the pre- and post-amplifiers and the output of which feeds the pre-detection filter. While initially neglecting the photodiode noise, the only noise in the receiver will be resulted by the preamplifier. The mean-square equivalent input noise current (A^2) is expressed by [6]:

$$\left\langle i_n{}^2 \right\rangle_c = \left(S_I + \frac{S_E}{R_{in}{}^2} \right) BI_2 + \left(2\pi C_T\right)^2 S_E B^3 I_3 \qquad (80)$$

Where S_I is a shunt noise generator (A^2/Hz), modeling the noise current due to the preamplifier first stage and the photodiode load resistor. S_E, the series noise generator(V^2/Hz), models the

preamplifier series noise sources. B is the PCM bit rate , which is 10^9 bits in the link. C_T is the total input capacitance which equals ($C_d + C_{in}$). I_2 and I_3 are bandwidth integrals which depend on the shape of the input and output pluses. As the receiver uses a pre-detection filter that generates pulses with a raised-cosine spectrum, $\alpha = 1$ (where α is the fraction of the time-slot occupied by the rectangular pulses) and thus the pulses fill the whole of the slot and having full-width or non-return-to zero, NRZ, rectangular pulses. The following table shows values of I_2 and I_3 for different rectangular input pulses [6]:

Rectangular input pulses										
α	0.1	0.2	0.3	0.4	0.5	0.6	0.7	0.8	0.9	1.0
I_2	0.376	0.379	0.384	0.392	0.403	0.417	0.436	0.463	0.501	0.564
I_3	0.030	0.031	0.032	0.034	0.036	0.040	0.044	0.053	0.064	0.087

Table 8. Values of I_2 and I_3 for different rectangular input pulses

Therefore, by using table 8, the values of I_2 and I_3 are $I_2 = 0.564$ and $I_3 = 0.087$ for $\alpha = 1$.

It can be noted that the preamplifier noise consists of a frequency-independent term of magnitude S_I (A^2/Hz), and an f^2 noise term of magnitude S_E (V^2/Hz). However, the series noise generator (S_E) has a negligible effect on the receiver noise in free space for PCM data rate of 1 Gbit/s because it is insignificant compared with S_I and the SOA shot noise which are much higher than S_E. Therefore, the mean-square equivalent input noise current (A^2) becomes:

$$\left\langle i_n^{\,2} \right\rangle_c = S_I B I_2 \qquad (81)$$

As mentioned before, S_I models the noise current due to the preamplifier first stage and the photodiode load resistor. However, Assuming the photodiode load resistor ($R_L = 50\Omega$, InGaAs PIN

photodiode C30637) is much smaller than the amplifier input impedance ($R_f = 50 \times 21 = 1050\Omega$ as $G = 20dB$ the Gain of SOA (IEEE 802.3av)). Consequently, the thermal noise of the photodiode load resistor is much greater than that of the amplifier input. Therefore, the shunt noise generator, S_I, which is considered here as the noise delivered to the input of the SOA from the source, N_I, equals the mean-square thermal (Johnson)noise current of load resistor and is given by:

$$S_I = N_I = \frac{4K_B T}{R_L} = 3.312 \times 10^{-22} \qquad (A^2/Hz) \qquad (82)$$

Where ($K_B = 1.38 \times 10^{-23} JK^{-1}$) is Boltzmann's Constant, ($T = 300$ Kelvin) is the absolute temperature. It should be noted that using different coding schemes requires using different bit rates. Thus, the mean-square equivalent input noise current becomes:

$$\left\langle i_n^{\,2} \right\rangle_c = \frac{4K_B T}{R_L} B_C I_2 \qquad (A^2) \qquad (83)$$

Where B_C is the bit rate which takes different values, for 3 bits of PCM, of $\frac{5}{3}B$, $\frac{2^3}{3}B$ and $2B$ for MPPM(5,2), DPPM and Dicode PPM , respectively. The results have been made for these three coding schemes as can be seen in table 10.

As discussed in chapter 2, the photodiode noise falls into two main categories- invariant dark current noise, and signal-dependent shot noise. In a PIN receiver the signal-dependent noise is often insignificant compared with the circuit noise. Taking into consideration the photodiode noise, the total, signal-independent, equivalent input noise current which includes the noise from the photodiode dark currents and any preamplifier noise is given by [6]:

$$\left\langle i_n^{\,2} \right\rangle_T = 2qI_D B_C I_2 + \left\langle i_n^{\,2} \right\rangle_c \qquad (A^2) \qquad (84)$$

Where ($q = 1.602 \times 10^{-19} C$) is electron charge, and I_D is the dark current of PIN photodiode ($I_D = 1 \times 10^{-9} A$, InGaAs PIN photodiode C30637). The results have been made for the three used coding schemes as can be seen in table 10.

Before moving on to determine the sensitivity of the selected optical receiver in the link, it is important to mention that there is an extra noise from the SOA which is the input noise of the device itself, N_A, and is expressed as:

$$N_A = N_I (F - 1) = 2.3 \times 10^{-21} \qquad (A^2/Hz) \qquad (85)$$

Where F is amplifier noise factor ($NF = 10\log(F) = 9(dB)$ is the amplifier noise figure of SOA (IEEE 802.3av)).

In order to determine the sensitivity of the used optical receiver in the link, the mean optical power required, P , is given by [6]:

$$P = \frac{Q}{R_o}(\sqrt{\langle i_n^{\,2} \rangle_T} + qB_C I_2 Q) \qquad (W \ , \ dB_m) \qquad (86)$$

Where Q is the signal-to-noise ratio parameter, Q=6 for an error rate of 1 in 10^9 pulses. R_o is the responsivity of PIN photodiode ($R_o = 0.95$ (*A/W*), InGaAs PIN photodiode C30637). The results have been made for the three used coding schemes as can be seen in table 10.

The signal-to-noise ratio parameter is expressed as:

$$Q = \frac{I}{\sqrt{\langle i_n^{\,2} \rangle_c}} = \frac{I}{\sqrt{\frac{4K_B T}{R_L} B_C I_2}} \qquad (87)$$

Where Q=6 for an error rate of 1 in 10^9 pulses, and $\langle i_n^{\,2} \rangle_c$ is already known. Thus, I which is the output current of PIN photodiode and given by:

$$I = Q\sqrt{\frac{4K_B T}{R_L} B_C I_2} \qquad (A) \qquad (88)$$

Thus, the received power is given by:

$$P_o = \frac{I}{R_o} \qquad (W) \qquad (89)$$

Therefore, the number of received photons is expressed as:

$$NP = P_o \lambda \frac{T_s}{h.c} \qquad (90)$$

Where λ is wavelength of operation (λ=1550 nm in the link), h is Planck's constant ($h = 6.624\times10^{-34}$ JS), c is velocity of light in a vacuum ($c = 3\times10^{8}$ m/s) and T_s is the slot time which takes different values for 3 bits of PCM of $\frac{3.T_b}{5}$, $\frac{3.T_b}{2^3}$ and $\frac{T_b}{2}$ for MPPM(5,2),DPPM and Dicode PPM, respectively. The results have been made for these three coding schemes as can be seen in table 10.

The following figure shows the flow chart of the aforementioned simulation for MPPM, DPPM and Dicode PPM, respectively, operating with 3 bits of PCM. This chart clarifies the process of the simulation and how the results have been yielded:

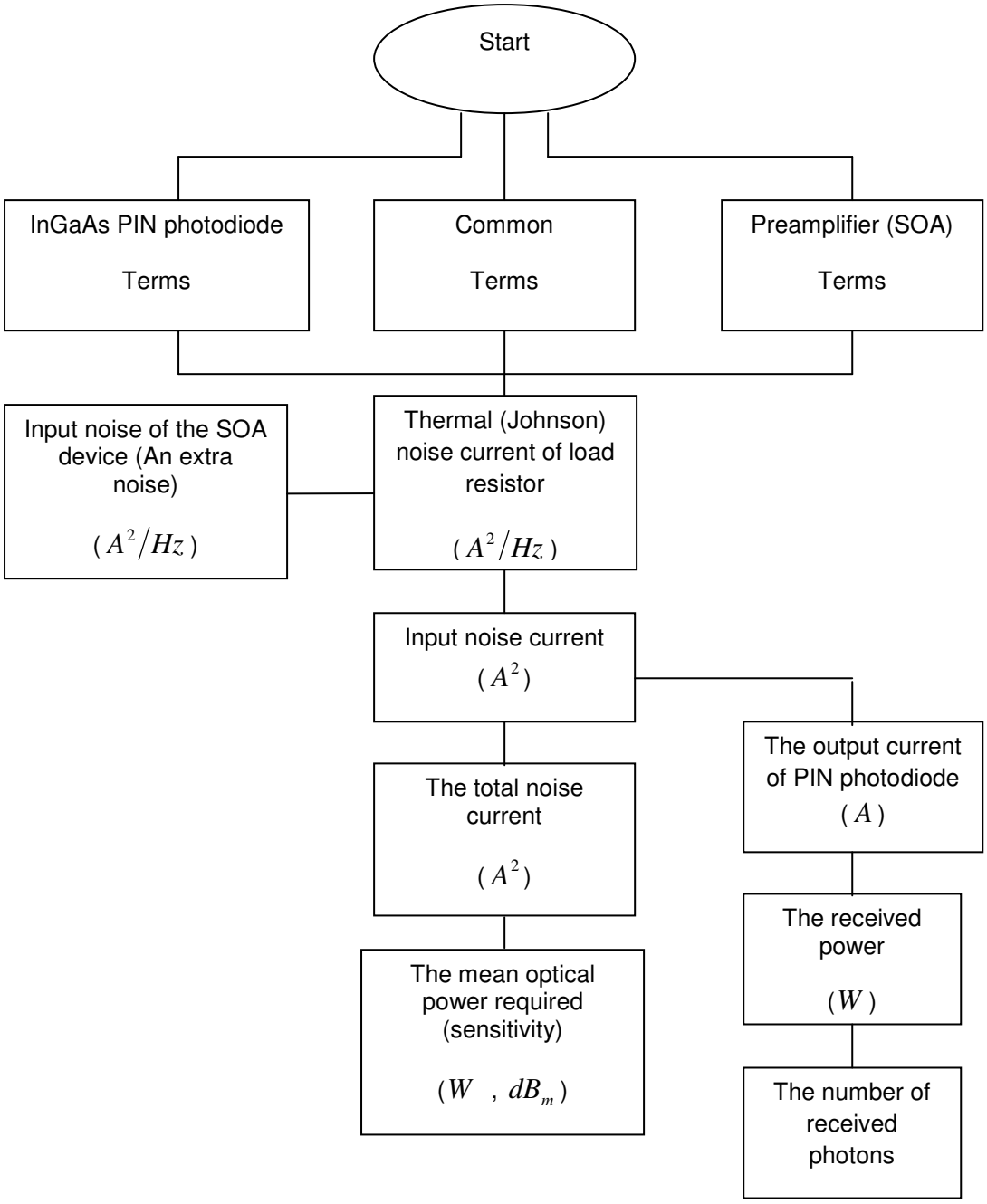

Figure 28. Flow chart of the simulation for examination of the performance of the used optical receiver with MPPM, DPPM and Dicode PPM coding 3 bits of PCM

As mentioned previously, A High speed InGaAs PIN photodiode C30637, @ 1550 nm (optoelectronics. PerkinElmer) and an SOA-High Power Operation (IEEE 802.3av) have been used as a photodetector and amplifier, respectively, (Datasheets are attached in appendixes A and B, respectively). Therefore, the simulation starts with SOA as preamplifier, PIN photodiode as photodetector and common terms. The following list of parameters shows these terms:

Preamplifier (SOA) (IEEE 802.3av) terms	
$G = 20dB$	Gain of SOA
λ =1550 nm	Wavelength of operation
$NF = 10\log(F) = 9(dB)$	Amplifier noise figure
$F = 7.943$	Amplifier noise factor
Common Terms	
$B = 10^9$	PCM bit rate
$T_b = 10^{-9}$	PCM bit time
$N = 3$	Number of PCM bits
$f_n = 10^6$	Channel bandwidth for free space
$q = 1.602 \times 10^{-19} C$	Electron charge
$K_B = 1.38 \times 10^{-23} JK^{-1}$	Boltzmann's Constant
$T = 300$ Kelvin	Absolute temperature
$h = 6.624 \times 10^{-34}$ JS	Planck's constant
$c = 3 \times 10^8$ m/s	Velocity of light in a vacuum
$B_C = \frac{5}{3}B, \frac{2^3}{3}B$ and $2B$	Bit rate for 3 bits PCM for MPPM(5,2), DPPM and Dicode PPM , respectively
$I_2 = 0.564$ and $I_3 = 0.087$	Bandwidth integrals
InGaAs PIN photodiode terms	
$I_D = 1 \times 10^{-9} A$	Dark current of PIN photodiode
$R_o = 0.95$ (A/W)	Responsivity of PIN photodiode @ 1550 nm
$R_L = 50\Omega$	Photodiode load resistor
$C = 0.4 \times 10^{-12} F$	Photodiode Capacitance

Table 9. List of parameters used in the simulation for examination of the performance of the used optical receiver with MPPM, DPPM and Dicode PPM coding 3 bits of PCM

The simulation results have been concluded by using the above parameters with the previous equations (82-90) in sequence in order to formulate the process of the simulation as shown in the aforementioned flow chart. These results are shown in table 10.

4. 3.2 Results and discussion:

The following table show summary of the results of the aforementioned simulation for MPPM, DPPM and Dicode PPM operating with 3 bits of PCM, in order to examine the noise performance of the selected optical receiver in the link, and hence determine its sensitivity and the number of received photons for each coding scheme (the simulation is attached in the appendix):

3 Bits PCM	MPPM	DPPM	Dicode PPM
Final Line Rate	1.7 ×PCM Data Rate (3 Bits)	2.7 × PCM Data Rate (3 Bits)	2 × PCM Data Rate (Fixed)
The Total Noise $\langle i_n^2 \rangle_T$, (A^2)	3.113×10^{-13}	4.981×10^{-13}	3.736×10^{-13}
The mean optical power required (sensitivity) $(W \ , dB_m)$	$3\cdot53\times10^{-6}(W\ )$ $-24\cdot523\ (dB_m)$	$4\cdot467\times10^{-6}(W\ )$ $-23\cdot5\,(dB_m)$	$3\cdot867\times10^{-6}(W\ )$ $-24\cdot126\,(dB_m)$
Slot Time (S)	6×10^{-10}	$3\cdot75\times10^{-10}$	5×10^{-10}
The number of received photons, *NP*	1.649×10^{4}	1.304×10^{4}	1.506×10^{4}

Table 10. Summary of the simulation results for examination of the performance of the used optical receiver with MPPM, DPPM and Dicode PPM, respectively, coding 3 bits of PCM

As can be seen, the final line rate for the MPPM (5, 2) scheme is 1.7 that of the PCM. This should be compared to DPPM that runs at a final line rate which is 2.7 times that of the original PCM data rate, and to Dicode PPM that has a fixed final line rate- twice the PCM rate.

Table 10 shows that the optical receiver offers the lowest total noise of 3.113×10^{-13} (A^2) when MPPM coding scheme is used because MPPM has the lowest speed and hence the lowest bandwidth requirement. The optical receiver used with DPPM coding scheme has a higher total noise of 4.981×10^{-13} (A^2) than that when Dicode PPM coding scheme is used (3.736×10^{-13} A^2) because Dicode PPM has lower speed and bandwidth than DPPM.

The optical receiver used with MPPM offers the best sensitivity because it needs the lowest main optical power required ($3\cdot53\times10^{-6}\,W$, $-24\cdot523\,dBm$) for an error rate of 1 bit in 10^9.In addition, the optical receiver used with Dicode PPM has better sensitivity than that uses DPPM coding scheme because it needs ($3\cdot867\times10^{-6}\,W$, $-24\cdot126\,dBm$) optical power required for the same error rate , whereas DPPM needs ($4\cdot467\times10^{-6}\,W$, $-23\cdot5\,dBm$) optical power required.

The optical receiver used with MPPM coding scheme has the largest number of received photons which is 1.649×10^4 (photons) because MPPM has the largest time slot width of 0.6 (ns). Dicode PPM has a time slot width of 0.5 (ns) and hence the optical receiver used with Dicode PPM has a higher number of received photons (1.506×10^4 Photons) than that uses DPPM (1.304×10^4 Photons).

4.4 Conclusion:

In the field of high bit rate long distance optical transmissions, photoreceivers producing both high sensitivity and high bandwidth are of great interest. The use of optical preamplification can be attractive in this case, since it results in separately optimise the noise performance of the receiver (mainly limited by the noise of the optical amplifier) and its speed (only given by the photodiode bandwidth).

A photodetector is needed at the receiver to convert the modulated light signal back into an electrical one. There are two types of detectors in use at present: avalanche photodiodes (APDs) or PIN photodiodes .The optimum choice depends on the wavelength of operation which, in turn, depends on how the laser source is to be modulated. In optical fibre communications it is common practice to modulate a continuous wave (CW) laser with an external Mach- Zehnder interferometer. As these devices operate at a wavelength of 1.55 µm, this must be the wavelength of operation for the link.

Comparative reviews and comprehensive treatments of the major aspects of both types of photodiodes have been presented to select the appropriate detector for the receiver through checking the possibility of using avalanche photodiodes (APDs) or PIN photodiodes with semiconductor optical amplifier (SOA), and to support selecting the appropriate semiconductor material that could be used in fabricating the suitable photodetector to be used in free space links and speed of 1 Gbit/s. These studies show that, unlike APD photodiodes, a PIN photodiode does not have multiplication and thus it has a lower excess noise and very good bandwidth. Whereas, an APD photodiode has multiplication that leads to increase of excess noise, which are dark and signal noise, and poor bandwidth. In addition, using an APD photodiode with SOA is not sufficient because the noise with the signal will be highly amplified. However, using a PIN photodiode with SOA has a very good bandwidth, multiplication and easy of use. Therefore, according to these considerations and investigations, using an optically preamplified receiver that consists of: a PIN photodiode as a photodetector, Semiconductor Optical Amplifier (SOA) as an amplifier, and a 3rd order Butterworth filter with central decision detection, is considered as a suitable design of the receiver to be used in optical intersatellite links in free space. Moreover, InGaAsP is the best choice as a semiconductor material to be used in fabricating a PIN photodiode in the link.

Since the lowest limit for the signals that can be processed is generally set by the noise sources operating in the receiver, noise considerations are significant in the design of optical receivers. Therefore, in order to examine the noise performance of the selected optical receiver, and hence determine its sensitivity and the number of received photons, a computer simulation model (using MCAD) has been carried out in such links and with using three different coding schemes for 3 bits of PCM: multiple pulse position modulation (MPPM); digital pulse position modulation (DPPM); Dicode pulse position modulation (Dicode PPM), respectively.

The results of this simulation show that the optical receiver offers the lowest total noise when MPPM coding scheme is used because MPPM has the lowest speed and hence the lowest bandwidth requirement. The optical receiver used with DPPM coding scheme has a higher total noise than that when Dicode PPM coding scheme is used. In addition, the optical receiver used with MPPM offers the best sensitivity as it needs the lowest main optical power required. The optical receiver used with Dicode PPM has better sensitivity than that uses DPPM coding scheme. Moreover, the optical receiver used with MPPM coding scheme has the largest number of received photons as MPPM has the largest time slot width. The optical receiver used with Dicode PPM has a higher number of received photons than the DPPM. Therefore, according to these considerations, it is concluded that the optical receiver, which uses PIN photodiode as a photodetector and SOA as an amplifier, used with MPPM coding 3 bits of PCM can be used in optical inter-satellite links in free space and PCM data rates of 1 Gbit/s.

5. The model of the link (Pulse Position Modulation Coding Schemes).

5.1 Introduction:

As mentioned in the last section of chapter 2, DPPM is currently the preferred coding scheme for use in optical inter-satellite links because it operates with very low average power and offers high sensitivity. However, it does suffer from a very large bandwidth expansion problem in that a scheme coding 5 bits of PCM will have a final line rate of 6.4 times the original PCM rate [16].This places a great strain on the processing electronics as the speed can be prohibitive. Comprehensive treatments of the major aspects of DPPM coding scheme are presented in various journals [70-95]

Many alternative coding schemes have been proposed that operate with a smaller bandwidth expansion. Of these, MPPM [16, 23-27] and Dicode PPM [20-22] appear to offer the lowest bandwidth expansion. The coding alphabet for DPPM and two alternative coding schemes, MPPM and Dicode PPM, has been presented in the last section of chapter 2. Additionally, basic information and previous comparisons between these three coding schemes in fibre optic have been discussed in chapter 2. These basic studies can be considered as a core concept to make a comprehensive comparison between these three coding schemes and hence select the appropriate and best coding scheme to be used in an optical intersatellite link in space.

In this chapter, work is presented to compare MPPM, DPPM and Dicode PPM coding schemes in terms of error weightings and coding efficiency through showing how the PCM error rate is affected by false alarm and erasure errors for MPPM, DPPM and Dicode PPM coding 3, 4, 5 and 6 bits of PCM. In addition, computer simulations models (using MCAD) have been carried out to compare these three coding schemes in terms of sensitivity and bandwidth efficiency.

Therefore, this chapter form this research project work is concerned with an in-depth analysis and comprehensive comparisons between these three coding schemes in terms of sensitivity, bandwidth efficiency, error weightings and coding efficiency. These comparisons support selecting the optimum PPM coding scheme to be used in optical intersatellite links in free space.

5.2 The importance of using PPM coding schemes in optical inter-satellite links:

Digital pulse position modulation (DPPM) is considered to be the most efficient modulation format for use in intersatellite laser communications when the ideal photon counting channel is utilised [96, 97]. It has also proved effective over the optical fibre channel when a threshold detection scheme is employed [98].

Cryan & Unwin [32] used the ideal photon counting channel as a model for optical detection in the deep space communications. This modulation format illustrated that the PPM format is the most efficient modulation format, and hence this efficiency has resulted in its widespread consideration for the optical satellite communications channel. In addition, the PPM format can be used to generate high peak power short duration pulses for semiconductor laser diodes which are both peak and average power limited and provided that the number of possible pulse positions or time slots is not as large as to lead to facet damage in the laser. This high peak power short duration pulses are easily distinguishable from background radiation and thermal noise.

Phillips et al [99] presented an original theoretical analysis for an optically preamplified direct-detection receiver employing the PPM transmission format in an optical fibre n-ary. They used the erbium-doped fibre amplifier (EDFA) as an optical preamplifier and the calculations were performed using physically realisable parameters and operating at a bit rate of 622 Mbit/s and a wavelength of 1.53μm. The results show that this receiver configuration with PPM system can surpass an equivalent PCM system by a 7.5 dB as a sensitivity benefit. In addition, a further demonstration was concluded by Phillips et al [99] that an optically preamplified PPM receiver can also offer sensitivities that significantly improve on the basic sensitivity limit of an optically preamplified PCM system and approach values achievable by coherent detection. This means that the theoretical sensitivity of a directly detected optically preamplified n-ary PPM system is equivalent to that of a shot noise limited coherent PCM system.

An optically preamplified on-off keyed (OOK) non-return to zero (NRZ) intersatellite system employing erbium-doped fibre amplifiers (EDFAs) was examined by Phillips et al [30,31], and hence the combination of optical preamplification, in particular erbium-doped fibre amplifiers (EDFAs), and PPM for an optical satellite communications receiver was investigated. An analysis is presented to help high bit rate operation for a PPM system employing threshold detection which is instead of employing a photon counting strategy and could be operated at high bit rates, thus allowing more efficient use of the wide bandwidth potential of optical intersatellite communications, whilst maximum likelihood detection is operated at much lower bit rates and has been considered as the common method of detecting optical PPM in the satellite channel. In addition, they mentioned that this presented analysis can be applied to semiconductor optical amplifiers, with some superficial modification [30, 31].

Phillips et al [30, 31] demonstrated the possibility of employing an optically preamplified receiver for the purposes of intersatellite laser communication employing PPM. The results showed that a possible receiver sensitivity of 13.5 photons/bit (at a BER of 10^{-6}) when operating at the STM-1 signalling bit rate of 155 Mbit/s, using conservative parameters and in the presence of background noise. This indicates to the considerable potential of the presented receiver formation for use in satellite communications. In addition, further demonstration was concluded by Phillips et al [30, 31] that receiver sensitivities up to 12.3 dB better than an equivalent EDFA OOK NRZ satellite receiver can be achieved by this threshold detection PPM scheme. Furthermore, the results showed that the PPM system can carry out at sensitivities beyond the basic optically preamplified OOK NRZ limit of 27.3photons/bit.

Phillips et al [100, 101] highlighted that digital pulse position modulation (DPPM) can provide a considerable receiver sensitivity improvement at the cost of fibre bandwidth. This leads to that DPPM is receiving a significant recent attention with respect to implementation over the optical fibre channel. They applied a Chernoff bound, by means of a recently developed moment-generating function (MGF), to the bit-error probability of an optically preamplified pulse position modulation (PPM) receiver in optical fibre channel for operation at the STM-4 bit rate of 622 Mbit/s, assuming Gaussian received pulse shapes, and using the erbium-

doped fibre amplifier (EDFA) as an optical preamplifier. The results show that this receiver configuration can achieve a sensitivity of 25.27 photons/bit, and can surpass an equivalent on-off-keyed non return-to-zero (OOK NRZ) system by 7.1 dB. Additionally, a further demonstration was concluded by Phillips et al [100, 101] that an optically preamplified PPM receiver can also offer sensitivities that improve on the basic sensitivity limit of an optically preamplified OOK NRZ receiver and approach values achievable by coherent detection.

Phillips et al [102] analysed an optically preamplified intersatellite digital pulse position modulation (DPPM) receiver using the optimal detection scheme of maximum likelihood detection (MLD). This analysis was made by means of using a Gaussian approximation (GA), which is the assumption of Gaussian received pulse shapes that gives an advantage in terms of ease and speed of computation, and Chernoff bound (CA) techniques. They used the erbium-doped fibre amplifier (EDFA) as an optical preamplifier, and additionally the calculations were performed using physically realisable parameters and operating at a bit rate of 25 Mbit/s and a wavelength of 1.54μm. The theoretical results show that the strong potential of this receiver configuration can offer impressive sensitivity, and can surpass an earlier optically preamplified PPM receiver by approximately 1.5 dB. In addition, a further demonstration was concluded by Phillips et al [102] that this optically preamplified intersatellite DPPM receiver can also offer sensitivities that improve on the basic sensitivity limit of an optically preamplified on-off-keyed non-return-to-zero (OOK NRZ) signalling. Furthermore, it should be noted that such impressive performance of this receiver configuration drives it to be the significant candidate for implementation in future laser intersatellite communications systems.

Phillips et al [102] clarified that the reason of the limited optimal scheme of maximum likelihood detection (MLD) is the relative complexity and associated speed limitations of the integrate and compare circuitry involved. This leads to the optimal scheme of MLD operating at a lower data rate than is normally possible for the leading edge threshold detection scheme which is usually found in fibre PPM and used in the first proposal of optically preamplified PPM for laser intersatellite communications [30].

Phillips et al [103] clarified that some of the abundant fibre bandwidth is exchanged by using DPPM over the optical fibre channel for impressive receiver sensitivity benefits. This justifies why DPPM was studied extensively in relation to different optically preamplified receiver configurations that has also an intense interest due to the recent emergence of practical optical amplifiers. In addition, they were particularly interested in using optical amplifiers as optical preamplifiers that boost the optical power level of an incoming photon steam directly before its impinging on the photodetector.

An optically preamplified digital pulse position modulation (DPPM) receiver with an improved electrical domain filtering regime, which consists of a matched filter in cascade with a proportional-derivative-delay (PDD) network, was thoroughly analysed for the first time by Phillips et al [103]. They used the erbium-doped fibre amplifier (EDFA) as an optical preamplifier, presented sensitivity curves and examined the behaviour of the pulse-shaping network under the assumption of Gaussian received pulse shapes, and additionally considered the penalty incurred by removing the pulse-shaping network to be about 1.9 dB for high PPM coding levels , but it is lower at the optimum coding level. The results show that the strong potential of this receiver configuration can offer impressive sensitivity of 21.54 photons/bit predicted at 622 Mbit/s, and can surpass an equivalent optically preamplified on-off-keyed nonreturn-to-zero (OOK NRZ) system by 8.1 dB. In addition, a further demonstration was concluded by Phillips et al [103] that this optically preamplified DPPM receiver can also offer sensitivities that improve on the basic sensitivity limit of an optically preamplified OOK NRZ receiver and approach values achievable by coherent detection systems. However, it should be noted that such impressive performance is achieved at the cost of bandwidth.

Phillips et al [104] highlighted that the operation of PPM coding scheme in relation to different receiver configurations significantly outperform receivers detecting standard on-off keyed non-return-to-zero (OOK NRZ) modulation in terms of sensitivity. However, this improvement comes at the expense of bandwidth. Consequently, this success leads to looking for an alternative modulation format that keeps some of the sensitivity benefits of PPM without the extreme bandwidth consumption. Therefore, Phillips et al [104] examined Dicode PPM that only produces a fourfold increase in the line rate over the OOK NRZ data rate and offers the sensitivity benefit. Whereas, line rates greater than 10 times the data rate might be required by the optimal PPM scheme.

Phillips et al [104] originally analysed and investigated the performance of an optically preamplified dicode pulse position modulation (Dicode PPM) receiver for the first time. They used the erbium-doped fibre amplifier (EDFA) as an optical preamplifier, and additionally the calculations were performed using physically realisable parameters and operating at two different bit rates of 622 Mbit/s and 2.5 Gbit/s. They concluded the new and accurate derivation for the average power of the Dicode PPM pulse stream, and additionally compared the sensitivity performance of this receiver configuration with that obtainable from equivalent optically preamplified pulse position modulation (PPM) and on-off keyed non-return-to-zero (OOK NRZ) systems. The theoretical results show that the strong potential of the optically preamplified Dicode PPM receiver configuration can offer impressive sensitivity, and can potentially surpass an optically preamplified OOK NRZ receiver by approximately 4.2 dB. However, a further demonstration was concluded by Phillips et al [104] that optically preamplified systems that use the optimal PPM scheme, which significantly outperforms OOK NRZ by 7.1 dB [100,101], can offer sensitivities that improve on those use Dicode PPM scheme by between 3 and 5 dB, depending on the normalised fibre bandwidth.

5.3 Error weightings for MPPM, DPPM and Dicode PPM coding schemes:

One of the major aspects of coding schemes is error weighting and coding efficiency. Sibley [16] examined the impact of detection errors on the resulting PCM data through considering a (12/2) multiple PPM scheme operating over graded-index plastic optical fibre. He found that PPM systems suffer from three types of detection error: wrong-slot, false alarm and erasure errors.

1. Wrong-slots error:

This error takes place when noise on the leading edge of a detected pulse results in the pulse to appear in adjacent time slots either before or after the current slot. Moreover, this error occurs in fibre optic and is not applicable in free space because it is minimized if the pulse is detected at the center of the time slot and thus the probability of a wrong-slot error, P_s, is:

$$P_s = 0.5 erfc(Q_s / \sqrt{2}) \tag{91}$$

Where

$$Q_s = \frac{T_s}{2} \frac{slope(t_d)}{\sqrt{\langle n_o^{\,2} \rangle}} \tag{92}$$

where $\langle n_o^{\,2} \rangle$ is the noise on the detected signal, T_s is the time slot width, and $slope(t_d)$ is the slope of the received pulse at the threshold crossing instant, t_d. Due to the dependency of the resulting PCM error on which slot the pulse appears to be in, this probability equation is that of a pulse moving by $T_s / 2$ in either direction.

2. False alarm error:

A false alarm error is caused by noise in an empty time slot generating a threshold crossing. This means that this error occurs in the interval between the beginning of the frame and the arrival of the signal pulse if noise boosts the receiver output voltage such that it crosses the threshold. The probability of this taking place, P_f , is given by:

$$P_f = \frac{T_s}{\tau_R} 0.5 erfc(Q_f / \sqrt{2}) \tag{93}$$

where T_s / τ_R is the number of uncorrelated samples per time slot and τ_R is the time at which the autocorrelation function of the filter has become small and Q_f is given by:

$$Q_f = \frac{v_d - v_o(t_d)}{\sqrt{\langle n_o^{\,2} \rangle}} \tag{94}$$

where $v_o(t_d)$ is the signal voltage in the slot considered, and v_d is the decision or threshold level voltage.

3. Erasures error:

An erasure error is caused by noise obliterating a valid pulse and making detection impossible. This means the amplitude of the pulse at the decision time, t_d , falls below the threshold voltage, v_d , when noise is present on it. The probability of this taking place, P_e , is given by:

$$P_e = 0.5 erfc(Q_e / \sqrt{2}) \tag{95}$$

where Q_e is expressed as:

$$Q_e = \frac{v_{pk} - v_d}{\sqrt{\langle n_o^{\,2} \rangle}} \tag{96}$$

where v_{pk} is the peak signal voltage within the time-slot.

Thus, when transmitting PPM over a slightly dispersive channel, such as optical fibre, the estimation of the arrival time of the pulse is affected by noise resulting in three types of error, namely, erasures, false alarms, and wrong-slot errors. Of these, only erasure and false alarm errors are relevant in free-space communications because wrong-slot error occurs in dispersive channels and so is not applicable in free space. Moreover, wrong-slot error is minimized by normally transmitting the pulses so that the desired threshold crossing instant takes place at the center of the time slot. Therefore, all PPM coding schemes operating in free space suffer from only two types of error: false alarm and erasure errors. As the original PCM code is converted into another code, these errors will cause the original PCM to be corrupted. In addition, inter-symbol interference (ISI) and inter-frame interference (IFI) do not affect on the detected pulse in free space because they result from pulse dispersion in optical fibre and thus they only exist in fibre optic. Moreover, the receiver in the link uses a pre-detection filter that generates pulses with a raised-cosine spectrum. Such a filter helps to minimise inter-symbol-interference. It can be approximated by a single pole preamplifier following by a 3^{rd} order Butterworth filter.

Work has been carried out to show how the PCM error rate is affected by false alarm and erasure errors for MPPM, DPPM and Dicode PPM operating with 3, 4, 5 and 6 bits of PCM. A maximum likelihood sequence detector (MLSD) is used in the decoder and so the PCM error weighting is as shown in tables 11, 12 and 13.

Original PCM Word	MPPM Code	MLSD	Probable MPPM words
000	11000	11100	01100 (100)
			10100 (001)
			11000 (000)
			Average of error = 0.666
		11010	01010 (101)
			10010 (010)
			11000 (000)
			Average of error = 1
		11001	01001 (110)
			10001 (011)
			11000 (000)
			Average of error = 1.333
Final average of error			0.999 for 3 bits 0.333 per bit

Table 11. Determination of PCM error when a false alarm occurs in (5, 2) multiple PPM

As an example, if the code 11000 MPPM, which is the code for 000 PCM, has a false alarm occurring in an empty slot in the code-word, three pulses are present and the MLSD operates as shown in table 11. The process is repeated for false alarms in all vacant slots and the average number of PCM error obtained. Consideration of all possible code-words yields the total average number of PCM bits in error due to false alarm detection errors as can be seen in table 14 (detailed results of false alarm error weightings are attached in the appendix).

Original PCM Word	DPPM Code	MLSD	Probable DPPM words
000	0000 0001	1000 0001	1000 0000 (111)
			0000 0001 (000)
			Average of error = 1.5
		0100 0001	0100 0000 (110)
			0000 0001 (000)
			Average of error = 1
		0010 0001	0010 0000 (101)
			0000 0001 (000)
			Average of error = 1
		0001 0001	0001 0000 (100)
			0000 0001 (000)
			Average of error = 0.5
		0000 1001	0000 1000 (011)
			0000 0001 (000)
			Average of error = 1
		0000 0101	0000 0100 (010)
			0000 0001 (000)
			Average of error = 0.5
		0000 0011	0000 0010 (001)
			0000 0001 (000)
			Average of error = 0.5
Final average of error			0.86 for 3 bits 0.286 per bit

Table 12. Determination of PCM error when a false alarm occurs in digital PPM

If the code 0000 0001 DPPM, which is the code for 000 PCM, experiences a false alarm in an empty slot in the code-word, two pulses are present and the MLSD operates as shown in table 12. Consideration of false alarms in all vacant slots will yield the average PCM error for that particular DPPM word. Consideration of all possible code-words yields the total average number of PCM bits in error due to a false alarm detection error as can be seen in table 14 (detailed results of false alarm error weightings are attached in the appendix).

Original PCM Word	MPPM Code	MLD	Probable MPPM words
000	11000	01000	11000 (000)
			01100 (100)
			01010 (101)
			01001 (110)
		10000	11000 (000)
			10100 (001)
			10010 (010)
			10001 (011)
Final average of error			1.125 for 3 Bits 0.375 per bit

Table 13. Determination of PCM error when an erasure occurs in (5, 2) multiple PPM

Taking the code 11000 MPPM, which is the code for 000 PCM, an erasure error leaves only one pulse in the detected code-word. As two pulses have to be present, the maximum likelihood sequence detector (MLSD) operates as shown in table 13.The same procedure applies if the second pulse is erased and the average error rate is obtained by taking each possible code-word in turn and averaging. Consideration of all possible code-words yields the

total average number of PCM bits in error due to an erasure detection error as can be seen in table 14 (detailed results of erasure error weightings are also attached in the appendix).

When a digital PPM pulse is erased, the decoded word is all zeroes. So the maximum likelihood sequence decoder assumes it could have been any word at all. Thus the output word will be the average word – 111 (max) 000 (min) giving an average of 1.5 errors. For a 4 bits digital PPM word it would be 1111 (max) 0000 (min) average of 2 errors, etc.

As regards the error weightings for dicode PPM, the erasure and false alarm errors weightings would be constant and independent of the coding level because the Dicode PPM system operates continuously.

The following table shows PCM errors weightings caused by false alarms and erasures for MPPM, DPPM and Dicode PPM coding 3, 4, 5 and 6 bits of PCM :

	False Alarm (Per Bit PCM)			**Erasure (Per Bit PCM)**		
	MPPM	**DPPM**	**Dicode PPM**	**MPPM**	**DPPM**	**Dicode PPM**
PCM (3 bits)	0.309	0.286	0.249	0.382	0.5	0.193
PCM (4 bits)	0.3088	0.266	0.249	0.419	0.5	0.193
PCM (5 bits)	0.305	0.258	0.249	0.440	0.5	0.193
PCM (6 bits)	0.310	0.253	0.249	0.433	0.5	0.193

Table 14. Summary of PCM errors weightings caused by false alarms and erasures for MPPM, DPPM and Dicode PPM coding 3, 4, 5 and 6 bits of PCM

This table shows the weighting that must be applied to the probability of false alarm and erasure errors for MPPM, DPPM and Dicode PPM. These weightings show how the PCM error rate is affected by false alarms and erasures for MPPM, DPPM and Dicode PPM operating with 3, 4, 5 and 6 bits of PCM. As can be seen, Dicode PPM is the best coding scheme in terms of error weightings because it has the lowest false alarm and erasure error weightings. In addition, DPPM is better than MPPM in terms of false alarm error weightings because it has fewer error weightings than MPPM. MPPM is better than DPPM in terms of erasure error weightings.

Dicode PPM is the best coding scheme in terms of coding efficiency and simplicity of coding method because it operates continuously and only transmits a pulse when there is a transition between levels. Thus, the erasure and false alarm weightings for Dicode PPM are independent of the coding level. MPPM uses two or more pulses in a frame to convey the original PCM word and DPPM codes *n* bits of PCM into a single pulse which occupies one of 2^n time slot. Therefore, the erasure and false alarm weightings for MPPM and DPPM are dependent on the coding level.

5. 4 Comparison between MPPM, DPPM and Dicode PPM schemes:

As mentioned earlier in this chapter, the main target of this chapter and hence this research project work is selecting the best and appropriate PPM coding scheme to be used in optical intersatellite links in free space and for PCM data rates of 1 Gbit/s. This requires making a comprehensive and complete comparison between these three PPM coding schemes. This comparison can be performed not only in terms of error weightings and coding efficiency, but also in terms of the sensitivity (in terms of photon per PCM bit), the noise bandwidth, the peak voltage and hence the bandwidth efficiency.

Therefore, in addition to the work that was presented in the last section to perform this comparison between MPPM, DPPM and Dicode PPM coding schemes operating with 3, 4, 5 and 6 bits of PCM in terms of error weightings and coding efficiency, twelve computer simulations models (using MCAD) have been carried out to perform this comparison between MPPM, DPPM and Dicode PPM coding schemes operating with 3, 4, 5 and 6 bits of PCM in terms of sensitivity and bandwidth efficiency (these simulations are attached in the appendix). The initial assumption is that the input speed is of the order of 128 Mbit/s and the output speed is of the order of 1 Gbit/s.

5. 4.1 Simulation Model:

Simulations have been performed with the three systems using MPPM, DPPM and Dicode PPM, respectively. These systems are operating in space at a wavelength of 1.55µm, a photodiode quantum efficiency of 100%, 3, 4, 5 and 6 bits of PCM, respectively, and PCM data rates of 1 Gbit/s. The following figure shows the block diagram of the receiver system under consideration:

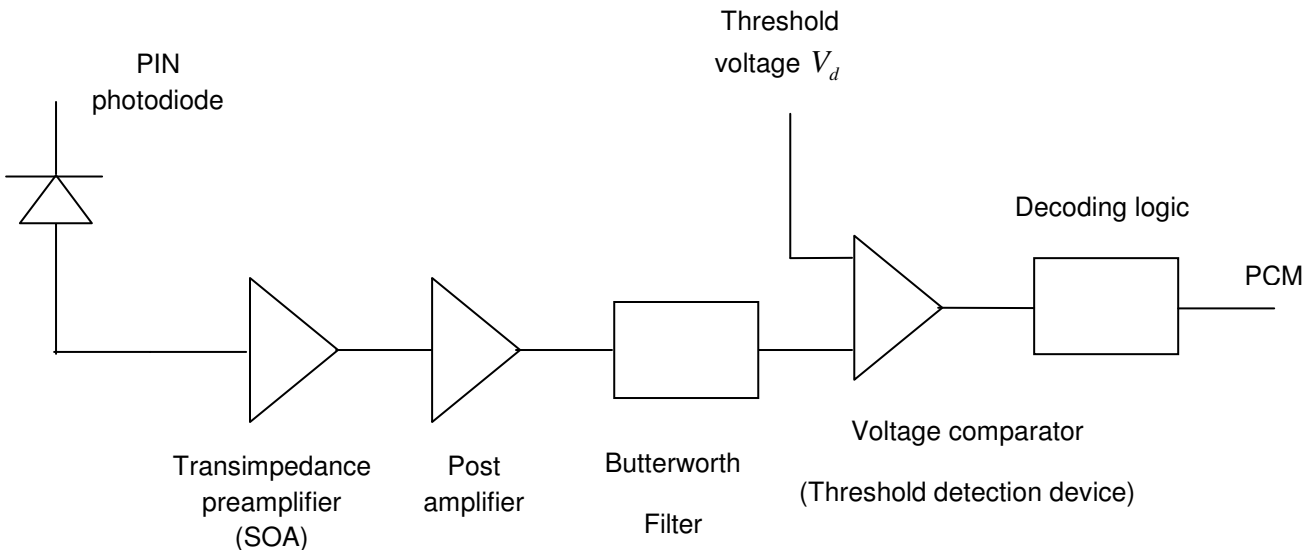

Figure 29. A block diagram of the receiver system in an optical intersatellite link in free space

Square pulses are assumed to be received with the following Fourier Transform (FT):

$$Pulse(\omega) = \frac{\sin(\frac{\omega.T_s}{2})}{(\frac{\omega.T_s}{2})} \qquad (97)$$

Normalising to the slot time gives:

$$Pulse_n(\omega) = \frac{\sin(\frac{\omega}{2})}{(\frac{\omega}{2})} \quad (98)$$

The receiver uses a pre-detection filter that generates pulses with a raised-cosine spectrum. Such a filter helps to minimise inter-symbol-interference. It can be approximated by a single pole preamplifier with bandwidth of $0.7 \times \frac{1}{T_s}$ following by a 3rd order Butterworth filter with bandwidth of $0.5 \times \frac{1}{T_s}$. Assuming ideal raised-cosine spectrum pulses, the pulse shape presented to the threshold detector [22] is

$$I_0(t) = \frac{\omega_{Pn}}{\pi.T_s}.\int_0^\infty Pulse_n(\omega).\left[\frac{a(\omega).\cos(\omega.(t-0.5)) + b(\omega).\sin(\omega.(t-0.5))}{a(\omega)^2 + b(\omega)^2}\right]d\omega \quad (99)$$

And the derivative of the pulse shape is:

$$I_1(t) = \frac{\omega_{Pn}}{\pi.T_s^{\,2}}.\int_0^\infty Pulse_n(\omega).\omega.\left[\frac{b(\omega).\cos(\omega.(t-0.5)) - a(\omega).\sin(\omega.(t-0.5))}{a(\omega)^2 + b(\omega)^2}\right]d\omega \quad (100)$$

where *a(ω), b(ω)* are variables and given by:

$$a(\omega) = \omega_{Pn} - 3.\frac{\omega^2}{\omega_{Bn}} - 3.\frac{\omega^2.\omega_{Pn}}{\omega_{Bn}^{\,2}} + \frac{\omega^4}{\omega_{Bn}^{\,3}} \quad (101)$$

$$b(\omega) = \omega + 3.\frac{\omega.\omega_{Pn}}{\omega_{Bn}} - 3.\frac{\omega^3}{\omega_{Bn}^{\,2}} - \frac{\omega^3.\omega_{Pn}}{\omega_{Bn}^{\,3}} \quad (102)$$

where ω_{Pn} is the preamplifier bandwidth, ω_{Bn} is the bandwidth of the Butterworth filter, T_s is the slot time which takes different values of $\frac{N.T_b}{M}$, $\frac{N.T_b}{2^N}$ and $\frac{T_b}{2}$ for MPPM(M,2), DPPM and Dicode PPM, respectively. Where N is the number of PCM bits, T_b is PCM bit time , and M is the number of slots used in MPPM which is 5, 7, 9 and 12 for 3, 4, 5 and 6 bits of PCM, respectively. Examples of time slots are shown in figure 12 in the last section of chapter 2 which shows examples of timing diagram for the MPPM, DPPM and Dicode PPM signals with the time slot width (T_s) for 3 bits of PCM and for each scheme.

A threshold-crossing detector makes a decision as to the presence or absence of a pulse in a particular time-slot. A normalised decision voltage, V_i, is given by:

$$V_i = \frac{V_d}{V_{pk}} \tag{103}$$

where V_d is the threshold crossing voltage and V_{pk} is the peak voltage of the pulse. For a given coding scheme, the pulse shape and noise can be determined and the optimum value of V_i that yields the lowest number of photons per pulse, b, can be found for a specified PCM error rate (1 in 10^9 in these simulations).

An algorithm was designed to generate results which can be used as comparative tools between MPPM, DPPM and Dicode PPM operating with 3, 4, 5 and 6 bits of PCM in terms of error weightings, coding efficiency, sensitivity and bandwidth efficiency. Consequently, the most appropriate coding scheme can be determined to be used in optical inter-satellite links in free space and for PCM data rates of 1 Gbit/s.

The following figure shows the flow chart of the aforementioned simulations for comparisons of the three used coding schemes MPPM, DPPM and Dicode PPM operating with 3, 4, 5 and 6 bits of PCM, respectively. This chart clarifies the process of the simulation and how the results were yielded:

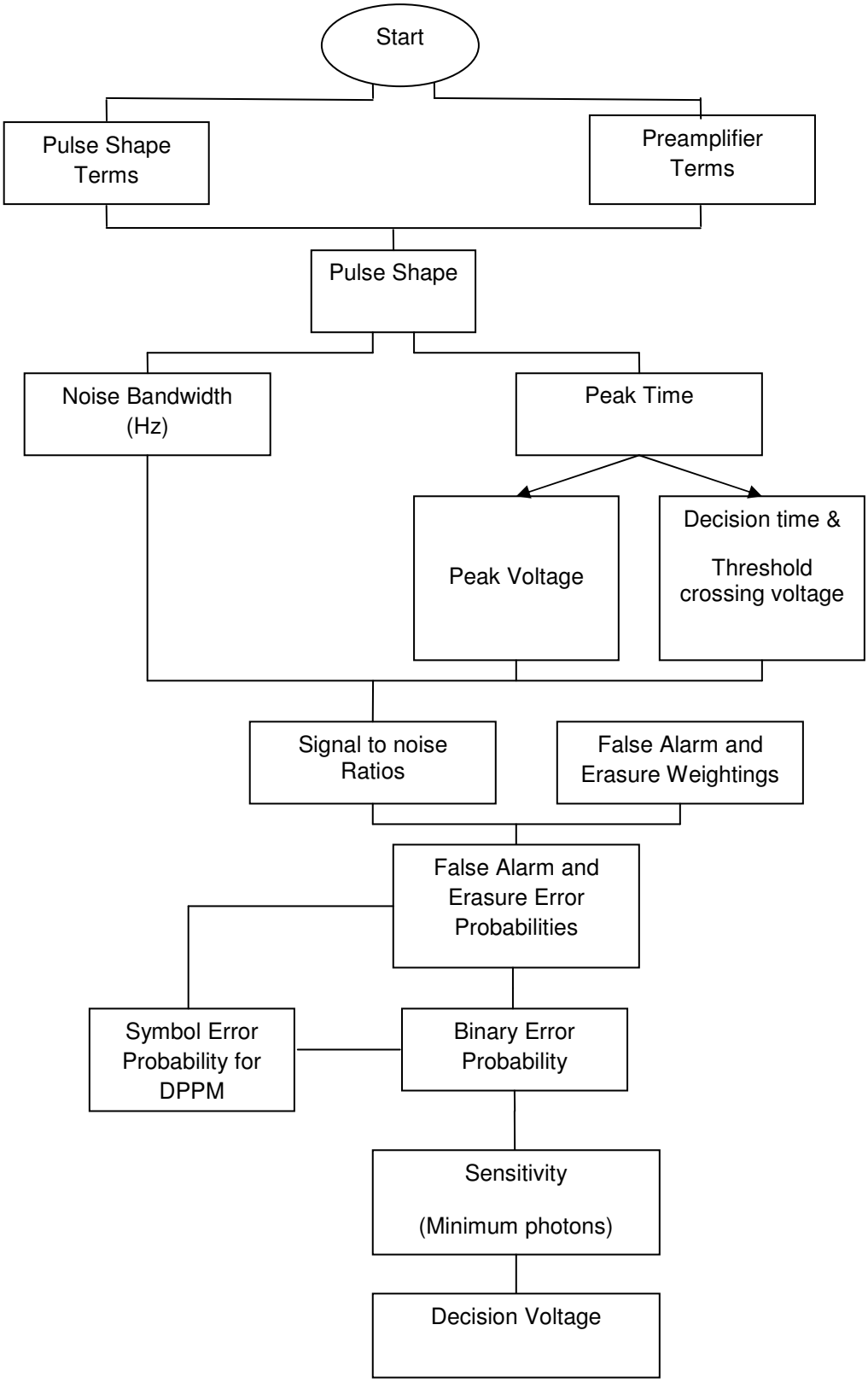

Figure 30. Flow chart of the simulations for comparisons of the three used coding schemes MPPM, DPPM and Dicode PPM coding 3, 4, 5 and 6 bits of PCM

As can be seen by figure 30, the simulations start with preamplifier and pulse shape terms. These preamplifier terms are shown by the following list of parameters:

Preamplifier Terms	
$S_o = 16\times10^{-24}$	Preamplifier noise at input-doublesided Philps TZA 3043
λ =1550 nm	Wavelength of operation
$B = 10^9$	PCM bit rate
$T_b = 10^{-9}$	PCM bit time
$n = 8$	Number of like symbols in PCM
$f_n = 10^6$	Channel bandwidth for free space
$N = 3$ or 4 or 5 or 6	Number of PCM bits
$\eta q = 1.6\times10^{-19}$	Quantum energy
$Photon\_energy = 12.832\times10^{-20}$	Photon energy
$R_o = 1.247$	Responsivity
$b = 5\times10^3$	Constant
$range = 1000$	Constant
$i = 0,1,.....20$	variable

Table 15. List of parameters used in the simulations for comparisons of the three used coding schemes MPPM, DPPM and Dicode PPM coding 3, 4, 5 and 6 bits of PCM

As regards the pulse shape terms, the most important parameter is the slot time, T_s, which takes different values of $\frac{N.T_b}{M}$, $\frac{N.T_b}{2^N}$ and $\frac{T_b}{2}$ for MPPM(M,2), DPPM and Dicode PPM, respectively. Where N is the number of PCM bits, T_b is PCM bit time , and M is the number

of slots used in MPPM which is 5, 7, 9 and 12 for 3, 4, 5 and 6 bits of PCM, respectively. Examples of time slots are shown in figure 12 in the last section of chapter 2 which shows examples of timing diagram for the MPPM, DPPM and Dicode PPM signals with the time slot width (T_s) for 3 bits of PCM and for each scheme.

As mentioned previously, the receiver uses a pre-detection filter that generates pulses with a raised-cosine spectrum. Such a filter helps to minimise inter-symbol-interference. It can be approximated by a single pole preamplifier with bandwidth of $0.7\times\frac{1}{T_s}$ following by a 3rd order Butterworth filter with bandwidth of $0.5\times\frac{1}{T_s}$. So, the preamplifier bandwidth, ω_{Pn}, and the bandwidth of the Butterworth filter, ω_{Bn}, are given by:

$$f_p = 0.7\frac{1}{T_s} \qquad f_B = 0.5\frac{1}{T_s} \tag{104}$$

$$\omega_B = 2\pi\times f_B \qquad \omega_{Bn} = 2\pi\times f_B\times T_s \tag{105}$$

$$\omega_p = 2\pi\times f_p \qquad \omega_{pn} = 2\pi\times f_p\times T_s \tag{106}$$

The Fourier Transform (FT):

$$H_p(\omega) = \frac{1}{1+j\frac{\omega}{\omega_p}} \qquad H_B(\omega) = \frac{{\omega_B}^3}{(j\omega+\omega_B)^3} \tag{107}$$

$$H_{p_n}(\omega) = \frac{1}{1+j\frac{\omega}{\omega_{p_n}}} \qquad H_{B_n}(\omega) = \frac{{\omega_{B_n}}^3}{(j\omega+\omega_{B_n})^3} \tag{108}$$

The autocorrelation time is given by:

$$\tau_R = \frac{8}{\omega_B} \qquad \tau_{Rn} = \frac{8}{\omega_B \times T_s} \tag{109}$$

By using values of these parameters into equations (101) and (102), the pulse shape presented to the threshold detector can be found as expressed by equation (99).

The noise bandwidth is given by:

$$noise = \frac{2}{2\pi.} \int_0^\infty \left\langle \left| H_p(\omega) \times H_B(\omega) \right| \right\rangle^2 d\omega \tag{110}$$

The peak time, t_{Pk} , can be found by using the pulse shape and the equation:

$$t_{pk} = root(I_1(t).T_s^{\,2}, t) \tag{111}$$

And so the peak voltage, V_{pk} , is given by:

$$V_{pk}(b) = b \times \eta q \times I_0(t_{pk}) \tag{112}$$

The decision time is expressed as:

$$t_{d_i} = root\left[\left\langle I_0(t) - V_i \times I_0(t_{pk}) \right\rangle T_s^{\,2}, t \right] \tag{113}$$

And so the threshold crossing voltage is given by:

$$V_d(b,i) = b \times \eta q \times I_0(t_{d_i}) \tag{114}$$

By using the noise bandwidth, equation (110), the peak voltage, equation (112), and the threshold crossing voltage, equation (114), the signal to noise ratios for false alarm and erasure errors can be found by the following equations:

For false alarm, threshold crossing:

$$Q_t(b,i) = \frac{V_d(b,i)}{\sqrt{S_0 \times noise}} \tag{115}$$

For erasure error:

$$Q_r(b,i) = \frac{V_{pk}(b) - V_d(b,i)}{\sqrt{S_0 \times noise}} \tag{116}$$

As mentioned previously, a maximum likelihood sequence detector (MLSD) has been used in the decoder in order to show how the PCM error rate is affected by false alarm and erasure errors for MPPM, DPPM and Dicode PPM operating with 3, 4, 5 and 6 bits of PCM. Examples have been presented throughout tables 11, 12 and 13 in order to show how MLSD was used. In addition, table 14 shows the results of PCM errors weightings caused by false alarms and erasures for MPPM, DPPM and Dicode PPM coding 3, 4, 5 and 6 bits of PCM.

By using these false alarm and erasure weightings, P_{fa} and P_{er}, respectively, and the signal to noise ratios, equations (115) and (116), the false alarm and erasure error probabilities can be found and are given by:

For false alarm error:

$$P_f(b,i) = 0.5 \times P_{fa} \times erfc\left(\frac{Q_t(b,i)}{\sqrt{2}}\right) \tag{117}$$

For erasure error:

$$P_r(b,i) = 0.5 \times P_{er} \times erfc\left(\frac{Q_r(b,i)}{\sqrt{2}}\right) \tag{118}$$

And so the binary error probability, $P_{eb}(b,i)$, for MPPM and Dicode PPM is given by:

$$P_{eb}(b,i) = P_f(b,i) + P_r(b,i) \tag{119}$$

Whereas the binary error probability for DPPM can be found through the symbol error probability, $P_{es}(b,i)$, that is given by:

$$P_{es}(b,i) = P_r(b,i) + \frac{n-1}{2} P_f(b,i) \quad (120)$$

And so the binary error probability for DPPM is given by:

$$P_{eb}(b,i) = \frac{n}{2(n-1)} P_{es}(b,i) \quad (121)$$

The minimum number of photons per PCM bit represents the sensitivity. Thus the sensitivity for MPPM and DPPM is given by:

$$Photons = \min(a)/N \quad (122)$$

Whereas the Dicode PPM system operates continuously and so its sensitivity is independent of the coding level and given regardless of the division on the number of PCM bits:

$$Photons = \min(a) \quad (123)$$

Where $pc(b,i)$, a_i are variable for a specified PCM error rate (1 in 10^9) and given by:

$$pc(b,i) = \langle \log(P_{eb}(b,i)) + 9 \rangle \quad (124)$$

$$a_i = root(pc(b,i), b) \quad (125)$$

The simulations results have been concluded by using the previous parameters with the above equations (97-125) in sequence in order to formulate the simulations process as shown in the aforementioned flow chart. These results are shown in tables 16, 17, 18 and 19 for MPPM, DPPM and Dicode PPM operating with 3, 4, 5 and 6 bits of PCM, respectively.

5. 4.2 Results and discussion:

The following tables16, 17, 18 and 19 show the summary of the results of these simulations for MPPM, DPPM and Dicode PPM operating with 3, 4, 5 and 6 bits of PCM, respectively:

3 Bits PCM	MPPM	DPPM	Dicode PPM
Weighting for False Alarm Errors	0.309	0.286	0.249
Weighting for Erasure Errors	0.382	0.5	0.193
Photon per PCM Bit	$2 \cdot 822 \times 10^{3}$	$2 \cdot 341 \times 10^{3}$	$7 \cdot 292 \times 10^{3}$
Noise Bandwidth (Hz)	8.776×10^{8}	1.404×10^{9}	1.053×10^{9}
Final Line Rate (B/W Expansion)	1.7 ×PCM Data Rate (3 Bits)	2.7 × PCM Data Rate (3 Bits)	2 × PCM Data Rate (Fixed)
Slot Time (S)	6×10^{-10}	$3 \cdot 75 \times 10^{-10}$	5×10^{-10}
Normalised Peak Voltage (V_{pk})	0.625	1	0.75
Decision Voltage ($V_i = \frac{V_d}{V_{pk}}$)	$0 \cdot 54$	$0 \cdot 566$	$0 \cdot 51$

Table 16. Summary of the results of simulations for comparisons of MPPM, DPPM and Dicode PPM operating with 3 bits of PCM

Table 16 shows the results of simulation for MPPM, DPPM and Dicode PPM coding 3 bits of PCM. As can be seen, MPPM offers the lowest noise bandwidth of 8.776×10^{8} Hz because it has the lowest speed and hence the lowest bandwidth requirement. DPPM has a higher noise bandwidth of 1.404×10^{9} Hz than Dicode PPM (1.053×10^{9} Hz) because Dicode PPM has lower speed and bandwidth than DPPM.

The peak voltage has been normalised to unity. MPPM has the lowest peak voltage which is 0.625 that of the DPPM because it has the largest time slot width of 0.6ns. Dicode PPM has a time slot width of 0.5ns and a peak voltage which is 0.75 that of the DPPM. The time slot width for MPPM (5, 2), DPPM and Dicode PPM signals is $\frac{3.T_b}{5}$, $\frac{3.T_b}{2^3}$ and $\frac{T_b}{2}$ respectively.

DPPM offers the best sensitivity in terms of photon per PCM bit because it requires $2\cdot341\times10^{3}$ Photons per PCM bit. In addition, MPPM has better sensitivity than Dicode PPM because it requires $2\cdot822\times10^{3}$ Photons per PCM bit, whereas Dicode PPM requires $7\cdot292\times10^{3}$ Photons per PCM bit.

4 Bits PCM	MPPM	DPPM	Dicode PPM
Weighting for False Alarm Errors	0.3088	0.266	0.249
Weighting for Erasure Errors	0.419	0.5	0.193
Photon per PCM Bit	$2 \cdot 071 \times 10^{3}$	$1 \cdot 434 \times 10^{3}$	$7 \cdot 292 \times 10^{3}$
Noise Bandwidth (Hz)	9.215×10^{8}	2.106×10^{9}	1.053×10^{9}
Final Line Rate (B/W Expansion)	1.75 × PCM Data Rate (4 Bits)	4 × PCM Data Rate (4 Bits)	2 × PCM Data Rate (Fixed)
Slot Time (S)	5.714×10^{-10}	$2 \cdot 5 \times 10^{-10}$	5×10^{-10}
Normalised Peak Voltage (V_{pk})	0.437	1	0.5
Decision Voltage ($V_i = \frac{V_d}{V_{pk}}$)	$0 \cdot 54$	$0 \cdot 566$	$0 \cdot 51$

Table 17. Summary of the results of simulations for comparisons of MPPM, DPPM and Dicode PPM operating with 4 bits of PCM

Table 17 shows the results of simulation for MPPM, DPPM and Dicode PPM coding 4 bits of PCM. As can be seen, MPPM has better sensitivity than Dicode PPM because it requires 2.071×10^{3} Photons per PCM bit. Whereas the required photons per PCM bit for Dicode PPM is independent of the coding level and equals 7.292×10^{3} Photons per PCM bit. In addition, this table shows that DPPM operating with 4 bits of PCM offers the best sensitivity in terms of photon per PCM bit because it requires 1.434×10^{3} Photons per PCM bit.

DPPM has a higher noise bandwidth of 2.106×10^{9} Hz than Dicode PPM (1.053×10^{9} Hz) for 4 bits of PCM because Dicode PPM has lower speed and bandwidth than DPPM. In addition, MPPM coding 4 bits of PCM offers the lowest noise bandwidth of 9.215×10^{8} Hz as it has the lowest speed and hence the lowest bandwidth requirement.

The peak voltage has been normalised to unity. Similar to operating with 3 bits of PCM, MPPM coding 4 bits of PCM has the lowest peak voltage which is 0.437 that of the DPPM for 4 bits of PCM because it has the largest time slot width of 0.5714 ns. Dicode PPM has a time slot width of 0.5 ns and a peak voltage that is 0.5 that of the DPPM. The time slot width for MPPM (7, 2), DPPM and Dicode PPM signals is $\frac{4.T_b}{7}$, $\frac{4.T_b}{2^4}$ and $\frac{T_b}{2}$ respectively.

5 Bits PCM	MPPM	DPPM	Dicode PPM
Weighting for False Alarm Errors	0.305	0.258	0.249
Weighting for Erasure Errors	0.440	0.5	0.193
Photon per PCM Bit	$1 \cdot 6358 \times 10^{3}$	$0 \cdot 9068 \times 10^{3}$	$7 \cdot 292 \times 10^{3}$
Noise Bandwidth (Hz)	9.478×10^{8}	3.37×10^{9}	1.053×10^{9}
Final Line Rate (B/W Expansion)	1.8 ×PCM Data Rate (5 Bits)	6.4 × PCM Data Rate (5 Bits)	2 × PCM Data Rate (Fixed)
Slot Time (S)	5.556×10^{-10}	$1 \cdot 563 \times 10^{-10}$	5×10^{-10}
Normalised Peak Voltage (V_{pk})	0.281	1	0.312
Decision Voltage ($V_i = \frac{V_d}{V_{pk}}$)	$0 \cdot 54$	$0 \cdot 566$	$0 \cdot 51$

Table 18. Summary of the results of simulations for comparisons of MPPM, DPPM and Dicode PPM operating with 5 bits of PCM

Table 18 shows the results of simulation for MPPM, DPPM and Dicode PPM coding 5 bits of PCM. As can be seen, the peak voltage has been normalised to unity. Since MPPM has the largest time slot width of 0.5556 ns, it has the lowest peak voltage which is 0.281 that of the DPPM for 5 bits of PCM. In addition, Dicode PPM has a time slot width of 0.5 ns and a peak voltage that is 0.312 that of the DPPM. The time slot width for MPPM (9, 2), DPPM and Dicode PPM signals is $\frac{5.T_b}{9}$, $\frac{5.T_b}{2^5}$ and $\frac{T_b}{2}$ respectively.

This table shows that Dicode PPM coding 5 bits of PCM has less sensitivity than MPPM as it requires 7.292×10^3 Photons per PCM bit, which is independent of the coding level. Whereas the required photons per PCM bit for MPPM is 1.6358×10^3 Photons per PCM bit for 5 bits of PCM. In addition, similar to 3 and 4 bits of PCM, DPPM operating with 5 bits of PCM offers the best sensitivity in terms of photon per PCM bit because it requires 0.9068×10^3 Photons per PCM bit.

Since Dicode PPM has lower speed and bandwidth than that of DPPM, it can be seen from this table that Dicode PPM has a lower noise bandwidth (1.053×10^9 Hz), which is also independent of the coding level, than DPPM which has noise bandwidth of 3.37×10^9 Hz for 5 bits of PCM. In addition, MPPM operating with 5 bits of PCM offers the lowest noise bandwidth of 9.478×10^8 Hz because it has the lowest speed and hence the lowest bandwidth requirement.

6 Bits PCM	MPPM	DPPM	Dicode PPM
Weighting for False Alarm Errors	0.310	0.253	0.249
Weighting for Erasure Errors	0.433	0.5	0.193
Photon per PCM Bit	$1 \cdot 2927 \times 10^3$	$0 \cdot 5854 \times 10^3$	$7 \cdot 292 \times 10^3$
Noise Bandwidth (Hz)	1.053×10^9	5.616×10^9	1.053×10^9
Final Line Rate (B/W Expansion	2 ×PCM Data Rate (6 Bits)	10.7 × PCM Data Rate (6 Bits)	2 × PCM Data Rate (Fixed)
Slot Time (S)	5×10^{-10}	$9 \cdot 375 \times 10^{-11}$	5×10^{-10}
Normalised Peak Voltage (V_{pk})	0.187	1	0.187
Decision Voltage ($V_i = \frac{V_d}{V_{pk}}$)	$0 \cdot 54$	$0 \cdot 566$	$0 \cdot 51$

Table 19. Summary of the results of simulations for comparisons of MPPM, DPPM and Dicode PPM operating with 6 bits of PCM

Table 19 shows the results of simulation for MPPM, DPPM and Dicode PPM coding 6 bits of PCM. This table shows that MPPM has better sensitivity than Dicode PPM because it requires 1.2927×10^{3} Photons per PCM bit for 6 bits of PCM. Whereas the required photons per PCM bit for Dicode PPM is independent of the coding level and equals 7.292×10^{3} Photons per PCM bit. In addition, similar to 3, 4 and 5 bits of PCM, DPPM operating with 6 bits of PCM offers the best sensitivity in terms of photon per PCM bit as it requires 0.5854×10^{3} Photons per PCM bit.

The peak voltage has been normalised to unity. MPPM has the lowest peak voltage which is 0.187 that of the DPPM for 6 bits of PCM because it has the largest time slot width of 0.5 ns. Dicode PPM has the same time slot width of MPPM (0.5 ns), and thus the same peak voltage that is 0.187 that of the DPPM.

As can be seen ,MPPM operating with 6 bits of PCM offers the lowest noise bandwidth of 1.053×10^{9} Hz as it has the lowest speed and hence the lowest bandwidth requirement. DPPM has a higher noise bandwidth of 5.616×10^{9} Hz than Dicode PPM (1.053×10^{9} Hz), which equals the noise bandwidth of MPPM, for 6 bits of PCM because Dicode PPM has lower speed and bandwidth than DPPM.

5.5 Conclusion:

DPPM is currently the preferred coding scheme for use in optical inter-satellite links because it operates with very low average power and offers a high sensitivity. However, it does suffer from a very large bandwidth expansion problem. Two alternative coding schemes have been examined in this research project work and a comparison has been made in terms of sensitivity, bandwidth efficiency, error weightings and coding efficiency.

Results show that Dicode PPM is the best coding scheme in terms of error weightings and coding efficiency because it has the lowest error weightings and operates continuously. In addition, it offers a fixed small bandwidth expansion - twice the PCM rate. MPPM can run at a lower speed - the final line rate for the MPPM (5, 2), (7, 2), (9, 2) and (12, 2) scheme are 1.7, 1.75, 1.8 and 2 that of the PCM, respectively. This should be compared to DPPM operating with 3, 4, 5 and 6 bits of PCM that run at a final line rate which are 2.7, 4, 6.4 and 10.7 times that of the original PCM data rate, respectively.

Despite the fact that Dicode PPM is the best coding scheme in terms of error weightings and coding efficiency, it requires the highest photons per PCM bit and thus has the lowest sensitivity. This is because the Dicode PPM system operates continuously and so its sensitivity, which is represented by the minimum number of photons per PCM bit, is independent of the coding level and given regardless of the division on the number of PCM bits as can be seen by equation (123). However, MPPM requires much lower photons per PCM bit compared to Dicode PPM, offers the lowest bandwidth expansion, has the lowest speed and offers the lowest noise bandwidth. Therefore, according to these considerations, it is concluded that MPPM coding 3, 4, 5 and 6 bits of PCM is the appropriate coding scheme to be used in optical inter-satellite links in free space.

6. Future work

In general, there is good correlation between computer predicted and theoretical results. This shows that the novel model of the link used in the theoretical analysis is reasonably accurate. Therefore, the author has achieved his objective of the research and demonstrated the suitable design of the model of optical inter-satellite link in free space and PCM data rates of 1 Gbit/s, and hence determined the most appropriate coding scheme to be used in such links. However, this research project work has discussed and investigated MPPM (5, 2), (7, 2), (9, 2) and (12, 2) coding 3, 4, 5 and 6 bits of PCM, respectively. Such techniques include random, linear, Hamming, Gary and Reed Solomon codes could be investigated. Therefore, this research project work could be the core concept for future work that is examining these code techniques in general and Reed Solomon in particular, for using in optical intersatellite links in free space in case of aforementioned MPPM systems (X/2) or maybe more than 12 slots such that an optimum can be found. In all cases the suitability for use in free space (power consumption and complexity) will be addressed.

On the other hand, this research project work could be the core concept for future work that is extending the comparisons in order to include more coding schemes such as Offset Pulse Position Modulation (OPPM) coding schemes for using in optical intersatellite links in free space in case of aforementioned PCM data rates of 1 Gbit/s or maybe more than 1 Gbit/s such that an optimum can be found.

7. Conclusion

This thesis described an analysis of intersatellite links in free space, with optical links using laser sources being considered in particular. The initial assumption was that the input speed is of the order of 128 Mbit/s and the output speed is of the order of 1 Gbit/s. This work has investigated a suitable design of the model of optical inter-satellite link in free space and has selected the most appropriate coding scheme to be used. The following block diagram summarises the results of the work:

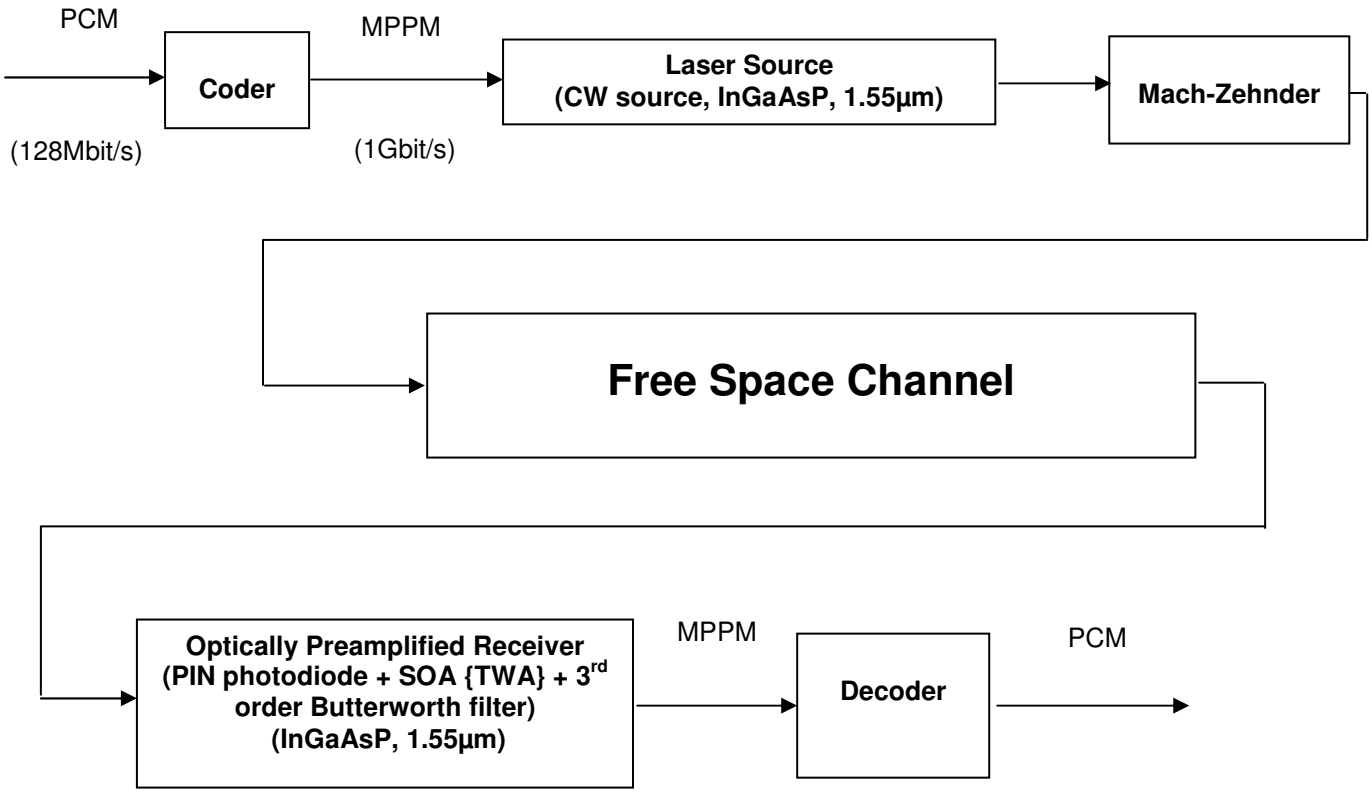

Figure 31. The block diagram represents the final results of design of the model for optical intersatellite links in free space and for PCM data rates of 1 Gbit/s

As can be seen from this diagram, the model of the link consists of: transmitter, receiver and coding system. This research project work started in chapter 2 with an in-depth analysis and

literature review of significant topics, which have formed the core concepts of the investigation into designing the model of the link.

The importance of using laser diodes as a light source in optical intersatellite links in space was presented in chapter 3. This chapter showed that a laser diode has many advantages: small size; high electrical to optical efficiencies; tightly focused beam. It is possible to adapt the technology used in fibre optic links to free-space communications and so multi-Gbit/s transmission is possible using readily available integrated driver chips. Investigations have been carried out throughout this chapter in order to establish the model of the transmitter. These investigations have concluded that emission wavelength of 1.55 μm and InGaAsP as the semiconductor material are the most suitable combination.

A theoretical model of an optically preamplified receiver has been developed throughout chapter 4. This model relied heavily on the basic structure of an optical receiver which consists of: a photodiode, a low-noise preamplifier, the front-end, further amplification stages, the post-amplifier and filtering. This chapter included studies and investigations in order to establish the model of the receiver. These studies have resulted in the conclusion that using an optically preamplified receiver that consists of: a PIN photodiode as a photodetector, Semiconductor Optical Amplifier (SOA) as an amplifier and a 3rd order Butterworth filter with central decision detection, is considered as a suitable combination in the design of the receiver to be used in optical intersatellite links in free space. Moreover, InGaAsP is the best choice as a semiconductor material to be used in fabricating a PIN photodiode in the link. This is because an APD photodiode has multiplication that leads to increase of excess noise, which are dark and signal noise, and poor bandwidth. In contrast, a PIN photodiode does not have multiplication and thus it has a lower excess noise and very good bandwidth. In addition, using an APD photodiode with SOA is not sufficient because the noise and the signal will be highly amplified. However, using a PIN photodiode with SOA has a very good bandwidth, multiplication and easy to use.

An original analysis of this novel technique of an optically preamplified receiver has also been presented in chapter 4 in order to examine the noise performance of the selected optical receiver, and hence determine its sensitivity and the number of received photons. This analysis was presented by using a computer simulation model (using MCAD) that has been carried out in such links and with using three different coding schemes for 3 bits of PCM: Multiple Pulse Position Modulation (MPPM), Digital Pulse Position Modulation (DPPM) and Dicode Pulse Position Modulation (Dicode PPM), respectively.

The results of this simulation have showed that the optical receiver offers the lowest total noise when MPPM coding scheme is used because MPPM has the lowest speed and hence the lowest bandwidth requirement. The optical receiver used with Dicode PPM coding scheme has a lower total noise than that when DPPM coding scheme is used. Additionally, the optical receiver used with MPPM offers the best sensitivity as it requires the lowest optical power. The optical receiver used with Dicode PPM has better sensitivity than that using DPPM coding scheme. Moreover, the optical receiver used with MPPM coding scheme has the largest number of photons received for a specified error rate as MPPM has the largest time slot width. The optical receiver used with DPPM has a lower number of photons received for a specified error rate than that uses Dicode PPM.

According to these results and investigations, it is concluded that the optical receiver, which uses PIN photodiode as a photodetector with SOA as an amplifier and a 3^{rd} order Butterworth filter with central decision detection, used with MPPM coding 3 bits of PCM is considered a suitable design for use in optical inter-satellite links in free space. This information has represented the main goal of designing the receiver in such links.

DPPM and two alternative coding schemes, which are MPPM and Dicode PPM, have been examined and analysed throughout chapter 5. This chapter included original algorithms that have been designed. The results can be used as comparative tools between MPPM, DPPM and Dicode PPM operating with 3, 4, 5 and 6 bits of PCM in terms of error weightings, coding efficiency, sensitivity and bandwidth efficiency. Consequently, the most appropriate coding

scheme can be determined to be used in optical inter-satellite links in free space and for PCM data rates of 1 Gbit/s.

Final investigations and results have resulted in the conclusion that Dicode PPM is the best coding scheme in terms of error weightings and coding efficiency because it has the lowest error weightings and operates continuously. In addition, it offers a fixed narrow bandwidth expansion - twice the PCM rate, but it requires the highest photons per PCM bit and thus has the lowest sensitivity. However, MPPM can run at a lower speed - the final line rate for the MPPM (5, 2), (7, 2), (9, 2) and (12, 2) scheme are 1.7, 1.75, 1.8 and 2 that of the PCM, respectively. This should be compared to DPPM operating with 3, 4, 5 and 6 bits of PCM that run at a final line rate which are 2.7, 4, 6.4 and 10.7 times that of the original PCM data rate, respectively. Moreover, MPPM requires much lower photons per PCM bit compared to Dicode PPM, offers the lowest bandwidth expansion, has the lowest speed and offers the lowest noise bandwidth.

Therefore, according to these investigations and considerations, it is concluded that MPPM coding 3, 4, 5 and 6 bits of PCM is the most appropriate coding scheme to be used in optical inter-satellite links in free space and for PCM data rates of 1 Gbit/s. This information has represented the main target of this research.

REFERENCES

[1] McCullagh , M. J., Wisely, D.R., Mobility Group, SRD. (1993, 14 October).A Comparison of Microwave and Optical Free Space point to Point links. *Revision: Issue 1, QA status: Reviewed, Project: 1634 Job 00.*

[2] Ekberg, J. (1970, 6 April).*Transmission Calculations for Infrared-Optical Links*. Helsinki, Finland: The STATE Institute for Technical Research.

[3] Toyoshima, M. Leeb, W. Kunimori, H. and Takano, T. Optical communications work best over relatively short distances in space. *SPIE Newsroom, DOI: 10.1117/2.1200602.0088*. Retrieved March 18, 2009, from http://spie.org/documents/Newsroom/Imported/0088/88_469_0_2006-02-27.pdf

[4] Lutz, H.P. (1997, August). Optical Communications in Space - Twenty Years of ESA Effort. *ESA Bulletin Nr.91*. Retrieved November 21, 2006, from http://www.esa.int/esapub/bulletin/bullet91/b91lutz.htm

[5] Japan Aerospace Exploration Agency (JAXA). (2006, November). *"Kirari" Optical Inter-Orbit Communications Engineering Test Satellite (OICETS)*. Retrieved November 16, 2006, from http://www.jaxa.jp/missions/projects/sat/tsushin/oicets/index_e.html

[6] Sibley, M. J. N. (1995). *Optical Communications* (2nd Ed). Houndmills, Basingstoke, Hampshire RG21 2XS, and London: The Macmillan Press LTD.

[7] Keiser, G. (2000). *Optical Fibre Communications* (3rd Ed). McGraw-Hill Higher Education: McGraw-Hill Companies, Inc.

[8] Yariv, A. (1991). *Optical Electronics* (4th Ed). The United States of America: Saunders College Publishing.

[9] Brain, M. C. & Smith, D. R. (1983, April). Phototransistors, APD-FET, and PINFET Optical Receivers for 1-1.6- μm Wavelength. *IEEE Transactions on Electron Devices, Vol. ED-30, No. 4.*

[10] Srinivasan, M. & Vilnrotter, V. (1998, August 15). Symbol-Error Probabilities for Pulse-Position Modulation Signaling With an Avalanche Photodiode Receiver and Gaussian Thermal Noise. *The Telecommunications and Mission Operations Progress Report 42-134, April {June 1998,* Jet Propulsion Laboratory, Pasadena, California, pp.1 {11. Retrieved March 20, 2007, from http://tmo.jpl.nasa.gov/progress_report/42-134/134E.pdf

[11] Srinivasan, M. & Vilnrotter, V. (2001, February 15). Avalanche Photodiode Arrays for Optical Communications Receivers. *The Telecommunications and Mission Operations Progress Report 42-144,* Jet Propulsion Laboratory, Pasadena, California, pp. 1{10. Retrieved March 20, 2007, from http://opticalcomm.jpl.nasa.gov/PAPERS/GOPR/144f.pdf

[12] McIntyre, R. J. (1966, January). Multiplication Noise in Uniform Avalanche Diodes. *IEEE Trans, Electron Devices (Special Issue on Semiconductor Bulk-Effect and Transit-Time Devices),* vol. **ED-13**, pp. 164-168.

[13] McIntyre, R. J. (1972, June). The Distribution of Gains in Uniformly Multiplying Avalanche Photodiodes: Theory. *IEEE Transactions on Electron Devices,* vol. **ED-19**, pp. 703-713.

[14] Vilnrotter, V., Simon, M., and Srinivasan, M. (1999, July 8). Maximum Likelihood Detection of PPM Signals Governed by Arbitrary Point-Process Plus Additive Gaussian Noise. *Electronics letters*, vol.35, pp. 1132{1133.

[15] Gagliardi, R. M. & Karp, S. (1995). *Optical Communications.* New York: John Wiley and Sons, Inc.

[16] Sibley, M. (2004, December). Analysis of multiple pulse position modulation when operating over graded-index plastic optical fiber. *IEE proc –Optoelectron.*, Vol. 151 , No. 6, December 2004 .

[17] Zwillinger, D. (1988). 'Differential PPM has a higher throughput than PPM for the band-limited and power-limited optical channel', *IEEE Trans. Inf. Theory*, 34, (5), pp. 1269-1273

[18] Shiu, D.S., and Kahn, J.M. (1999). 'Differential pulse-position modulation for power-efficient optical communication'*, IEEE Trans. Commun.*, 47, (8), pp. 1201-1210

[19] Shalaby, H.M.H. (1999). 'A performance analysis of optical overlapping PPM-CDMA communication systems'*, IEEE J. Lightw. Technol.*, 17, (3), pp. 426-434

[20] Sibley, M.J.N. (2003). 'Dicode pulse position modulation – a novel coding scheme for optical fibre communications', *IEE Proc., Optoelectron*, 150, (2), pp. 125-131

[21] Sibley, M.J.N. (2003). ' Analysis of dicode pulse position modulation using a PINFET receiver and a slightly/highly dispersive optical channel', *IEE Proc., Optoelectron*, 150, (3), pp. 205-209

[22] Sibley, M.J.N. (2004). 'Sub-optimal filtering in a zero guard, dicode PPM system operating over dispersive optical channels', *IEE Proc., Optoelectron*, 151, pp. 237-243

[23] Sugiyama, H., and Nosu, K. (1989). 'MPPM: A method for improving the band-utilization efficiency in optical PPM'*, IEEE J. Lightw. Technol*, 7, (3), pp. 465-472

[24] Atkin, G.E., and Fung, K.-S. (1994).' Coded multipulse modulation in optical communication systems', *IEEE Trans. Commun*, 42, (2/3/4), pp. 574-582

[25] Park, H., and Barry, J.R. (1995). 'Modulation analysis for wireless infrared communications'. Proc. *IEEE Int. Conf. on communications*, pp. 1182-1186

[26] Park, H., and Barry, J.R. (1996). 'Performance analysis and channel capacity for multiple-pulse position modulation on multipath channels'. Proc*. IEEE Int. Symp. On Personal, Indoor and Mobile radio communications*, pp. 247-251

[27] Park, H., and Barry, J.R. (2003). 'Partial-response precoding scheme for multiple pulse-position modulation'*, IEE Proc., Optoelectron*,150, (2), pp. 133-137

[28] Allen, C., Cobanoglu, Y., Chong, S.K. & Gogineni, S. (2000). Development of a 1310-nm, coherent laser radar with RF pulse compression. *Geoscience and Remote Sensing Symposium, 2000. Proceedings. IGARSS 2000. IEEE 2000 International*. Volume 4, Issue, 2000 Page(s):1784 - 1786 vol.4. Retrieved June 27, 2007, from

http://ieeexplore.ieee.org/Xplore/login.jsp?url=/iel5/6913/18598/00857345.pdf

[29] Wree, C. Collier, C. P. Lane, S. Turney, A. Armentrout, B. Yates, J. Francis, N., and Joshi, A. (2008). 'Ten Gb/s optically pre-amplified RZ-DPSK for FSO communications systems with very large link losses'. *SPIE*, Vol.7091, 709103-1. Doi: 10.1117/12.793784

[30] Phillips, A.J., Cryan, R.A. and Senior, J.M. (1995, February). Novel laser intersatellite communication system employing optically preamplified PPM receivers. *IEE Proceedings Communications,* Vol. 142, No. 1, pp. 15-20.

[31] Phillips, A.J., Cryan, R.A. and Senior, J.M. (1994, May). . An optically preamplified PPM threshold detection receiver for satellite communications. *Microwave and Optical Technology Letters,* Vol. 7, No. 7, pp. 324-327.

[32] Cryan, R.A. & Unwin, R.T. (1992). "Optical space communications employing pulse position modulation*," Proc. IEE Colloquium on Advanced Modulation and Coding Techniques for Satellite Communications*., London, 1992, Digest No. 1992/019, pp. 7/1-7/5.

[33] Ferrier, R., Johnson, A.D., and Fletcher, G.D. (1990). Intersatellite coherent optical communications. *Proc. IEE colloquium on Coherent Optical Communications*, 1990, Digest No. 116, pp. 8/1-6.

[34] Kressel, H. and Butler, J. K. (1977). *Semiconductor Lasers and Heterojunction LEDs*, Academic Press, New York.

[35] Kressel, H. (Ed.) (1980). *Semiconductor Devices for Optical Communications*, *Vol. 39, Topics in Applied Physics*, Springer-Verlag, New York.

[36] Casey, H. C. and Panish, M. B. (1978). *Heterostructure Lasers,* Part A: *Fundamental Principles and* Part B: *Materials and Operating Characteristics*, Academic Press, New York.

[37] Yariv, A. (1991). *Optical Electronics*, 4th edn, HRW Ltd, Orlando, Florida.

[38] Nayar, B. K. and Booth, R. C. (1986). 'An introduction to integrated optics', *British Telecom Technology Journal*, **3**, 5-15.

[39] Brierley, M. C. and France, P. W. (1987). 'Neodynium doped fluorozirconate fibre laser', *Electronics Letters*, **23**, 815-817.

[40] Mikhrin, S.S., Kovsh, A. R., Krestnikov, I. L., Kozhukhov, A. V., Livshits, D. A., Ledentsov, N.N., Shernyakov, Yu.M., Novikov, I.I., Maximov, M.V., Ustinov, V.M.& Alferov Zh. I. (2005, May). High power temperature-insensitive 1.3 μm InAs/InGaAs/GaAs quantum dot lasers. *IOP/ Electronic journals. Semiconductor Science and Technology. et al 2005 Semicond. Sci. Technol.* **20** 340-342 doi:10.1088/0268-1242/20/5/002. Received 26 July 2004, in final form 19 January 2005. Published 28 February 2005. Retrieved June 27, 2007, from

http://www.iop.org/EJ/abstract/0268-1242/20/5/002

[41] Eric, P., Jaques, B., Claudine, D. & Olivier, M. (1999, December). Reliability of 1300-nm laser diode for space applications. Proc. *SPIE Vol. 3872, p. 139-147, Photonics for Space and Radiation Environments, Edward W. Taylor; Francis Berghmans; Eds*. Retrieved June 27, 2007, from

http://adsabs.harvard.edu/abs/1999SPIE.3872..139P

[42] Rabinovich, W. S., Mahon, R., Burris, H. R., Gilbreath, G. C., Goetz, P. G., Moore, C. I., Stell, M. F., Vilcheck, M. J., Witkowsky, J. L., Swingen, L., Suite, M. R., Oh, E. & Koplow, J. (2005, May). Free-space optical communications link at 1550 nm using multiple-quantum-well modulating retroreflectors in a marine environment. *Optical Engineering 44(5), 056001*. Retrieved June 27, 2007, from

http://www.nrl.navy.mil/fpco/publications/FreespaceOpticalCommunicationLink.pdf

[43] Personick, S. D. (1973). 'Receiver design for digital fiber optic communication systems, Parts I and II', *Bell System Tech. J.*, **52**, 843-886.

[44] Smith, D. R. and Garrett, I. (1978). 'A simplified approach to digital receiver design', *Optical and Quantum Electronics*, **10**, 211-221.

[45] Ducellier, T., Goix, M., Hebert, J.P., Legouezigou, O., N*"Go,* R., Pommereau, F., Tscherptner, N., Pasquier, J., Gaborit, F., Pagnod, P., Grard, E., Artigaud, S**.,** Blanconnier, P. and Giraudet, L. (1997, 13th March). Compact high sensitivity 10 Gbit/s SOA-filter- pin receiver module. *Electronics Letters, vol. 33, No.6,* 509-510. Retrieved June 27, 2007, from http://ieeexplore.ieee.org/xpl/freeabs_all.jsp?isnumber=12683&arnumber=585071&count=73&index=51

[46] LIVAS, J.c.: 'High sensitivity optically preamplified 10Gbit/s receivers'. OFC'96, San Jose, 1996, Paper PD4.

[47] YUN, T.Y., HAN, J.H., and PARK, M.s.: '10Gbit/s optical receiver of lossless tuned pin-HEMT with high performance', Electron. Lett., 1998, 31, (19), pp. 1688-1689.

[48] YUN, T.Y., PARK, M.s., HAN, J.H., WATANABE, I., and MAKITA, K.: '10Gbi/s optical receiver with superlattice APD and lossless tuned transimpedance HEMT amplifier'. ECOC'96, Oslo, 1996, Paper ThC. 1 .5

[49] SCHIMPE, R., CREMER, c., HOFFMANN, L., ROMER, D., SCHIER, M., BAUMEISTER, G., EBBINGHAUS, G., KRISTEN, G., and MORVAN, M.: 'InP-based 2.5 Gbitis optically preamplified WDM receiver', Electron. Lett., 1996, 32, (12), pp. 1141-1142.

[50] MIKKELSEN, B., DURHUUS, T., JOERGENSEN, C., STUBKJAER, K E., DOUSSIERE, P., GARABEDIAN, G., GRAVER, c., and LECLERC, D.: 'High performance semiconductor optical amplifiers as in-line and preamplifiers'. ECOC'94, Firenze, 1994.

[51] Heim, P.J.S.; Dagenais, M.; Krainak, M.A.; Leavitt, R. (1996, 21st Nov). High-sensitivity semiconductor optically preamplified 25 GHz receiver**.** *Lasers and Electro-Optics Society Annual Meeting, 1996. LEOS 96., IEEE.* Volume 2, Issue , Page(s):254 – 255.

[52] H. de Waardt, L.F. Tiemeijer, and B.H. Verbeek, "89 km 10 Gbit/s 1310 repeaterless transmission experiments using direct laser modulation and two SL-MQW laser preamplifiers with low polarization sensitivity", *IEEE Photon Techn. Lett.*, vol. 6, pp. 645-647, 1994.

[53] I-Hsing, C-K Sun, K.S. Giboney, J.E. Bowers, E.L. Hu, B.I. Miller, and R.J. Capik, "120-GHz long wavelength low-capacitance photodetector with an air-bridge coplanar metal waveguide", *IEEE Photon. Techn. Lett.,* vol. 7, pp. 1477-1482, 1995.

[54] Legros, E., Barrou, Th., Vuye, S., Giraudet, L., Joly, C., Blache, F., Ducellier, T. & Goix, M. (1998, 20-24 September). High-sensitivity high-gain SOA-filter-PIN-PHEMT 40-Gb/s photoreceiver. *Optical communication, 1998. 24th European Conference.* Volume 1, Issue, 20-24 Sep 1998 Page(s) 69-70 vol.1. Retrieved June 27, 2007, from http://ieeexplore.ieee.org/Xplore/login.jsp?url=/iel4/5897/15800/00732440.pdf?arnumber=732440

[55] Xia, F., Wei, J., Menon, V. & Forrest, S.R. (2003, March). Monolithic integration of a semiconductor optical amplifier and a high bandwidth p-i-n photodiode using asymmetric twin-waveguide technology. *Photonics Technology Letters, IEEE.* Volume 15, Issue 3, March 2003 Page(s):452 – 454. Retrieved June 27, 2007, from http://ieeexplore.ieee.org/Xplore/login.jsp?url=/iel5/68/26551/01182788.pdf

[56] Sysak, M.N., Barton, J.S., Johansson, L.A., Raring, J.W., Skogen, E.J., Masanovic, M.L., Blumenthal, D.J. & Coldren L.A. (2004, September). Single-chip wavelength conversion using a photocurrent-driven EAM integrated with a widely tunable sampled-grating DBR laser. *Photonics Technology Letters, IEEE.* Volume 16, Issue 9, Sept. 2004 Page(s):2093 – 2095. Retrieved June 27, 2007, from http://ieeexplore.ieee.org/Xplore/login.jsp?url=/iel5/68/29327/01325243.pdf

[57] Shiu, K.-T., Agashe, S.S. & Forrest, S.R. (2006, April**).** A simple monolithically integrated optical receiver consisting of an optical preamplifier and a p-i-n photodiode. *Photonics Technology Letters, IEEE*. Volume 18, Issue 8, April 2006 Page(s):956 – 958. Retrieved June 27, 2007, from http://ieeexplore.ieee.org/Xplore/login.jsp?url=/iel5/68/33824/01613982.pdf

[58] Stillman, G. E. *et al*. (1983). 'InGaAsP photodiodes'*, IEEE Transactions: Electronic Devices*, **ED-30**, 364-381.

[59] Kressel, H. (Ed.) (1980). *Semiconductor Devices for Optical Communications*, *Vol.39, Topics in Applied Physics*, Springer-Verlag, New York.

[60] R.J. Manning and D.A.O. Davies, "Three-wavelength device for all-optical signal processing," Optics letters, June 15, 1994, Vol. 19, No. 12, pp. 889-891

[61] Mitsuru Sugawara, Nobuyuki Hatori, Tomoyuki Akiyama, etc, "Quantum-Dot Semiconductor Optical Amplifiers for High Bit-Rate Signal Processing over 40 Gbit/s,"Jpn,Vol. 40(2001) pp. L488-L491

[62] Tommy W. Berg and Jesper Mork, "Ultrafast Optical Signal Processing usgin Semiconductor Quantum Dot Amplifiers," S. L. Chuang, *Physics of Optoelectronic Devices*, pp.357, New York : Wiley (1995).

[63] EMCORE global communications and power at the speed of light (2005). *Semiconductor Optical Amplifiers*. Retrieved April 20, 2008, from http://www.fiber-optics.info/articles/op-amp.htm

[64] INPHENIX, Inc., Application Instruction 001 (2004, September). *The Enhanced Functionalities of Semiconductor Optical Amplifiers and their Role in Advanced Optical Networking*. Retrieved April 20, 2008, from http://www.inphenix.com/pdfdoc/Application_Notes_for_SOAs.pdf

[65] Constable, J.A., White, I.H., Coles, A.N. & Cunningham, D.G. (1993, November 11th). Reduction of harmonic distortion and noise in a semiconductor optical amplifier using bias current feedback. *Electronics Letters*. Volume 29, Issue 23, 11 Nov 1993 Page(s):2042 – 2044. Retrieved June 24, 2007, from http://ieeexplore.ieee.org/Xplore/login.jsp?url=/iel1/2220/6464/00253944.pdf?arnumber=253944

[66] Mathlouthi, W., Lemieux, P. & Rusch, L. A. Optimal SOA-based Noise Reduction Schemes for Incoherent Spectrum-Sliced PONs. *Université Laval, Québec, QC G1K 7P4, Canada, rusch@gel.ulaval.ca* : Centre d'optique, photonique et laser (COPL), Department of Electrical and Computer Engineering. Retrieved June 24, 2007, from http://www.copl.ulaval.ca/publications/uploadPDF/publication_1813.pdf

[67] Broeke (1), R.G., Binsma (2), J.J.M., van Geemert (2), M., Heinrichsdorff (2), F., van Dongen (2), T., van Zantvoort (1), J.H.C., Leijtens (1), X.J.M., Oei (1), Y.S.& Smit (1), M.K. All-Optical Wavelength Converter With A Monolithically Integrated Digitally Tunable Laser. *1: Eindhoven University* of Technology-COBRA/DIMES, Department of Electrical Engineering, Den Dolech 2, 5612 AZ Eindhoven, The Netherlands & *2: JDS Uniphase, Prof. Holstlaan 4*, 5656 AA Eindhoven, The Netherlands . Retrieved June 24, 2007, from http://tte.ele.tue.nl/oed/publications/OED%20pubs%202002/Broeke%20all-optical%20wavelength%20ECOC%2002.pdf

[68] Cao, S.-C. & Cartledge, J.C. Senior Member, IEEE. (2002, July). Time- and Frequency-Domain Characterization of the Modulated ASE Noise in SOA-MZI Wavelength Converters. *Photonics Technology Letters, IEEE*. Volume 14, Issue 7, Jul 2002 Page(s):962 – 964. Retrieved June 24, 2007, from http://ieeexplore.ieee.org/Xplore/login.jsp?url=/iel5/68/21809/01012399.pdf

[69] Liu, Y., Hill, M. T., Tangdiongga, E., de Waardt, H., Calabretta, N., Khoe , G. D. & Dorren, H. J. S. All-optical wavelength converter based on cross-polarization modulation in a single semiconductor optical amplifier. *COBRA Research Institute, Eindhoven University of Technology*, P. O. Box 513, 5600 MB Eindhoven, The Netherlands. Retrieved June 24, 2007, from http://tte.ele.tue.nl/optical/Publications/ECO%20pubs%202002/Liu%20all-optical%20wavelength%20ECOC%2002%20poster%202.14.pdf

[70] Garrett, I.: 'Pulse-position modulation for transmission over optical fibres with direct or heterodyne detection', *IEEE Trans. Commun.*,1983, **31**, pp. 518–527.

[71] Garrett, I.: 'Digital pulse-position modulation over dispersive optical fibre channels'. Presented at Int. Workshop on Digital Communications, Tirrenia, Italy, 15–19 August 1983.

[72] Garrett, I.: 'Digital pulse-position modulation over slightly dispersive optical fibre channels'. Proc. Int. Symp. on Information Theory, St. Jovite, Canada, 1983, pp. 78–79.

[73] Cryan, R.A., Unwin, R.T., Garrett, I., Sibley, M.J.N., and Calvert, N.M.: 'Optical fibre digital pulse-position modulation assuming a Gaussian received pulse shape', *IEE Proc. J, Optoelectron.*, 1990, **137**, (4), pp. 89–96.

[74] Garrett, I., Calvert, N.M., Sibley, M.J.N., Unwin, R.T., and Cryan, R.A.: 'Optical fibre digital pulse position modulation', *Br. Telecom Technol. J.*, 1989, **7**, (3), pp. 5–11.

[75] Sibley, M.J.N., and Massarella, A.J.: 'Detection of digital pulse position modulation over highly/slightly dispersive optical channels', *Proc. SPIE–Int. Soc. Opt. Eng.*, 1993, **1974**, pp. 99–110.

[76] Audeh, M.D., Kahn, J.M., and Barry, J.R.: 'Performance of pulse position modulation on measured nondirected indoor infrared channels', *IEEE Trans. Commun.*, 1996, **44**, (6), pp. 654–659.
[77] Sibley, M.J.N.: 'Design implications of high speed digital PPM', *Proc. SPIE–Int. Soc. Opt. Eng.,* 1993, **2024**, pp. 342–352.

[78] Calvert, N. M., Sibley. M. J. N., and Unwin, R.T.: 'Experimental optical fibre digital pulse-position modulation system'. *Electron. Lett.*,1988, **24**. pp. 129-131.

[79] Massarella, A.J., and Sibley. M.J.N.: 'Experimental results on sub-optimal filtering for optical digital pulse-position modulation', *Electron. Lett.*, 1991, **27**, (I) , pp. 1953-1954.

[80] Cryan, R.A., and Unwin, R.T.: 'Optimal and suboptimal detection of optical fibre digital PPM', *IEE Proc. J, Optoelectron,* 1993, **140**, (6). Pp. 367-375.

[81] Calvert, N.M., Sibley. M.J.N., Unwin, R.T., Garett, I., and Cryan, R.A.: 'Optimal filtering of digital PPM transmitted over optical fibre channels'. IEE Colloquium on Electronic filters. Dig. 1989/97, June 1989, pp. 5/1-5.

[82] Cryan. R.A., Unwin. R.T., Massarella, A.J., Sibley, M.J.N., Garrett, I., and Calvert. N.M.: 'Optical fibre digital PPM: theoretical and experimental results'. Presented at the UK-USSR Symposium on Communication and applications, 1991.

[83] Barry, J.R.: 'Sequence detection and equalization for pulse-position modulation'. Proceedings of the International Conference on Communications, New Orleans, 1994, pp. 1561-1565.

[84] Audeh. M.D., Kahn, J.M., and Barry, J.R.: 'Decision-feedback equalization of pulse-position modulation on measured nondirected indoor infrared channels', *IEEE Trans. Commun.,* 1999, **47,** (4), pp**.** 500**-**503.

[85] Ghassemlooy, Z., Hayes, A.R., Seed, N.L., and Kaluarachchi, E.D.: 'Digital pulse interval modulation for optical communications', *IEEE Commun. Mag.*, 1998, **36**, pp. 95–99.

[86] Hayes, A.R., Ghassemlooy, Z., Seed, N.L., and McLaughlin, R.: 'Baseline-wander effects on systems employing digital pulse interval modulation', *IEE Proc., Optoelectron.*, 2000, **147**, pp. 295–300.

[87] Ghassemlooy, Z., Hayes, A.R., and Wilson, B.: 'Reducing the effects of intersymbol interference in diffuse DPIM optical wireless communications', *IEE Proc., Optoelectron.*, 2003, **150**, pp. 445–452.

[88] Aldibbiat, N.M., Ghassemlooy, Z., and McLaughlin, R.: 'Performance of dual header-pulse interval modulation (DH-PIM) for optical wireless communication systems', *Proc. SPIE-Int. Soc. Opt. Eng.*,2001, **4214**, pp. 144–152.

[89] Aldibbiat, N.M., Ghassemlooy, Z., and McLaughlin, R.: 'Dual header pulse interval modulation for dispersive indoor optical wireless communication systems', *IEE Proc., Circuits Devices Syst.*, 2002,**149**, pp. 187–192.

[90] Lee, D.C., Khan, J.M., and Audeh, M.D.: 'Trellis-coded pulse position modulation for wireless indoor infrared communications', *IEEE Trans. Commun.*, 1997, **45**, pp. 1080–1087.

[91] Park, H., and Barry, J.R.: 'Trellis-coded multiple-pulse-position modulation for wireless infrared communications', *IEEE Trans. Commun.*, 2004, **52**, pp. 643–651.

[92] Lee, D.C.M., and Khan, J.M.: 'Coding and equalisation for PPM on wireless infrared channels', *IEEE Trans. Commun.,* 1999, **47**, pp. 255–260.

[93] Bar-David, I., and Kaplan, G.: 'Information rates of photon-limited overlapping pulse position modulation channels'*. IEEE Trans. Inf. Theory*, 1984, **30**, (3), pp.455-464.
[94] Cattermole, K.W.: 'Representation and analysis of digital line codes', in 'Mathematical topics in telecommunications'. Vol. 2 (Pentech Press, London, 1984).

[95] Pires, J. J. O., and da Rocha, J. R. F.: 'Digital pulse position modulation over optical fibres with avalanche photodiode receivers,' *IEE Proc. Pt. J.*, Vol. 133, No. 5, 1986, pp. 309-313.

[96] Pierce, J.R. (1978). Optical channels: Practical limits on photon counting, *IEEE Trans. Commun.*, 1978, **COM-26**, (12), pp. 1819-1821.

[97] Cryan, R.A. Space communications employing optical pulse position modulation. *Proc. IEE 3rd European Conference on Satellite Communications (ECSC-3), Manchester*, 1993, pp. 192-195.

[98] Cryan, R.A., and Unwin, R.T. (1992). Reed-Solomon coded homodyne digital pulse position modulation*, IEE Proc. I, Commun., Speech Vis.*, 1992, **139**, (2), pp. 140-146.

[99] Phillips, A.J., Cryan, R.A. and Senior, J.M. (1994, May). Performance evaluation of optically pre-amplified PPM systems. IEEE Photonics Technology Letters, Vol. 6, No. 5, pp. 651-653.

[100] Phillips, A.J., Cryan, R.A. and Senior, J.M. (1995, October). An improved analysis for optically preamplified pulse-position modulation receivers in optical fibre systems. Microwave and Optical Technology Letters, Vol. 10, No. 2, pp. 108-111.

[101] Phillips, A.J., Cryan, R.A. and Senior, J.M. (1996, April). Optically preamplified pulse-position modulation for fibre-optic communication systems. IEE Proceedings- Optoelectronics, Vol. 143, No. 2, pp. 153-159.

[102] Phillips, A.J., Cryan, R.A. and Senior, J.M. (1996, May). An optically preamplified intersatellite PPM receiver employing maximum likelihood detection. IEEE Photonics Technology Letters, Vol. 8, No. 5, pp. 691-693.

[103] Phillips, A.J., Cryan, R.A. and Senior, J.M. (1997, January). An optically preamplified digital PPM receiver with improved suboptimum filtering. *Microwave and Optical Technology Letters*, Vol. 14, No. 1, pp. 23-28.

[104] Phillips, A.J., AL-Suleimani, I.H. and Woolfson, M.S., (2008). Performance evaluation of optically preamplified dicode pulse position modulation receivers*. European Trans. Telecomm*, 19(1), 47-52.

SENSOR SOLUTIONS

DATASHEET

High Speed InGaAs PIN Photodiodes

C30616, C30637, C30617, C30618 Series

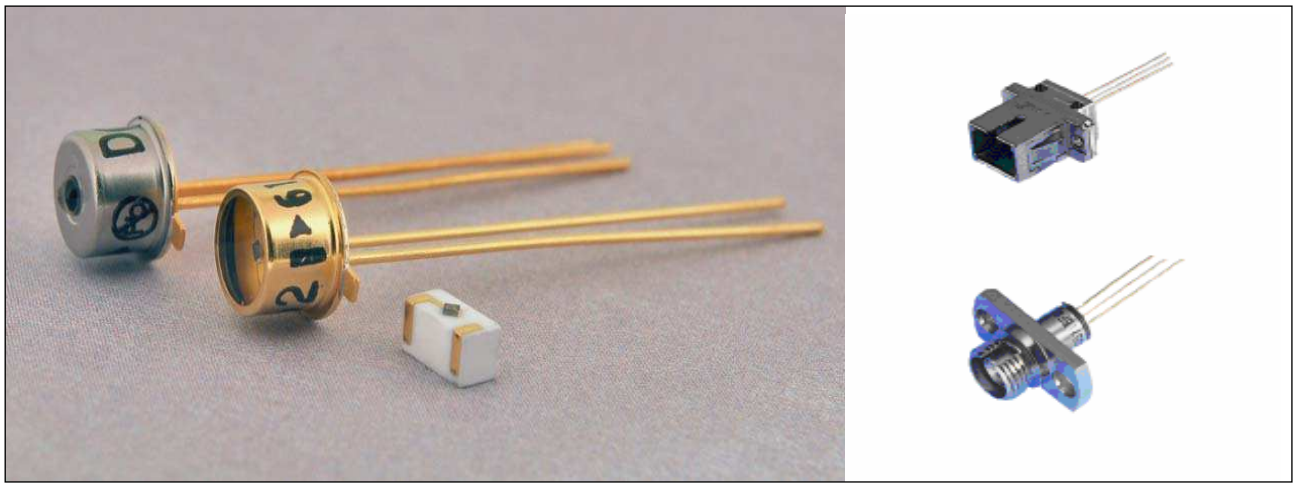

Overview

This series of high speed InGaAs photodiodes is designed for use in OEM fiber-optic communications systems and high-speed receiver applications including trunk line, LAN, fiber-in-the-loop and data communications. Ceramic sub-mount packages are available for easy integration into high speed SONET, FDDI, data link receiver modules, or as back facet power monitors in laser diode modules.

Available in hermetic TO-18 packages, or in connectorized receptacle packages with industry standard FC or SC connectors, these photodiodes are designed to function with either single or multimode fibers. Receptacle packages use a ball-lens TO-18 package to maximize coupling efficiency. All devices are planar passivated and feature proven, high reliability mounting and contacting.

Recognizing that different applications have different performance requirements, PerkinElmer offers a wide range of customization of these photodiodes to meet your design challenges. Responsivity and noise screening, custom device testing and packaging are among many of the application specific solutions available

Features and Benefits

- Available in various packages
- 50, 75, 100, 350 µm diameters
- High responsivity at 1300 and 1550 nm
- Low capacitance for high bandwidths (to 3.5 GHz)
- RoHS Compliant

Applications

- Telecommunications
- Instrumentation
- Data transmission
- High speed switching
- Data links and LANs

PerkinElmer® precisely.

Table of Contents

Table 1. Mechanical and Optical Characteristics

	C30616	C30637	C30617	C30618	Unit
Shape	Circular	Circular	Circular	Circular	
Useful Area	0.002	0.004	0.008	0.096	mm^2
Useful Diameter	50	75	100	350	µm
Package Types[1]	Rectangular ceramic	Rectangular ceramic	TO-18 Ball Lens, Rectangular ceramic, FC, SC receptacle	TO-18, Rectangular ceramic, FC receptacle	
Window Type			Ball Lens Glass	Flat Glass	

1. See Figures 5-10 for package dimension details.

Table 2. Typical Electrical Characteristics at T_A = 22 °C, @ V_R=Vop typical

Parameter	C30616			C30637			Units
	Min	Typ	Max	Min	Typ	Max	
Operating voltage (Vop)	1	5	10	1	5	10	V
Breakdown voltage	25	100	-	25	100	-	V
Responsivity @ 1300 nm TO-18, ceramic FC/ST/SC receptacle	0.80 -	0.90 -	- -	0.80 -	0.90 -	- -	A/W
Responsivity @ 1550 nm TO-18, ceramic FC/ST/SC receptacle	0.85 -	0.95 -	- -	0.85 -	0.95 -	- -	A/W
Dark Current	-	<1.0	2.0	-	<1.0	2.0	nA
Spectral Noise current (10KHz, 1.0 Hz)	-	<0.02	0.15	-	<0.02	0.15	pA/√Hz
Capacitance @ V_R=V_{OP} Ceramic TO-18	-	0.35 -	0.55 -	-	0.40 -	0.60 -	pF
Rise/Fall time (10%-90%)	-	0.07	0.5	-	0.07	0.5	ns
Bandwidth (-3dB, R_L=50Ω)	-	3.5	-	-	3.5	-	GHz
Maximum Forward Current	-	-	10	-	-	10	mA
Power Dissipation	-	-	100	-	-	100	mW
Storage Temperature	-60		125	-60		125	°C
Operating Temperature	-40		125	-40		125	°C

Parameter	C30617			C30618			Units
	Min	Typ	Max	Min	Typ	Max	
Operating voltage	1	5	10	1	5	10	V
Breakdown voltage	25	100	-	25	80	-	V
Responsivity @ 1300 nm TO-18, ceramic FC/ST/SC receptacle[2]	 0.80 0.65	 0.90 0.75	 - -	 0.80 0.65	 0.90 0.75	 - -	A/W
Responsivity @ 1550nm TO-18, ceramic FC/ST/SC receptacle[2]	 0.85 0.70	 0.95 0.80	 - -	 0.85 0.70	 0.95 0.80	 - -	A/W
Dark Current Ceramic package TO-18 package	 -	 <1.0 -	 2.0 4.0	 -	 1.0 -	 5.0 -	nA
Spectral Noise current (10 KHz, 1.0 Hz)	-	<0.02	0.15	-	0.02	0.20	pA/√Hz
Capacitance @ V_R=V_{OP} Ceramic TO-18	-	 0.6 0.8	 0.8 1.0	-	 4.0 4.0	 6.0 6.0	pF
Rise/Fall time (10%-90%)	-	0.07	0.5	-	0.5	1.0	ns
Bandwidth (-3dB, R_L=50Ω)	-	3.5	-	-	0.75	-	GHz
Maximum Forward Current	-	-	10	-	-	10	mA
Power Dissipation	-	-	100	-	-	100	mW
Storage Temperature[3]	-60		125	-60		125	°C
Operating Temperature[3]	-40		125	-40		125	°C

2. Coupled from 62.5 µm, 0.28NA, graded index multi-mode fiber using 1300 nm SLED source.
3. Maximum storage and operating temperature of connectorized /receptacle devices is +85°C.

Table 3. Ordering Guide

Package Type	C30616	C30637	C30617	C30618
TO-18 ball glass lens	-	-	C30617BH	-
TO-18 flat glass lens	-	-	-	C30618GH
Rectangular ceramic	C30616ECERH	C30637ECERH	C30617ECERH	C30618ECERH
TO-18 ball lens with FC receptacle	-	-	C30617BFCH	C30618BFCH
TO-18 ball lens with SC receptacle	-	-	C30617BSCH	-

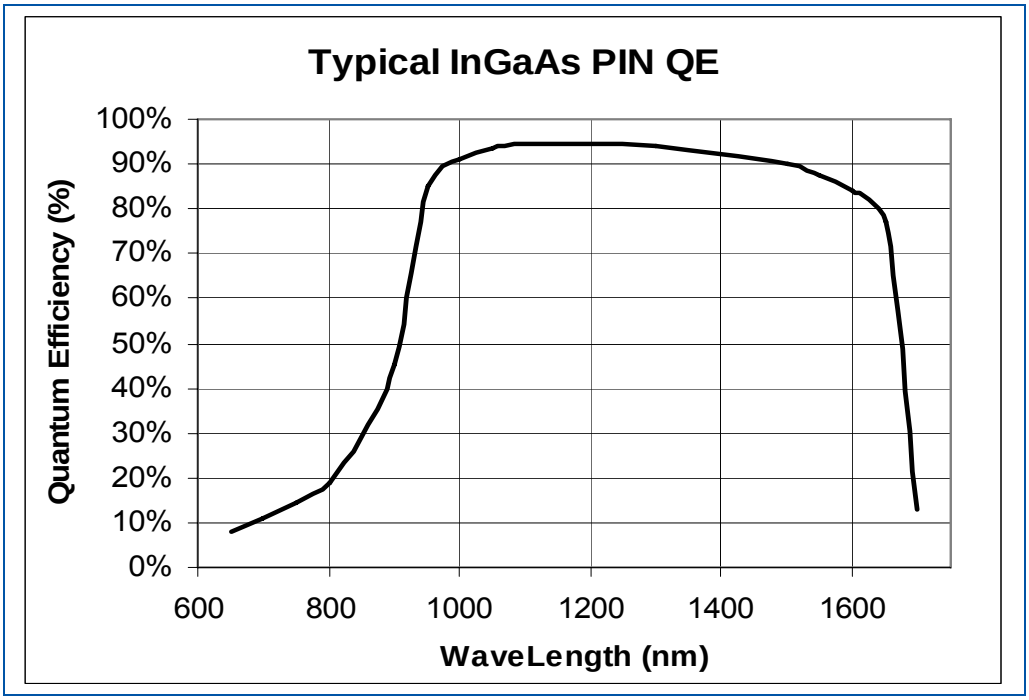

Figure 1
Typical Quantum Efficiency vs. Wavelength

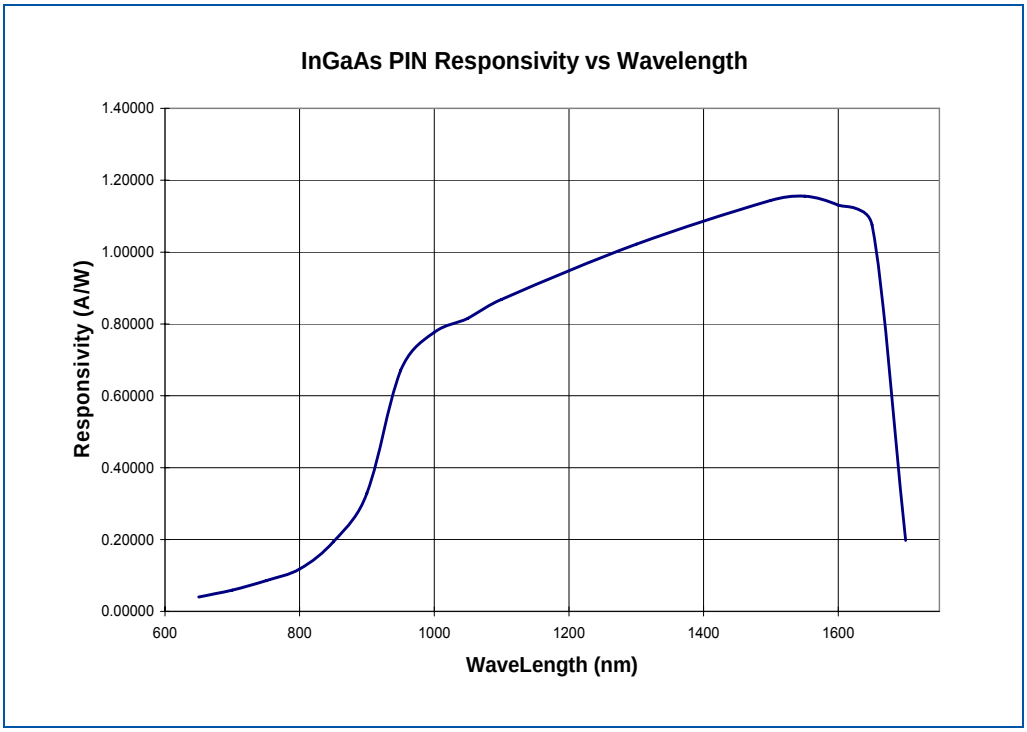

Figure 2
Typical Responsivity vs. Wavelength

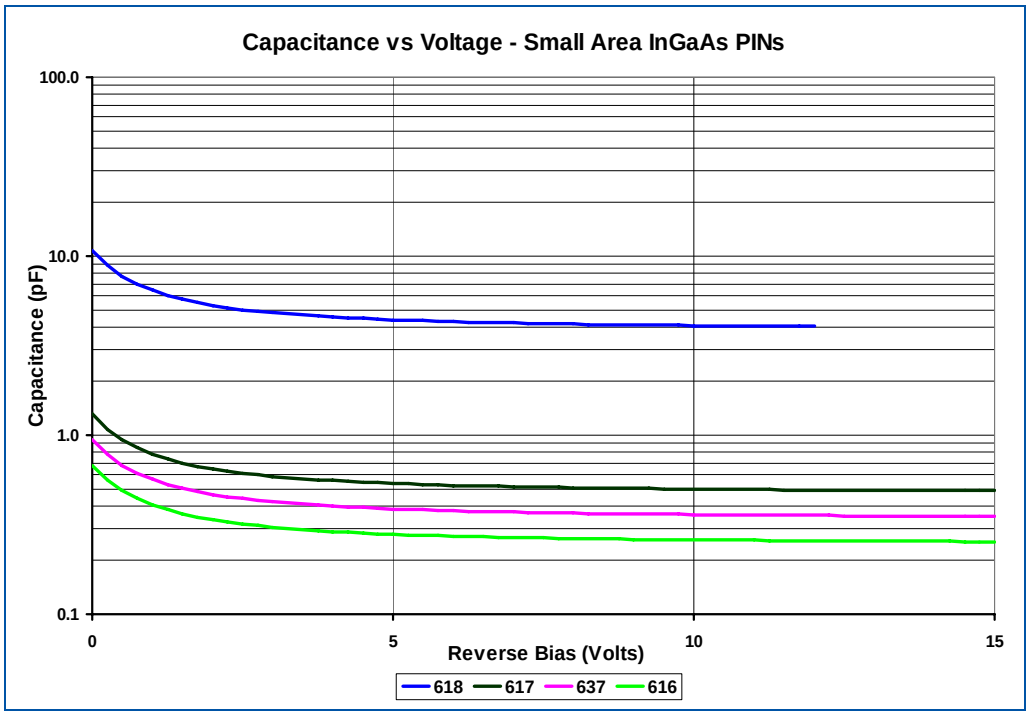

Figure 3
Typical Capacitance vs. Operating Voltage

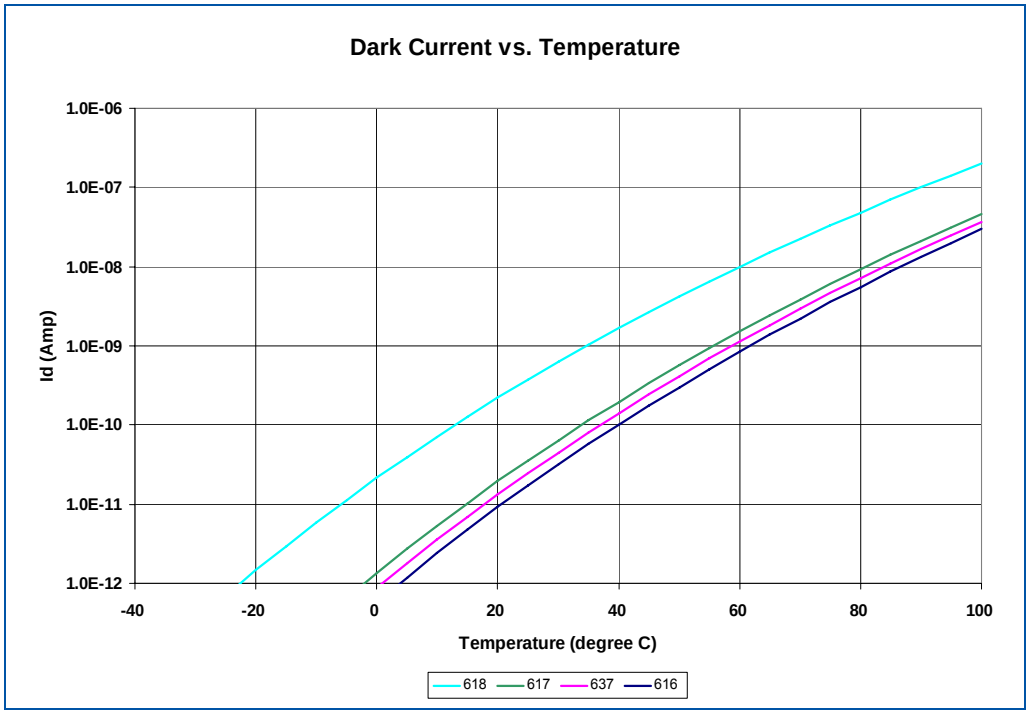

Figure 4
Typical Dark Current vs. Temperature

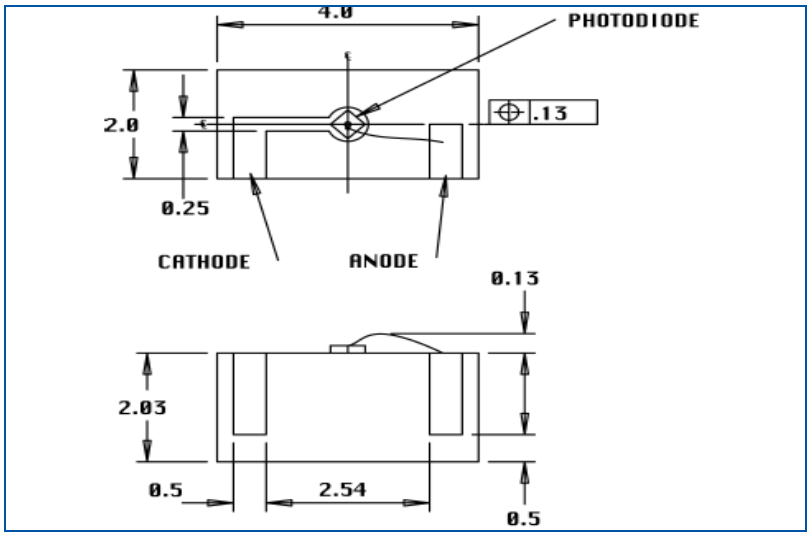

Figure 5
Package dimension for rectangular ceramic ECERH types, in mm, for reference only

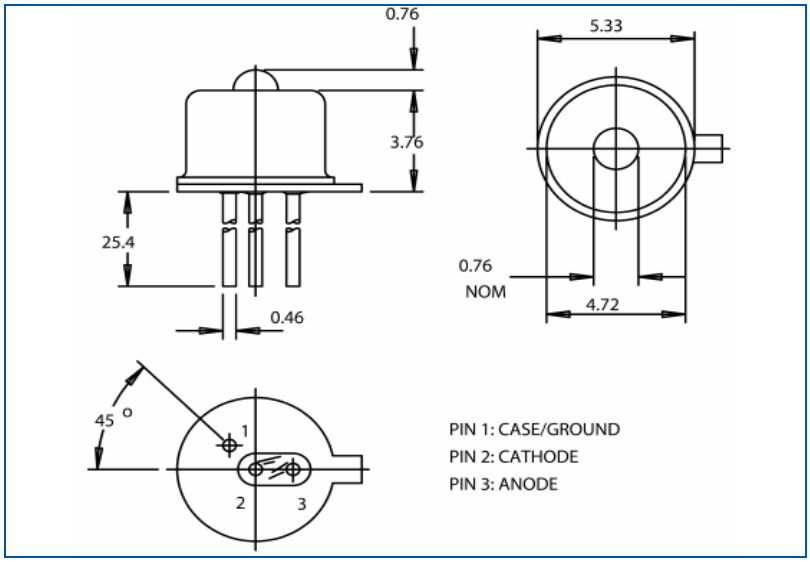

Figure 6
Package dimension for TO-18 ball lens BH types, in mm, for reference only

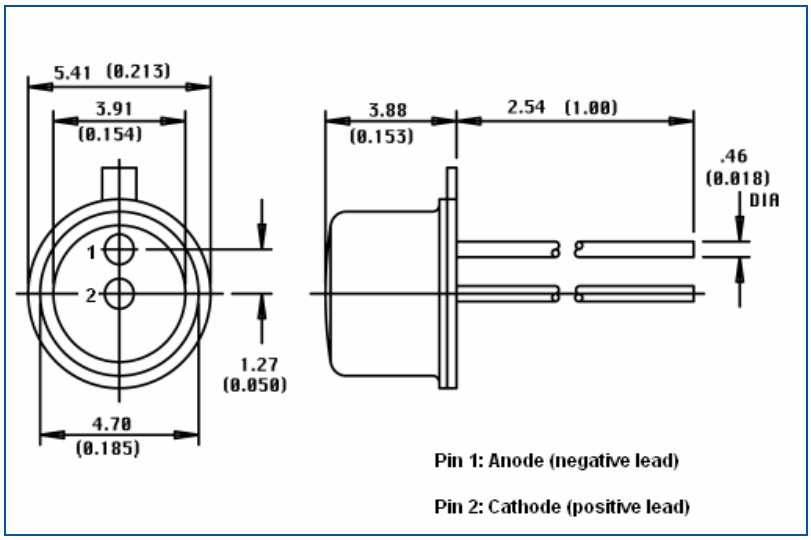

Figure 7
Package dimension for TO-18 flat glass lens GH types, in mm, for reference only

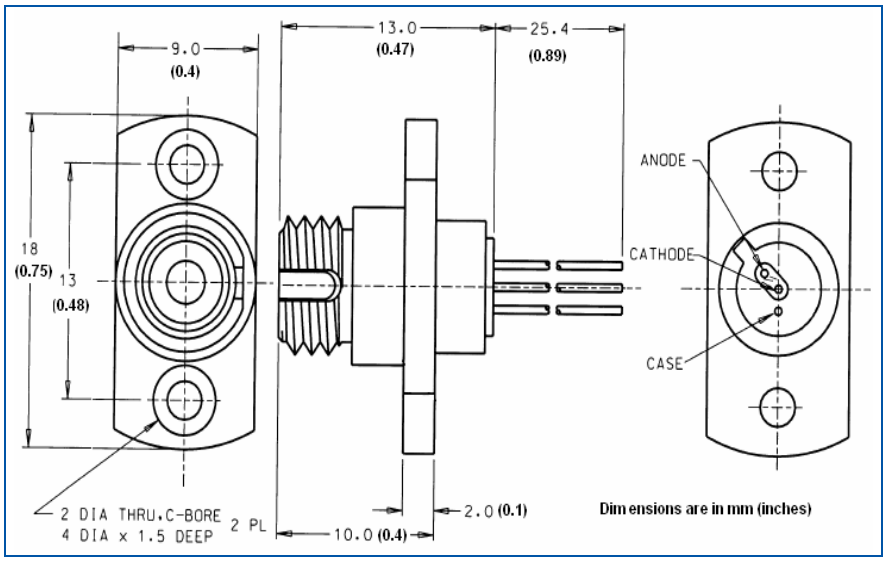

Figure 8
Package dimension for TO-18 ball lens FC receptacle BFC types, in mm (inches), for reference only

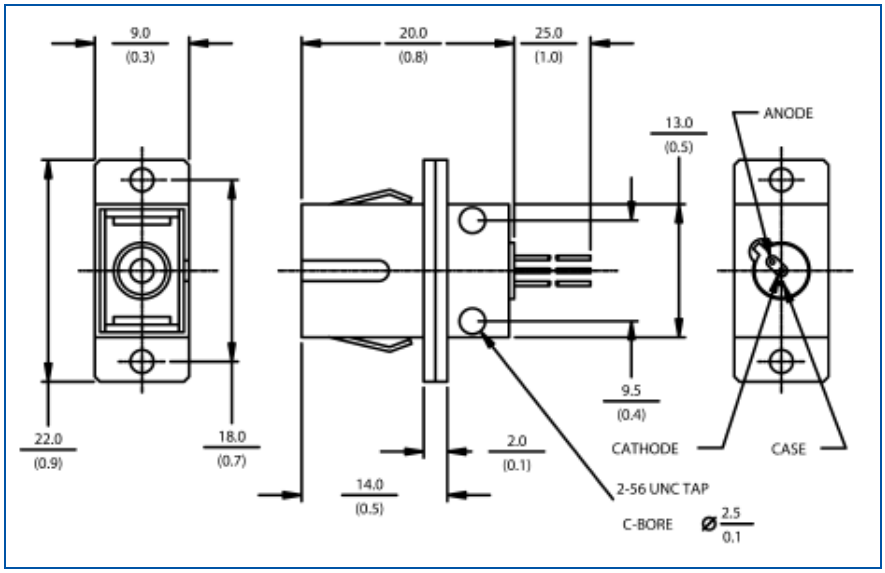

Figure 9
Package dimension for TO-18 ball lens SC receptacle BSC types, in mm (inches), for reference only

RoHS Compliance

This series of photodiodes is designed and built to be fully compliant with the European Union Directive 2002/95EEC – Restriction of the use of certain Hazardous Substances in Electrical and Electronic equipment.

Warranty

A standard 12-month warranty following shipment applies. Any warranty is null and void if the photodiode window has been opened.

Your Partner of Choice

With a broad customer base in all major markets, built on ninety years of solid trust and cooperation with our customers, PerkinElmer is recognized as a reliable partner that delivers high quantity, customized, and superior "one-stop" solutions. Our products – from single photocells to complex x-ray inspection systems - meet the highest quality and environmental standards. Our worldwide Centres of Excellence, along with our Customer and Technical Support teams, always work with you to find the best solutions for your specific needs.

PerkinElmer Optoelectronics

PerkinElmer Optoelectronics is a global technology leader providing market-driven, integrated solutions for a wide range of applications, which leverage our lighting, sensors, and imaging expertise. Our technologies, services and support are enhancing our customers' productivity, optimizing performance, and accelerating time to market. So contact us and put PerkinElmer's expertise to work in your demanding applications. We will show how our innovations will help you deliver the perfect product.

North America
Customer Support Hub
PerkinElmer Optoelectronics
22001 Dumberry Road
Vaudreuil-Dorion, Québec
Canada J7V 8P7
Telephone: +1 450-424-3300,
(+1) 866-574-6786 (toll-free)
Fax: +1 450-424-3345
Email: opto@perkinelmer.com
www.optoelectronics.perkinelmer.com

European Headquarters
PerkinElmer Optoelectronics
Wenzel-Jaksch-Str. 31
65199 Wiesbaden, Germany
Telephone: (+49) 611-492-247
Fax: (+49) 611-492-170
Email: opto.Europe@perkinelmer.com

Asia Headquarters
PerkinElmer Optoelectronics
47 Ayer Rajah Crescent #06-12
Singapore 139947
Telephone: (+65) 6775-2022
Fax: (+65) 6775-1008
Email: opto.Asia@perkinelmer.com

For a complete listing of our global offices, visit www.optoelectronics.perkinelmer.com

600252_01 DTS0308

Semiconductor Optical Amplifiers – High Power Operation

Boris Stefanov, Leo Spiekman, David Piehler
Alphion Corporation

IEEE 802.3av Task Force Meeting, Orlando, 13-15 March 2007

Two 10 Gb/s downstream solutions

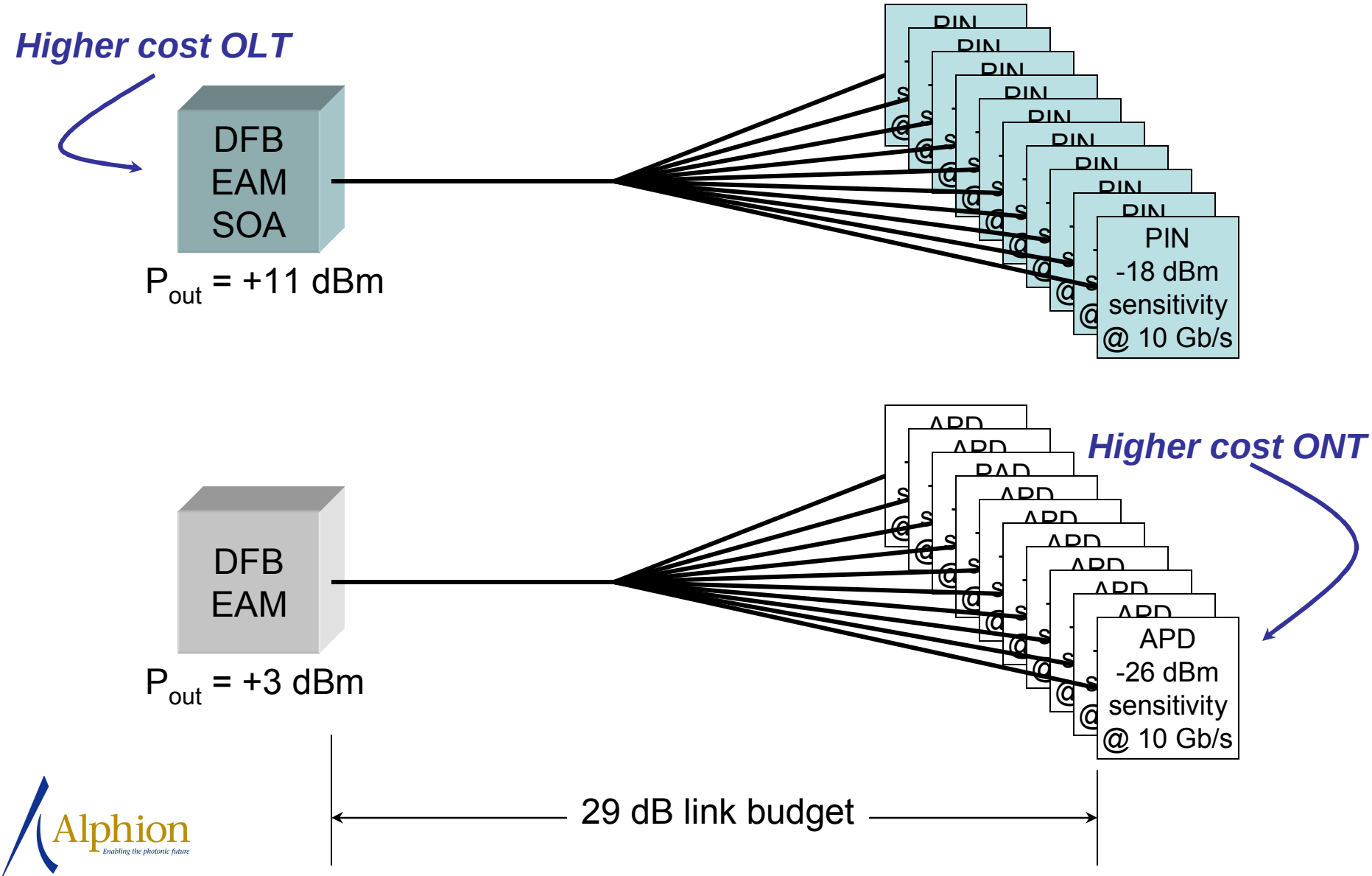

SOA vendor survey

From:
http://www.ieee802.org/3/av/public/2006_11/3av_0611_lee_1.pdf
(November 2006 meeting)

Availability of SOAs

- **Off the shelf** in the spectral band of 1550 nm and 1310 nm
- **Saturation power is > 11 dBm** typically, and 14 dBm maximum
- **Gain is > 10 dB typically**, and 22 dB maximum

Vendor	Wavelength (nm)	Gain (dB)			3dB Saturation Power (dBm)		NF (dB)
		min	typ	max	min	typ	typ
A	1310		14.0			11.0	8.0
B		18.0	22.0			10.0	7.0
		13.0	16.0		10.0		7.0
C		10.0			8.0		6.0
		16.0			8.0		6.0
A	1550		14.0			13.0	7.0
		4.0		8.0		13.0	7.0
B		10.0	13.0		12.0	14.0	8.0
C		12.0	15.0			10.0	9.0
		18.0	20.0			10.0	9.0
D		20.0			10.0	11.0	6.0
		10.0			10.0	11.0	6.0
		15.0			12.0	13.0	6.0
E		10.0		16.0	14.0		6.5

6 IEEE 802.3av 10Gb/s EPON TF, November 2006

Note 1 – SOA saturation power is measured with a cw source. For a modulated signal with P_{ave} = Psat(3dB), the peak,"1," power will be well into saturation, while the "0" will be below saturation.

Production SOAs operating in the 1490 nm range, as well as SOAs with peak gain > 25 dB are also available on the market.

Alphion
Enabling the photonic future

SOA questions

- Performance
  - What happens when SOA operates near saturation?
- State of the art
  - What kind of saturation power are available using present technology?
  - Are there any physical limits to higher saturation powers?
- Feasibility
  - Is SOA technology mature?
  - Are there any lifetime issues when operating SOAs at very high saturation power?
  - What kind of power does such a device draw; what cooling is necessary?

Alphion
Enabling the photonic future

SOAs operating near saturation

- Near saturation
  - Waveform distortion increases
  - Chirp increases

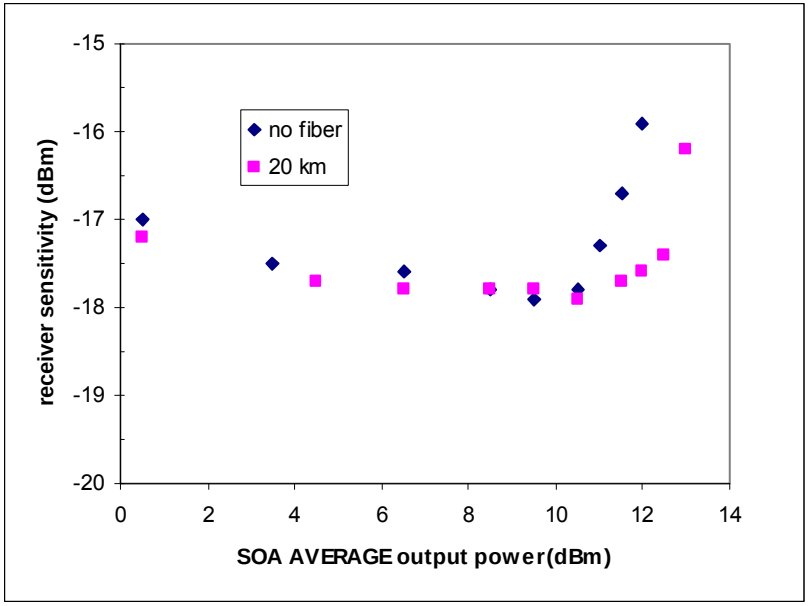

10 Gb/s RZ signal at 0.5 dB into saturation

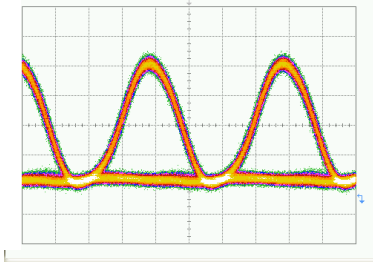

10 Gb/s RZ signal at 6.0 dB into saturation

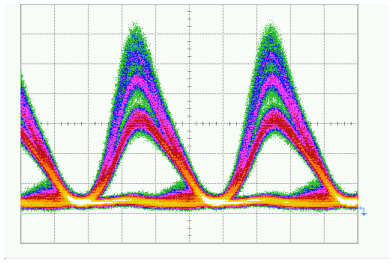

Conditions:

10 Gb/s signal modulation
C-band SOA
P_{sat} (1 dB) = 10 dBm
P_{sat} (3 dB) = 12 dBm
PIN receiver (no optical filter)
~7 GHz electronic filter
Receiver sensitivity measured at 10^{-9} s^{-1} BER

(Note that chirp + dispersion can counteract waveform distortion)

Alphion
Enabling the photonic future

SOAs near saturation

Under the following conditions:

- 10 Gb/s data rate
- Wavelength in the 1480 to 1600 nm range
- Average power at or below the 1 dB (cw) saturation point*
- Through 20 km of G.652 fiber
- Using a PIN receiver

Power penalty will be less than 1 dB compared to operation in the linear regime

*another way to look at this is that the peak power is ~ 4 dB into saturation

Alphion
Enabling the photonic future

SOA state of the art

- Most SOAs marketed today are in-line amplifiers with polarization dependant gain minimized.
  - Since booster amplifiers are matched with a single polarization source, they do not need polarization independent gain.
  - With this constraint removed, higher saturation powers can be obtained.

- Commercially available P_{sat}(1dB) = +10 dBm SOA exist today.

Alphion
Enabling the photonic future

"Semiconductor Optical Amplifiers – High Power Operation" IEEE 802.3av Meeting, Orlando, 13-15 March 2007

SOA hero experiments

"**8×10 Gb/s DWDM transmission over 240 km of standard fiber using a cascade of semiconductor optical amplifiers**," Spiekman, L.H.; Wiesenfeld, J.M.; Gnauck, A.H.; Garrett, L.D.; van den Hoven, G.N.; van Dongen, T.; Sander-Jochem, M.J.H.; Binsma, J.J.M.; Photonics Technology Letters, IEEE Volume 12, Issue 8, Aug. 2000 Page(s):1082 – 1084
(SOAs are operated with P_{ave} at the 1 dB (cw) saturation point with ~ 1dB power penalty)

"**High saturation power (>16.5 dBm) and low noise figure (<6 dB) semiconductor optical amplifier for C-band operation**," Borghesani, A.; Fensom, N.; Scott, A.; Crow, G.; Johnston, L.; King, J.; Rivers, L.; Cole, S.; Perrin, S.; Scrase, D.; Bonfrate, G.; Ellis, A.; Lealman, I.; Crouzel, G.; Chun, L.H.K.; Lupu, A.; Mahe, E.; Maigne, P.; Optical Fiber Communications Conference, 2003. 23-28 March 2003 Page(s):534 - 536 vol.2

"**Record high saturation power (+22 dBm) and low noise figure (5.7 dB) polarization-insensitive SOA module**," Morito, K.; Tanaka, S.; Photonics Technology Letters, IEEE Volume 17, Issue 6, June 2005 Page(s):1298 - 1300

"**An ultrawide-band (120 nm) semiconductor optical amplifier having an extremely-high penalty-free output power of 23 dBm realized with quantum-dot active layers**," Akiyama, T.; Ekawa, M.; Sugawara, M.; Sudo, H.; Kawaguchi, K.; Kuramata, A.; Ebe, H.; Morito, K.; Imai, H.; Arakawa, Y.; Optical Fiber Communication Conference, 2004. Volume 2, 23-27 Feb. 2004

Alphion
Enabling the photonic future

SOA feasibility

- SOAs use the identical InP technology used in
  - 1550 nm DFB lasers
  - EA modulators
  - 1480 nm EDFA pump lasers
    - These devices use similar materials and waveguide dimensions and output > 300 mW (24.8 dBm)
- Fabrication, packaging, and lifetime are well understood.

Alphion
Enabling the photonic future

Powering

- A SOA operating at +12 dBm output power requires:
  - 400 mA of current (with a 1.8 V drop)
  - 3 W of TEC power to operate at 25℃ chip temperature over a case temperature of -40 to 65℃

Alphion
Enabling the photonic future

Physical Limits

- Output power is limited by heating due to the injection of carriers in the active stripe.
- In concept, one could have SOAs with output powers as high as 1480 nm EDFA pump lasers (> 300 mW)
  - In fact Morito, *et al.* demonstrated essentially this in their *Hero* paper.

Alphion
Enabling the photonic future

Summary

- For the 10G – EPON downstream application, SOA-based OLT transmitters can reliably provide required performance with present day technology.

Alphion
Enabling the photonic future

PCM (3 Bits)	DPPM False Alarm Per PCM Bit	MPPM (5,2) False Alarm Per PCM Bit	Dicode PPM False Alarm Per PCM Bit
000	0.286	0.333	0.249
001	0.286	0.314	0.249
010	0.286	0.351	0.249
011	0.286	0.259	0.249
100	0.286	0.277	0.249
101	0.286	0.37	0.249
110	0.286	0.314	0.249
111	0.286	0.259	0.249
Average	**0.286**	**0.309**	**0.249**

PCM (3 Bits)	DPPM Erasure Per PCM Bit	MPPM Erasure Per PCM Bit	Dicode PPM Erasure Per PCM Bit
000	0.5	0.375	0.193
001	0.5	0.38	0.193
010	0.5	0.428	0.193
011	0.5	0.333	0.193
100	0.5	0.333	0.193
101	0.5	0.4285	0.193
110	0.5	0.388	0.193
111	0.5	0.388	0.193
Average	0.5	0.382	0.193

PCM (4Bits)	DPPM False Alarm Per PCM Bit	MPPM (7,2) False Alarm Per PCM Bit	Dicode PPM False Alarm Per PCM Bit
0000	0.266	0.2833	0.249
0001	0.266	0.33325	0.249
0010	0.266	0.3083	0.249
0011	0.266	0.3416	0.249
0100	0.266	0.2833	0.249
0101	0.266	0.31665	0.249
0110	0.266	0.3999	0.249
0111	0.266	0.3666	0.249
1000	0.266	0.32495	0.249
1001	0.266	0.3166	0.249
1010	0.266	0.3	0.249
1011	0.266	0.3166	0.249
1100	0.266	0.29995	0.249
1101	0.266	0.2583	0.249
1110	0.266	0.27495	0.249
1111	0.266	0.2166	0.249
Average	**0.266**	**0.3088**	**0.249**

PCM (4Bits)	DPPM Erasure Per PCM Bit	MPPM (7,2) Erasure Per PCM Bit	Dicode PPM Erasure Per PCM Bit
0000	0.5	0.354	0.193
0001	0.5	0.4375	0.193
0010	0.5	0.4	0.193
0011	0.5	0.45	0.193
0100	0.5	0.388	0.193
0101	0.5	0.444	0.193
0110	0.5	0.5	0.193
0111	0.5	0.475	0.193
1000	0.5	0.425	0.193
1001	0.5	0.444	0.193
1010	0.5	0.416	0.193
1011	0.5	0.425	0.193
1100	0.5	0.425	0.193
1101	0.5	0.361	0.193
1110	0.5	0.388	0.193
1111	0.5	0.375	0.193
Average	**0.5**	**0.419**	**0.193**

PCM (5 Bits)	DPPM False Alarm Per PCM Bit	MPPM (9,2) False Alarm Per PCM Bit	Dicode PPM False Alarm Per PCM Bit
00000	0.258	0.266	0.249
00001	0.258	0.266	0.249
00010	0.258	0.323	0.249
00011	0.258	0.323	0.249
00100	0.258	0.3142	0.249
00101	0.258	0.280	0.249
00110	0.258	0.280	0.249
00111	0.258	0.247	0.249
01000	0.258	0.285	0.249
01001	0.258	0.304	0.249
01010	0.258	0.304	0.249
01011	0.258	0.314	0.249
01100	0.258	0.276	0.249
01101	0.258	0.280	0.249
01110	0.258	0.271	0.249
01111	0.258	0.438	0.249

10000	0.258	0.304	0.249
10001	0.258	0.323	0.249
10010	0.258	0.299	0.249
10011	0.258	0.323	0.249
10100	0.258	0.309	0.249
10101	0.258	0.361	0.249
10110	0.258	0.3428	0.249
10111	0.258	0.347	0.249
11000	0.258	0.347	0.249
11001	0.258	0.323	0.249
11010	0.258	0.299	0.249
11011	0.258	0.309	0.249
11100	0.258	0.304	0.249
11101	0.258	0.285	0.249
11110	0.258	0.242	0.249
11111	0.258	0.252	0.249
Average	***0.258***	***0.305***	***0.249***

PCM (5 Bits)	DPPM Erasure Per PCM Bit	MPPM (9,2) Erasure Per PCM Bit	Dicode PPM Erasure Per PCM Bit
00000	0.5	0.35	0.193
00001	0.5	0.35	0.193
00010	0.5	0.4375	0.193
00011	0.5	1.0625	0.193
00100	0.5	0.426	0.193
00101	0.5	0.4	0.193
00110	0.5	0.4	0.193
00111	0.5	0.369	0.193
01000	0.5	0.375	0.193
01001	0.5	0.4	0.193
01010	0.5	0.4	0.193
01011	0.5	0.426	0.193
01100	0.5	0.4	0.193
01101	0.5	0.4	0.193
01110	0.5	0.4	0.193
01111	0.5	0.575	0.193
10000	0.5	0.4	0.193

10001	0.5	0.44	0.193
10010	0.5	0.428	0.193
10011	0.5	0.457	0.193
10100	0.5	0.446	0.193
10101	0.5	0.475	0.193
10110	0.5	0.453	0.193
10111	0.5	0.428	0.193
11000	0.5	0.485	0.193
11001	0.5	0.461	0.193
11010	0.5	0.4	0.193
11011	0.5	0.428	0.193
11100	0.5	0.428	0.193
11101	0.5	0.415	0.193
11110	0.5	0.384	0.193
11111	0.5	0.4	0.193
Average	***0.5***	***0.440***	***0.193***

PCM (6 Bits)	DPPM False Alarm Per PCM Bit	MPPM (12,2) False Alarm Per PCM Bit	Dicode PPM False Alarm Per PCM Bit
000000	0.253	0.233	0.249
000001	0.253	0.2666	0.249
000010	0.253	0.255	0.249
000011	0.253	0.283	0.249
000100	0.253	0.288	0.249
000101	0.253	0.277	0.249
000110	0.253	0.34995	0.249
000111	0.253	0.338	0.249
001000	0.253	0.291	0.249
001001	0.253	0.311	0.249
001010	0.253	0.302	0.249
001011	0.253	0.311	0.249
001100	0.253	0.327	0.249
001101	0.253	0.327	0.249
001110	0.253	0.32215	0.249
001111	0.253	0.355	0.249
010000	0.253	0.316	0.249

010001	0.253	0.349	0.249
010010	0.253	0.316	0.249
010011	0.253	0.330	0.249
010100	0.253	0.3083	0.249
010101	0.253	0.3166	0.249
010110	0.253	0.361	0.249
010111	0.253	0.311	0.249
011000	0.253	0.3555	0.249
011001	0.253	0.272	0.249
011010	0.253	0.3166	0.249
011011	0.253	0.2722	0.249
011100	0.253	0.302	0.249
011101	0.253	0.2694	0.249
011110	0.253	0.399	0.249
011111	0.253	0.394	0.249
100000	0.253	0.327	0.249
100001	0.253	0.322	0.249
100010	0.253	0.344	0.249
100011	0.253	0.327	0.249
100100	0.253	0.324	0.249

100101	0.253	0.308	0.249
100110	0.253	0.294	0.249
100111	0.253	0.2944	0.249
101000	0.253	0.299	0.249
101001	0.253	0.333	0.249
101010	0.253	0.294	0.249
101011	0.253	0.3083	0.249
101100	0.253	0.302	0.249
101101	0.253	0.333	0.249
101110	0.253	0.338	0.249
101111	0.253	0.327	0.249
110000	0.253	0.336	0.249
110001	0.253	0.349	0.249
110010	0.253	0.324	0.249
110011	0.253	0.3166	0.249
110100	0.253	0.305	0.249
110101	0.253	0.2916	0.249
110110	0.253	0.308	0.249
110111	0.253	0.266	0.249
111000	0.253	0.2777	0.249

111001	0.253	0.263	0.249
111010	0.253	0.2805	0.249
111011	0.253	0.283	0.249
111100	0.253	0.297	0.249
111101	0.253	0.288	0.249
111110	0.253	0.274	0.249
111111	0.253	0.283	0.249
Average	***0.253***	***0.310***	***0.249***

PCM (6 Bits)	DPPM Erasure Per PCM Bit	MPPM (12,2) Erasure Per PCM Bit	Dicode PPM Erasure Per PCM Bit
000000	0.5	0,318	0.193
000001	0.5	0.363	0.193
000010	0.5	0.356	0.193
000011	0.5	0.386	0.193
000100	0.5	0.393	0.193
000101	0.5	0.378	0.193
000110	0.5	0.477	0.193
000111	0.5	0.462	0.193
001000	0.5	0.420	0.193
001001	0.5	0.436	0.193
001010	0.5	0.441	0.193
001011	0.5	0.4318	0.193
001100	0.5	0.446	0.193
001101	0.5	0.446	0.193
001110	0.5	0.439	0.193
001111	0.5	0.484	0.193
010000	0.5	0.4318	0.193

010001	0.5	0.477	0.193
010010	0.5	0.444	0.193
010011	0.5	0.460	0.193
010100	0.5	0.441	0.193
010101	0.5	0.4318	0.193
010110	0.5	0.492	0.193
010111	0.5	0.424	0.193
011000	0.5	0.484	0.193
011001	0.5	0.371	0.193
011010	0.5	0.431	0.193
011011	0.5	0.380	0.193
011100	0.5	0.428	0.193
011101	0.5	0.383	0.193
011110	0.5	0.545	0.193
011111	0.5	0.537	0.193
100000	0.5	0.446	0.193
100001	0.5	0.439	0.193
100010	0.5	0.469	0.193
100011	0.5	0.460	0.193
100100	0.5	0.460	0.193

100101	0.5	0.45	0.193
100110	0.5	0.401	0.193
100111	0.5	0.401	0.193
101000	0.5	0.409	0.193
101001	0.5	0.454	0.193
101010	0.5	0.412	0.193
101011	0.5	0.428	0.193
101100	0.5	0.433	0.193
101101	0.5	0.454	0.193
101110	0.5	0.462	0.193
101111	0.5	0.446	0.193
110000	0.5	0.476	0.193
110001	0.5	0.492	0.193
110010	0.5	0.475	0.193
110011	0.5	0.431	0.193
110100	0.5	0.416	0.193
110101	0.5	0.412	0.193
110110	0.5	0.436	0.193
110111	0.5	0.391	0.193
111000	0.5	0.378	0.193

111001	0.5	0.373	0.193
111010	0.5	0.396	0.193
111011	0.5	0.416	0.193
111100	0.5	0.420	0.193
111101	0.5	0.404	0.193
111110	0.5	0.4	0.193
111111	0.5	0.425	0.193
Average	***0.5***	***0.433***	***0.193***

Pulse position modulation coding schemes for optical intersatellite links

F.J. Ghosna and M.J.N. Sibley

The rapid and significant development of communications links between satellites has made it possible to use various applications such as relay voice, video, multimedia, etc. As a result, much research has been carried out in this field during recent years to reduce power consumption and increase transmission reliability. This reported work focuses on analysis of intersatellite links in free space, with optical links using laser sources being considered in particular. The use of several different coding schemes are discussed for use in such links: multiple pulse position modulation (MPPM); digital pulse position modulation (DPPM); Dicode pulse position modulation (Dicode PPM). Work has been carried out to compare these coding schemes in terms of error weightings and coding efficiency through showing how the PCM error rate is affected by false alarm and erasure errors for MPPM, DPPM and Dicode PPM coding 3 bits of PCM. Comparison between these coding schemes is drawn in terms of sensitivity and bandwidth efficiency.

Introduction: The competing technologies of optical and microwave systems have been examined by McCullagh *et al.* [1] and Ekberg [2]. These studies show that, in general, microwave radio systems can receive much lower power levels and operate in the atmosphere more efficiently than optical ones [1]. However, in space, optical systems can operate with much lower path loss and are considered superior to microwave ones [2]. In addition, they have the potential of operation at Gbit/s data rates. Therefore, according to these considerations, optical links in space are receiving a great deal of attention.

The first significant optical intersatellite link, in 2000, was the Semiconductor Laser Intersatellite Link Experiment (SILEX) by the European Space Agency (ESA) using semiconductor laser diode technology [3]. The most recent project, in 2006, is the Optical Inter-orbit Communications Engineering Test Satellite (OICETS) 'Kirari' by the Japan Aerospace Exploration Agency (JAXA) using laser utilising communications equipment (LUCE) [4]. This was an optical inter-orbit communications system using a high-power semiconductor laser between satellites that are tens of thousands of kilometres apart. As a source, laser diodes have many advantages: small size; high electrical to optical efficiencies; tightly focused beam. In addition, it is possible to adapt the technology used in fibre-optic links to free-space communications and so multi-Gbit/s transmission is possible using readily available integrated driver chips.

As these devices operate at a wavelength of 1.55 μm, this must be the wavelength of operation for the link.

Coding schemes: Digital pulse position modulation (DPPM) is currently the preferred coding scheme for use in optical inter-satellite links because it operates with very low average power and offers high sensitivity. However, it suffers from a very large bandwidth expansion problem [5]. This places great strain on the processing electronics as the speed can be prohibitive.

Many alternatives have been proposed that operate with a smaller bandwidth expansion. Of these, multiple PPM (MPPM) [5] and Dicode PPM [6] appear to offer lowest bandwidth expansion. MPPM uses two or more pulses in a frame with the pulse positions being determined by the original PCM word, whereas Dicode PPM only transmits a pulse when there is a transition between levels. Sibley [5] examined the impact of detection errors on the resulting PCM data through considering a (12/2) multiple PPM scheme operating over graded-index plastic optical fibre. He found that PPM systems suffer from three types of detection error: wrong-slot, false alarm and erasure errors. Wrong-slot error occurs in dispersive channels and is not applicable in free space. Therefore, only erasure and false alarm errors are relevant in free-space communications. A false alarm is caused by noise in an empty time slot generating a threshold crossing and an erasure is caused by noise obliterating a valid pulse. As the original PCM code is converted into another code, these errors will cause the original PCM to be corrupted. The coding alphabet for MPPM and DPPM for 3 bits of PCM is shown in Table 1.

Work has been carried out to show how the PCM error rate is affected by false alarm and erasure errors for MPPM, DPPM and Dicode PPM operating with 3 bits of PCM. A maximum likelihood sequence detector (MLSD) is used in the decoder with the same method as mentioned by Sibley [5].The process is repeated for false alarms and erasures in all vacant slots and the average number of PCM errors obtained. Consideration of all possible codewords yields the total average number of PCM bits in error due to false alarm and erasure detection errors as can be seen in Table 2. The erasure and false alarm weightings for Dicode PPM are independent of the coding level because the Dicode system operates continuously.

Table 1: Alphabet for coding 3 bits of PCM into MPPM and DPPM

PCM (3 bits)	MPPM (5,2)	DPPM
000	11000 (1,2)	0000 0001
001	10100 (1,3)	0000 0010
010	10010 (1,4)	0000 0100
011	10001 (1,5)	0000 1000
100	01100 (2,3)	0001 0000
101	01010 (2,4)	0010 0000
110	01001 (2,5)	0100 0000
111	00110 (3,4)	1000 0000

Table 2: Summary of results of simulations for MPPM, DPPM and DPPM operating with 3 bits of PCM

3 bits PCM	MPPM	DPPM	Dicode PPM
Weighting for false alarm errors	0.309	0.286	0.249
Weighting for erasure errors	0.382	0.5	0.193
Photon per PCM bit	2.822×10^3	2.341×10^3	7.292×10^3
Noise bandwidth (Hz)	8.776×10^8	1.404×10^9	1.053×10^9
Final line rate (B/W expansion)	1.7 × PCM data rate (3 bits)	2.7 × PCM data rate (3 bits)	2 × PCM data rate (fixed)
Slot time (S)	6×10^{-10}	3.75×10^{-10}	5×10^{-10}
Normalised peak voltage (V_{pk})	0.625	1	0.75
Decision voltage $\left(V_i = \frac{V_d}{V_{pk}}\right)$	0.54	0.566	0.51

Simulation model: Simulations were performed with the three systems using MPPM, DPPM and Dicode PPM, respectively. These systems are operating in space at a wavelength of 1.55 μm, a photodiode quantum efficiency of 100%, 3 bits PCM and PCM data rates of 1 Gbit/s.

Square pulses are assumed to be received with the following Fourier transform (FT):

$$Pulse(\omega) = \frac{\sin(\omega T_s/2)}{(\omega T_s/2)} \tag{1}$$

Normalising to the slot time, T_s, gives:

$$Pulse_n(\omega) = \frac{\sin(\omega/2)}{(\omega/2)} \tag{2}$$

The receiver uses a pre-detection filter that generates pulses with a raised-cosine spectrum. Such a filter helps to minimise inter-symbol-interference. It can be approximated by a single pole preamplifier with bandwidth of $0.7 \times 1/T_s$ followed by a third-order Butterworth filter with bandwidth of $0.5 \times 1/T_s$. Assuming ideal raised-cosine spectrum pulses, the pulse shape presented to the threshold detector [6] is

$$I_0(t) = \frac{\omega_{Pn}}{\pi T_s} \int_0^\infty Pulse_n(\omega) \left[\frac{a(\omega)\cos(\omega(t-0.5)) + b(\omega)\sin(\omega(t-0.5))}{a(\omega)^2 + b(\omega)^2} \right] d\omega \tag{3}$$

where $a(\omega)$, $b(\omega)$ are variables and given by:

$$a(\omega) = \omega_{Pn} - 3\frac{\omega^2}{\omega_{Bn}} - 3\frac{\omega^2\,\omega_{Pn}}{\omega_{Bn}^2} + \frac{\omega^4}{\omega_{Bn}^3} \tag{4}$$

$$b(\omega) = \omega + 3\frac{\omega\,\omega_{Pn}}{\omega_{Bn}} - 3\frac{\omega^3}{\omega_{Bn}^2} - \frac{\omega^3\,\omega_{Pn}}{\omega_{Bn}^3}$$

where ω_{Pn} is the preamplifier bandwidth, ω_{Bn} the bandwidth of the Butterworth filter, T_s the slot time which takes different values of

Techset Composition Ltd, Salisbury Doc: {IEE}EI/ISSUE/46-4/Pagination/EL58966.3d
Optical communication

$3T_b/5$, $3T_b/2^3$ and $T_b/2$ for MPPM (5,2), DPPM and Dicode PPM, respectively.

A threshold-crossing detector makes a decision as to the presence or absence of a pulse in a particular time-slot. A normalised decision voltage, V_i, is given by:

$$V_i = \frac{V_d}{V_{pk}} \tag{5}$$

where V_d is the threshold crossing voltage and V_{pk} is the peak voltage of the pulse. For a given coding scheme, the pulse shape and noise can be determined and the optimum value of V_i that yields the lowest number of photons per pulse, b, can be found for a specified PCM error rate (1 in 10^9 in these simulations).

An algorithm was designed to generate results which can be used as comparative tools between MPPM, DPPM and Dicode PPM operating with 3 bits of PCM in terms of error weightings, coding efficiency, sensitivity and bandwidth efficiency. Consequently, the appropriate coding scheme can be determined for use in optical intersatellite links in free space.

Results and discussion: Table 2 shows the weighting that must be applied to the probability of false alarm and erasure errors for MPPM, DPPM and Dicode PPM. These weightings show how the PCM error rate is affected by false alarms and erasures for MPPM, DPPM and Dicode PPM operating with 3 bits of PCM. As can be seen, Dicode PPM is the best coding scheme in terms of error weightings because it has the lowest false alarm and erasure weightings. In addition, DPPM is better than MPPM in terms of false alarm weightings because it has fewer errors than MPPM. MPPM is better than DPPM in terms of erasure weightings.

Dicode PPM is the best coding scheme in terms of coding efficiency because it operates continuously and only transmits a pulse when there is a transition between levels. Thus, the erasure and false alarm weightings for Dicode PPM are independent of the coding level. MPPM uses two or more pulses in a frame to convey the original PCM word and DPPM codes n bits of PCM into a single pulse which occupies one of 2^n time slot. Therefore, the erasure and false alarm weightings for MPPM and DPPM are dependent on the coding level.

MPPM offers the lowest noise bandwidth of 8.776×10^8 Hz because it has the lowest speed and hence the lowest bandwidth requirement. DPPM has a higher noise bandwidth of 1.404×10^9 Hz than Dicode PPM (1.053×10^9 Hz) because Dicode PPM has lower speed and bandwidth than DPPM.

The peak voltage has been normalised to unity. MPPM has the lowest peak voltage which is 0.625 that of the DPPM because it has the largest time slot width of 0.6 ns. Dicode PPM has a time slot width of 0.5 ns and a peak voltage which is 0.75 that of the DPPM.

DPPM offers the best sensitivity in terms of photon per PCM bit because it requires 2.341×10^3 photons per PCM bit. In addition, MPPM has better sensitivity than Dicode PPM because it requires 2.822×10^3 photons per PCM bit, whereas Dicode PPM requires 7.292×10^3 photons per PCM bit.

Conclusion: DPPM coding can operate with very low average power and offer a high sensitivity. However, it does suffer from a very large bandwidth expansion problem. Two alternative schemes have been examined in this Letter and a comparison has been made in terms of sensitivity, bandwidth efficiency, error weightings and coding efficiency.

Results show that Dicode PPM is the best coding scheme in terms of error weightings and coding efficiency because it has the lowest error weightings and operates continuously. In addition, it offers a fixed small bandwidth expansion – twice the PCM rate. MPPM can run at a lower speed – the final line rate for the MPPM (5, 2) scheme is 1.7 that of the PCM. This should be compared to DPPM that runs at a final line rate which is 2.7 times that of the original PCM data rate.

Dicode PPM requires the highest photons per PCM bit and thus has the lowest sensitivity. However, MPPM requires much lower photons per PCM bit compared to Dicode PPM, offers the lowest bandwidth expansion, has the lowest speed and offers the lowest noise bandwidth. In addition, MPPM has the lowest peak voltage as it has the largest time slot width. Therefore, according to these considerations, it is concluded that MPPM coding 3 bits of PCM is the appropriate coding scheme for use in optical intersatellite links in free space.

19 October 2009
doi: 10.1049/el.2010.3650

F.J. Ghosna and M.J.N. Sibley (*Department of Engineering and Technology, School of Computing and Engineering, University of Huddersfield, Queensgate, Huddersfield HD1 3DH, United Kingdom*)

E-mail: m.j.n.sibley@hud.ac.uk

References

1 McCullagh, M.J., and Wisely, D.R., Mobility Group, SRD. (1993, 14 October). A Comparison of Microwave and Optical Free Space Point to Point Links. *Revision: Issue 1, QA status: Reviewed, Project: 1634 Job 00*
2 Ekberg, J. (1970, 6 April). *Transmission Calculations for Infrared-Optical Links*. Helsinki, Finland: The STATE Institute for Technical Research
3 Lutz, H.P. (1997, August). Optical Communications in Space – Twenty Years of ESA Effort. *ESA Bulletin Nr.91*. Retrieved November 21, 2006, from http://www.esa.int/esapub/bulletin/bullet91/b91lutz.htm
4 Japan Aerospace Exploration Agency (JAXA). (2006, November). *'Kirari' Optical Inter-Orbit Communications Engineering Test Satellite (OICETS)*. Retrieved 16 November, 2006, from http://www.jaxa.jp/missions/projects/sat/tsushin/oicets/index_e.html
5 Sibley, M.: 'Analysis of multiple pulse position modulation when operating over graded-index plastic optical fiber', *IEE Proc., Optoelectron.*, 2004, **151**, (6)
6 Sibley, M.J.N.: 'Sub-optimal filtering in a zero guard, dicode PPM system operating over dispersive optical channels', *IEE Proc., Optoelectron.*, 2004, **151**, pp. 237–243

DicodePPM using a Butterworth Filter and zero guard with 1Gbit/s data and 3 PCM BITS for Free Space

Preamplifier terms

$S_o := 16 \cdot 10^{-24}$ Preamp noise at input - double sided Philips TZA 3043

$B := 1 \cdot 10^{9}$ Bit rate

$T_b := \frac{1}{B}$ PCM bit time

$i := 0, 1 .. 20$

$v_i := v_{off} + \frac{i}{range}$

$n := 8$ Number of like symbols in PCM

$f_n := 1 \cdot 10^{6}$ Channel Bandwidth for free space

$N := 3$ Number of PCM Bits

$T_s := \frac{T_b}{2}$ Slot Time for DicodePPM

$\eta q := 1.6 \cdot 10^{-19}$ Quantum energy

$\lambda := 1.55 \cdot 10^{-6}$ This is the wavelength of operation

$$photon\_energy := \frac{6.63 \cdot 10^{-34} \cdot 3 \cdot 10^{8}}{\lambda}$$

$$R_o := \frac{\eta q}{photon\_energy} \qquad R_o := 1.247$$

Pulse shape terms

$T_s = 5 \cdot 10^{-10}$

$f_p := 0.7 \cdot \frac{1}{T_s}$ $f_B := 0.5 \cdot \frac{1}{T_s}$

$\alpha := \frac{0.1874 \cdot T_b}{f_n}$ $\alpha_n := \frac{0.1874 \cdot T_b}{f_n \cdot T_s}$

$\omega_B := 2 \cdot \pi \cdot f_B$ $\omega_{Bn} := \omega_B \cdot T_s$

$\omega_p := 2\cdot\pi\cdot f_p$ $\omega_{pn} := 2\cdot\pi\cdot f_p\cdot T_s$

$\tau_R := \frac{8}{\omega_B}$ $\tau_{Rn} := \frac{8}{\omega_B\cdot T_s}$

$Pulse(\omega) := \frac{\sin\left(\frac{\omega\cdot T_s}{2}\right)}{\left(\frac{\omega\cdot T_s}{2}\right)}$ $Pulse_n(\omega) := \frac{\sin\left(\frac{\omega}{2}\right)}{\left(\frac{\omega}{2}\right)}$

$H_{pre}(\omega) := \frac{1}{1 + j\cdot\frac{\omega}{\omega_p}}$ $H_B(\omega) := \frac{\omega_B^{\,3}}{\left(j\cdot\omega + \omega_B\right)^3}$

$H_{pren}(\omega) := \frac{1}{1 + j\cdot\frac{\omega}{\omega_{pn}}}$ $H_{Bn}(\omega) := \frac{\omega_{Bn}^{\,3}}{\left(j\cdot\omega + \omega_{Bn}\right)^3}$

Pulse shape

$$I_0(t) := \frac{1}{\pi}\cdot\int_0^{1\cdot 10^{11}} Pulse(\omega)\cdot Re\left[H_{pre}(\omega)\cdot H_B(\omega)\cdot\exp\left[i\cdot\omega\cdot(t-0.5)\cdot T_s\right]\right]d\omega$$

$$a(\omega) := \omega_{pn} - 3\cdot\frac{\omega^2}{\omega_{Bn}} - 3\cdot\frac{\omega^2\cdot\omega_{pn}}{\omega_{Bn}^{\,2}} + \frac{\omega^4}{\omega_{Bn}^{\,3}}$$

$$b1(\omega) := \omega + 3\cdot\frac{\omega\cdot\omega_{pn}}{\omega_{Bn}} - 3\cdot\frac{\omega^3}{\omega_{Bn}^{\,2}} - \frac{\omega^3\cdot\omega_{pn}}{\omega_{Bn}^{\,3}}$$

$$I_0(t) := \frac{\omega_{pn}}{\pi\cdot T_s}\cdot\int_0^{100} Pulse_n(\omega)\cdot\left[\frac{a(\omega)\cdot\cos(\omega\cdot(t-0.5)) + b1(\omega)\cdot\sin(\omega\cdot(t-0.5))}{a(\omega)^2 + b1(\omega)^2}\right]d\omega$$

$$I_1(t) := \frac{\omega_{pn}}{\pi\cdot T_s^{\,2}}\cdot\int_0^{100} Pulse_n(\omega)\cdot\omega\cdot\frac{b1(\omega)\cdot\cos(\omega\cdot(t-0.5)) - a(\omega)\cdot\sin(\omega\cdot(t-0.5))}{a(\omega)^2 + b1(\omega)^2}d\omega$$

$t := -1, -0.99 .. 6$

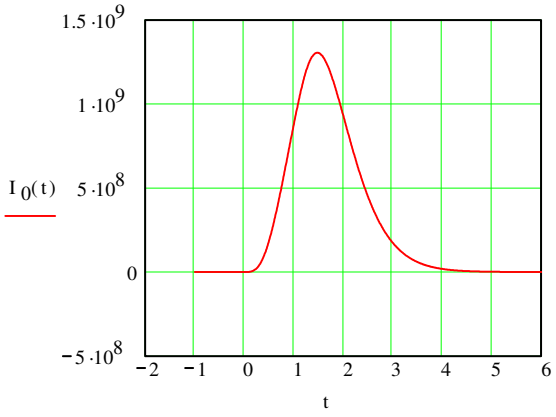

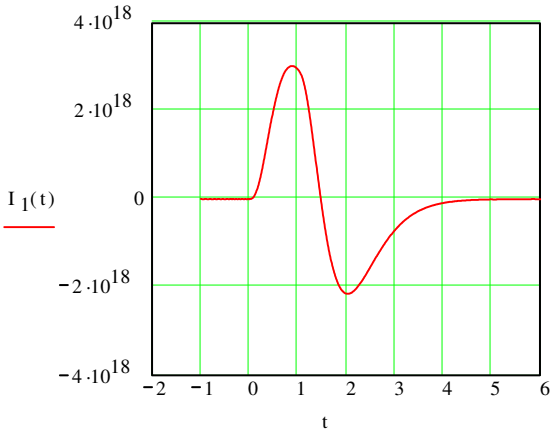

$$noise := \frac{2}{2\cdot\pi}\cdot\int_{0}^{1\cdot10^{11}} \left| H_{pre}(\omega)\cdot H_B(\omega) \right|^2 d\omega$$

$$noise = 1.053\cdot10^{9}$$

$t := 1.474$

$t_{pk} := root\left(I_1(t)\cdot T_s^{\,2}, t\right)$

$$t_{pk} = 1.474$$

$v_{pk}(b) := b\cdot\eta q\cdot I_0\left(t_{pk}\right)$

$v_{pk}(b) = 1.044\cdot10^{-6}$

$$b\cdot\eta q\cdot I_0\left(t_{pk}\right) = 1.044\cdot10^{-6}$$

$t := 0.853$

$t_{d_i} := \text{root}\left[\left(I_0(t) - v_i \cdot I_0\left(t_{pk}\right)\right) \cdot T_s^{\,2}, t\right]$

$v_d(b,i) := b \cdot \eta q \cdot I_0\left(t_{d_i}\right)$

$t_{d_5} = 0.853$

Erasure Error

$$Q_r(b,i) := \frac{v_{pk}(b) - v_d(b,i)}{\sqrt{S_o \cdot noise}}$$

$P_{er} := 0.193$ **3 Bits PCM error caused by Erasure in Dicode PPM**

$$P_r(b,i) := 0.5 \cdot P_{er} \cdot \text{erfc}\left(\frac{Q_r(b,i)}{\sqrt{2}}\right)$$ ***Erasure Error Probability***

False Alarm Error

$$Q_t(b,i) := \frac{v_d(b,i)}{\sqrt{S_o \cdot noise}}$$

$P_{fa} := 0.249$ **3 Bits PCM error caused by False Alarm in Dicode PPM**

$$P_f(b,i) := 0.5 \cdot \text{erfc}\left(\frac{Q_t(b,i)}{\sqrt{2}}\right) \cdot P_{fa}$$ [redacted]

$P_{eb}(b,i) := P_r(b,i) + P_f(b,i)$ ***Binary Error Probability***

$pc(b,i) := \left(\log\left(P_{eb}(b,i)\right) + 9\right)$ Set for 1 in 10^9 errors

$a_i := root(pc(b,i),b)$ Find the root to give 1 in 10^9

$minimum := min(a)$

$range \equiv 1000$

$minimum = 7.292 \cdot 10^3$

$b \equiv 5 \cdot 10^3$

$minimum = 7.292 \cdot 10^3$

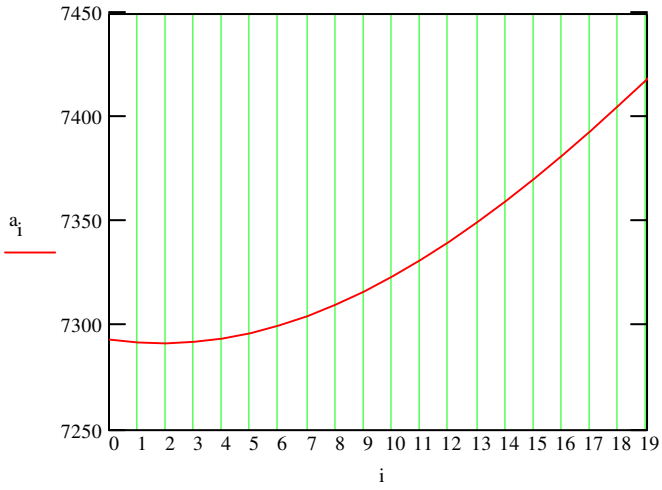

$v_{off} \equiv 0.5$

$N \equiv 3$

$f_n \equiv 1 \cdot 10^6$

$v_{10} = 0.51$

$P_r(b,i) =$

$5.62 \cdot 10^{-6}$
$5.815 \cdot 10^{-6}$
$6.016 \cdot 10^{-6}$
$6.224 \cdot 10^{-6}$
$6.439 \cdot 10^{-6}$
$6.66 \cdot 10^{-6}$
$6.889 \cdot 10^{-6}$
$7.126 \cdot 10^{-6}$
$7.37 \cdot 10^{-6}$
$7.621 \cdot 10^{-6}$
$7.881 \cdot 10^{-6}$
$8.15 \cdot 10^{-6}$
$8.427 \cdot 10^{-6}$
$8.713 \cdot 10^{-6}$
$9.008 \cdot 10^{-6}$
$9.313 \cdot 10^{-6}$

$P_f(b,i) =$

$7.25 \cdot 10^{-6}$
$7.007 \cdot 10^{-6}$
$6.771 \cdot 10^{-6}$
$6.543 \cdot 10^{-6}$
$6.322 \cdot 10^{-6}$
$6.109 \cdot 10^{-6}$
$5.902 \cdot 10^{-6}$
$5.701 \cdot 10^{-6}$
$5.508 \cdot 10^{-6}$
$5.32 \cdot 10^{-6}$
$5.138 \cdot 10^{-6}$
$4.963 \cdot 10^{-6}$
$4.793 \cdot 10^{-6}$
$4.628 \cdot 10^{-6}$
$4.469 \cdot 10^{-6}$
$4.315 \cdot 10^{-6}$

Appendix E: Simulation 2

DicodePPM using a Butterworth Filter and zero guard with 1Gbit/s data and 4 PCM BITS for Free Space

Preamplifier terms

$S_o := 16 \cdot 10^{-24}$ Preamp noise at input - double sided Philips TZA 3043

$B := 1 \cdot 10^{9}$ Bit rate

$T_b := \frac{1}{B}$ PCM bit time

$i := 0, 1 .. 20$

$v_i := v_{off} + \frac{i}{range}$

$n := 8$ Number of like symbols in PCM

$f_n := 1 \cdot 10^{6}$ Channel Bandwidth for free space

$N := 4$ Number of PCM Bits

$T_s := \frac{T_b}{2}$ Slot Time for DicodePPM

$\eta q := 1.6 \cdot 10^{-19}$ Quantum energy

$\lambda := 1.55 \cdot 10^{-6}$ This is the wavelength of operation

$$photon\_energy := \frac{6.63 \cdot 10^{-34} \cdot 3 \cdot 10^{8}}{\lambda}$$

$R_o := \frac{\eta q}{photon\_energy}$ $R_o := 1.247$

Pulse shape terms

$T_s = 5 \cdot 10^{-10}$

$f_p := 0.7 \cdot \frac{1}{T_s}$ $f_B := 0.5 \cdot \frac{1}{T_s}$

$\alpha := \frac{0.1874 \cdot T_b}{f_n}$ $\alpha_n := \frac{0.1874 \cdot T_b}{f_n \cdot T_s}$

$\omega_B := 2 \cdot \pi \cdot f_B$ $\omega_{Bn} := \omega_B \cdot T_s$

$\omega_p := 2\cdot\pi\cdot f_p$ $\omega_{pn} := 2\cdot\pi\cdot f_p\cdot T_s$

$\tau_R := \frac{8}{\omega_B}$ $\tau_{Rn} := \frac{8}{\omega_B\cdot T_s}$

$\text{Pulse}(\omega) := \frac{\sin\left(\frac{\omega\cdot T_s}{2}\right)}{\left(\frac{\omega\cdot T_s}{2}\right)}$ $\text{Pulse}_n(\omega) := \frac{\sin\left(\frac{\omega}{2}\right)}{\left(\frac{\omega}{2}\right)}$

$H_{pre}(\omega) := \frac{1}{1 + j\cdot\frac{\omega}{\omega_p}}$ $H_B(\omega) := \frac{\omega_B^{\,3}}{\left(j\cdot\omega + \omega_B\right)^3}$

$H_{pren}(\omega) := \frac{1}{1 + j\cdot\frac{\omega}{\omega_{pn}}}$ $H_{Bn}(\omega) := \frac{\omega_{Bn}^{\,3}}{\left(j\cdot\omega + \omega_{Bn}\right)^3}$

Pulse shape

$$I_0(t) := \frac{1}{\pi}\cdot\int_0^{1\cdot 10^{11}} \text{Pulse}(\omega)\cdot\text{Re}\left[H_{pre}(\omega)\cdot H_B(\omega)\cdot\exp\left[i\cdot\omega\cdot(t-0.5)\cdot T_s\right]\right]d\omega$$

$$a(\omega) := \omega_{pn} - 3\cdot\frac{\omega^2}{\omega_{Bn}} - 3\cdot\frac{\omega^2\cdot\omega_{pn}}{\omega_{Bn}^{\,2}} + \frac{\omega^4}{\omega_{Bn}^{\,3}}$$

$$b1(\omega) := \omega + 3\cdot\frac{\omega\cdot\omega_{pn}}{\omega_{Bn}} - 3\cdot\frac{\omega^3}{\omega_{Bn}^{\,2}} - \frac{\omega^3\cdot\omega_{pn}}{\omega_{Bn}^{\,3}}$$

$$I_0(t) := \frac{\omega_{pn}}{\pi\cdot T_s}\cdot\int_0^{100} \text{Pulse}_n(\omega)\cdot\left[\frac{a(\omega)\cdot\cos(\omega\cdot(t-0.5)) + b1(\omega)\cdot\sin(\omega\cdot(t-0.5))}{a(\omega)^2 + b1(\omega)^2}\right]d\omega$$

$$I_1(t) := \frac{\omega_{pn}}{\pi\cdot T_s^{\,2}}\cdot\int_0^{100} \text{Pulse}_n(\omega)\cdot\omega\cdot\frac{b1(\omega)\cdot\cos(\omega\cdot(t-0.5)) - a(\omega)\cdot\sin(\omega\cdot(t-0.5))}{a(\omega)^2 + b1(\omega)^2}d\omega$$

$t := -1, -0.99 .. 6$

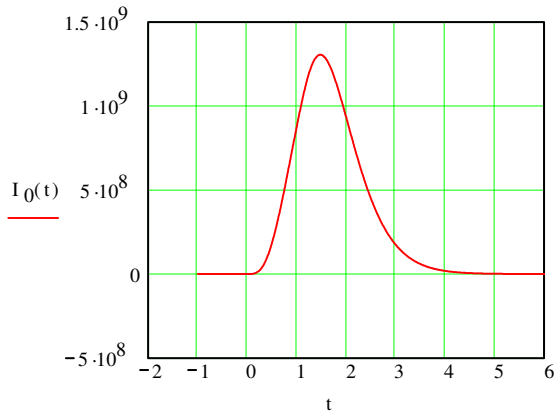

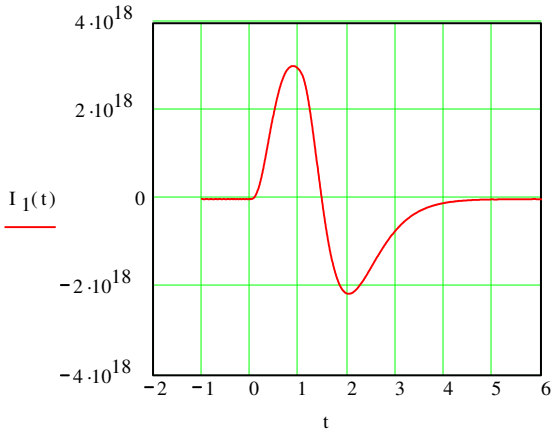

$$noise := \frac{2}{2 \cdot \pi} \cdot \int_{0}^{1 \cdot 10^{11}} \left| H_{pre}(\omega) \cdot H_B(\omega) \right|^2 d\omega$$

$noise = 1.053 \cdot 10^{9}$

$t := 1.474$

$t_{pk} := root\left(I_1(t) \cdot T_s^{\,2}, t\right)$

$t_{pk} = 1.474$

$v_{pk}(b) := b \cdot \eta q \cdot I_0\left(t_{pk}\right)$

$v_{pk}(b) = 1.044 \cdot 10^{-6}$

$b \cdot \eta q \cdot I_0\left(t_{pk}\right) = 1.044 \cdot 10^{-6}$

$t := 0.853$

$t_{d_i} := \text{root}\left[\left(I_0(t) - v_i \cdot I_0\left(t_{pk}\right)\right) \cdot T_s^{\,2}, t\right]$

$v_d(b,i) := b \cdot \eta q \cdot I_0\left(t_{d_i}\right)$

$t_{d_5} = 0.853$

Erasure Error

$$Q_r(b,i) := \frac{v_{pk}(b) - v_d(b,i)}{\sqrt{S_o \cdot noise}}$$

$P_{er} := 0.193$ **4 Bits PCM error caused by Erasure in Dicode PPM**

$$P_r(b,i) := 0.5 \cdot P_{er} \cdot \text{erfc}\left(\frac{Q_r(b,i)}{\sqrt{2}}\right)$$ ***Erasure Error Probability***

False Alarm Error

$$Q_t(b,i) := \frac{v_d(b,i)}{\sqrt{S_o \cdot noise}}$$

$P_{fa} := 0.249$ **4 Bits PCM error caused by False Alarm in Dicode PPM**

$$P_f(b,i) := 0.5 \cdot \text{erfc}\left(\frac{Q_t(b,i)}{\sqrt{2}}\right) \cdot P_{fa}$$ [redacted]

$P_{eb}(b,i) := P_r(b,i) + P_f(b,i)$ ***Binary Error Probability***

$pc(b,i) := \left(\log\left(P_{eb}(b,i)\right) + 9\right)$ Set for 1 in 10^9 errors

$a_i := root(pc(b,i),b)$ Find the root to give 1 in 10^9

$minimum := min(a)$

$range \equiv 1000$

$minimum = 7.292 \cdot 10^3$

$b \equiv 5 \cdot 10^3$

$minimum = 7.292 \cdot 10^3$

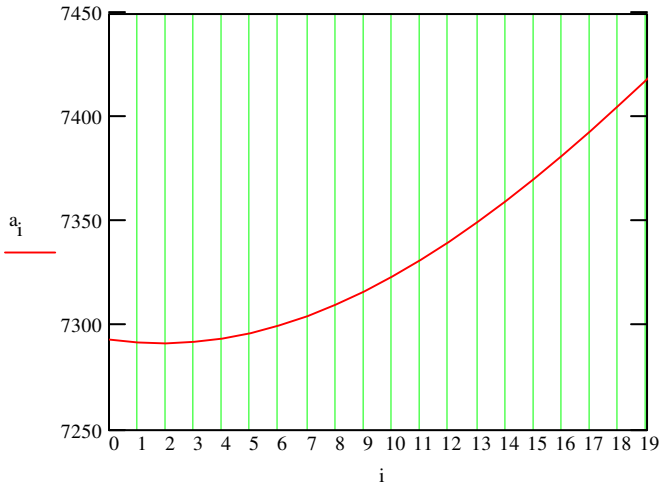

$v_{off} \equiv 0.5$

$N \equiv 4$

$f_n \equiv 1 \cdot 10^6$

$v_{10} = 0.51$

$P_r(b,i) =$

$5.62 \cdot 10^{-6}$
$5.815 \cdot 10^{-6}$
$6.016 \cdot 10^{-6}$
$6.224 \cdot 10^{-6}$
$6.439 \cdot 10^{-6}$
$6.66 \cdot 10^{-6}$
$6.889 \cdot 10^{-6}$
$7.126 \cdot 10^{-6}$
$7.37 \cdot 10^{-6}$
$7.621 \cdot 10^{-6}$
$7.881 \cdot 10^{-6}$
$8.15 \cdot 10^{-6}$
$8.427 \cdot 10^{-6}$
$8.713 \cdot 10^{-6}$
$9.008 \cdot 10^{-6}$
$9.313 \cdot 10^{-6}$

$P_f(b,i) =$

$7.25 \cdot 10^{-6}$
$7.007 \cdot 10^{-6}$
$6.771 \cdot 10^{-6}$
$6.543 \cdot 10^{-6}$
$6.322 \cdot 10^{-6}$
$6.109 \cdot 10^{-6}$
$5.902 \cdot 10^{-6}$
$5.701 \cdot 10^{-6}$
$5.508 \cdot 10^{-6}$
$5.32 \cdot 10^{-6}$
$5.138 \cdot 10^{-6}$
$4.963 \cdot 10^{-6}$
$4.793 \cdot 10^{-6}$
$4.628 \cdot 10^{-6}$
$4.469 \cdot 10^{-6}$
$4.315 \cdot 10^{-6}$

Appendix E: Simulation 5

DicodePPM using a Butterworth Filter and zero guard with 1Gbit/s data and 5 PCM BITS for Free Space

Preamplifier terms

$S_o := 16 \cdot 10^{-24}$ Preamp noise at input - double sided Philips TZA 3043

$B := 1 \cdot 10^{9}$ Bit rate

$T_b := \frac{1}{B}$ PCM bit time

$i := 0, 1 .. 20$

$v_i := v_{off} + \frac{i}{range}$

$n := 8$ Number of like symbols in PCM

$f_n := 1 \cdot 10^{6}$ Channel Bandwidth for free space

$N := 5$ Number of PCM Bits

$T_s := \frac{T_b}{2}$ Slot Time for DicodePPM

$\eta q := 1.6 \cdot 10^{-19}$ Quantum energy

$\lambda := 1.55 \cdot 10^{-6}$ This is the wavelength of operation

$$photon\_energy := \frac{6.63 \cdot 10^{-34} \cdot 3 \cdot 10^{8}}{\lambda}$$

$R_o := \frac{\eta q}{photon\_energy}$ $R_o := 1.247$

Pulse shape terms

$T_s = 5 \cdot 10^{-10}$

$f_p := 0.7 \cdot \frac{1}{T_s}$ $f_B := 0.5 \cdot \frac{1}{T_s}$

$\alpha := \frac{0.1874 \cdot T_b}{f_n}$ $\alpha_n := \frac{0.1874 \cdot T_b}{f_n \cdot T_s}$

$\omega_B := 2 \cdot \pi \cdot f_B$ $\omega_{Bn} := \omega_B \cdot T_s$

$\omega_p := 2\cdot\pi\cdot f_p$ $\omega_{pn} := 2\cdot\pi\cdot f_p\cdot T_s$

$\tau_R := \frac{8}{\omega_B}$ $\tau_{Rn} := \frac{8}{\omega_B\cdot T_s}$

$\text{Pulse}(\omega) := \frac{\sin\left(\frac{\omega\cdot T_s}{2}\right)}{\left(\frac{\omega\cdot T_s}{2}\right)}$ $\text{Pulse}_n(\omega) := \frac{\sin\left(\frac{\omega}{2}\right)}{\left(\frac{\omega}{2}\right)}$

$H_{pre}(\omega) := \frac{1}{1 + j\cdot\frac{\omega}{\omega_p}}$ $H_B(\omega) := \frac{\omega_B^3}{\left(j\cdot\omega + \omega_B\right)^3}$

$H_{pren}(\omega) := \frac{1}{1 + j\cdot\frac{\omega}{\omega_{pn}}}$ $H_{Bn}(\omega) := \frac{\omega_{Bn}^3}{\left(j\cdot\omega + \omega_{Bn}\right)^3}$

Pulse shape

$$I_0(t) := \frac{1}{\pi}\cdot\int_0^{1\cdot 10^{11}} \text{Pulse}(\omega)\cdot\text{Re}\left[H_{pre}(\omega)\cdot H_B(\omega)\cdot\exp\left[i\cdot\omega\cdot(t-0.5)\cdot T_s\right]\right]d\omega$$

$$a(\omega) := \omega_{pn} - 3\cdot\frac{\omega^2}{\omega_{Bn}} - 3\cdot\frac{\omega^2\cdot\omega_{pn}}{\omega_{Bn}^2} + \frac{\omega^4}{\omega_{Bn}^3}$$

$$b1(\omega) := \omega + 3\cdot\frac{\omega\cdot\omega_{pn}}{\omega_{Bn}} - 3\cdot\frac{\omega^3}{\omega_{Bn}^2} - \frac{\omega^3\cdot\omega_{pn}}{\omega_{Bn}^3}$$

$$I_0(t) := \frac{\omega_{pn}}{\pi\cdot T_s}\cdot\int_0^{100} \text{Pulse}_n(\omega)\cdot\left[\frac{a(\omega)\cdot\cos(\omega\cdot(t-0.5)) + b1(\omega)\cdot\sin(\omega\cdot(t-0.5))}{a(\omega)^2 + b1(\omega)^2}\right]d\omega$$

$$I_1(t) := \frac{\omega_{pn}}{\pi\cdot T_s^2}\cdot\int_0^{100} \text{Pulse}_n(\omega)\cdot\omega\cdot\frac{b1(\omega)\cdot\cos(\omega\cdot(t-0.5)) - a(\omega)\cdot\sin(\omega\cdot(t-0.5))}{a(\omega)^2 + b1(\omega)^2}d\omega$$

$t := -1, -0.99 .. 6$

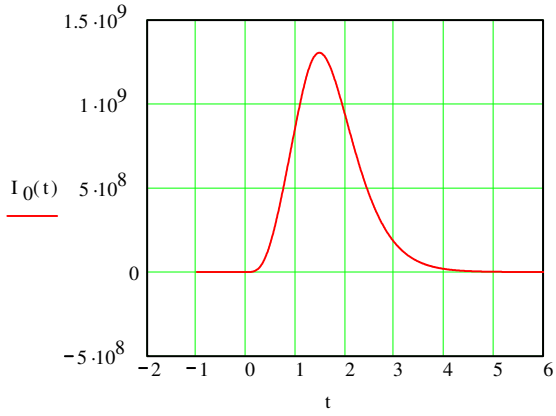

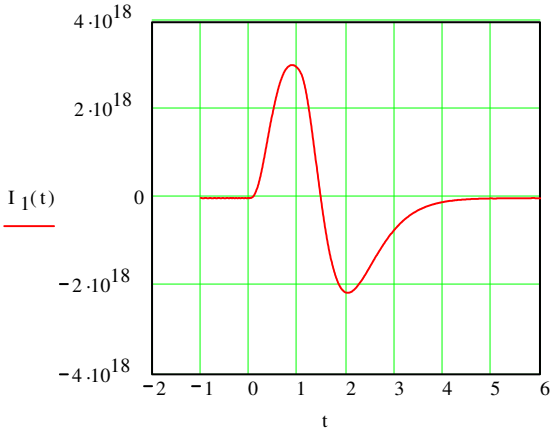

$$noise := \frac{2}{2 \cdot \pi} \cdot \int_0^{1 \cdot 10^{11}} \left| H_{pre}(\omega) \cdot H_B(\omega) \right|^2 d\omega$$

$$noise = 1.053 \cdot 10^9$$

$t := 1.474$

$t_{pk} := root\left(I_1(t) \cdot T_s^{\,2}, t\right)$

$$t_{pk} = 1.474$$

$v_{pk}(b) := b \cdot \eta q \cdot I_0\left(t_{pk}\right)$

$$v_{pk}(b) = 1.044 \cdot 10^{-6}$$

$$b \cdot \eta q \cdot I_0\left(t_{pk}\right) = 1.044 \cdot 10^{-6}$$

$t := 0.853$

$t_{d_i} := \text{root}\left[\left(I_0(t) - v_i \cdot I_0\left(t_{pk}\right)\right) \cdot T_s^{\,2}, t\right]$

$v_d(b,i) := b \cdot \eta q \cdot I_0\left(t_{d_i}\right)$

$t_{d_5} = 0.853$

Erasure Error

$$Q_r(b,i) := \frac{v_{pk}(b) - v_d(b,i)}{\sqrt{S_o \cdot noise}}$$

$P_{er} := 0.193$ **5 Bits PCM error caused by Erasure in Dicode PPM**

$$P_r(b,i) := 0.5 \cdot P_{er} \cdot \text{erfc}\left(\frac{Q_r(b,i)}{\sqrt{2}}\right)$$ ***Erasure Error Probability***

False Alarm Error

$$Q_t(b,i) := \frac{v_d(b,i)}{\sqrt{S_o \cdot noise}}$$

$P_{fa} := 0.249$ **5 Bits PCM error caused by False Alarm in Dicode PPM**

$$P_f(b,i) := 0.5 \cdot \text{erfc}\left(\frac{Q_t(b,i)}{\sqrt{2}}\right) \cdot P_{fa}$$ [redacted]

$P_{eb}(b,i) := P_r(b,i) + P_f(b,i)$ ***Binary Error Probability***

$pc(b,i) := \left(\log\left(P_{eb}(b,i)\right) + 9\right)$ Set for 1 in 10^9 errors

$a_i := root(pc(b,i),b)$ Find the root to give 1 in 10^9

$minimum := min(a)$

$range \equiv 1000$

$minimum = 7.292 \cdot 10^3$

$b \equiv 5 \cdot 10^3$

$minimum = 7.292 \cdot 10^3$

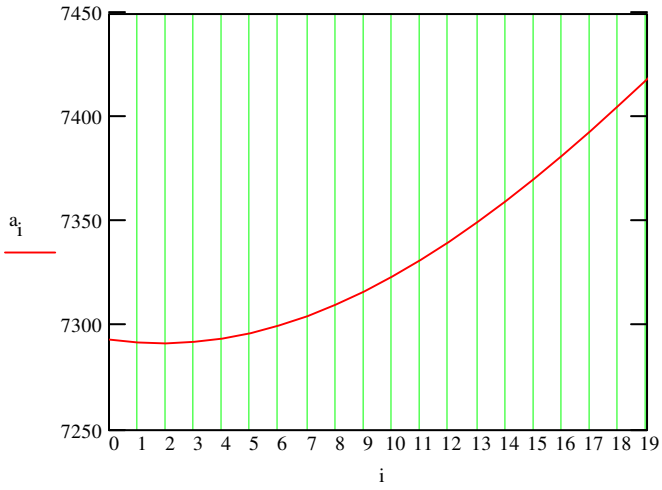

$v_{off} \equiv 0.5$

$N \equiv 5$

$f_n \equiv 1 \cdot 10^6$

$v_{10} = 0.51$

$P_r(b,i) =$

$5.62 \cdot 10^{-6}$
$5.815 \cdot 10^{-6}$
$6.016 \cdot 10^{-6}$
$6.224 \cdot 10^{-6}$
$6.439 \cdot 10^{-6}$
$6.66 \cdot 10^{-6}$
$6.889 \cdot 10^{-6}$
$7.126 \cdot 10^{-6}$
$7.37 \cdot 10^{-6}$
$7.621 \cdot 10^{-6}$
$7.881 \cdot 10^{-6}$
$8.15 \cdot 10^{-6}$
$8.427 \cdot 10^{-6}$
$8.713 \cdot 10^{-6}$
$9.008 \cdot 10^{-6}$
$9.313 \cdot 10^{-6}$

$P_f(b,i) =$

$7.25 \cdot 10^{-6}$
$7.007 \cdot 10^{-6}$
$6.771 \cdot 10^{-6}$
$6.543 \cdot 10^{-6}$
$6.322 \cdot 10^{-6}$
$6.109 \cdot 10^{-6}$
$5.902 \cdot 10^{-6}$
$5.701 \cdot 10^{-6}$
$5.508 \cdot 10^{-6}$
$5.32 \cdot 10^{-6}$
$5.138 \cdot 10^{-6}$
$4.963 \cdot 10^{-6}$
$4.793 \cdot 10^{-6}$
$4.628 \cdot 10^{-6}$
$4.469 \cdot 10^{-6}$
$4.315 \cdot 10^{-6}$

Appendix E: Simulation 8

DicodePPM using a Butterworth Filter and zero guard with 1Gbit/s data and 6 PCM BITS for Free Space

Preamplifier terms

$S_o := 16 \cdot 10^{-24}$ Preamp noise at input - double sided Philips TZA 3043

$B := 1 \cdot 10^{9}$ Bit rate

$T_b := \frac{1}{B}$ PCM bit time

$i := 0, 1 .. 20$

$v_i := v_{off} + \frac{i}{range}$

$n := 8$ Number of like symbols in PCM

$f_n := 1 \cdot 10^{6}$ Channel Bandwidth for free space

$N := 6$ Number of PCM Bits

$T_s := \frac{T_b}{2}$ Slot Time for DicodePPM

$\eta q := 1.6 \cdot 10^{-19}$ Quantum energy

$\lambda := 1.55 \cdot 10^{-6}$ This is the wavelength of operation

$$photon\_energy := \frac{6.63 \cdot 10^{-34} \cdot 3 \cdot 10^{8}}{\lambda}$$

$R_o := \frac{\eta q}{photon\_energy}$ $R_o := 1.247$

Pulse shape terms

$T_s = 5 \cdot 10^{-10}$

$f_p := 0.7 \cdot \frac{1}{T_s}$ $f_B := 0.5 \cdot \frac{1}{T_s}$

$\alpha := \frac{0.1874 \cdot T_b}{f_n}$ $\alpha_n := \frac{0.1874 \cdot T_b}{f_n \cdot T_s}$

$\omega_B := 2 \cdot \pi \cdot f_B$ $\omega_{Bn} := \omega_B \cdot T_s$

$\omega_p := 2\cdot\pi\cdot f_p$ $\omega_{pn} := 2\cdot\pi\cdot f_p\cdot T_s$

$\tau_R := \frac{8}{\omega_B}$ $\tau_{Rn} := \frac{8}{\omega_B\cdot T_s}$

$\text{Pulse}(\omega) := \frac{\sin\left(\frac{\omega\cdot T_s}{2}\right)}{\left(\frac{\omega\cdot T_s}{2}\right)}$ $\text{Pulse}_n(\omega) := \frac{\sin\left(\frac{\omega}{2}\right)}{\left(\frac{\omega}{2}\right)}$

$H_{pre}(\omega) := \frac{1}{1 + j\cdot\frac{\omega}{\omega_p}}$ $H_B(\omega) := \frac{\omega_B^3}{\left(j\cdot\omega + \omega_B\right)^3}$

$H_{pren}(\omega) := \frac{1}{1 + j\cdot\frac{\omega}{\omega_{pn}}}$ $H_{Bn}(\omega) := \frac{\omega_{Bn}^3}{\left(j\cdot\omega + \omega_{Bn}\right)^3}$

Pulse shape

$$I_0(t) := \frac{1}{\pi}\cdot\int_0^{1\cdot 10^{11}} \text{Pulse}(\omega)\cdot\text{Re}\left[H_{pre}(\omega)\cdot H_B(\omega)\cdot\exp\left[i\cdot\omega\cdot(t-0.5)\cdot T_s\right]\right]d\omega$$

$$a(\omega) := \omega_{pn} - 3\cdot\frac{\omega^2}{\omega_{Bn}} - 3\cdot\frac{\omega^2\cdot\omega_{pn}}{\omega_{Bn}^2} + \frac{\omega^4}{\omega_{Bn}^3}$$

$$b1(\omega) := \omega + 3\cdot\frac{\omega\cdot\omega_{pn}}{\omega_{Bn}} - 3\cdot\frac{\omega^3}{\omega_{Bn}^2} - \frac{\omega^3\cdot\omega_{pn}}{\omega_{Bn}^3}$$

$$I_0(t) := \frac{\omega_{pn}}{\pi\cdot T_s}\cdot\int_0^{100} \text{Pulse}_n(\omega)\cdot\left[\frac{a(\omega)\cdot\cos(\omega\cdot(t-0.5)) + b1(\omega)\cdot\sin(\omega\cdot(t-0.5))}{a(\omega)^2 + b1(\omega)^2}\right]d\omega$$

$$I_1(t) := \frac{\omega_{pn}}{\pi\cdot T_s^2}\cdot\int_0^{100} \text{Pulse}_n(\omega)\cdot\omega\cdot\frac{b1(\omega)\cdot\cos(\omega\cdot(t-0.5)) - a(\omega)\cdot\sin(\omega\cdot(t-0.5))}{a(\omega)^2 + b1(\omega)^2}d\omega$$

$t := -1, -0.99 .. 6$

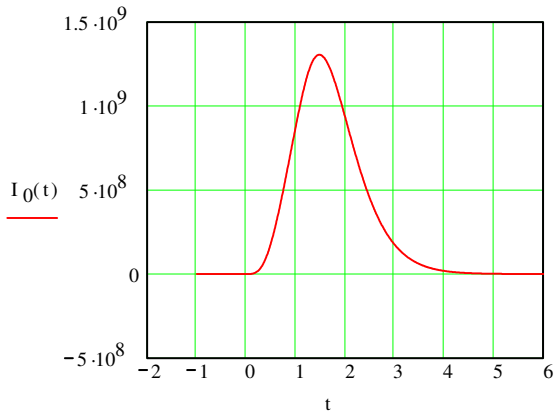

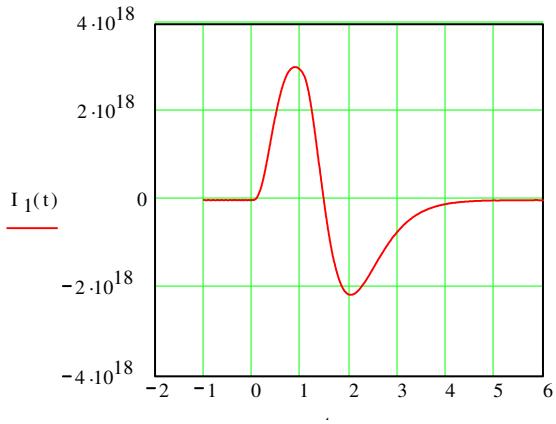

$$noise := \frac{2}{2\cdot\pi}\cdot\int_{0}^{1\cdot10^{11}} \left| H_{pre}(\omega)\cdot H_B(\omega) \right|^2 d\omega$$

$noise = 1.053\cdot10^{9}$

$t := 1.474$

$t_{pk} := root\left(I_1(t)\cdot T_s^{\,2}, t\right)$

$t_{pk} = 1.474$

$v_{pk}(b) := b\cdot\eta q\cdot I_0\left(t_{pk}\right)$

$v_{pk}(b) = 1.044\cdot10^{-6}$

$b\cdot\eta q\cdot I_0\left(t_{pk}\right) = 1.044\cdot10^{-6}$

$t := 0.853$

$t_{d_i} := \text{root}\left[\left(I_0(t) - v_i \cdot I_0\left(t_{pk}\right)\right) \cdot T_s^{\,2}, t\right]$

$v_d(b,i) := b \cdot \eta q \cdot I_0\left(t_{d_i}\right)$

$t_{d_5} = 0.853$

Erasure Error

$$Q_r(b,i) := \frac{v_{pk}(b) - v_d(b,i)}{\sqrt{S_o \cdot noise}}$$

$P_{er} := 0.193$ **6 Bits PCM error caused by Erasure in Dicode PPM**

$$P_r(b,i) := 0.5 \cdot P_{er} \cdot erfc\left(\frac{Q_r(b,i)}{\sqrt{2}}\right)$$ ***Erasure Error Probability***

False Alarm Error

$$Q_t(b,i) := \frac{v_d(b,i)}{\sqrt{S_o \cdot noise}}$$

$P_{fa} := 0.249$ **6 Bits PCM error caused by False Alarm in Dicode PPM**

$$P_f(b,i) := 0.5 \cdot erfc\left(\frac{Q_t(b,i)}{\sqrt{2}}\right) \cdot P_{fa}$$ [redacted]

$P_{eb}(b,i) := P_r(b,i) + P_f(b,i)$ ***Binary Error Probability***

$pc(b,i) := \left(\log\left(P_{eb}(b,i)\right) + 9\right)$ Set for 1 in 10^9 errors

$a_i := root(pc(b,i), b)$ Find the root to give 1 in 10^9

$minimum := min(a)$

$minimum = 7.292 \cdot 10^3$

$range \equiv 1000$

$b \equiv 5 \cdot 10^3$

$minimum = 7.292 \cdot 10^3$

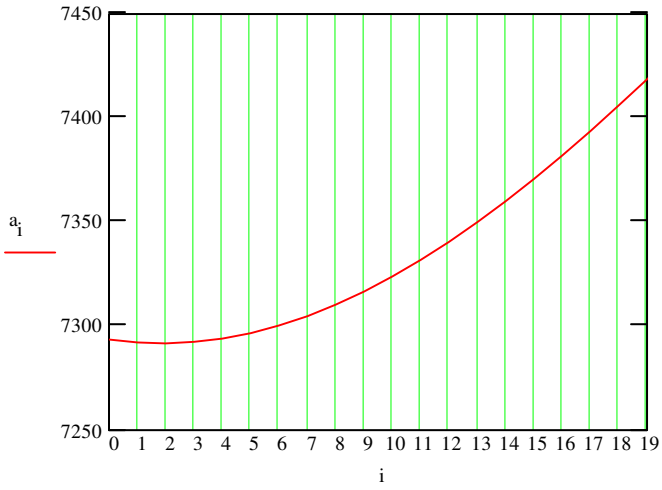

$v_{off} \equiv 0.5$

$N \equiv 6$

$f_n \equiv 1 \cdot 10^6$

$v_{10} = 0.51$

$P_r(b,i) =$

$5.62 \cdot 10^{-6}$
$5.815 \cdot 10^{-6}$
$6.016 \cdot 10^{-6}$
$6.224 \cdot 10^{-6}$
$6.439 \cdot 10^{-6}$
$6.66 \cdot 10^{-6}$
$6.889 \cdot 10^{-6}$
$7.126 \cdot 10^{-6}$
$7.37 \cdot 10^{-6}$
$7.621 \cdot 10^{-6}$
$7.881 \cdot 10^{-6}$
$8.15 \cdot 10^{-6}$
$8.427 \cdot 10^{-6}$
$8.713 \cdot 10^{-6}$
$9.008 \cdot 10^{-6}$
$9.313 \cdot 10^{-6}$

$P_f(b,i) =$

$7.25 \cdot 10^{-6}$
$7.007 \cdot 10^{-6}$
$6.771 \cdot 10^{-6}$
$6.543 \cdot 10^{-6}$
$6.322 \cdot 10^{-6}$
$6.109 \cdot 10^{-6}$
$5.902 \cdot 10^{-6}$
$5.701 \cdot 10^{-6}$
$5.508 \cdot 10^{-6}$
$5.32 \cdot 10^{-6}$
$5.138 \cdot 10^{-6}$
$4.963 \cdot 10^{-6}$
$4.793 \cdot 10^{-6}$
$4.628 \cdot 10^{-6}$
$4.469 \cdot 10^{-6}$
$4.315 \cdot 10^{-6}$

DPPM using a Butterworth Filter and zero guard with 1Gbit/s data and 3 PCM BITS for Free Space

Preamplifier terms

$S_o := 16 \cdot 10^{-24}$ Preamp noise at input - double sided Philips TZA 3043

$B := 1 \cdot 10^{9}$ Bit rate

$T_b := \frac{1}{B}$ PCM bit time

$i := 0, 1 .. 20$

$v_i := v_{off} + \frac{i}{range}$

$n := 8$ Number of like symbols in PCM

$f_n := 1 \cdot 10^{6}$ Channel Bandwidth for free space

$N := 3$ Number of PCM Bits

$T_s := \frac{N \cdot T_b}{2^N}$ Slot Time for DPPM

$\eta q := 1.6 \cdot 10^{-19}$ Quantum energy

$\lambda := 1.55 \cdot 10^{-6}$ This is the wavelength of operation

$photon\_energy := \frac{6.63 \cdot 10^{-34} \cdot 3 \cdot 10^{8}}{\lambda}$

$R_o := \frac{\eta q}{photon\_energy}$ $R_o := 1.247$

Pulse shape terms

$T_s = 3.75 \cdot 10^{-10}$

$f_p := 0.7 \cdot \frac{1}{T_s}$ $f_B := 0.5 \cdot \frac{1}{T_s}$

$\alpha := \frac{0.1874 \cdot T_b}{f_n}$ $\alpha_n := \frac{0.1874 \cdot T_b}{f_n \cdot T_s}$

$\omega_B := 2 \cdot \pi \cdot f_B$ $\omega_{Bn} := \omega_B \cdot T_s$

$\omega_p := 2\cdot\pi\cdot f_p$ $\omega_{pn} := 2\cdot\pi\cdot f_p\cdot T_s$

$\tau_R := \frac{8}{\omega_B}$ $\tau_{Rn} := \frac{8}{\omega_B\cdot T_s}$

$Pulse(\omega) := \frac{\sin\left(\frac{\omega\cdot T_s}{2}\right)}{\left(\frac{\omega\cdot T_s}{2}\right)}$ $Pulse_n(\omega) := \frac{\sin\left(\frac{\omega}{2}\right)}{\left(\frac{\omega}{2}\right)}$

$H_{pre}(\omega) := \frac{1}{1 + j\cdot\frac{\omega}{\omega_p}}$ $H_B(\omega) := \frac{\omega_B^{\,3}}{\left(j\cdot\omega + \omega_B\right)^3}$

$H_{pren}(\omega) := \frac{1}{1 + j\cdot\frac{\omega}{\omega_{pn}}}$ $H_{Bn}(\omega) := \frac{\omega_{Bn}^{\,3}}{\left(j\cdot\omega + \omega_{Bn}\right)^3}$

Pulse shape

$$I_0(t) := \frac{1}{\pi}\cdot\int_0^{1\cdot 10^{11}} Pulse(\omega)\cdot Re\left[H_{pre}(\omega)\cdot H_B(\omega)\cdot\exp\left[i\cdot\omega\cdot(t-0.5)\cdot T_s\right]\right]d\omega$$

$$a(\omega) := \omega_{pn} - 3\cdot\frac{\omega^2}{\omega_{Bn}} - 3\cdot\frac{\omega^2\cdot\omega_{pn}}{\omega_{Bn}^{\,2}} + \frac{\omega^4}{\omega_{Bn}^{\,3}}$$

$$b1(\omega) := \omega + 3\cdot\frac{\omega\cdot\omega_{pn}}{\omega_{Bn}} - 3\cdot\frac{\omega^3}{\omega_{Bn}^{\,2}} - \frac{\omega^3\cdot\omega_{pn}}{\omega_{Bn}^{\,3}}$$

$$I_0(t) := \frac{\omega_{pn}}{\pi\cdot T_s}\cdot\int_0^{100} Pulse_n(\omega)\cdot\left[\frac{a(\omega)\cdot\cos(\omega\cdot(t-0.5)) + b1(\omega)\cdot\sin(\omega\cdot(t-0.5))}{a(\omega)^2 + b1(\omega)^2}\right]d\omega$$

$$I_1(t) := \frac{\omega_{pn}}{\pi\cdot T_s^{\,2}}\cdot\int_0^{100} Pulse_n(\omega)\cdot\omega\cdot\frac{b1(\omega)\cdot\cos(\omega\cdot(t-0.5)) - a(\omega)\cdot\sin(\omega\cdot(t-0.5))}{a(\omega)^2 + b1(\omega)^2}d\omega$$

$t := -1, -0.99 .. 6$

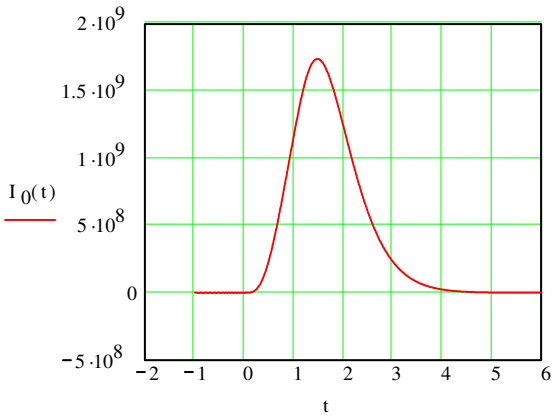

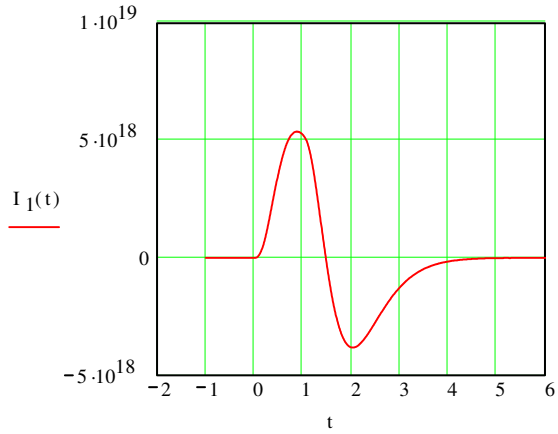

$$noise := \frac{2}{2\cdot\pi}\cdot\int_0^{1\cdot10^{11}} \left| H_{pre}(\omega)\cdot H_B(\omega) \right|^2 d\omega$$

$noise = 1.404\cdot10^{9}$

$t := 1.474$

$t_{pk} := root\left(I_1(t)\cdot T_s^{\,2}, t\right)$

$t_{pk} = 1.474$

$v_{pk}(b) := b\cdot\eta q\cdot I_0\left(t_{pk}\right)$

$v_{pk}(b) = 1.391\cdot10^{-6}$

$t := 0.901$

$t_{d_i} := root\left[\left(I_0(t) - v_i\cdot I_0\left(t_{pk}\right)\right)\cdot T_s^{\,2}, t\right]$

$v_d(b,i) := b\cdot\eta q\cdot I_0\left(t_{d_i}\right)$

$t_{d_5} = 0.901$

Erasure Error

$$Q_r(b,i) := \frac{v_{pk}(b) - v_d(b,i)}{\sqrt{S_o \cdot noise}}$$

$P_{er} := 0.5$ **3 Bits PCM error caused by erasure in DPPM**

$$P_r(b,i) := 0.5 \cdot P_{er} \cdot erfc\left(\frac{Q_r(b,i)}{\sqrt{2}}\right)$$ ***Erasure Error Probability***

False Alarm Error

$$Q_t(b,i) := \frac{v_d(b,i)}{\sqrt{S_o \cdot noise}}$$

$P_{fa} := 0.286$ **3 Bits PCM error caused by Flase Alarm in DPPM**

$$P_f(b,i) := 0.5 \cdot erfc\left(\frac{Q_t(b,i)}{\sqrt{2}}\right) \cdot P_{fa}$$ [redacted]

$$P_{es}(b,i) := P_r(b,i) + \frac{n-1}{2} \cdot P_f(b,i)$$ ***Symbol Error Probability***

$$P_{eb}(b,i) := \frac{n}{2 \cdot (n-1)} \cdot P_{es}(b,i)$$ ***Binary Error Probability***

$pc(b,i) := \left(\log\left(P_{eb}(b,i)\right) + 9\right)$ Set for 1 in 10^9 errors

$a_i := root(pc(b,i),b)$ Find the root to give 1 in 10^9

$minimum := min(a)$

$minimum = 7.025 \cdot 10^3$

$range \equiv 1000$

$b \equiv 5 \cdot 10^3$

$minimum = 7.025 \cdot 10^3$

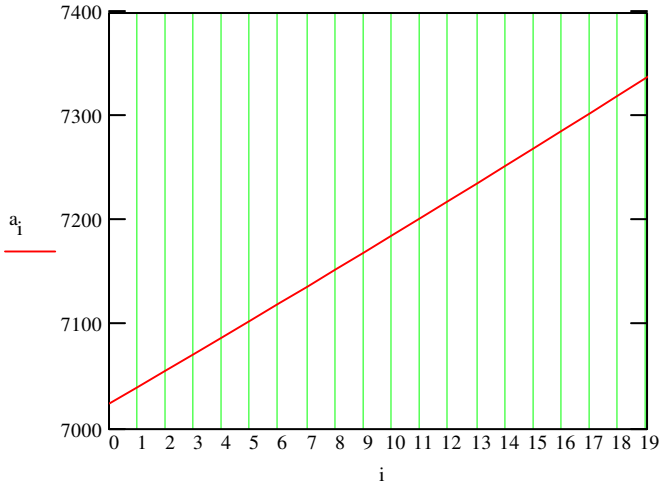

$v_{off} \equiv 0.556$

$N \equiv 3$

$f_n \equiv 1 \cdot 10^6$

$v_{10} = 0.566$

$P_r(b,i) =$

$9.396 \cdot 10^{-6}$
$9.782 \cdot 10^{-6}$
$1.018 \cdot 10^{-5}$
$1.06 \cdot 10^{-5}$
$1.103 \cdot 10^{-5}$
$1.148 \cdot 10^{-5}$
$1.195 \cdot 10^{-5}$
$1.243 \cdot 10^{-5}$
$1.294 \cdot 10^{-5}$
$1.346 \cdot 10^{-5}$
$1.4 \cdot 10^{-5}$
$1.457 \cdot 10^{-5}$
$1.515 \cdot 10^{-5}$
$1.576 \cdot 10^{-5}$
$1.639 \cdot 10^{-5}$
$1.704 \cdot 10^{-5}$

$P_f(b,i) =$

$3.502 \cdot 10^{-8}$
$3.332 \cdot 10^{-8}$
$3.171 \cdot 10^{-8}$
$3.016 \cdot 10^{-8}$
$2.87 \cdot 10^{-8}$
$2.73 \cdot 10^{-8}$
$2.596 \cdot 10^{-8}$
$2.469 \cdot 10^{-8}$
$2.349 \cdot 10^{-8}$
$2.233 \cdot 10^{-8}$
$2.124 \cdot 10^{-8}$
$2.019 \cdot 10^{-8}$
$1.92 \cdot 10^{-8}$
$1.825 \cdot 10^{-8}$
$1.735 \cdot 10^{-8}$
$1.649 \cdot 10^{-8}$

DPPM using a Butterworth Filter and zero guard with 1Gbit/s data and 4 PCM BITS for Free Space

Preamplifier terms

$S_o := 16 \cdot 10^{-24}$ Preamp noise at input - double sided Philips TZA 3043

$B := 1 \cdot 10^{9}$ Bit rate

$T_b := \frac{1}{B}$ PCM bit time

$i := 0, 1 .. 20$

$v_i := v_{off} + \frac{i}{range}$

$n := 8$ Number of like symbols in PCM

$f_n := 1 \cdot 10^{6}$ Channel Bandwidth for free space

$N := 4$ Number of PCM Bits

$T_s := \frac{N \cdot T_b}{2^N}$ Slot Time for DPPM

$\eta q := 1.6 \cdot 10^{-19}$ Quantum energy

$\lambda := 1.55 \cdot 10^{-6}$ This is the wavelength of operation

$photon\_energy := \frac{6.63 \cdot 10^{-34} \cdot 3 \cdot 10^{8}}{\lambda}$

$R_o := \frac{\eta q}{photon\_energy}$ $R_o := 1.247$

Pulse shape terms

$T_s = 2.5 \cdot 10^{-10}$

$f_p := 0.7 \cdot \frac{1}{T_s}$ $f_B := 0.5 \cdot \frac{1}{T_s}$

$\alpha := \frac{0.1874 \cdot T_b}{f_n}$ $\alpha_n := \frac{0.1874 \cdot T_b}{f_n \cdot T_s}$

$\omega_B := 2 \cdot \pi \cdot f_B$ $\omega_{Bn} := \omega_B \cdot T_s$

$\omega_p := 2\cdot\pi\cdot f_p$ $\omega_{pn} := 2\cdot\pi\cdot f_p\cdot T_s$

$\tau_R := \frac{8}{\omega_B}$ $\tau_{Rn} := \frac{8}{\omega_B\cdot T_s}$

$Pulse(\omega) := \frac{\sin\left(\frac{\omega\cdot T_s}{2}\right)}{\left(\frac{\omega\cdot T_s}{2}\right)}$ $Pulse_n(\omega) := \frac{\sin\left(\frac{\omega}{2}\right)}{\left(\frac{\omega}{2}\right)}$

$H_{pre}(\omega) := \frac{1}{1 + j\cdot\frac{\omega}{\omega_p}}$ $H_B(\omega) := \frac{\omega_B^{\,3}}{\left(j\cdot\omega + \omega_B\right)^3}$

$H_{pren}(\omega) := \frac{1}{1 + j\cdot\frac{\omega}{\omega_{pn}}}$ $H_{Bn}(\omega) := \frac{\omega_{Bn}^{\,3}}{\left(j\cdot\omega + \omega_{Bn}\right)^3}$

Pulse shape

$$I_0(t) := \frac{1}{\pi}\cdot\int_0^{1\cdot 10^{11}} Pulse(\omega)\cdot Re\left[H_{pre}(\omega)\cdot H_B(\omega)\cdot\exp\left[i\cdot\omega\cdot(t-0.5)\cdot T_s\right]\right]d\omega$$

$$a(\omega) := \omega_{pn} - 3\cdot\frac{\omega^2}{\omega_{Bn}} - 3\cdot\frac{\omega^2\cdot\omega_{pn}}{\omega_{Bn}^{\,2}} + \frac{\omega^4}{\omega_{Bn}^{\,3}}$$

$$b1(\omega) := \omega + 3\cdot\frac{\omega\cdot\omega_{pn}}{\omega_{Bn}} - 3\cdot\frac{\omega^3}{\omega_{Bn}^{\,2}} - \frac{\omega^3\cdot\omega_{pn}}{\omega_{Bn}^{\,3}}$$

$$I_0(t) := \frac{\omega_{pn}}{\pi\cdot T_s}\cdot\int_0^{100} Pulse_n(\omega)\cdot\left[\frac{a(\omega)\cdot\cos(\omega\cdot(t-0.5)) + b1(\omega)\cdot\sin(\omega\cdot(t-0.5))}{a(\omega)^2 + b1(\omega)^2}\right]d\omega$$

$$I_1(t) := \frac{\omega_{pn}}{\pi\cdot T_s^{\,2}}\cdot\int_0^{100} Pulse_n(\omega)\cdot\omega\cdot\frac{b1(\omega)\cdot\cos(\omega\cdot(t-0.5)) - a(\omega)\cdot\sin(\omega\cdot(t-0.5))}{a(\omega)^2 + b1(\omega)^2}d\omega$$

$t := -1, -0.99 .. 6$

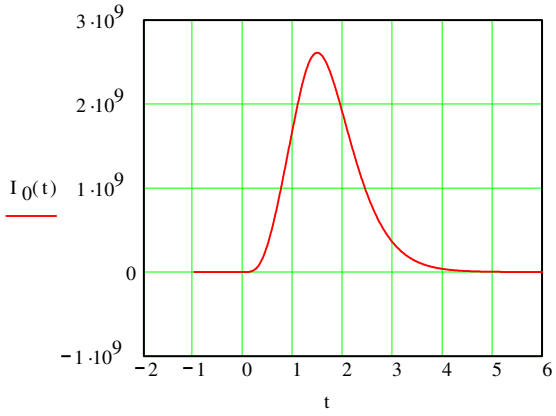

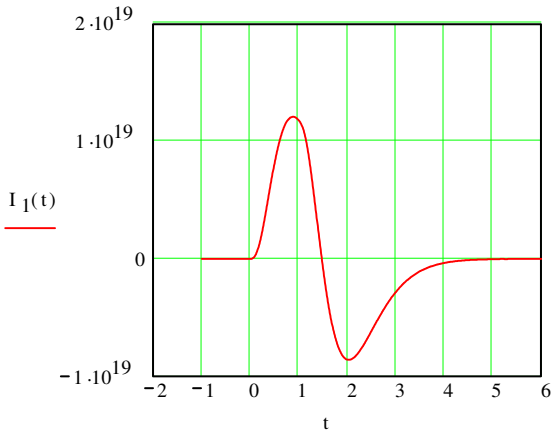

$$noise := \frac{2}{2\cdot\pi}\cdot\int_{0}^{1\cdot10^{11}} \left| H_{pre}(\omega)\cdot H_B(\omega) \right|^2 d\omega$$

$noise = 2.106\cdot10^{9}$

$t := 1.474$

$t_{pk} := root\left(I_1(t)\cdot T_s^{\,2}, t\right)$

$t_{pk} = 1.474$

$v_{pk}(b) := b\cdot\eta q\cdot I_0\left(t_{pk}\right)$

$v_{pk}(b) = 2.087\cdot10^{-6}$

$t := 0.901$

$t_{d_i} := \text{root}\left[\left(I_0(t) - v_i \cdot I_0\left(t_{pk}\right)\right) \cdot T_s^{\,2}, t\right]$

$v_d(b,i) := b \cdot \eta q \cdot I_0\left(t_{d_i}\right)$

$t_{d_5} = 0.901$

Erasure Error

$$Q_r(b,i) := \frac{v_{pk}(b) - v_d(b,i)}{\sqrt{S_o \cdot noise}}$$

$P_{er} := 0.5$ **4 Bits PCM error caused by erasure in DPPM**

$$P_r(b,i) := 0.5 \cdot P_{er} \cdot \text{erfc}\left(\frac{Q_r(b,i)}{\sqrt{2}}\right)$$ ***Erasure Error Probability***

False Alarm Error

$$Q_t(b,i) := \frac{v_d(b,i)}{\sqrt{S_o \cdot noise}}$$

$P_{fa} := 0.266$ **4 Bits PCM error caused by Flase Alarm in DPPM**

$$P_f(b,i) := 0.5 \cdot \text{erfc}\left(\frac{Q_t(b,i)}{\sqrt{2}}\right) \cdot P_{fa}$$ [redacted]

$$P_{es}(b,i) := P_r(b,i) + \frac{n-1}{2} \cdot P_f(b,i)$$ ***Symbol Error Probability***

Binary Error Probability

$$P_{eb}(b,i) := \frac{n}{2\cdot(n-1)}\cdot P_{es}(b,i)$$

$$pc(b,i) := \left(\log\left(P_{eb}(b,i)\right) + 9\right)$$

Set for 1 in 10^9 errors

$$a_i := root(pc(b,i),b)$$

Find the root to give 1 in 10^9

$$minimum := min(a)$$

$$range \equiv 1000$$

$$minimum = 5.736\cdot 10^3$$

$$b \equiv 5\cdot 10^3$$

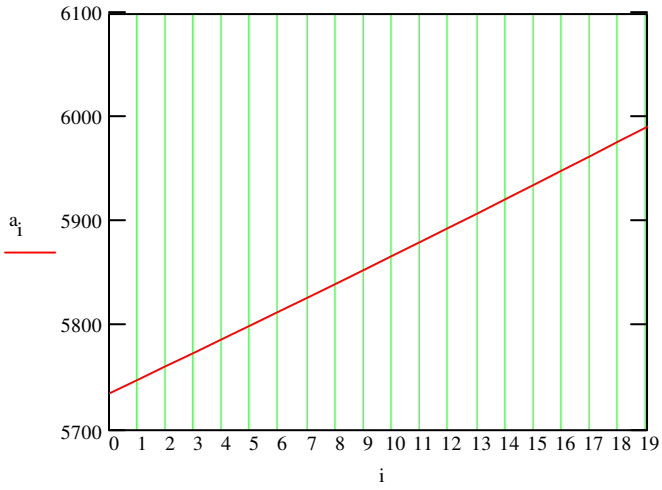

$$minimum = 5.736\cdot 10^3$$

$$v_{off} \equiv 0.556$$

$$N \equiv 4$$

$$f_n \equiv 1\cdot 10^6$$

$P_r(b,i) =$

$1.115\cdot 10^{-7}$
$1.183\cdot 10^{-7}$
$1.256\cdot 10^{-7}$
$1.332\cdot 10^{-7}$
$1.413\cdot 10^{-7}$
$1.499\cdot 10^{-7}$
$1.59\cdot 10^{-7}$
$1.686\cdot 10^{-7}$
$1.788\cdot 10^{-7}$
$1.895\cdot 10^{-7}$
$2.009\cdot 10^{-7}$
$2.129\cdot 10^{-7}$
$2.256\cdot 10^{-7}$
$2.391\cdot 10^{-7}$
$2.533\cdot 10^{-7}$
$2.683\cdot 10^{-7}$

$P_f(b,i) =$

$3.443\cdot 10^{-11}$
$3.198\cdot 10^{-11}$
$2.971\cdot 10^{-11}$
$2.759\cdot 10^{-11}$
$2.562\cdot 10^{-11}$
$2.379\cdot 10^{-11}$
$2.209\cdot 10^{-11}$
$2.05\cdot 10^{-11}$
$1.903\cdot 10^{-11}$
$1.766\cdot 10^{-11}$
$1.639\cdot 10^{-11}$
$1.521\cdot 10^{-11}$
$1.411\cdot 10^{-11}$
$1.309\cdot 10^{-11}$
$1.214\cdot 10^{-11}$
$1.126\cdot 10^{-11}$

$$v_{10} = 0.566$$

DPPM using a Butterworth Filter and zero guard with 1Gbit/s data and 5 PCM BITS for Free Space

Preamplifier terms

$S_o := 16 \cdot 10^{-24}$ Preamp noise at input - double sided Philips TZA 3043

$B := 1 \cdot 10^{9}$ Bit rate

$T_b := \frac{1}{B}$ PCM bit time

$i := 0, 1 .. 20$

$v_i := v_{off} + \frac{i}{range}$

$n := 8$ Number of like symbols in PCM

$f_n := 1 \cdot 10^{6}$ Channel Bandwidth for free space

$N := 5$ Number of PCM Bits

$T_s := \frac{N \cdot T_b}{2^N}$ Slot Time for DPPM

$\eta q := 1.6 \cdot 10^{-19}$ Quantum energy

$\lambda := 1.55 \cdot 10^{-6}$ This is the wavelength of operation

$photon\_energy := \frac{6.63 \cdot 10^{-34} \cdot 3 \cdot 10^{8}}{\lambda}$

$R_o := \frac{\eta q}{photon\_energy}$ $R_o := 1.247$

Pulse shape terms

$T_s = 1.563 \cdot 10^{-10}$

$f_p := 0.7 \cdot \frac{1}{T_s}$ $f_B := 0.5 \cdot \frac{1}{T_s}$

$\alpha := \frac{0.1874 \cdot T_b}{f_n}$ $\alpha_n := \frac{0.1874 \cdot T_b}{f_n \cdot T_s}$

$\omega_B := 2 \cdot \pi \cdot f_B$ $\omega_{Bn} := \omega_B \cdot T_s$

$\omega_p := 2\cdot\pi\cdot f_p$ $\omega_{pn} := 2\cdot\pi\cdot f_p\cdot T_s$

$\tau_R := \frac{8}{\omega_B}$ $\tau_{Rn} := \frac{8}{\omega_B\cdot T_s}$

$Pulse(\omega) := \frac{\sin\left(\frac{\omega\cdot T_s}{2}\right)}{\left(\frac{\omega\cdot T_s}{2}\right)}$ $Pulse_n(\omega) := \frac{\sin\left(\frac{\omega}{2}\right)}{\left(\frac{\omega}{2}\right)}$

$H_{pre}(\omega) := \frac{1}{1 + j\cdot\frac{\omega}{\omega_p}}$ $H_B(\omega) := \frac{\omega_B^{\,3}}{\left(j\cdot\omega + \omega_B\right)^3}$

$H_{pren}(\omega) := \frac{1}{1 + j\cdot\frac{\omega}{\omega_{pn}}}$ $H_{Bn}(\omega) := \frac{\omega_{Bn}^{\,3}}{\left(j\cdot\omega + \omega_{Bn}\right)^3}$

Pulse shape

$$I_0(t) := \frac{1}{\pi}\cdot\int_0^{1\cdot 10^{11}} Pulse(\omega)\cdot Re\left[H_{pre}(\omega)\cdot H_B(\omega)\cdot\exp\left[i\cdot\omega\cdot(t-0.5)\cdot T_s\right]\right]d\omega$$

$$a(\omega) := \omega_{pn} - 3\cdot\frac{\omega^2}{\omega_{Bn}} - 3\cdot\frac{\omega^2\cdot\omega_{pn}}{\omega_{Bn}^{\,2}} + \frac{\omega^4}{\omega_{Bn}^{\,3}}$$

$$b1(\omega) := \omega + 3\cdot\frac{\omega\cdot\omega_{pn}}{\omega_{Bn}} - 3\cdot\frac{\omega^3}{\omega_{Bn}^{\,2}} - \frac{\omega^3\cdot\omega_{pn}}{\omega_{Bn}^{\,3}}$$

$$I_0(t) := \frac{\omega_{pn}}{\pi\cdot T_s}\cdot\int_0^{100} Pulse_n(\omega)\cdot\left[\frac{a(\omega)\cdot\cos(\omega\cdot(t-0.5)) + b1(\omega)\cdot\sin(\omega\cdot(t-0.5))}{a(\omega)^2 + b1(\omega)^2}\right]d\omega$$

$$I_1(t) := \frac{\omega_{pn}}{\pi\cdot T_s^{\,2}}\cdot\int_0^{100} Pulse_n(\omega)\cdot\omega\cdot\frac{b1(\omega)\cdot\cos(\omega\cdot(t-0.5)) - a(\omega)\cdot\sin(\omega\cdot(t-0.5))}{a(\omega)^2 + b1(\omega)^2}d\omega$$

$t := -1, -0.99 .. 6$

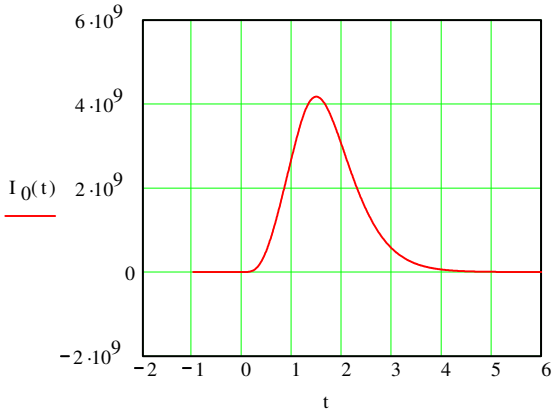

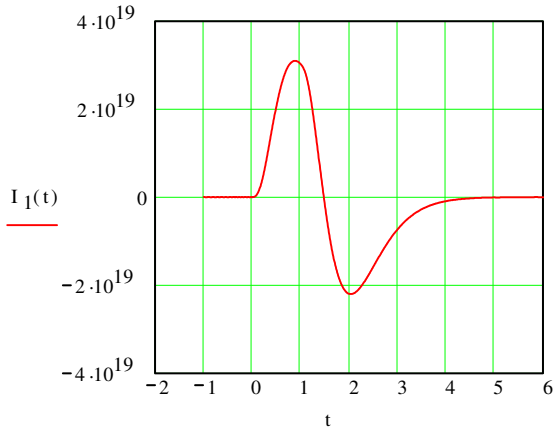

$$noise := \frac{2}{2 \cdot \pi} \cdot \int_{0}^{1 \cdot 10^{11}} \left| H_{pre}(\omega) \cdot H_B(\omega) \right|^2 d\omega$$

$$noise = 3.37 \cdot 10^{9}$$

$t := 1.474$

$t_{pk} := root\left(I_1(t) \cdot T_s^{\,2}, t\right)$

$$t_{pk} = 1.474$$

$v_{pk}(b) := b \cdot \eta q \cdot I_0\left(t_{pk}\right)$

$$v_{pk}(b) = 3.34 \cdot 10^{-6}$$

$t := 0.901$

$t_{d_i} := root\left[\left(I_0(t) - v_i \cdot I_0\left(t_{pk}\right)\right) \cdot T_s^{\,2}, t\right]$

$v_d(b,i) := b \cdot \eta q \cdot I_0\left(t_{d_i}\right)$

$t_{d_5} = 0.901$

Erasure Error

$$Q_r(b,i) := \frac{v_{pk}(b) - v_d(b,i)}{\sqrt{S_o \cdot noise}}$$

$P_{er} := 0.5$ **5 Bits PCM error caused by erasure in DPPM**

$$P_r(b,i) := 0.5 \cdot P_{er} \cdot erfc\left(\frac{Q_r(b,i)}{\sqrt{2}}\right)$$ ***Erasure Error Probability***

False Alarm Error

$$Q_t(b,i) := \frac{v_d(b,i)}{\sqrt{S_o \cdot noise}}$$

$P_{fa} := 0.258$ **5 Bits PCM error caused by Flase Alarm in DPPM**

$$P_f(b,i) := 0.5 \cdot erfc\left(\frac{Q_t(b,i)}{\sqrt{2}}\right) \cdot P_{fa}$$ [redacted]

$$P_{es}(b,i) := P_r(b,i) + \frac{n-1}{2} \cdot P_f(b,i)$$ ***Symbol Error Probability***

$$P_{eb}(b,i) := \frac{n}{2\cdot(n-1)}\cdot P_{es}(b,i)$$

Binary Error Probability

$$pc(b,i) := \left(\log\left(P_{eb}(b,i)\right) + 9\right)$$

Set for 1 in 10^9 errors

$a_i := root(pc(b,i),b)$ Find the root to give 1 in 10^9

$minimum := min(a)$

$minimum = 4.534\cdot10^{3}$

$range \equiv 1000$

$b \equiv 5\cdot10^{3}$

$minimum = 4.534\cdot10^{3}$

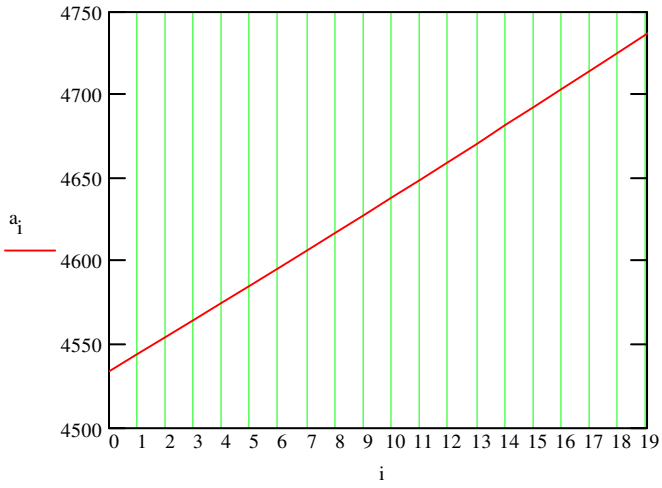

$v_{off} \equiv 0.556$

$N \equiv 5$

$f_n \equiv 1\cdot10^{6}$

$P_r(b,i) =$

$4.269\cdot10^{-11}$
$4.69\cdot10^{-11}$
$5.15\cdot10^{-11}$
$5.655\cdot10^{-11}$
$6.208\cdot10^{-11}$
$6.814\cdot10^{-11}$
$7.477\cdot10^{-11}$
$8.203\cdot10^{-11}$
$8.998\cdot10^{-11}$
$9.867\cdot10^{-11}$
$1.082\cdot10^{-10}$
$1.186\cdot10^{-10}$
$1.3\cdot10^{-10}$
$1.424\cdot10^{-10}$
$1.56\cdot10^{-10}$
$1.709\cdot10^{-10}$

$P_f(b,i) =$

0
0
0
0
0
0
0
0
0
0
0
0
0
0
0
0

$v_{10} = 0.566$

DPPM using a Butterworth Filter and zero guard with 1Gbit/s data and 6 PCM BITS for Free Space

Preamplifier terms

$S_o := 16 \cdot 10^{-24}$ Preamp noise at input - double sided Philips TZA 3043

$B := 1 \cdot 10^{9}$ Bit rate

$T_b := \frac{1}{B}$ PCM bit time

$i := 0, 1 .. 20$

$v_i := v_{off} + \frac{i}{range}$

$n := 8$ Number of like symbols in PCM

$f_n := 1 \cdot 10^{6}$ Channel Bandwidth for free space

$N := 6$ Number of PCM Bits

$T_s := \frac{N \cdot T_b}{2^N}$ Slot Time for DPPM

$\eta q := 1.6 \cdot 10^{-19}$ Quantum energy

$\lambda := 1.55 \cdot 10^{-6}$ This is the wavelength of operation

$photon\_energy := \frac{6.63 \cdot 10^{-34} \cdot 3 \cdot 10^{8}}{\lambda}$

$R_o := \frac{\eta q}{photon\_energy}$ $R_o := 1.247$

Pulse shape terms

$T_s = 9.375 \cdot 10^{-11}$

$f_p := 0.7 \cdot \frac{1}{T_s}$ $f_B := 0.5 \cdot \frac{1}{T_s}$

$\alpha := \frac{0.1874 \cdot T_b}{f_n}$ $\alpha_n := \frac{0.1874 \cdot T_b}{f_n \cdot T_s}$

$\omega_B := 2 \cdot \pi \cdot f_B$ $\omega_{Bn} := \omega_B \cdot T_s$

$\omega_p := 2\cdot\pi\cdot f_p$ $\omega_{pn} := 2\cdot\pi\cdot f_p\cdot T_s$

$\tau_R := \frac{8}{\omega_B}$ $\tau_{Rn} := \frac{8}{\omega_B\cdot T_s}$

$Pulse(\omega) := \frac{\sin\left(\frac{\omega\cdot T_s}{2}\right)}{\left(\frac{\omega\cdot T_s}{2}\right)}$ $Pulse_n(\omega) := \frac{\sin\left(\frac{\omega}{2}\right)}{\left(\frac{\omega}{2}\right)}$

$H_{pre}(\omega) := \frac{1}{1 + j\cdot\frac{\omega}{\omega_p}}$ $H_B(\omega) := \frac{\omega_B^{\,3}}{\left(j\cdot\omega + \omega_B\right)^3}$

$H_{pren}(\omega) := \frac{1}{1 + j\cdot\frac{\omega}{\omega_{pn}}}$ $H_{Bn}(\omega) := \frac{\omega_{Bn}^{\,3}}{\left(j\cdot\omega + \omega_{Bn}\right)^3}$

Pulse shape

$$I_0(t) := \frac{1}{\pi}\cdot\int_0^{1\cdot 10^{11}} Pulse(\omega)\cdot Re\left[H_{pre}(\omega)\cdot H_B(\omega)\cdot\exp\left[i\cdot\omega\cdot(t-0.5)\cdot T_s\right]\right]d\omega$$

$$a(\omega) := \omega_{pn} - 3\cdot\frac{\omega^2}{\omega_{Bn}} - 3\cdot\frac{\omega^2\cdot\omega_{pn}}{\omega_{Bn}^{\,2}} + \frac{\omega^4}{\omega_{Bn}^{\,3}}$$

$$b1(\omega) := \omega + 3\cdot\frac{\omega\cdot\omega_{pn}}{\omega_{Bn}} - 3\cdot\frac{\omega^3}{\omega_{Bn}^{\,2}} - \frac{\omega^3\cdot\omega_{pn}}{\omega_{Bn}^{\,3}}$$

$$I_0(t) := \frac{\omega_{pn}}{\pi\cdot T_s}\cdot\int_0^{100} Pulse_n(\omega)\cdot\left[\frac{a(\omega)\cdot\cos(\omega\cdot(t-0.5)) + b1(\omega)\cdot\sin(\omega\cdot(t-0.5))}{a(\omega)^2 + b1(\omega)^2}\right]d\omega$$

$$I_1(t) := \frac{\omega_{pn}}{\pi\cdot T_s^{\,2}}\cdot\int_0^{100} Pulse_n(\omega)\cdot\omega\cdot\frac{b1(\omega)\cdot\cos(\omega\cdot(t-0.5)) - a(\omega)\cdot\sin(\omega\cdot(t-0.5))}{a(\omega)^2 + b1(\omega)^2}d\omega$$

$t := -1, -0.99 .. 6$

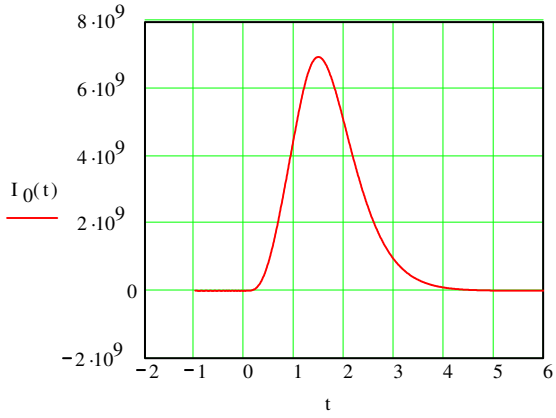

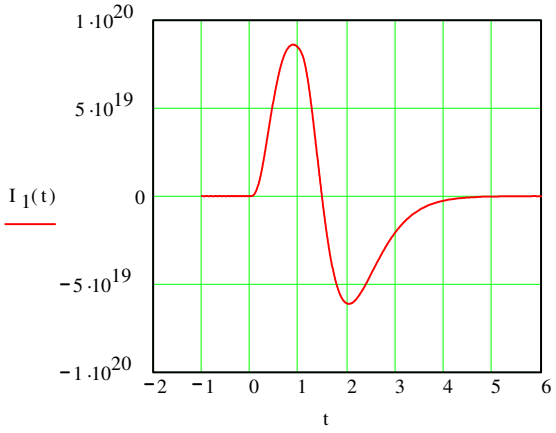

$$noise := \frac{2}{2\cdot\pi}\cdot\int_{0}^{1\cdot10^{11}} \left| H_{pre}(\omega)\cdot H_B(\omega) \right|^2 d\omega$$

$noise = 5.616\cdot10^{9}$

$t := 1.474$

$t_{pk} := root\left(I_1(t)\cdot T_s^{\,2}, t\right)$

$t_{pk} = 1.474$

$v_{pk}(b) := b\cdot\eta q\cdot I_0\left(t_{pk}\right)$

$v_{pk}(b) = 5.566\cdot10^{-6}$

$t := 0.901$

$t_{d_i} := \text{root}\left[\left(I_0(t) - v_i \cdot I_0\left(t_{pk}\right)\right) \cdot T_s^{\,2}, t\right]$

$v_d(b,i) := b \cdot \eta q \cdot I_0\left(t_{d_i}\right)$

$t_{d_5} = 0.901$

Erasure Error

$$Q_r(b,i) := \frac{v_{pk}(b) - v_d(b,i)}{\sqrt{S_o \cdot noise}}$$

$P_{er} := 0.5$ **6 Bits PCM error caused by erasure in DPPM**

$$P_r(b,i) := 0.5 \cdot P_{er} \cdot \text{erfc}\left(\frac{Q_r(b,i)}{\sqrt{2}}\right)$$ ***Erasure Error Probability***

False Alarm Error

$$Q_t(b,i) := \frac{v_d(b,i)}{\sqrt{S_o \cdot noise}}$$

$P_{fa} := 0.253$ **6 Bits PCM error caused by Flase Alarm in DPPM**

$$P_f(b,i) := 0.5 \cdot \text{erfc}\left(\frac{Q_t(b,i)}{\sqrt{2}}\right) \cdot P_{fa}$$ [redacted]

$$P_{es}(b,i) := P_r(b,i) + \frac{n-1}{2} \cdot P_f(b,i)$$ ***Symbol Error Probability***

$$P_{eb}(b,i) := \frac{n}{2 \cdot (n-1)} \cdot P_{es}(b,i)$$ ***Binary Error Probability***

$pc(b,i) := \left(\log\left(P_{eb}(b,i)\right) + 9\right)$ Set for 1 in 10^9 errors

$a_i := root(pc(b,i),b)$ Find the root to give 1 in 10^9

$minimum := min(a)$

$range \equiv 1000$

$minimum = 3.512 \cdot 10^3$

$b \equiv 5 \cdot 10^3$

$minimum = 3.512 \cdot 10^3$

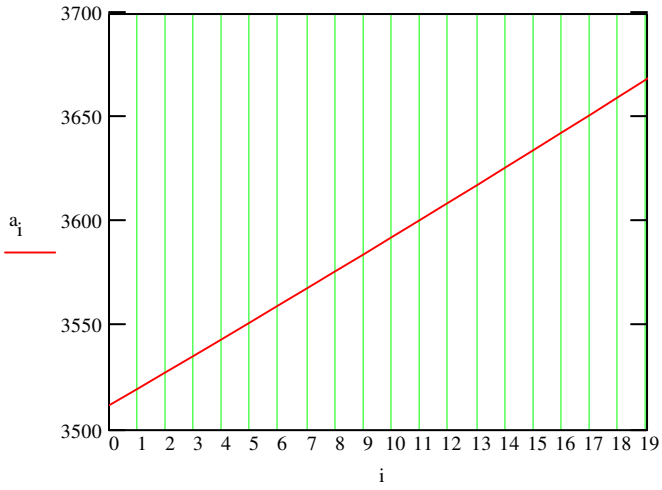

$v_{off} \equiv 0.556$

$N \equiv 6$

$f_n \equiv 1 \cdot 10^6$

$v_{10} = 0.566$

$P_r(b,i) =$

0
0
0
0
0
0
0
0
0
0
0
0
0
0
0
0
0
0
0

$P_f(b,i) =$

0
0
0
0
0
0
0
0
0
0
0
0
0
0
0
0
0
0
0

MPPM using a Butterworth Filter and zero guard with 1Gbit/s data and 3 PCM BITS for Free Space

Preamplifier terms

$S_o := 16 \cdot 10^{-24}$ Preamp noise at input - double sided Philips TZA 3043

$B := 1 \cdot 10^{9}$ Bit rate

$T_b := \frac{1}{B}$ PCM bit time

$i := 0, 1 .. 20$

$v_i := v_{off} + \frac{i}{range}$

$n := 8$ Number of like symbols in PCM

$f_n := 1 \cdot 10^{6}$ Channel Bandwidth for free space

$N := 3$ Number of PCM Bits

$T_s := \frac{3 \cdot T_b}{5}$ Slot Time for MPPM(5,2)

$\eta q := 1.6 \cdot 10^{-19}$ Quantum energy

$\lambda := 1.55 \cdot 10^{-6}$ This is the wavelength of operation

$photon\_energy := \frac{6.63 \cdot 10^{-34} \cdot 3 \cdot 10^{8}}{\lambda}$

$R_o := \frac{\eta q}{photon\_energy}$ $R_o := 1.247$

Pulse shape terms

$T_s = 6 \cdot 10^{-10}$

$f_p := 0.7 \cdot \frac{1}{T_s}$ $f_B := 0.5 \cdot \frac{1}{T_s}$

$\alpha := \frac{0.1874 \cdot T_b}{f_n}$ $\alpha_n := \frac{0.1874 \cdot T_b}{f_n \cdot T_s}$

$\omega_B := 2 \cdot \pi \cdot f_B$ $\omega_{Bn} := \omega_B \cdot T_s$

$\omega_p := 2\cdot\pi\cdot f_p$ $\omega_{pn} := 2\cdot\pi\cdot f_p\cdot T_s$

$\tau_R := \frac{8}{\omega_B}$ $\tau_{Rn} := \frac{8}{\omega_B\cdot T_s}$

$Pulse(\omega) := \frac{\sin\left(\frac{\omega\cdot T_s}{2}\right)}{\left(\frac{\omega\cdot T_s}{2}\right)}$ $Pulse_n(\omega) := \frac{\sin\left(\frac{\omega}{2}\right)}{\left(\frac{\omega}{2}\right)}$

$H_{pre}(\omega) := \frac{1}{1 + j\cdot\frac{\omega}{\omega_p}}$ $H_B(\omega) := \frac{\omega_B^{\,3}}{\left(j\cdot\omega + \omega_B\right)^3}$

$H_{pren}(\omega) := \frac{1}{1 + j\cdot\frac{\omega}{\omega_{pn}}}$ $H_{Bn}(\omega) := \frac{\omega_{Bn}^{\,3}}{\left(j\cdot\omega + \omega_{Bn}\right)^3}$

Pulse shape

$$I_0(t) := \frac{1}{\pi}\cdot\int_0^{1\cdot 10^{11}} Pulse(\omega)\cdot Re\left[H_{pre}(\omega)\cdot H_B(\omega)\cdot\exp\left[i\cdot\omega\cdot(t-0.5)\cdot T_s\right]\right]d\omega$$

$$a(\omega) := \omega_{pn} - 3\cdot\frac{\omega^2}{\omega_{Bn}} - 3\cdot\frac{\omega^2\cdot\omega_{pn}}{\omega_{Bn}^{\,2}} + \frac{\omega^4}{\omega_{Bn}^{\,3}}$$

$$b1(\omega) := \omega + 3\cdot\frac{\omega\cdot\omega_{pn}}{\omega_{Bn}} - 3\cdot\frac{\omega^3}{\omega_{Bn}^{\,2}} - \frac{\omega^3\cdot\omega_{pn}}{\omega_{Bn}^{\,3}}$$

$$I_0(t) := \frac{\omega_{pn}}{\pi\cdot T_s}\cdot\int_0^{100} Pulse_n(\omega)\cdot\left[\frac{a(\omega)\cdot\cos(\omega\cdot(t-0.5)) + b1(\omega)\cdot\sin(\omega\cdot(t-0.5))}{a(\omega)^2 + b1(\omega)^2}\right]d\omega$$

$$I_1(t) := \frac{\omega_{pn}}{\pi\cdot T_s^{\,2}}\cdot\int_0^{100} Pulse_n(\omega)\cdot\omega\cdot\frac{b1(\omega)\cdot\cos(\omega\cdot(t-0.5)) - a(\omega)\cdot\sin(\omega\cdot(t-0.5))}{a(\omega)^2 + b1(\omega)^2}d\omega$$

$t := -1, -0.99 .. 6$

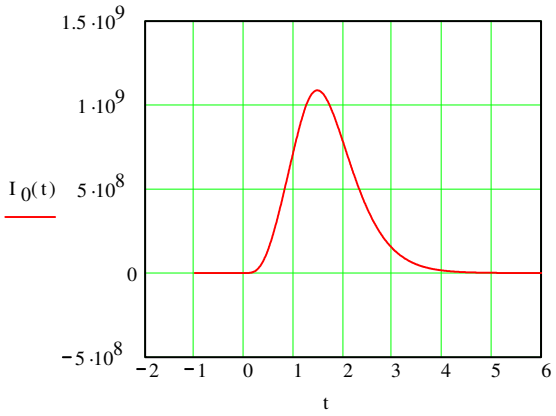

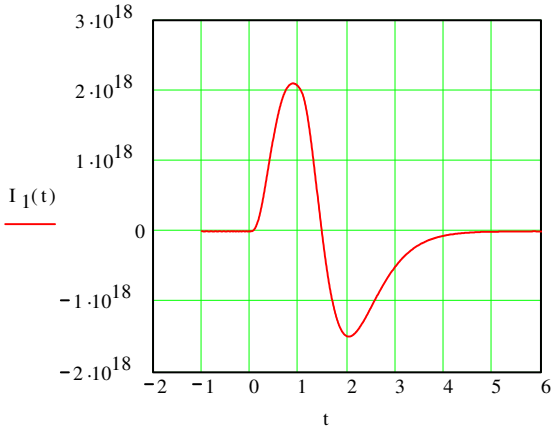

$$noise := \frac{2}{2\cdot\pi}\cdot\int_{0}^{1\cdot10^{11}} \left| H_{pre}(\omega)\cdot H_B(\omega) \right|^2 d\omega$$

$noise = 8.776\cdot10^{8}$

$t := 1.474$

$t_{pk} := root\left(I_1(t)\cdot T_s^{\,2}, t\right)$

$t_{pk} = 1.474$

$v_{pk}(b) := b\cdot\eta q\cdot I_0\left(t_{pk}\right)$

$v_{pk}(b) = 8.697\cdot10^{-7}$

$t := 0.878$

$t_{d_i} := \text{root}\left[\left(I_0(t) - v_i \cdot I_0\left(t_{pk}\right)\right) \cdot T_s^{\,2}, t\right]$

$v_d(b,i) := b \cdot \eta q \cdot I_0\left(t_{d_i}\right)$

$t_{d_5} = 0.878$

Erasure Error

$$Q_r(b,i) := \frac{v_{pk}(b) - v_d(b,i)}{\sqrt{S_o \cdot noise}}$$

$P_{er} := 0.382$ **3 Bits PCM error caused by erasure in MPPM**

$$P_r(b,i) := 0.5 \cdot P_{er} \cdot \text{erfc}\left(\frac{Q_r(b,i)}{\sqrt{2}}\right)$$ ***Erasure Error Probability***

False Alarm Error

$$Q_t(b,i) := \frac{v_d(b,i)}{\sqrt{S_o \cdot noise}}$$

$P_{fa} := 0.309$ **3 Bits PCM error caused by False Alarm in MPPM**

$$P_f(b,i) := 0.5 \cdot \text{erfc}\left(\frac{Q_t(b,i)}{\sqrt{2}}\right) \cdot P_{fa}$$ [redacted]

$P_{eb}(b,i) := P_r(b,i) + P_f(b,i)$ ***Binary Error Probability***

$pc(b,i) := \left(\log\left(P_{eb}(b,i)\right) + 9\right)$ Set for 1 in 10^9 errors

$a_i := root(pc(b,i),b)$ Find the root to give 1 in 10^9

$minimum := min(a)$

$minimum = 8.466 \cdot 10^3$

$range \equiv 1000$

$b \equiv 5 \cdot 10^3$

$minimum = 8.466 \cdot 10^3$

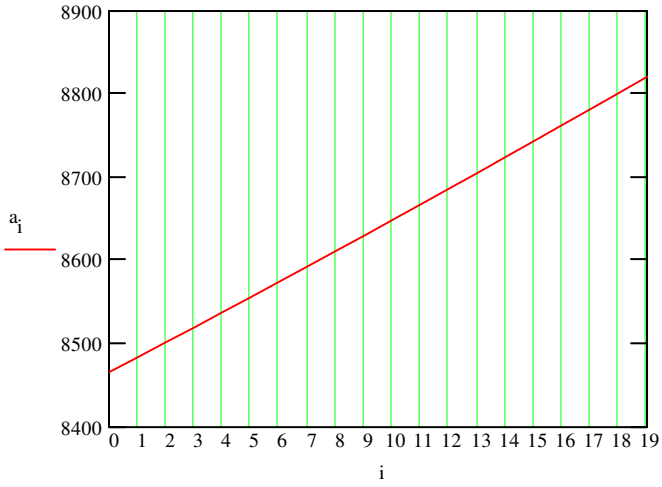

$v_{off} \equiv 0.53$

$N \equiv 3$

$f_n \equiv 1 \cdot 10^6$

$v_{10} = 0.54$

$P_r(b,i) =$

$1.073 \cdot 10^{-4}$
$1.103 \cdot 10^{-4}$
$1.133 \cdot 10^{-4}$
$1.164 \cdot 10^{-4}$
$1.196 \cdot 10^{-4}$
$1.228 \cdot 10^{-4}$
$1.262 \cdot 10^{-4}$
$1.296 \cdot 10^{-4}$
$1.332 \cdot 10^{-4}$
$1.368 \cdot 10^{-4}$
$1.405 \cdot 10^{-4}$
$1.443 \cdot 10^{-4}$
$1.481 \cdot 10^{-4}$
$1.521 \cdot 10^{-4}$
$1.562 \cdot 10^{-4}$
$1.604 \cdot 10^{-4}$

$P_f(b,i) =$

$1.55 \cdot 10^{-5}$
$1.504 \cdot 10^{-5}$
$1.459 \cdot 10^{-5}$
$1.415 \cdot 10^{-5}$
$1.373 \cdot 10^{-5}$
$1.332 \cdot 10^{-5}$
$1.292 \cdot 10^{-5}$
$1.253 \cdot 10^{-5}$
$1.215 \cdot 10^{-5}$
$1.178 \cdot 10^{-5}$
$1.143 \cdot 10^{-5}$
$1.108 \cdot 10^{-5}$
$1.074 \cdot 10^{-5}$
$1.042 \cdot 10^{-5}$
$1.01 \cdot 10^{-5}$
$9.792 \cdot 10^{-6}$

MPPM using a Butterworth Filter and zero guard with 1Gbit/s data and 4 PCM BITS for Free Space

Preamplifier terms

$S_o := 16 \cdot 10^{-24}$ Preamp noise at input - double sided Philips TZA 3043

$B := 1 \cdot 10^{9}$ Bit rate

$T_b := \frac{1}{B}$ PCM bit time

$i := 0, 1 .. 20$

$v_i := v_{off} + \frac{i}{range}$

$n := 8$ Number of like symbols in PCM

$f_n := 1 \cdot 10^{6}$ Channel Bandwidth for free space

$N := 4$ Number of PCM Bits

$T_s := \frac{4 \cdot T_b}{7}$ Slot Time for MPPM(7,2)

$\eta q := 1.6 \cdot 10^{-19}$ Quantum energy

$\lambda := 1.55 \cdot 10^{-6}$ This is the wavelength of operation

$photon\_energy := \frac{6.63 \cdot 10^{-34} \cdot 3 \cdot 10^{8}}{\lambda}$

$R_o := \frac{\eta q}{photon\_energy}$ $R_o := 1.247$

Pulse shape terms

$T_s = 5.714 \cdot 10^{-10}$

$f_p := 0.7 \cdot \frac{1}{T_s}$ $f_B := 0.5 \cdot \frac{1}{T_s}$

$\alpha := \frac{0.1874 \cdot T_b}{f_n}$ $\alpha_n := \frac{0.1874 \cdot T_b}{f_n \cdot T_s}$

$\omega_B := 2 \cdot \pi \cdot f_B$ $\omega_{Bn} := \omega_B \cdot T_s$

$\omega_p := 2\cdot\pi\cdot f_p$ $\omega_{pn} := 2\cdot\pi\cdot f_p\cdot T_s$

$\tau_R := \frac{8}{\omega_B}$ $\tau_{Rn} := \frac{8}{\omega_B\cdot T_s}$

$\text{Pulse}(\omega) := \frac{\sin\left(\frac{\omega\cdot T_s}{2}\right)}{\left(\frac{\omega\cdot T_s}{2}\right)}$ $\text{Pulse}_n(\omega) := \frac{\sin\left(\frac{\omega}{2}\right)}{\left(\frac{\omega}{2}\right)}$

$H_{pre}(\omega) := \frac{1}{1 + j\cdot\frac{\omega}{\omega_p}}$ $H_B(\omega) := \frac{\omega_B^{\,3}}{\left(j\cdot\omega + \omega_B\right)^3}$

$H_{pren}(\omega) := \frac{1}{1 + j\cdot\frac{\omega}{\omega_{pn}}}$ $H_{Bn}(\omega) := \frac{\omega_{Bn}^{\,3}}{\left(j\cdot\omega + \omega_{Bn}\right)^3}$

Pulse shape

$$I_0(t) := \frac{1}{\pi}\cdot\int_0^{1\cdot 10^{11}} \text{Pulse}(\omega)\cdot\text{Re}\left[H_{pre}(\omega)\cdot H_B(\omega)\cdot\exp\left[i\cdot\omega\cdot(t-0.5)\cdot T_s\right]\right]d\omega$$

$$a(\omega) := \omega_{pn} - 3\cdot\frac{\omega^2}{\omega_{Bn}} - 3\cdot\frac{\omega^2\cdot\omega_{pn}}{\omega_{Bn}^{\,2}} + \frac{\omega^4}{\omega_{Bn}^{\,3}}$$

$$b1(\omega) := \omega + 3\cdot\frac{\omega\cdot\omega_{pn}}{\omega_{Bn}} - 3\cdot\frac{\omega^3}{\omega_{Bn}^{\,2}} - \frac{\omega^3\cdot\omega_{pn}}{\omega_{Bn}^{\,3}}$$

$$I_0(t) := \frac{\omega_{pn}}{\pi\cdot T_s}\cdot\int_0^{100} \text{Pulse}_n(\omega)\cdot\left[\frac{a(\omega)\cdot\cos(\omega\cdot(t-0.5)) + b1(\omega)\cdot\sin(\omega\cdot(t-0.5))}{a(\omega)^2 + b1(\omega)^2}\right]d\omega$$

$$I_1(t) := \frac{\omega_{pn}}{\pi\cdot T_s^{\,2}}\cdot\int_0^{100} \text{Pulse}_n(\omega)\cdot\omega\cdot\frac{b1(\omega)\cdot\cos(\omega\cdot(t-0.5)) - a(\omega)\cdot\sin(\omega\cdot(t-0.5))}{a(\omega)^2 + b1(\omega)^2}d\omega$$

$t := -1, -0.99 .. 6$

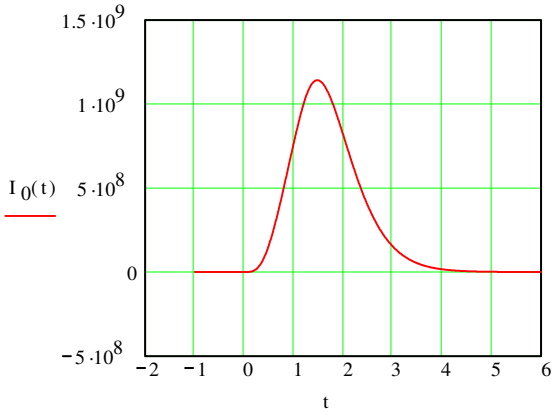

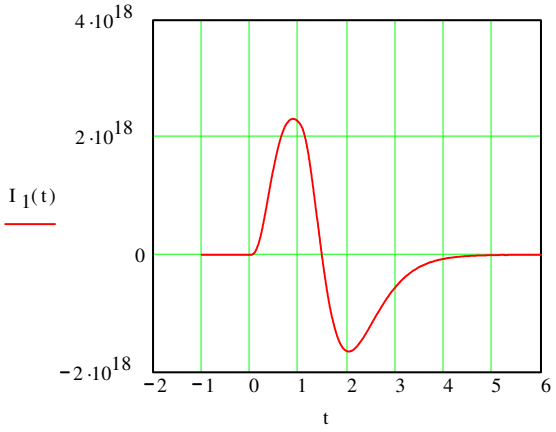

$$noise := \frac{2}{2 \cdot \pi} \cdot \int_{0}^{1 \cdot 10^{11}} \left| H_{pre}(\omega) \cdot H_B(\omega) \right|^2 d\omega$$

$noise = 9.215 \cdot 10^{8}$

$t := 1.474$

$t_{pk} := root\left(I_1(t) \cdot T_s^{\,2}, t\right)$

$t_{pk} = 1.474$

$v_{pk}(b) := b \cdot \eta q \cdot I_0\left(t_{pk}\right)$

$v_{pk}(b) = 9.132 \cdot 10^{-7}$

$t := 0.878$

$t_{d_i} := root\left[\left(I_0(t) - v_i \cdot I_0\left(t_{pk}\right)\right) \cdot T_s^{\,2}, t\right]$

$v_d(b,i) := b \cdot \eta q \cdot I_0\left(t_{d_i}\right)$

$t_{d_5} = 0.878$

Erasure Error

$$Q_r(b,i) := \frac{v_{pk}(b) - v_d(b,i)}{\sqrt{S_o \cdot noise}}$$

$P_{er} := 0.419$ **4 Bits PCM error caused by erasure in MPPM**

$$P_r(b,i) := 0.5 \cdot P_{er} \cdot erfc\left(\frac{Q_r(b,i)}{\sqrt{2}}\right)$$ ***Erasure Error Probability***

False Alarm Error

$$Q_t(b,i) := \frac{v_d(b,i)}{\sqrt{S_o \cdot noise}}$$

$P_{fa} := 0.3088$ **4 Bits PCM error caused by False Alarm in MPPM**

$$P_f(b,i) := 0.5 \cdot erfc\left(\frac{Q_t(b,i)}{\sqrt{2}}\right) \cdot P_{fa}$$ ***False Alarm Error probability***

$P_{eb}(b,i) := P_r(b,i) + P_f(b,i)$ ***Binary Error probability***

$pc(b,i) := \left(\log\left(P_{eb}(b,i)\right) + 9\right)$ Set for 1 in 10^9 errors

$a_i := root(pc(b,i),b)$ Find the root to give 1 in 10^9

$minimum := min(a)$

$minimum = 8.284 \cdot 10^3$

$range \equiv 1000$

$b \equiv 5 \cdot 10^3$

$minimum = 8.284 \cdot 10^3$

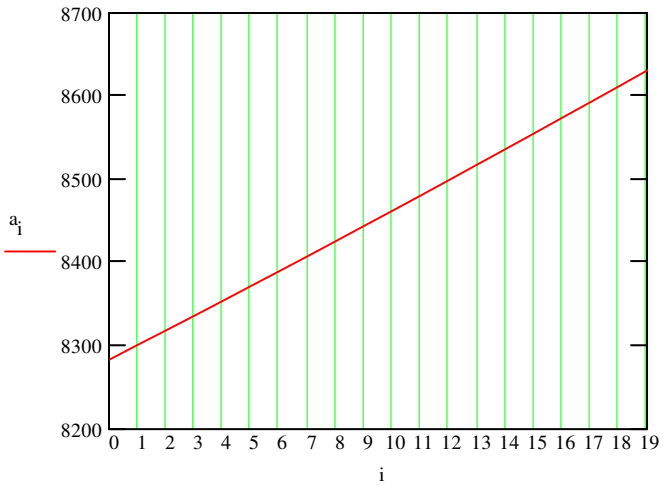

$v_{off} \equiv 0.53$

$N \equiv 4$

$f_n \equiv 1 \cdot 10^6$

$v_{10} = 0.54$

$P_r(b,i) =$

$8.556 \cdot 10^{-5}$
$8.803 \cdot 10^{-5}$
$9.056 \cdot 10^{-5}$
$9.316 \cdot 10^{-5}$
$9.583 \cdot 10^{-5}$
$9.857 \cdot 10^{-5}$
$1.014 \cdot 10^{-4}$
$1.043 \cdot 10^{-4}$
$1.072 \cdot 10^{-4}$
$1.103 \cdot 10^{-4}$
$1.134 \cdot 10^{-4}$
$1.166 \cdot 10^{-4}$
$1.199 \cdot 10^{-4}$
$1.233 \cdot 10^{-4}$
$1.268 \cdot 10^{-4}$
$1.303 \cdot 10^{-4}$

$P_f(b,i) =$

$1.038 \cdot 10^{-5}$
$1.006 \cdot 10^{-5}$
$9.744 \cdot 10^{-6}$
$9.439 \cdot 10^{-6}$
$9.143 \cdot 10^{-6}$
$8.856 \cdot 10^{-6}$
$8.577 \cdot 10^{-6}$
$8.307 \cdot 10^{-6}$
$8.045 \cdot 10^{-6}$
$7.79 \cdot 10^{-6}$
$7.543 \cdot 10^{-6}$
$7.304 \cdot 10^{-6}$
$7.072 \cdot 10^{-6}$
$6.847 \cdot 10^{-6}$
$6.629 \cdot 10^{-6}$
$6.417 \cdot 10^{-6}$

MPPM using a Butterworth Filter and zero guard with 1Gbit/s data and 5 PCM BITS for Free Space

Preamplifier terms

$S_o := 16 \cdot 10^{-24}$ Preamp noise at input - double sided Philips TZA 3043

$B := 1 \cdot 10^{9}$ Bit rate

$T_b := \frac{1}{B}$ PCM bit time

$i := 0, 1 .. 20$

$v_i := v_{off} + \frac{i}{range}$

$n := 8$ Number of like symbols in PCM

$f_n := 1 \cdot 10^{6}$ Channel Bandwidth for free space

$N := 5$ Number of PCM Bits

$T_s := \frac{5 \cdot T_b}{9}$ Slot Time for MPPM(9,2)

$\eta q := 1.6 \cdot 10^{-19}$ Quantum energy

$\lambda := 1.55 \cdot 10^{-6}$ This is the wavelength of operation

$photon\_energy := \frac{6.63 \cdot 10^{-34} \cdot 3 \cdot 10^{8}}{\lambda}$

$R_o := \frac{\eta q}{photon\_energy}$ $R_o := 1.247$

Pulse shape terms

$T_s = 5.556 \cdot 10^{-10}$

$f_p := 0.7 \cdot \frac{1}{T_s}$ $f_B := 0.5 \cdot \frac{1}{T_s}$

$\alpha := \frac{0.1874 \cdot T_b}{f_n}$ $\alpha_n := \frac{0.1874 \cdot T_b}{f_n \cdot T_s}$

$\omega_B := 2 \cdot \pi \cdot f_B$ $\omega_{Bn} := \omega_B \cdot T_s$

$\omega_p := 2\cdot\pi\cdot f_p$ $\omega_{pn} := 2\cdot\pi\cdot f_p\cdot T_s$

$\tau_R := \frac{8}{\omega_B}$ $\tau_{Rn} := \frac{8}{\omega_B\cdot T_s}$

$\text{Pulse}(\omega) := \frac{\sin\left(\frac{\omega\cdot T_s}{2}\right)}{\left(\frac{\omega\cdot T_s}{2}\right)}$ $\text{Pulse}_n(\omega) := \frac{\sin\left(\frac{\omega}{2}\right)}{\left(\frac{\omega}{2}\right)}$

$H_{pre}(\omega) := \frac{1}{1 + j\cdot\frac{\omega}{\omega_p}}$ $H_B(\omega) := \frac{\omega_B^{\,3}}{\left(j\cdot\omega + \omega_B\right)^3}$

$H_{pren}(\omega) := \frac{1}{1 + j\cdot\frac{\omega}{\omega_{pn}}}$ $H_{Bn}(\omega) := \frac{\omega_{Bn}^{\,3}}{\left(j\cdot\omega + \omega_{Bn}\right)^3}$

Pulse shape

$$I_0(t) := \frac{1}{\pi}\cdot\int_0^{1\cdot 10^{11}} \text{Pulse}(\omega)\cdot\text{Re}\left[H_{pre}(\omega)\cdot H_B(\omega)\cdot\exp\left[i\cdot\omega\cdot(t-0.5)\cdot T_s\right]\right]d\omega$$

$$a(\omega) := \omega_{pn} - 3\cdot\frac{\omega^2}{\omega_{Bn}} - 3\cdot\frac{\omega^2\cdot\omega_{pn}}{\omega_{Bn}^{\,2}} + \frac{\omega^4}{\omega_{Bn}^{\,3}}$$

$$b1(\omega) := \omega + 3\cdot\frac{\omega\cdot\omega_{pn}}{\omega_{Bn}} - 3\cdot\frac{\omega^3}{\omega_{Bn}^{\,2}} - \frac{\omega^3\cdot\omega_{pn}}{\omega_{Bn}^{\,3}}$$

$$I_0(t) := \frac{\omega_{pn}}{\pi\cdot T_s}\cdot\int_0^{100} \text{Pulse}_n(\omega)\cdot\left[\frac{a(\omega)\cdot\cos(\omega\cdot(t-0.5)) + b1(\omega)\cdot\sin(\omega\cdot(t-0.5))}{a(\omega)^2 + b1(\omega)^2}\right]d\omega$$

$$I_1(t) := \frac{\omega_{pn}}{\pi\cdot T_s^{\,2}}\cdot\int_0^{100} \text{Pulse}_n(\omega)\cdot\omega\cdot\frac{b1(\omega)\cdot\cos(\omega\cdot(t-0.5)) - a(\omega)\cdot\sin(\omega\cdot(t-0.5))}{a(\omega)^2 + b1(\omega)^2}d\omega$$

$t := -1, -0.99 .. 6$

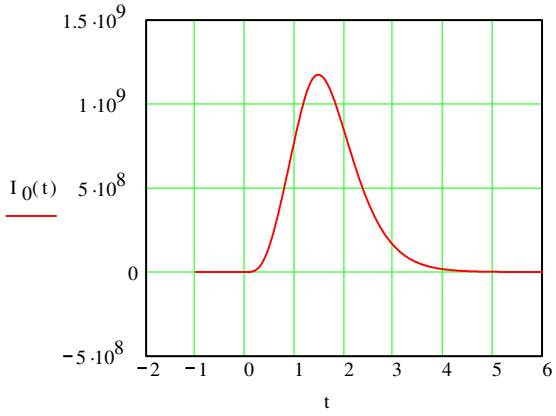

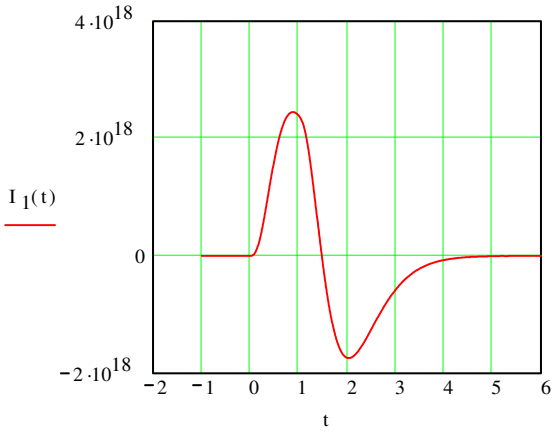

$$noise := \frac{2}{2\cdot\pi}\cdot\int_{0}^{1\cdot10^{11}} \left| H_{pre}(\omega)\cdot H_B(\omega) \right|^2 d\omega$$

$noise = 9.478\cdot10^{8}$

$t := 1.474$

$t_{pk} := root\left(I_1(t)\cdot T_s^{\,2}, t\right)$

$t_{pk} = 1.474$

$v_{pk}(b) := b\cdot\eta q\cdot I_0\left(t_{pk}\right)$

$v_{pk}(b) = 9.392\cdot10^{-7}$

$t := 0.878$

$t_{d_i} := root\left[\left(I_0(t) - v_i \cdot I_0\left(t_{pk}\right)\right) \cdot T_s^{\,2}, t\right]$

$v_d(b,i) := b \cdot \eta q \cdot I_0\left(t_{d_i}\right)$

$t_{d_5} = 0.878$

Erasure Error

$$Q_r(b,i) := \frac{v_{pk}(b) - v_d(b,i)}{\sqrt{S_o \cdot noise}}$$

$P_{er} := 0.440$ **5 Bits PCM error caused by erasure in MPPM**

$$P_r(b,i) := 0.5 \cdot P_{er} \cdot erfc\left(\frac{Q_r(b,i)}{\sqrt{2}}\right)$$ ***Erasure Error Probability***

False Alarm Error

$$Q_t(b,i) := \frac{v_d(b,i)}{\sqrt{S_o \cdot noise}}$$

$P_{fa} := 0.305$ **5 Bits PCM error caused by False Alarm in MPPM**

$$P_f(b,i) := 0.5 \cdot erfc\left(\frac{Q_t(b,i)}{\sqrt{2}}\right) \cdot P_{fa}$$ [redacted]

$P_{eb}(b,i) := P_r(b,i) + P_f(b,i)$ ***Binary Error Probability***

$pc(b,i) := \left(\log\left(P_{eb}(b,i)\right) + 9\right)$ Set for 1 in 10^9 errors

$a_i := root(pc(b,i),b)$ Find the root to give 1 in 10^9

$minimum := min(a)$

$minimum = 8.179 \cdot 10^3$

$range \equiv 1000$

$b \equiv 5 \cdot 10^3$

$minimum = 8.179 \cdot 10^3$

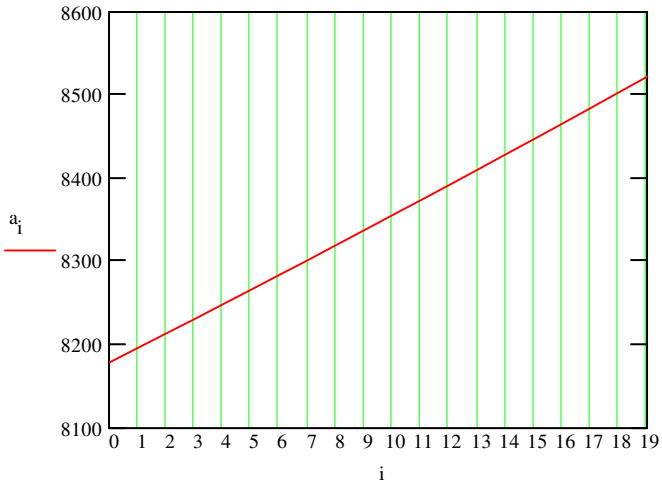

$v_{off} \equiv 0.53$

$N \equiv 5$

$f_n \equiv 1 \cdot 10^6$

$v_{10} = 0.54$

$P_r(b,i) =$

$7.423 \cdot 10^{-5}$
$7.643 \cdot 10^{-5}$
$7.869 \cdot 10^{-5}$
$8.101 \cdot 10^{-5}$
$8.34 \cdot 10^{-5}$
$8.585 \cdot 10^{-5}$
$8.837 \cdot 10^{-5}$
$9.096 \cdot 10^{-5}$
$9.362 \cdot 10^{-5}$
$9.635 \cdot 10^{-5}$
$9.915 \cdot 10^{-5}$
$1.02 \cdot 10^{-4}$
$1.05 \cdot 10^{-4}$
$1.08 \cdot 10^{-4}$
$1.112 \cdot 10^{-4}$
$1.144 \cdot 10^{-4}$

$P_f(b,i) =$

$8.069 \cdot 10^{-6}$
$7.811 \cdot 10^{-6}$
$7.56 \cdot 10^{-6}$
$7.317 \cdot 10^{-6}$
$7.082 \cdot 10^{-6}$
$6.853 \cdot 10^{-6}$
$6.632 \cdot 10^{-6}$
$6.417 \cdot 10^{-6}$
$6.209 \cdot 10^{-6}$
$6.007 \cdot 10^{-6}$
$5.812 \cdot 10^{-6}$
$5.623 \cdot 10^{-6}$
$5.439 \cdot 10^{-6}$
$5.261 \cdot 10^{-6}$
$5.089 \cdot 10^{-6}$
$4.922 \cdot 10^{-6}$

MPPM using a Butterworth Filter and zero guard with 1Gbit/s data and 6 PCM BITS for Free Space

Preamplifier terms

$S_o := 16 \cdot 10^{-24}$ Preamp noise at input - double sided Philips TZA 3043

$B := 1 \cdot 10^{9}$ Bit rate

$T_b := \frac{1}{B}$ PCM bit time

$i := 0, 1 .. 20$

$v_i := v_{off} + \frac{i}{range}$

$n := 8$ Number of like symbols in PCM

$f_n := 1 \cdot 10^{6}$ Channel Bandwidth for free space

$N := 6$ Number of PCM Bits

$T_s := \frac{6 \cdot T_b}{12}$ Slot Time for MPPM(12,2)

$\eta q := 1.6 \cdot 10^{-19}$ Quantum energy

$\lambda := 1.55 \cdot 10^{-6}$ This is the wavelength of operation

$$photon\_energy := \frac{6.63 \cdot 10^{-34} \cdot 3 \cdot 10^{8}}{\lambda}$$

$R_o := \frac{\eta q}{photon\_energy}$ $R_o := 1.247$

Pulse shape terms

$T_s = 5 \cdot 10^{-10}$

$f_p := 0.7 \cdot \frac{1}{T_s}$ $f_B := 0.5 \cdot \frac{1}{T_s}$

$\alpha := \frac{0.1874 \cdot T_b}{f_n}$ $\alpha_n := \frac{0.1874 \cdot T_b}{f_n \cdot T_s}$

$\omega_B := 2 \cdot \pi \cdot f_B$ $\omega_{Bn} := \omega_B \cdot T_s$

$\omega_p := 2\cdot\pi\cdot f_p$ $\omega_{pn} := 2\cdot\pi\cdot f_p\cdot T_s$

$\tau_R := \frac{8}{\omega_B}$ $\tau_{Rn} := \frac{8}{\omega_B\cdot T_s}$

$\text{Pulse}(\omega) := \frac{\sin\left(\frac{\omega\cdot T_s}{2}\right)}{\left(\frac{\omega\cdot T_s}{2}\right)}$ $\text{Pulse}_n(\omega) := \frac{\sin\left(\frac{\omega}{2}\right)}{\left(\frac{\omega}{2}\right)}$

$H_{pre}(\omega) := \frac{1}{1 + j\cdot\frac{\omega}{\omega_p}}$ $H_B(\omega) := \frac{\omega_B^{\,3}}{\left(j\cdot\omega + \omega_B\right)^3}$

$H_{pren}(\omega) := \frac{1}{1 + j\cdot\frac{\omega}{\omega_{pn}}}$ $H_{Bn}(\omega) := \frac{\omega_{Bn}^{\,3}}{\left(j\cdot\omega + \omega_{Bn}\right)^3}$

Pulse shape

$$I_0(t) := \frac{1}{\pi}\cdot\int_0^{1\cdot 10^{11}} \text{Pulse}(\omega)\cdot\text{Re}\left[H_{pre}(\omega)\cdot H_B(\omega)\cdot\exp\left[i\cdot\omega\cdot(t-0.5)\cdot T_s\right]\right]d\omega$$

$$a(\omega) := \omega_{pn} - 3\cdot\frac{\omega^2}{\omega_{Bn}} - 3\cdot\frac{\omega^2\cdot\omega_{pn}}{\omega_{Bn}^{\,2}} + \frac{\omega^4}{\omega_{Bn}^{\,3}}$$

$$b1(\omega) := \omega + 3\cdot\frac{\omega\cdot\omega_{pn}}{\omega_{Bn}} - 3\cdot\frac{\omega^3}{\omega_{Bn}^{\,2}} - \frac{\omega^3\cdot\omega_{pn}}{\omega_{Bn}^{\,3}}$$

$$I_0(t) := \frac{\omega_{pn}}{\pi\cdot T_s}\cdot\int_0^{100} \text{Pulse}_n(\omega)\cdot\left[\frac{a(\omega)\cdot\cos(\omega\cdot(t-0.5)) + b1(\omega)\cdot\sin(\omega\cdot(t-0.5))}{a(\omega)^2 + b1(\omega)^2}\right]d\omega$$

$$I_1(t) := \frac{\omega_{pn}}{\pi\cdot T_s^{\,2}}\cdot\int_0^{100} \text{Pulse}_n(\omega)\cdot\omega\cdot\frac{b1(\omega)\cdot\cos(\omega\cdot(t-0.5)) - a(\omega)\cdot\sin(\omega\cdot(t-0.5))}{a(\omega)^2 + b1(\omega)^2}d\omega$$

$t := -1, -0.99 .. 6$

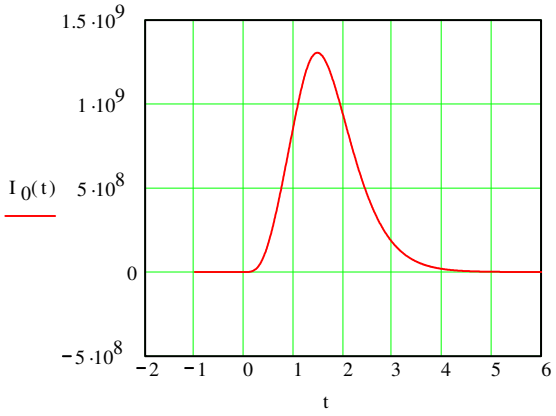

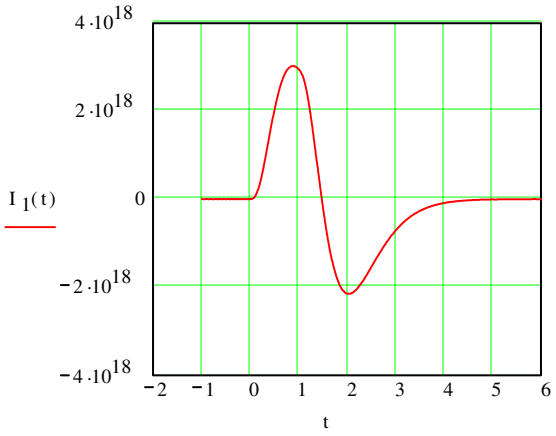

$$noise := \frac{2}{2\cdot\pi}\cdot\int_0^{1\cdot10^{11}} \left| H_{pre}(\omega)\cdot H_B(\omega) \right|^2 d\omega$$

$noise = 1.053\cdot10^{9}$

$t := 1.474$

$t_{pk} := root\left(I_1(t)\cdot T_s^{\,2}, t\right)$

$t_{pk} = 1.474$

$v_{pk}(b) := b\cdot\eta q\cdot I_0\left(t_{pk}\right)$

$v_{pk}(b) = 1.044\cdot10^{-6}$

$t := 0.878$

$t_{d_i} := \text{root}\left[\left(I_0(t) - v_i \cdot I_0\left(t_{pk}\right)\right) \cdot T_s^{\,2}, t\right]$

$v_d(b,i) := b \cdot \eta q \cdot I_0\left(t_{d_i}\right)$

$t_{d_5} = 0.878$

Erasure Error

$$Q_r(b,i) := \frac{v_{pk}(b) - v_d(b,i)}{\sqrt{S_o \cdot noise}}$$

$P_{er} := 0.433$ **6 Bits PCM error caused by erasure in MPPM**

$$P_r(b,i) := 0.5 \cdot P_{er} \cdot erfc\left(\frac{Q_r(b,i)}{\sqrt{2}}\right)$$ ***Erasure Error Probability***

False Alarm Error

$$Q_t(b,i) := \frac{v_d(b,i)}{\sqrt{S_o \cdot noise}}$$

$P_{fa} := 0.310$ **6 Bits PCM error caused by False Alarm in MPPM**

$$P_f(b,i) := 0.5 \cdot erfc\left(\frac{Q_t(b,i)}{\sqrt{2}}\right) \cdot P_{fa}$$ [redacted]

$P_{eb}(b,i) := P_r(b,i) + P_f(b,i)$ ***Binary Error Probability***

$pc(b,i) := \left(\log\left(P_{eb}(b,i)\right) + 9\right)$ Set for 1 in 10^9 errors

$a_i := root(pc(b,i),b)$ Find the root to give 1 in 10^9

$minimum := min(a)$

$range \equiv 1000$

$minimum = 7.756 \cdot 10^3$

$b \equiv 5 \cdot 10^3$

$minimum = 7.756 \cdot 10^3$

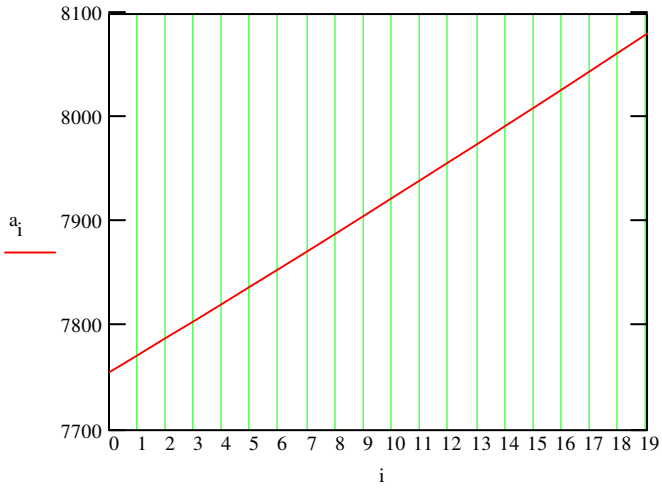

$v_{off} \equiv 0.53$

$N \equiv 6$

$f_n \equiv 1 \cdot 10^6$

$v_{10} = 0.54$

$P_r(b,i) =$

$3.414 \cdot 10^{-5}$
$3.526 \cdot 10^{-5}$
$3.641 \cdot 10^{-5}$
$3.76 \cdot 10^{-5}$
$3.882 \cdot 10^{-5}$
$4.009 \cdot 10^{-5}$
$4.139 \cdot 10^{-5}$
$4.273 \cdot 10^{-5}$
$4.411 \cdot 10^{-5}$
$4.553 \cdot 10^{-5}$
$4.7 \cdot 10^{-5}$
$4.851 \cdot 10^{-5}$
$5.007 \cdot 10^{-5}$
$5.167 \cdot 10^{-5}$
$5.332 \cdot 10^{-5}$
$5.502 \cdot 10^{-5}$

$P_f(b,i) =$

$3.154 \cdot 10^{-6}$
$3.043 \cdot 10^{-6}$
$2.935 \cdot 10^{-6}$
$2.831 \cdot 10^{-6}$
$2.73 \cdot 10^{-6}$
$2.633 \cdot 10^{-6}$
$2.539 \cdot 10^{-6}$
$2.448 \cdot 10^{-6}$
$2.361 \cdot 10^{-6}$
$2.276 \cdot 10^{-6}$
$2.194 \cdot 10^{-6}$
$2.115 \cdot 10^{-6}$
$2.039 \cdot 10^{-6}$
$1.966 \cdot 10^{-6}$
$1.894 \cdot 10^{-6}$
$1.826 \cdot 10^{-6}$

The model of the noise performance and sensitivity for an optically Pre-amplified Receiver (SOA + PIN) with 1 Gb/S and 3 Bits of PCM in Free Space

Preamplifier (SOA) terms

$G := 20$ Gain of SOA (dB) (SOA-High Power Operation)(IEEE 802.3av)

$\lambda := 1550 \cdot 10^{-9}$ Wavelength of operation (m)

$NF := 9$ Amplifier noise figure (dB)

$F := 10^{\frac{NF}{10}}$ Amplifier noise factor

$F = 7.943$

Common terms

$B := 1 \cdot 10^{9}$ PCM bit rate

$T_b := \frac{1}{B}$ PCM bit time

$N := 3$ Number of PCM Bits

$f_n := 1 \cdot 10^{6}$ Channel Bandwidth for free space

$q := 1.602 \cdot 10^{-19}$ Electron Charge

$K_B := 1.38 \cdot 10^{-23}$ Boltzmann's Constant

$T := 300$ The absolute temperature (Kelvin)

$h := 6.624 \cdot 10^{-34}$ Planck's Constant(JS)

$c := 3 \cdot 10^{8}$ Velocity of light in a vacuum (m/s)

InGaAs PIN Photodiode terms

$I_D := 1 \cdot 10^{-9}$ Dark Current (A) (High speed InGaAs PIN photodiode C30637, @ 1550 nm, optoelectronics.PerkinElmer)

$R_o := 0.95$ Resposivity (A/W) @ 1550 nm

$R_L := 50$ Photodiode Load Resistor (Ω)

$C := 0.4 \cdot 10^{-12}$ Photodiode Capacitance (F)

For Dicode PPM :

$T_{s1} := \frac{T_b}{2}$ Slot time for Dicode PPM for 3 Bits of PCM

$B_1 := 2 \cdot B$ Bit rate for DicodePPM for 3 Bits of PCM

$I_2 := 0.564$

$I_3 := 0.087$

Bandwidth integrals which depend on the shape of the input and output pulses, output pulse shape is raised-cosine spectrum pulse.
these values are for α=1 pulses fill the whole of the slot (rectangular pulses)

$N_i := \frac{4 \cdot K_B \cdot T}{R_L}$

The noise delivered to the input of SOA from the source, which is The mean-square thermal (Johnson) noise current of load resistor (A^2/Hz). Assumption to the photodiode load resistor is much smallar than the amplifier input impedance.Therfore, it's thermal noise is much greater than that of the amplifier input.

$N_i = 3.312 \cdot 10^{-22}$

$S_i := N_i$

The shunt noise generator, models the noise current due to the preamplifier first stage and the photodiode load resistor(A^2/Hz)

$N_{input} := S_i \cdot B_1 \cdot I_2$ The mean-square equivalent input noise current (A^2)

$N_{input} = 3.736 \cdot 10^{-13}$

$$N_{total} := 2 \cdot q \cdot I_D \cdot B_1 \cdot I_2 + N_{input}$$

The total, signal-independent, equivalent input noise current which includes the noise from the photodiode dark currents and any preamplifier noise (A^2)

$$N_{total} = 3.736 \cdot 10^{-13}$$

$$N_A := N_i \cdot (F - 1)$$

The input noise of the SOA device which is considered as an extra noise (A^2/Hz)

$$N_A = 2.3 \cdot 10^{-21}$$

$$Q := 6$$

This value is for an error rate of 1 in 10^9 pulses

$$P := Q \cdot \frac{\left(\sqrt{N_{total}} + q \cdot B_1 \cdot I_2 \cdot Q\right)}{R_o}$$

The mean optical power required (Sensitivity)

$$P = 3.867 \cdot 10^{-6}$$

$$Y := 6$$

The signal to noise ratio, which equals 6 for an error rate of 1 in 10^9 pulses

$$I := Y \cdot \sqrt{N_{input}}$$

$$I = 3.667 \cdot 10^{-6}$$

$$P_o := \frac{I}{R_o}$$

The received power (W)

$$P_o = 3.86 \cdot 10^{-6}$$

$$NP := P_o \cdot \lambda \cdot \frac{T_{s1}}{h \cdot c}$$

The number of received photons for Dicode PPM for 3 Bits of PCM

$$NP = 1.506 \cdot 10^{4}$$

For DPPM :

$$T_{s2} := \frac{3 \cdot T_b}{2^3}$$

Slot time for DPPM for 3 Bits of PCM

$$B_2 := \frac{2^3 \cdot B}{3}$$

Bit rate for DPPM for 3 Bits of PCM

$I_2 := 0.564$

$I_3 := 0.087$

Bandwidth integrals which depend on the shape of the input and output pulses, output pulse shape is raised-cosine spectrum pulse.
these values are for α=1 pulses fill the whole of the slot (rectangular pulses)

$$N_i := \frac{4 \cdot K_B \cdot T}{R_L}$$

$N_i = 3.312 \cdot 10^{-22}$

The noise delivered to the input of SOA from the source, which is The mean-square thermal (Johnson) noise current of load resistor (A^2/Hz). Assumption to the photodiode load resistor is much smallar than the amplifier input impedance.Therfore, it's thermal noise is much greater than that of the amplifier input.

$$S_i := N_i$$

The shunt noise generator, models the noise current due to the preamplifier first stage and the photodiode load resistor(A^2/Hz)

$$N_{input} := S_i \cdot B_2 \cdot I_2$$

The mean-square equivalent input noise current (A^2)

$N_{input} = 4.981 \cdot 10^{-13}$

$$N_{total} := 2 \cdot q \cdot I_D \cdot B_2 \cdot I_2 + N_{input}$$

The total, signal-independent, equivalent input noise current which includes the noise from the photodiode dark currents and any preamplifier noise (A^2)

$N_{total} = 4.981 \cdot 10^{-13}$

$N_A := N_i \cdot (F - 1)$ The input noise of the SOA device which is considered as an extra noise (A^2/Hz)

$N_A = 2.3 \cdot 10^{-21}$

$Q := 6$ This value is for an error rate of 1 in 10^9 pulses

$$P := Q \cdot \frac{\left(\sqrt{N_{total}} + q \cdot B_2 \cdot I_2 \cdot Q\right)}{R_o}$$

The mean optical power required (Sensitivity)

$P = 4.467 \cdot 10^{-6}$

$Y := 6$ The signal to noise ratio, which equals 6 for an error rate of 1 in 10^9 pulses

$I := Y \cdot \sqrt{N_{input}}$

$I = 4.235 \cdot 10^{-6}$

$$P_o := \frac{I}{R_o}$$

The received power (W)

$P_o = 4.458 \cdot 10^{-6}$

$$NP := P_o \cdot \lambda \cdot \frac{T_{s2}}{h \cdot c}$$

The number of received photons for DPPM for 3 Bits of PCM

$NP = 1.304 \cdot 10^4$

For MPPM (5,2) :

$T_{s3} := \frac{3 \cdot T_b}{5}$ Slot time for MPPM(5,2) for 3 Bits of PCM

$B_3 := \frac{5 \cdot B}{3}$ Bit rate for MPPM(5,2) for 3 Bits of PCM

$I_2 := 0.564$

$I_3 := 0.087$

Bandwidth integrals which depend on the shape of the input and output pulses, output pulse shape is raised-cosine spectrum pulse. these values are for α=1 pulses fill the whole of the slot (rectangular pulses)

$N_i := \frac{4 \cdot K_B \cdot T}{R_L}$

$N_i = 3.312 \cdot 10^{-22}$

The noise delivered to the input of SOA from the source, which is The mean-square thermal (Johnson) noise current of load resistor (A^2/Hz). Assumption to the photodiode load resistor is much smallar than the amplifier input impedance.Therfore, it's thermal noise is much greater than that of the amplifier input.

$S_i := N_i$ The shunt noise generator, models the noise current due to the preamplifier first stage and the photodiode load resistor(A^2/Hz)

$N_{input} := S_i \cdot B_3 \cdot I_2$ The mean-square equivalent input noise current (A^2)

$N_{input} = 3.113 \cdot 10^{-13}$

$N_{total} := 2 \cdot q \cdot I_D \cdot B_3 \cdot I_2 + N_{input}$ The total, signal-independent, equivalent input noise current which includes the noise from the photodiode dark currents and any preamplifier noise (A^2)

$N_{total} = 3.113 \cdot 10^{-13}$

$N_A := N_i \cdot (F - 1)$ The input noise of the SOA device which is considered as an extra noise (A^2/Hz)

$N_A = 2.3 \cdot 10^{-21}$

$Q := 6$ This value is for an error rate of 1 in 10^9 pulses

$P := Q \cdot \frac{\left(\sqrt{N_{total}} + q \cdot B_3 \cdot I_2 \cdot Q\right)}{R_o}$ The mean optical power required (Sensitivity)

$P = 3.53 \cdot 10^{-6}$

$Y := 6$ The signal to noise ratio, which equals 6 for an error rate of 1 in 10^9 pulses

$I := Y \cdot \sqrt{N_{input}}$

$I = 3.348 \cdot 10^{-6}$

$P_o := \frac{I}{R_o}$ The received power (W)

$P_o = 3.524 \cdot 10^{-6}$

$NP := P_o \cdot \lambda \cdot \frac{T_{s3}}{h \cdot c}$ The number of received photons for MPPM(5,2) for 3 Bits of PCM

$NP = 1.649 \cdot 10^4$

Appendix E: Simulation 1

Appendix E: Simulation 1

Appendix E: Simulation 1